On Quantitative Issues Pertaining to the Detection of Epistatic Genetic Architectures

by
Carleigh Woodward

B.A. (Hons.), Simon Fraser University, 2015

Thesis Submitted in Partial Fulfillment of the
Requirements for the Degree of
Master of Arts

in the
Department of Psychology
Faculty of Arts and Social Sciences

SIMON FRASER UNIVERSITY
Spring 2021

Declaration of Committee

Name:	**Carleigh Woodward**
Degree:	**Master of Arts**
Thesis title:	**On Quantitative Issues Pertaining to the Detection of Epistatic Genetic Architectures**
Committee:	**Chair:** **Lara Aknin** Associate Professor, Psychology
	Michael Maraun Supervisor Professor, Psychology
	Rachel Fouladi Committee Member Associate Professor, Psychology
	Michael Neale Examiner Professor Psychiatry and Human Molecular Genetics Virginia Commonwealth University

Abstract

Converging empirical evidence portrays epistasis (i.e., gene-gene interaction) as a ubiquitous property of genetic architectures and protagonist in complex trait variability. While researchers employ sophisticated technologies to detect epistasis, the scarcity of robust instances of detection in human populations is striking. To evaluate the empirical issues pertaining to epistatic detection, we analytically characterize the statistical detection problem and elucidate two candidate explanations. The first examines whether population-level manifestations of epistasis arising in nature are small; consequently, for sample-sizes employed in research, the power delivered by detectors may be disadvantageously small. The second considers whether gene-environmental association generates bias in estimates of genotypic values diminishing the power of detection. By simulation study, we adjudicate the merits of both explanations and the power to detect epistasis under four digenic architectures. In agreement with both explanations, our findings implicate small epistatic effect-sizes and gene-environmental association as mechanisms that obscure the detection of epistasis.

Keywords: epistasis; gene-environment association; detection theory; omnibus *F*-test of interaction; quantitative genetics; simulation study

Acknowledgements

Foremost, I would like to express my sincere gratitude to my research supervisor and mentor, Prof. Dr. M. Maraun. The opportunity to study under his invaluable guidance has been the utmost privilege. His expertise, innovative ideas, patience, and sincerity have deeply inspired me. To my committee members, for their support and expertise. To my family, Léandre, and Matéo for their love, understanding, and continuing encouragement. Finally, to my colleague Paul, for both his camaraderie and invaluable technical help on the project.

Table of Contents

List of Tables

List of Figures

Glossary

Additive Models	Additive model: $Z_{ij}= a_i + \beta_j$ (Cordell, 2002). Specified on either the penetrance scale $p_{ij} = a_i + \beta_j$ or a log-odds scale $log\left(\frac{p_{ij}}{1-p_{ij}}\right)=a_i + \beta_j$ (Cordell, 2002). SNP coding: AA=0, Aa=1, aa=2.
Admixture and Migration	Admixture and migration refer to gene flow between populations
Attributes	Attributes are typically genomic variants of interest to the researcher (typically SNPs).
Batch Effects	Batch effects refer to a difference between samples based on processing and measurement differences unrelated to biological variation during the experiment (e.g., laboratory conditions, the instruments used, and time of day).
Bayes Factors	Bayes Factors (BF) initially suggested by Laplace (1774; reprinted in 1986) are a criterion to compare a discrete set of models by the ratio of their respective marginal likelihood, reporting the probability of the data under each hypothesis, averaged over the uncertainty in the parameters.
Bayes Theorem	Bayes Theorem (Bayes and Price, 1763) is used to calculate conditional posterior probabilities based on both prior distributions of parameters and the observed data (Wei, Hemani, & Haley, 2014). In particular, the conditional posterior probability is the product of the likelihood function and prior probability of an event A, divided by the marginal likelihood of event B: $P(A\|B) = \frac{P(B\|A)P(A)}{P(B)}$ (Kaplan & Depoli, 2013).
Bayesian Network	Bayesian Networks are a directed acyclic graph, the structure of which represents the joint probability distribution and conditional independence of a set of random variables (Han et al., 2012). For epistatic detection, SNP markers are nodes with their probability distribution. A Markov property is encoded by the network based on the *independence* or *conditional dependence* of a node to its parent nodes. Dependencies

	between each node are graphically depicted as an edge or interaction. Herein, edges between nodes determine the structure of the graph.
Bayesian Model Averaging	Bayesian Model Averaging improves average predictive abilities by way of conditioning all probability distributions and derived probabilities on the average of *all models* (Madigan & Raftery,1994, as cited by Hoeting, Madigan, Raferty, & Volinsky, 1999).
Cross-Validation	Cross-validation is a method to evaluate model performance by partitioning a dataset into subsamples. The first subset is used to perform the analysis, and the second to test how well the analysis worked. Multiple rounds of cross-validation are employed with different partitions of the data. However, cross-validation may lead to issues in a model overfitting the current dataset. In such a case, the model may no longer be generalizable to future data sets (Cordell, 2009).
Complex Traits	Complex traits are thought to result from a small to a moderate number of common variants based on the assumption of the *common disease common variant hypothesis* (CDCV) (Zeigler, Konig, Thompson, 2008).
Common Disease Common Variant Hypothesis (CDCV)	The CDCV hypothesis suggests that common sequence differences (SNPs) may confer at least some of the genetic risk for common diseases, with multiple common genetic variants influencing multi-locus traits each with low penetrance or effect size (Bush & Moore, 2012).
Curse of Dimensionality	Characteristics of data sparsity. Herein the requirement for a large sample size n grows exponentially with test dimensionality.
Direct Association	Direct association in the context of GWAS occurs when the genetic marker is the casual locus of the phenotype. Indirect association occurs when the genetic marker is in linkage disequilibrium (LD) (i.e., associated) with the causal locus, and thus also has a degree of association with the disease. GWAS typically employs *indirect association*, assuming LD between variants of interest and the casual locus.
Differential Bias	Differential bias refers to variability in the process of assigning genotypes to subjects: 1) variations in the preparation of DNA samples across different laboratories or differences in well-plates before genotyping; 2) degeneration of arrays over time; and 3) subject-level variability due to differences in DNA concentration differences, variations during the hybridization process and probe affinities (see Zeigler, Konig, & Thompson (2008).

Dominance Disease Model	In dominance disease models the dominant allele must be present at both loci (Zeigler et al., 2012). Consequently, only genotypes containing dominant alleles A and B are at risk (Neuman, Rice, 1992). Binary SNP coding of dominant models are as follows: AA=1, Aa + aa =0.
Dirichlet Prior	Dirichlet priors are a family of multivariate probability distributions, pdf:$f(x_1, \ldots, x_K; \alpha_1, \ldots, \alpha_K) = \frac{1}{B(\boldsymbol{\alpha})} \prod_{i=1}^{K} x_i^{\alpha_i - 1}$. In which a is a concentration parameter vector of all real numbers. Dirichlet priors are commonly used as conjugate priors to Bernoulli and multinomial parameters, as they yield a Dirichlet posterior distribution.
EM Algorithm	The Expectation-Maximization (EM) algorithm is a two-step algorithm designed to estimate maximum a-posterior point estimates (MAPs). The EM algorithm is an iterative method which consists of two steps: 1) E (e.g., creates a function for the expectation of the log-likelihood evaluated based on the current estimate of parameters); 2) and M (e.g., maximization step which computes the parameters which maximize the expected log-likelihood). Herein, each step is repeated until convergence and the algorithm derives maximum a posteriori point estimates of the posterior mode, model coefficients, standard error, p-values, and AICs (Yi, Kaklamani, and Pasche, 2012). EM algorithms are used in hybrid methods to compare model fit (Yi, Kaklamani, and Pasche, 2012).
Exhaustive Search Algorithms	Exhaustive Search is optimization algorithms that aim to generate and check all candidate solutions (e.g., brute force and branch- bound algorithms, which respectively employ an exponential search tree, and node sorting and pruning). Generation of candidate solutions includes looping nearest-neighbor pairs, candidate packing, and permutations. Typically, the selection process is based upon the satisfaction of a particular statement. Algorithm issues include scalability for both storage, memory, and performance.
Evolutionary Algorithms	Evolutionary algorithms are optimization algorithms that build models designed to predict class membership (e.g., disease status) by generating a population of solutions evaluated by a fitness function. Model selection is based on those with the highest *fitness* (McKinney et al., 2006).
Feature Selection	The aims of feature selection or variable selection is to identify a subset of features relevant to predictor/outcome variables (conducted before modeling), to reduce over-fitting, improve accuracy, and reduce training time. Feature selection methods include: 1) *wrapper algorithms* which use a predictive model to score feature subsets and are used for model training and evaluation (e.g., stepwise regression, which is a greedy

	algorithm that adds the best feature each iteration); 2) *filter algorithms* which score a feature subset on a proxy measure (e.g., PPMC, intra-class distance, pointwise mutual information); 3) *embedded algorithms* as a part of the model construction process (e.g., LASSO- where any non-zero regression coefficients following L1 penalty shrinking are 'selected').
Fine Fitting Mapping	Fine fitting mapping refers to the sequencing of all variants in an associated region.
Gene Conversion	Gene conversion occurs during meiosis when a short stretch of the copied chromosome is transferred to the other yielding two very closely spaced recombination events.
Genetic Drift	Genetic drift describes the generational change in gene and haplotype frequencies in a population of a finite number of offspring due to random sampling of gametes. Herein frequency changes are accentuated in small populations and the increased drift of small stable populations tends to increase LD as haplotypes are lost from the population (Ardlie, Kruglyak, & Seielstad, 2002).
Genetic Marker	Genetic markers include *tag* variants such as single-nucleotide polymorphisms (SNPs).
Genome Sequencing	Genome sequencing for ~3 million nucleotide markers and other potential sources of genomic variation is conducted using high-throughput microarrays. Sequencing is the process in which the order of nucleotide sequence for a given DNA fragment is determined based upon thousands of unique nucleotide probe sequences designed to hybridize with a target nucleic acid molecule (Zeigler, Zonig, & Thompson, 2008). The intensity of hybridization between a probe and the target in the sample is measured. The hybridization intensity is a function of DNA quality and affinity of hybridization (LaFramboise, Harrington, & Wier, 2006).
Genetic Variant	Genetic variants refer to changes in the nucleotide sequence due to mutations such as single nucleotide base pair change (bp) to rearrangement of large sections on a chromosome, loss of heterozygosity (LOH), and genomic copy number variants (CNV). CNVs refer to changes in 'expression levels' of a particular protein associated with deletions and duplications of the segment of DNA~20 kilo-bases in length.

Gini importance	Gini importance or mean decrease impurity (MDI) is the average of a variables total decrease in node impurity (weighted by the probability of reaching a particular node), averaged over all trees in the ensemble (i.e., the higher the MDI, the higher the variable importance). Gini impurity is a metric regarding the probability of incorrect classification at a given node in a decision tree based on training data.
Haplotype	Haplotype refers to a combination of alleles (i.e., a sequence of nucleotides on a single homolog). A pair of haplotypes is a diplotype (i.e., one variant of all possible combinations of the haplotypes that exist in the population).
Heuristic Search Algorithms	Heuristic search algorithms are used in state-space search problems to find a single path or conditional structure like an acyclic graph (e.g., to map states a sequence of actions to optimize the solution quality) (Hasen & Zilberstein, 2001).
Implicit Tests of Interaction	According to Cordell (2009) there exist various association tests to detect epistasis: 1) tests of *association* - epistasis is defined as the positive association between two linkage signals (Li & Reich, 1999); 2) *association with the potential for interaction* (Cordell, 2009) – testing a saturated versus reduced model or the joint association; 3) *clustering, association rules, linear models, and tree-based classifiers* to detect dependencies between attributes that improve model prediction (Cordell, 2009).
Imputation	Imputation methods used to account for missing variants include k-nearest neighbor, nonlinear iterative partial least-squares, Bayesian, and Least-squares methods to increase statistical power for detection and narrow down the distance between causal variants and candidate markers (see Rao, Sheperd, Bruno, Liu, and Miecznikowski, 2013; Wei, Hemani, & Haley, 2014).
Iterative Search Algorithm (Greedy Search)	The iterative improvement search technique is a greedy search algorithm that selects SNP combinations with maximum interactive effects. However, given SNPs are initially selected using a univariate test, these methods will not detect SNP interactions when the marginal effects of SNPs are weak or absent (Yoshida & Koike, 2011).
Linkage Analysis	A small number of variants are measured across several generations of a family to discern the associated patterns of inheritance.

Minor Allele Frequency (MAF)	MAF is the occurrence of the *minor allele* across a population. Common SNPs have a MAF in at least 5% of a given population while rare SNPs have a MAF< 5% in a given population.
Markov-Chain Monte-Carlo (MCMC)	MCMC is a sampler that traverses all potential models and parameter values. To do so, MCMC employs a Markov chain to sample from a targeted distribution of interest and Monte Carlo integration to approximate the expectation. Recall that a Markov chain is a sequence of random variables θ, θ^1, θ^2… such that θ^t depends on θ^{t-1}, and the general form of Monte Carlo integration for the expectation of the chain is as follows, $\int_S \ g(\theta)p(\theta)d(\theta) \cong \frac{1}{N}\sum_{t=1}^{n} g(\theta^t)$. Wherein θ^t are samples from the prior distribution $p(\theta)$ and approximates the expected value of the afore noted functions. Here, MCMC generates samples from a posterior density yielding approximate expectations for several quantities of interest. As such, MCMC sampling generates a large representative sample of credible parameter values from the conditional posterior distribution. The sample size or *chain length* is distinct from the sample of empirical data (Krushchke, 2013). As such, a longer MCMC chain indicates a higher resolution of the posterior distribution and its parameter values given the observable data.
Markov Blanket	Markov blanket of a variable T, (MB(T)), is as a minimal set for which (X $\perp T \mid MB(T)$, for all X $\in$V $-${T}$-$ MB(T) where V is the variable set (Han, Park, & Chen, 2010).
Naïve Bayes Classifiers	Naive Bayes Classifiers are a family of classification algorithms that assumes the independence of each feature from the others given a class variable. As such, Naive Bayes is a function that assigns a class label, based on Bayes's theorem and a decision rule. If one uses an event model there are several distributions used depending on the type of features (e.g., for discrete data - multi-nominal or binomial distribution. For continuous data - Gaussian distribution).
Network Learning	Based on information theory and probability theory, the mutual information (MI) between two random variables is a measure of mutual dependence, and MI is used as an association measure for feature selection algorithms (see Sun et al., 2017).
Permutation Tests	Permutation tests refer to the generation of the empirical distribution of a test-statistic by permuting the sample multiple times and re-calculating the value of the test

	statistic in each dataset. Each permuted sample is considered to be a sample of the population under the null hypothesis (Cordell, 2009)
Pleiotropy	Pleiotropy is the phenomenon in which a genetic factor influences more than one phenotype.
Recessive Genetic Models	Quantitative trait variation of this sort is proposed to be due to the presence of two recessive alleles. SNP coding for recessive: AA+Aa=0, aa=1.
Stochastic Search Algorithms	Stochastic search algorithms employ randomized initialization search steps controlled by noise parameters and are typically more efficient than systematic search for combinatorial problems.
Statistical Ranking Procedures	Statistical ranking procedures are based on statistically significant single-marker tests. Common metrics for statistical significance used for single-locus tests include p-values, power for replication, false positives report probability (FPRP), and minimum p-value across test-statistics for additive, recessive, and dominant genetic models (Zeigler, König, & Pahlke, 2010).
Single Nucleotide Polymorphism (SNP)	A single-nucleotide polymorphism (SNP) is a point mutation: 1) one base-pair (bp) for a particular locus differs across a population; 2) the variation is stable across generations; 3) correlated with nearby genomic variants; 4) occurring on average ~ 1 in every 300 bps. ~90% of human variation is proposed to be due to missense single point mutations in the nucleic acid structure of a gene (which include short tandem repeats, substitutions, or additions of motifs, typically around 2-5 bases). ~> 3 million SNPs within a genome. These permeant changes in the DNA sequence may occur spontaneously due to cell division or environmental agents (e.g., ionizing radiation, chemicals) within germline and somatic cells. Main mutation categories are: 1) *substitutions* (exchange of base pairs); 2) *insertions* (extra base pair is added); 3) *deletions* (base pair is removed); 4) and *frameshift* (incorrect codon). Wherein the amino acid structure required for protein synthesis will be either: 1) changed but functionally different (missense); 2) functional (nonsense); 3) or unchanged and functional (silent).
Single Association Tests	Single association tests are partitioned based on trait-type and SNP coding: 1) disease traits: Cochrane Armitage trend test, logistic regression, odds-ratio, Fishers Exact tests; 2) quantitative traits: ANOVA, linear regression, t-

	test; 3) survival data - Cox proportional hazard regression (Zeigler, König, & Pahlke, 2010; Zeng et al., 2015).
Simpsons paradox	The phenomena in which a spurious association or sign reversal occurs in the presence of a third variable.
Supervised Learning Algorithm	In supervised learning, the learning process is based upon the output variable, wherein the algorithm predicts the output variable given some input variables (McKinney et al., 2006).
Unsupervised Learning Algorithm	In unsupervised learning the output variable is unknown, and the goal of the algorithm is in pattern detection (McKinney et al., 2006)
Quality Control (QC)	Quality control techniques are measures used in genome-wide data analyses to identify and ameliorate sources of experimental error: 1) genotype calling and signal intensity plots; 2) cross-platform and cross-technology comparisons to ensure the reproducibility of genotypes (e.g., same platform concordance of 99% and cross-platform concordance at 95%); 3) SNP quality control metrics (e.g., identification and filtering outlying call rates, departures from HWE testing each SNP using the asymptomatic chi-squared test or Fisher's exact test. SNPs with p-values less than 10^{-5} or 10^{-6} removed from further analysis), non-random missing SNPs, and low minor allele frequency (1-2% MAF filter applied)); 4) utility of a control group; 5) subject-level quality control (e.g., identification and filtering of individuals with discordant sex information, outlying call rate, departures from homozygosity, cryptic relatedness in population case and control data); 6) Genomic control for population structure, sex checks, and population stratification. For further details please see the works of Zeigler, Konig, and Thompson (2008), and Zheng, Van Hulle, and Rathouz (2015).

Chapter 1. Introduction

1.1. Background

Considerable attention has been afforded to the task of delineating the relative contributions of genetics (G) and environment (E) to the engenderment of complex phenotypes (Z), or, in other words, elucidating the function f –the *phenotypic architecture* – which relates the values Z_i of individuals, to their genotype G_i, and their environmental exposures E_i,

$$Z_i = f(G_i, E_i). \tag{1.1}$$

One possible choice for f which has been foundational for much work in quantitative genetics goes by the name, Standard Biometric Model (SBM). The SBM portrays the dependency of the phenotype upon environment and genetics in terms of a linear equation in four latent variables and set of moment restrictions (see, e.g., Holzinger, 1929; Jinks & Fulker, 1970; Schonemann, 1997; Rijsdijk & Sham, 2002; Vitzhum, 2003). It is expressed as

$$Z = A + D + C + E \tag{1.2}$$

wherein A, D, C, and E are, respectively, additive (A)[1] and dominance (D) latent genetic variables, a latent environmental impact variable (C)[2], and measurement error (E)[3]. The moment restrictions assert that all latent variables have expectations of zero and are pairwise uncorrelated. However, a growing body of literature suggests that the SBM severely misportrays, via an oversimplification, the joint impact of genetics and environment (see Schönemann, 1979; Falconer, 1989; Kempthrone 1997; Schönemann, 1997; Vizthum, 2003; Shalizi, 2007). Among the flaws thought to be inherent in the SBM are the omission of intrauterine, maternal effects, developmental noise, cultural

[1] Within twin designs, these are genetic factors (additive and dominance) for which MZ twins share (100%) and DZ share (50%).

[2] Within twin designs, shared environmental factors contribute equally to the similarity for MZ and DZ twins.

[3] Within twin designs, unique environmental factors and measurement error contribute to differences between twins.

transmission, and shared familial/community-based environmental impacts, suggesting unaccounted dependencies between genetic and environmental effects (Kempthrone 1997; Shalizi, 2007). Recently, the fact that the SBM makes no mention of *epistasis* has received considerable attention (Vizthum, 2003; Zuk, Hechter, Sunyaev, & Lander, 2012; Wei, Hemani, & Haley, 2014).

Epistasis refers to the interaction between two or more genes at different loci. Although there exists debate, nowadays, over its definition[4], the term was coined by William Bateson (1909) to designate the circumstance where an allele[5] at one locus *masks*, *modifies*, or *interacts* with the phenotypic expression of another (i.e., 'allomorphic pair')[6]; the latter circumstance, proposed as an explanation for the novel and absent classes of traits observed in dihybrid crosses[7]. In contemporary literature, converging evidence suggests a ubiquitous role for epistasis within both prokaryotic and eukaryotic[8]

---

[4] The empirical literature on epistasis suggests several working definitions which vary across fields (see Cordell 2002; Phillips, 2008): 1) *functional, physiological, compositional*, and *statistical* epistasis are described based on the effects of two or more alleles at separate gene loci (see Wei, Hemani, & Haley, 2014; Phillips, 2008). Herein *functional* or *physiological* epistasis is feature of a particular genetic architecture, which occurs when differences in genotypic values at one locus vary depending on the genotype present at the second locus (Cheverud and Routman, 1994). *Compositional* epistasis as the the blocking of allelic effects by combinatorially substituting one allele against a standard background, and more generally, the composition of a particular genotype and the impact genetic background has on the effects of a set of alleles (Phillips, 2008). *Statistical* epistasis as its population-level effect. The differences being that *functional/physiological/compositional* do not take into account a populations allele frequencies while *statistical* epistasis does (Cheverud & Routman, 1994); 2) unidimensional (i.e., directional epistasis) and multidimensional epistasis describe the interaction of mutations with genetic background (see de Visser, Cooper, & Elena, 2011). Unidimensional epistasis is defined as negative or positive deviations from mean log fitness on a multiplicity scale and the number of alleles affecting fitness (de Visser, Cooper, & Elena, 2011). Wherein negative epistasis is described as antagonistic (amongst deleterious mutations), and positive epistasis is described as synergistic (amongst beneficial mutations). Multidimensional epistasis is defined as the individual interactions among a set of alleles and describes the interactions within a fitness landscape (de Visser, Cooper, & Elena, 2011).

[5] An allele is a *version* of a gene found at a particular *locus* (i.e., location along a chromosome). In diploid species, a dominant (A_1) and/or recessive (A_2) allele is inherited from each parent. Dominance (A_1) and recessive (A_2) alleles form three possible genotypes: homozygous dominant (A_1A_1), heterozygous (A_1A_2), and homozygous recessive (A_2 A_2).

[6] Refers to all the genes in the genome and their ability to modify or influence the effects of novel mutations.

[7] In this experimental procedure for bi-allelic species heterozygous parental lines (F1) with alternative alleles at two unlinked loci are respectively crossed and fixed, yielding the segregation of nine genotypes, four gametes per parent and sixteen combinations of alleles in the F2 generation. Herein, epistasis is defined upon the generation of phenotypic ratios which depart from 9:3:3:1.

[8] Select eukaryotic species – the majority of well-replicated research on epistasis has been conducted on model organisms (i.e., plants, yeast, drosophila, mice). As the study of model organisms provides researchers dominion over genetics and environment (afforded by inbred – isogenic - chromosome substitution lines, artificial selection, and di-allelic crosses), researchers are

multilocus genetic architecture[9] (Wright 1931; Wright 1961; Wolf, Broodie & Wade, 2000), and the evolving understanding of mapping genotype to phenotype (i.e., Genotype-Phenotype (GP) maps)[10] (Lewontin, 1974; Alberch, 1991; Wagner & Altenberg, 1996; Hansen, 2006; Wagner, Pavlicev, & Cheverud, 2007; Phillips 2008; Pigliucci, 2010; Sailor & Harms, 2017). To this end, a wealth of empirical literature demonstrating the importance of epistasis as a scientific phenomenon is roughly classifiable into two categories of scientific import, relating to both ultimate[11] and proximate[12] causation.

Concerning the former, literature in the field of evolutionary biology focuses on the role of epistasis as a metaphorical actor in the unfolding evolutionary history of diverse populations of organisms: 1) in the evolution of sexual reproduction and recombination[13] (Wright 1932 ; Kondrashov, 1998; De Visser & Elena, 2007; Otto & Gerstein 2006; Gandon & Otto, 2007; MacCarthy & Bergman, 2007); 2) de-canalization[14]

able to experimentally evaluate with high resolution both the particular interactions between gene loci within an individual, induce novel mutations, and evaluate the impact of epistasis over generations. In contrast, the study of epistasis within human populations is limited to observational or association studies (e.g., familial studies, genome-wide association studies) which are both riddled with practical and quantitative limitations.

[9] Defined as the complete description of genetic factors influencing trait variation (Wei, Hemani & Haley, 2014).

[10] GP maps are based on the works of Lewontin (1974) and Alberch (1991) in which, the authors suggest a functional relationship that maps from genotype space to phenotype space (ie., $G \rightarrow Z$) (see, e.g., Pigliucci, 2010).

[11] Ultimate causation - originally based on the works of Mayr (1961), Tinbergen (1963) describes the kinds of questions which evaluate both phylogeny (i.e., traits evolutionary history), and adaptive significance (i.e., how does trait variation impact a species fitness).

[12] Proximate causation - originally based on the works of Mayr (1961), Tinbergen (1963) describing the traits composition (i.e., what is the structure of the trait) or ontogeny (i.e., species-specific trait development).

[13] There exists several hypotheses for the evolution of sex and recombination. One hypothesis suggests that negative epistasis acts as a form of selection and generates negative associations between alleles (i.e., negative linkage disequilibrium). As such, sex and recombination yields a higher combination of alleles (either favourable or deleterious) on the same chromosome, increasing fitness variance and the response to selection. In such a scenario, it is the case favourable alleles rise in frequency within a population while deleterious alleles are more efficiently removed (Otto & Gertein, 2006). According to this particular hypothesis, epistasis needs to be weak and negative. However, single model simulations also suggest the evolution of recombination is governed by fluctuations in epistasis (i.e., temporal, speed, and shape) and linkage disequilibrium (Gandon & Otto, 2007).

[14] Canalization is the reduced sensitivity or variability of a phenotype to perturbations in the underlying genetic and environmental factors, which determine its expression (Flatt, 2005). As such, canalized genotypes (i.e., wild types) may accumulate mutations and maintain alleles that are not phenotypically expressed. This mutation accumulation yields a de-canalizing event, which is thought to be due to epistasis. As mutation accumulation is expected to lead to an accelerating increase of additive genetic variance (Hansen &Wagner, 2001; as cited by Flatt, 2005).

(Waddington 1942; Wade, 2002; Burch & Chao, 2004; Flatt 2005); 3) speciation[15] (Wade, Winther, Agrawal, & Goodnight, 2001; Pesgravses, 2007); 4) evolution of pleiotrophy (Guillaume & Otto, 2012; Rueffler, Hermission, & Wagner, 2012; Pavlicev & Wagner, 2012). Narrowing the scope slightly, literature in the field of structural-molecular evolution proposes epistasis as one mechanism by which, over generations, mutations (ie., deleterious, permissive) interact with genetic-background[16] to impact the adaptive significance of a traits fitness and function (Phillips, 2008; Elena, Solé, & Sardanyés, 2010; Starr & Thornton, 2016; De Visser, & Hoekstra, 1998)[17]. Empirical illustrations of this sort: 1) leaf area and plant height in maize (Iqal, Khan, Rahman, & Sher, 2010); 2) photoperiod sensitivity in rice (Lin, Yamamoto, Saski, & Yano, 2000); 3) earworm resistance in corn (Pang et al., 2012); 4) length of flowering (Visser, & Hoekstra, 1998); 5) disease resistance in the *vesicular stomatitis virus* (Sanjuan, Moya, & Elena, 2004); 6) functional specificity of the mineralocorticoid and glucocorticoid receptor[18] (Orlund, Bridgham, Redinbo & Thornton, 2007); and 7) drug resistance of the *human immunodeficiency virus* following monotherapy[19] (Molla et al.,1996).

Concerning the latter, in the fields of systems and developmental biology, epistasis is viewed as a proximate mechanism responsible for the orchestration of gene-networks, metabolic pathways in manifold biological contexts, among which: 1) human pathology (e.g., multiple sclerosis (Ramagopalan & Ebers, 2009; Gregersen et al., 2006); type I and II Diabetes (Yu et al., 2014; Wiltshire et al., 2006); Alzheimer's disease (Rhinn et al., 2013; Lehmann et al., 2012; Kolsch et al., 2012; Heun et al., 2012); ankylosing

---

[15] Speciation refers to the phenomena where under reproductive isolation, genes that function well in con-specific genetic backgrounds (i.e., same species), function poorly when combined in interspecific hybrids (ie., between different species) (Wade, Winther, Agrawal, Goodnight, 2001).

[16] Genetic background – refers to all genes within the genome, wherein the particular constellation of genes within a species genome may influence or modify the effects of mutations.

[17] In this particular context, epistasis is defined as the difference in phenotype of a double mutant which cannot be predicted by the sum of single mutants (Mackay, 2014). Moreover, in the case the phenotype of a double mutant is more severe than predicted by the additive effects of single mutants, epistatic effects are categorized as "synergistic, enhancing, aggravating and negative", whereas if the phenotype of the double mutant is less severe than predicted by the additive effects of single mutants, epistasis is said to be "antagonistic, suppressing, alleviating, and positive" (Mackay, 2014).

[18] In the former, epistatic interactions between new deleterious mutations and pre-existing permissive mutations permit conformational re-modeling of receptor-ligand and intra-protein contact structure yielding the receptor differences seen today (Orlund, Bridgham, Redinbo & Thornton, 2007).

[19] Select strains of HIV-1 showed drug resistance to monotherapy as a result of the epistatic sequential stepwise function between 9 codon substitutions (Molla et al.,1996).

spondylitis[20] (see Evans et al., 2011; Brown, Kenna, & Wordsworth, 2015; Cortes et al., 2015); Bechet's disease[21] (Kirino et al., 2013); breast cancer (Ritchie et al., 2001); psoriasis (see Bergboer, Zeeuwen, & Schalkwijk, 2012; Strange et al., 2010); schizophrenia (Burdick et al., 2008; Lin, Lei, Zhang, Dai, & Lu, 2015; Weinberger, 2014); autism spectrum disorder (Coutinho et al., 2007; Mitra et al., 2017); and Hirschsprung's disease[22] (de Pontual et al., 2009)); 2) a species unfolding ontogeny[23] (e.g., mammalian coat colour variation in mice and labrador retriever dogs (Bennett & Lamoreux, 2003; Hoekstra, 2006; Everts, Routhuizen, & Oost, 2000); body-weight in chickens (Le Rouzic, Álvarez-Castro, & Carlborg, 2008); and sensitivity of mutagen methyl-methanesulfonate (MMS) in yeast (Ong et al., 2007)); and 3) scale-independent higher-order epistasis (Sailor & Harms, 2017) (e.g., scattered genomic mutations implicated in *Escherichia coli* fitness (Khan, Dinh, Schneider, Lenksi, Cooper, 2011); chromosomes in asexual fungi for *Aspergillus niger* fitness (de Visser, Park, & Pope, 2009); biosynthetic networks for *Saccharomyces cerevisiae* haploid and diploid growth rate (Hall, Agan, & Hope, 2010); point-mutations and bacterial fitness (Weinreich, Delaney, DePristo, Hartl, 2006); and point-mutations in DNA protein binding affinity (Anderson, McKeown, & Thornton,2015)).

As such, the omission of epistasis from depictions of phenotypic- genetic architecture is problematic for manifold reasons, each classifiable as either broadly scientific or practical. Of the former, the most obvious is, that if epistasis is indeed an important scientific phenomenon, to omit it from scientific accounts is to misportray. Of the latter, perhaps the most striking relates to the mis-estimation[24] of narrow-sense (h^2)[25] and broad-sense heritability (H^2)[26] (see Fisher, 1951; Kempthrone, 1997; Shalizi, 2007; Vizthum, 2004; Hemani, Knott, & Haley, 2013), which serves as a potential explanation

[20] Ankylosing spondylitis is an inflammatory arthritis predominantly affecting the spine and pelvis that occurs in approximately 5 out of 1,000 adults of European descent.

[21] Inflammatory disease.

[22] Congenital disease impacting the large intestine (absence of particular nerve cells) and bowel movements.

[23] Species-specific development

[24] Missing heritability – the observation that genetic effects uncovered by GWAS are not equal to estimates of narrow heritability (Wei, Hemani, & Haley, 2012).

[25] Narrow-sense heritability is defined as the maximum proportion of phenotypic variance accounted for by a linear function of allele counts.

[26] Broad-sense heritability is defined as the proportion of phenotypic variance associated with all genetic effects.

of the phenomenon of *phantom heritability*[27] observed in contemporary genome-wide association studies (GWAS) (see Zuk, Hechter, Sunyaev, Lander, 2012); and inflated additive variance (see Cheverud, Routman, 1995; Templeton, 2000; Hemani, Knott, & Haley, 2013).

In light of the aforementioned role of epistasis in multi-locus genetic architectures of model organisms, it is not surprising that a great deal of effort has gone into its detection. Within human populations, epistatic detectors utilize both data-generation and data-processing methods designed to mitigate the large computational and statistical burden of high dimensional genomic data structure (Cordell 2009; Wei, Hemani, & Haley, 2012). However, despite their sophistication and the ostensive ubiquity of epistasis, it is striking, the dearth of robust[28] instances of detection uncovered for human populations. It would appear that, for reasons currently unknown, epistasis manifests in ways that render its detection particularly challenging. Though there would appear to be no shortage of candidate explanations for this phenomenon, there are two which are notably compelling. The first relates to the possibility the population-level manifestations of epistasis, are by their nature, *small*. Consequently, for the sorts of sample sizes employed in research, the power delivered by epistatic tools of detection may be disadvantageously small. The second relates to whether the presence of gene-environmental association generates bias in estimates of genotypic values[29] and, in so doing, systematically diminishes the power of epistatic detectors.

1.2. Thesis Aims

Broadly speaking the aims of the thesis are, by means of analysis and simulation study, to shed light on the empirical issue of why epistasis is difficult to detect.

---

[27] Phantom heritability was proposed by Zuk and colleagues (2012) as a reason for the phenomena of 'missing heritability', due to an overestimation of the total heritability based on unaccounted genetic interactions. This missing heritability is proposed to account for the deviation between heritability estimates and empirical observations under genome-wide sequencing designs.

[28] Robust examples of epistasis are those which demonstrate scale-invariant interaction effects between the same genetic loci, replicated independently. These include HLAC and ERAP1 in Psoriasis (Strange et al., 2010); ERAP1 and HLAB27 in ankylosing spondylitis (Brown, Kenna, & Wordsworth, 2015; Cortes et al., 2015); and RYN and RNF219, which are implicated in decreasing the risk of Alzheimer's disease in APOE4 non-carriers (Rhinn et al., 2013; Lehmann et al., 2012; Kolsch et al., 2012; Heun et al., 2012).

[29] Genotypic values are taken, variously, to be either theoretical values or $E(Z \mid \boldsymbol{g})$ (see Chapter 2 for further detail).

Specifically, we will: 1) provide a careful characterization of epistasis founded on an elucidation of the distinctions between the frequently conflated elements of the following pairs: i) *individual level* engendering architecture and *population-level* variance components; ii) *Fisherian decomposition of phenotypic values* and models of *phenotypic-genetic architecture*; 2) survey and analytically consider methods of epistasis detection available to the researcher; 3) analytically characterize the *statistical detection* problem and elucidate two candidate explanations for the apparent difficulty inherent to detecting epistasis; 4) finally, via simulation studies, we will adjudicate the merits of both candidate explanations and evaluate the power to detect epistasis under a series of four biologically plausible digenic epistatic architectures.

1.3. Thesis Outline

The thesis is composed of nine chapters. Chapters 2 through 5 provide background information and present the quantitative foundations on which the thesis rests. Specifically, in Chapter 2, we provide the reader with an introduction to quantitative genetics and its core definitions. In Chapter 3, we provide a technical survey of methods, heretofore invented for employment in detecting epistasis, and explore a series of pitfalls implicate to the empirical setting of epistatic detection. In Chapter 4, we provide the technical foundations of the property of epistasis and its engendering architecture, the notion of genotype-specific epistatic effects, and epistatic detection in the empirical setting. In Chapter 5, we provide a review of factors that bear on the probability of detection and present two candidate explanations for the difficulty inherent in detecting epistasis. In Chapter 6, we lay forth the technical elements in the construction of all four epistatic architectures, the general aims of simulation studies I and II, their focal quantities, and the set of criteria employed to adjudicate the merits of both candidate explanations. In Chapters 7 and 8, we present the results of the first and second simulation study. Finally, in Chapter 9, we conclude the thesis with a recapitulation of the findings as they bear on the two candidate explanations. Discussed, also, are corollary relationships, limitations, and areas for further exploration.

Chapter 2. Basics of Quantitative Genetics

Introduction

The issue of why the phenomenon of epistasis might be difficult to detect is a problem drawing from theory located within manifold domains, notably those of quantitative detection theory and genetics. Its roots lie most particularly, however, within the rich soil of quantitative genetics. Accordingly, in this chapter, we review elements of quantitative genetics relevant to the work undertaken. Sections are devoted to each of: 1) the quantitative elements of single and multi-locus engendering phenotypic-genetic (*ApAg*) architectures; 2) the Fisherian decomposition and population-level genetic variance components; 3) the quantities h^2, H^2, and σ_Z^2; and 4) a preliminary definition of epistasis.

2.1. Engendering Phenotypic-Genetic *(ApAg)* Architecture

Let it be the case that: i) Z is a quantitative or disease trait[30]; ii) each individual i belonging to a population P of humans has a score on Z; iii) for all i, Z_i depends genetically on s biallelic loci. In bi-allelic species, such as humans, each gene locus has two alleles. Let the alleles at locus 1 be $\{A_1, A_2\}$, at locus 2, $\{B_1, B_2\}$, etc. It follows then that, at each of the s loci, three *locus-specific genotypes* are defined (eg., at locus 1, $\{A_1A_1, A_1A_2, A_2A_2\}$, at locus 2=$\{B_1B_1, B_1B_2, B_2B_2\}$, etc.), these yielding 3^s genotypes with respect to Z[31]. Define g_j, $j = 1..s$, as the *gene content* of locus j, or, the number of copies of the second allele (A_2, B_2,…) present in a locus j-specific genotype. For the locus 1 specific genotypes A_1A_1, A_1A_2, and A_2A_2, for example, g_1 is equal to 0, 1, and 2, respectively. Clearly, each of the 3^s genotypes is uniquely associated with a value of the s-vector $\boldsymbol{g}$ the j^{th} element of which is g_j. We define the *genetic architecture* to be the scalar function $\Psi'(\boldsymbol{g})$ which maps each of the 3^s genotypes (equivalently, 3^s distinct values $\boldsymbol{g}^*$ of $\boldsymbol{g}$) into a *genotypic value*; i.e., $\Psi'(\boldsymbol{g}^*)$: $\boldsymbol{g}^* \subset \boldsymbol{R}^n \rightarrow \boldsymbol{R}$ (Lynch & Walsh, 1998). A genetic architecture

---

[30] If Z is a disease trait, then it is an [0,1] dichotomous variable that is taken to have arisen on the basis of a dichotomization, by unknown parameter τ, of an underlying quantitative trait, or "liability" Z^*, as follows: if $Z^* \geq \tau$, then Z=1; else, Z=0 (Zuk et. al., 2012).

[31] E.g., in the case $s = 2$, the nine genotypes are: $\{A_1A_1B_1B_1, A_1A_1B_1B_2, A_1A_1B_2B_2, A_1A_2B_1B_1, A_1A_2B_1B_2, A_1A_2B_2B_2, A_2A_2B_1B_1, A_2A_2B_1B_2, A_2A_2B_2B_2\}$.

is said to be *single locus* if $s = 1$, and *multi-locus*, otherwise[32]. The *phenotypic value* is the (*individual level*) scalar function

$$Z_i = \Psi'(\boldsymbol{g_i}) + \gamma(E)_i, \tag{2.1}$$

wherein, $\gamma(E)_i = Z_i - \Psi'(\boldsymbol{g}_i)$ is a residual representing the aggregate impact on Z of all effects – both main and interaction- involving environment[33]. Because each $i_{\in} P$ has a set of values $\{\boldsymbol{g}_i, \gamma(E)_i\}$, the induced distribution of Z in P is determined by the joint distribution of $\{\boldsymbol{g}, \gamma(E)\}$.

2.2. Fisherian Decomposition and Population Genetic Variance Components

In the case of a single locus architecture, the Fisherian decomposition of $\Psi'(g_1)$ is

$$\Psi'(g_1) = \Psi'(g_1)_{\text{Lin}} + \delta(g_1), \tag{2.2}$$

in which $\Psi'(g_1)_{\text{Lin}}$ is the linear predictor of genotypic value on the basis of gene content, and is called the *additive component*, and $\delta(g_1)$ is the residual, or quadratic fit, to the three genotypic values, and is called the *dominance component*. The additive and dominance components can be expressed as

$$\Psi'(g_1)_{\text{Lin}} = [\alpha + \beta g_1], \tag{2.3}$$

and

$$\delta(g_1) = \Psi'(g_1) - \Psi'(g_1)_{\text{Lin}}, \tag{2.4}$$

respectively, in which $\beta = \frac{\sigma_{\Psi'(g_1),g_1}}{\sigma^2_{g_1}}$ and $\alpha = \mu_{\Psi'_{(g_1)}} - \beta\mu_{(g_1)}$.

Given that $\Psi'(g_1)_{\text{Lin}}$ and $\delta(g_1)$ are orthogonal by construction (2.2) implies that the population genetic variance can be decomposed as follows

$$\text{V}(\Psi'(g_1) = V(\Psi'(g_1)_{\text{Lin}}) + V(\delta(g_1)) = \sigma^2_A + \sigma^2_D, \tag{2.5}$$

---

[32] In the multi-locus case when *s=2* an architecture is said to be digenic, and when *s>2,* polygenic.

[33] As afore noted, genotypic values are taken, variously, to be either theoretical values or $\text{E}(Z \mid \boldsymbol{g})$ (see Lynch & Walsh, 1998). In the latter case, the function $\Psi'(.)$ *is*, then, simply the conditional mean function, in which case $\text{E}\gamma(E) = 0$.

wherein σ_A^2 is called the *additive variance component*, and σ_D^2, the *dominance variance component*. Symbolize P(A_2) - the proportion of alleles in *P* of type A_2- as φ, and let it be the case that the probability of occurrence of each of the three genotypes is governed by the Hardy-Weinberg principle and Linkage Equilibrium[34] (see Lynch & Walsh, 1998), in which case P(A_1A_1) =(1- φ)^2 , P(A_1A_2) = 2 φ (1- φ), and P(A_2A_2) = φ^2. It can be proven, then, that

$$\sigma_A^2 = \beta^2\sigma_{g_1}^2 = \frac{\sigma^2_{\Psi'(g_1),g_1}}{\sigma^2_{g_1}} = \frac{\sigma^2_{\Psi'(g_1),g_1}}{2\varphi(1-\varphi)}, \tag{2.6}$$

and

$$\sigma_D^2 = \mathrm{V}(\Psi'(g_1)) - \sigma_A^2. \tag{2.7}$$

It is useful to parameterize the genotypic values as follows: $\Psi'(g_1=0) = 0$, $\Psi'(g_1=1) = (k+1)a$, and $\Psi'(g_1=2) = 2a$. Parameter a controls the linear rate of change of $\Psi'(g_1)$, conditional on g_1, and parameter k, the degree of non-linearity. Specifically, if $k = 0$, then $\Psi'(g_1)$ is a linear function of gene content (g_1); else, it is a quadratic function, in which the genotypic value for A_1A_2 (g_1=1) lies non-equidistant between those for $A_1A_1(g_1 = 0)$ and A_2A_2 (g_1=2) (see Lynch & Walsh, 1998).

Under the {ak} parameterization (Lynch & Walsh, 1998),

$$\sigma_A^2 = 2\varphi(1-\varphi)[\,a(1+k(2\varphi-1))]^2, \tag{2.8}$$

and

$$\sigma_D^2 = (2\varphi(1-\varphi)\,ak)^2. \tag{2.9}$$

In the multi-locus case, the Fisherian decomposition of $\Psi'(\boldsymbol{g})$ is

$$\Psi'(\boldsymbol{g}) = \mu_{\Psi\prime(g)} + \sum_{j=1}^{s} B_{(g_j)} + \sum_{j=1}^{s} \delta_{(g_j)} + \sum_{l=1}^{m} I_{(g_l)}, \tag{2.10}$$

in which: $B_{(g_j)} = \Psi'(\boldsymbol{g})_{\mathrm{Lin}j} - \mu_{\Psi\prime(g)}$; $\Psi'(\boldsymbol{g})_{\mathrm{Lin}j} = a_j + \beta_j g_j$ is the linear predictor of $\Psi'(\boldsymbol{g})$ on the basis of g_j; $\delta(g_j) = \Psi'(\boldsymbol{g}) - \Psi'(\boldsymbol{g})_{\mathrm{Lin}j}$; and the $I_{(g_l)}$ are $m=\sum_{r=2}^{s}\binom{s}{r}=(2^s-s-1)$ *locus-locus interactions*, there being $\binom{s}{r}$ interactions of the r^{th} order, $r = 2 \ldots s$. As the latter three components are orthogonal by construction, (2.10) implies that

[34] In the case *s>1*, unlinked loci are assumed such that $\mathrm{P}(\boldsymbol{g} = \boldsymbol{g}^*) = \prod_{j=1}^{s} P(g_j = \boldsymbol{g}_j^*)$.

$$\mathrm{V}(\Psi'(\boldsymbol{g})) = \sigma_A^2 + \sigma_D^2 + \sigma_{EP}^2, \tag{2.11}$$

wherein σ_{EP}^2 is the variance component due to epistasis.

2.3. The Quantities h^2, H^2, and σ_z^2

By definition, narrow- and broad-sense heritability are, respectively,

$$h^2 = \frac{\sigma_A^2}{\sigma_Z^2} \tag{2.12}$$

and

$$H^2 = \frac{\mathrm{V}(\Psi'(\boldsymbol{g}))}{\sigma_Z^2}. \tag{2.13}$$

Because, from (2.1), $Z = \Psi'(\boldsymbol{g}) + \gamma(E)$, it follows that

$$Z|\boldsymbol{g} \sim (\Psi'(\boldsymbol{g}) + \varepsilon(\boldsymbol{g}),\ \sigma_{\mathrm{E}|\boldsymbol{g}}^2), \tag{2.14}$$

wherein $\varepsilon(\boldsymbol{g}) = E(\gamma(E)|\boldsymbol{g})$ and $\sigma_{E|\boldsymbol{g}}^2 = V(\gamma(E)|\boldsymbol{g})$. Conditional on $\boldsymbol{g}$, $\Psi'(\boldsymbol{g})$, the genotypic value is a constant, and, unless $\varepsilon(\boldsymbol{g}) = 0$, it will not be equal to $\mathrm{E}(Z \mid \boldsymbol{g})$. From (2.14), it can be deduced that the unconditional distribution of Z is

$$\begin{aligned}
Z \sim\ & (\mu_{\mathrm{G}} + \mu_{\mathrm{E}},\ V(E(Z|\boldsymbol{g})) + E(\mathrm{V}(Z|\boldsymbol{g})))\\
& (\mu_{\mathrm{G}} + \mu_{\mathrm{E}},\ V(\Psi'(\boldsymbol{g}) + \varepsilon(\boldsymbol{g})) + E(\sigma_{E|\boldsymbol{g}}^2))\\
& (\mu_{\mathrm{G}} + \mu_{\mathrm{E}},\ V(\Psi'(\boldsymbol{g})) + \mathrm{V}(\varepsilon(\boldsymbol{g})) + 2\rho_{\Psi'(\boldsymbol{g}),\varepsilon(\boldsymbol{g})}\sigma_{\varepsilon(\boldsymbol{g})}\sigma_{\Psi'(\boldsymbol{g})} + \sigma_R^2)\\
& (\mu_{\mathrm{G}} + \mu_{\mathrm{E}},\ [\sigma_A^2 + \sigma_D^2 + \sigma_{EP}^2] + 2\rho_{\Psi'(\boldsymbol{g}),\varepsilon(\boldsymbol{g})}\sigma_{\varepsilon(\boldsymbol{g})}\sigma_{\Psi'(\boldsymbol{g})} + [\sigma_{\varepsilon(\boldsymbol{g})}^2 + \sigma_R^2])\\
& (\mu_{\mathrm{G}} + \mu_{\mathrm{E}},\ [\sigma_A^2 + \sigma_D^2 + \sigma_{EP}^2] + 2\rho_{\Psi'(\boldsymbol{g}),\varepsilon(\boldsymbol{g})}\sigma_{\varepsilon(\boldsymbol{g})}\sigma_{\Psi'(\boldsymbol{g})} + \sigma_E^2),
\end{aligned} \tag{2.15}$$

in which: $\mu_{\mathrm{G}} = E(\Psi'(\boldsymbol{g}))$; $\mu_{\mathrm{E}} = E(\varepsilon(\boldsymbol{g}))$; $\sigma_R^2 = E(\sigma_{E|\boldsymbol{g}}^2)$; $\sigma_{\varepsilon(\boldsymbol{g})}^2 = V(E(\gamma(\mathrm{E})|\boldsymbol{g}))$; and $\sigma_E^2 = \sigma_R^2 + \sigma_{\varepsilon(\boldsymbol{g})}^2$. Observe that $\mathrm{E}(\gamma(\mathrm{E}) \mid \boldsymbol{g}) = \varepsilon(\boldsymbol{g})$ is the mean environmental impact conditional on genotype, from which it follows that there does not exist a genetic-environment association *if and only if* $\varepsilon(\boldsymbol{g}) = c$. It follows then, that $\sigma_{\varepsilon(\boldsymbol{g})}^2$ is the variance in Z due to genetic-environment association. Another way of thinking about this is that $\sigma_{\varepsilon(\boldsymbol{g})}^2$ is the

variance in Z associated with environment that is inseparable from genetics, and σ_R^2 is the variance in Z that is. We observe, also, that, because

$$\rho_{\Psi'(\boldsymbol{g}),E} = \rho_{\Psi'(\boldsymbol{g}),\varepsilon(\boldsymbol{g})} = \frac{\mathrm{E}[E(\gamma(\mathrm{E})|\boldsymbol{g}) - \Psi'(\boldsymbol{g})] - \mu_{\mathrm{G}}\mu_{\mathrm{E}}}{\sigma_{\Psi'(\boldsymbol{g})}\sigma_{\varepsilon(\boldsymbol{g})}} = \mathrm{E}[\varepsilon(\boldsymbol{g}) * \Psi'(\boldsymbol{g})] - \mu_{\mathrm{G}}\mu_{\mathrm{E}}, \quad (2.16)$$

it follows that, under condition that $\varepsilon(\boldsymbol{g}) = c$,

$$\rho_{\Psi'(\boldsymbol{g}),\mathrm{E}} = E[\mathrm{c} * E(\Psi'(\boldsymbol{g})] - \mu_{\mathrm{G}} * \mathrm{c} = \mathrm{c} * \mu_{\mathrm{G}} - \mu_{\mathrm{G}} * \mathrm{c} = 0. \quad (2.17)$$

In other words, in order that $\rho_{\Psi'(\boldsymbol{g}),\mathrm{E}} \neq 0$, it must be the case that $\sigma^2_{\varepsilon(\boldsymbol{g})} > 0$.

All told, then, from (2.1), it follows that

$$\sigma_Z^2 = \sigma^2_{\Psi'(\boldsymbol{g})} + \sigma^2_{\gamma(\mathrm{E})} + 2\sigma_{\Psi'(\boldsymbol{g}),\gamma(\mathrm{E})}. \quad (2.18)$$

Symbolizing Var(γ(E)) = $\sigma^2_{\gamma(\mathrm{E})}$ as σ_E^2, (2.5) and (2.18) jointly imply that, in the single locus case,

$$\sigma_Z^2 = \sigma_A^2 + \sigma_D^2 + \sigma_E\ (\sigma_E + 2\rho_{\Psi_{(g_1)_{Lin}},\gamma(\mathrm{E})}\sigma_A + 2\rho_{\delta_{(g_1)},\gamma(\mathrm{E})}\sigma_D). \quad (2.19)$$

For the multi-locus case,(2.11) and (2.18) imply that

$$\sigma_Z^2 = \sigma_A^2 + \sigma_D^2 + \sigma_{EP}^2 + \sigma_E(\sigma_E + 2\rho_{\sum_{j=1}^{s}\mathrm{B}_{(g_j)},\gamma(\mathrm{E})}\sigma_A + 2\rho_{\sum_{j=1}^{s}\delta_{(g_j)},\gamma(\mathrm{E})}\sigma_D + 2\rho_{\sum_{l=1}^{m}I_{(g)l},\gamma(\mathrm{E})}\sigma_{EP}). \quad (2.20)$$

The rho parameters- $\rho_{\Psi_{(g_1)_{Lin}},\gamma(\mathrm{E})}$, $\rho_{\delta_{(g_1)},\gamma(\mathrm{E})}$, $\rho_{\sum_{j=1}^{s}\mathrm{B}_{(g_j)},\gamma(\mathrm{E})}$, $\rho_{\sum_{j=1}^{s}\delta_{(g_j)},\gamma(\mathrm{E})}$, and $\rho_{\sum_{l=1}^{m}I_{(g)l},\gamma(\mathrm{E})}$- are, of course, gene-environment correlations.

2.4. Definition of Epistasis

Let $\Psi'(\boldsymbol{g}^*)_{\mathrm{Main}}$ stand for the *main effect fitted values* of $\Psi'(\boldsymbol{g}^*)$, on the basis of gene content; i.e., $\mu_{\Psi'_{(\boldsymbol{g})}} + \sum_{j=1}^{s} B_{(g_{j^*})} + \sum_{j=1}^{s}\delta_{(g_{j^*})}$. An architecture has the property of epistasis, under the condition that a) s >1 and b) for *at least 2* of the 3^s genotypes $\boldsymbol{g}^*$,

$$\Psi'(\boldsymbol{g}^*) - \Psi'(\boldsymbol{g}^*)_{\mathrm{Main}} \neq 0. \quad (2.23)$$

A number of prominent authors draw a distinction between *functional* and *statistical* epistasis, wherein, by the former, they mean a *property* of a genetic architecture, and, by the latter, a non-zero value of the population variance component σ^2_{EP}. It is our view that the latter – ie., the magnitude of the chunk of phenotypic variance engendered by epistasis – should not be labelled epistasis. It is, rather, a (population level) *effect* of epistasis. Accordingly, we deny the legitimacy of the functional- and statistical epistasis distinction.

Chapter 3. Epistasis and its Detection

Introduction

Herein we aim to survey and analytically consider contemporary methods of epistatic detection available to the researcher. To this end, we will review: 1) genome-wide association studies (GWAS), the primary experimental design to wit contemporary human epistasis detection relies[35]; 2) a selection of epistatic detectors based on regression, data-mining/machine learning, and Bayesian model selection technologies; and 3) finally explore a series of pitfalls implicate to epistatic detection.

3.1. Genome Wide Association Studies

Genome-wide association studies (GWAS) are non-experimental designs[36] built to estimate trait outcomes and delineate the biological mechanisms implicate in trait variation. To do so, GWAS indirectly associate complex traits to genetic variants, by selecting a subset of genetic markers[37], which serve as proxies to causal variants vis-a-vis linkage disequilibrium (LD)[38] (see Hirschhorn & Daly, 2005; Wang, Barratt, Clayton, & Todd, 2005; Lander, 1996; Bush & Moore, 2012). To this end, high-throughput

[35] While previous study designs for human populations such as *linkage analysis* assess a small number of variants measured across several generations of a family to discern patterns of inheritance associated with the subset of variants, GWAS is the first to evaluate the genetic factors which influence trait variation on a genome-wide scale.

[36] GWAS designs are observational in nature and implement either between-subject (i.e., case-control, case-family) or within-subject (i.e., case-only, and population cohort) test procedures, where each individual is genotyped and classified based on group-membership.

[37] While ideally, one wishes to identify genetic variants whose linear or non-linear effects are *causal* in trait-outcomes, GWAS are designed to capture genome-wide variation across individuals, vis-à-vis, selecting a subset of genetic variants or genetic markers a priori. Genomic markers typically used in GWAS designs are tag *single-nucleotide polymorphisms* (SNPs). SNPs are a point mutation or the change of one base-pair (bp) at a particular locus, which differs across a population. SNPs are stable across generations, correlated with nearby genomic variants, and occur on average ~ 1 in every 300 bps. There are ~ > 3 million SNPs within a genome, accounting for ~90% of human variation.

[38] Linkage Disequilibrium (LD) describes the degree of co-inheritance of two alleles at different loci within a particular population. As such, LD is defined technically as the degree of statistical dependence between loci, $D = P(AB) - P(A)P(B)$. Typically values of $D \geq 0.8$ between a tag SNP (genetic marker) and a causal SNP (casual variant) are required for "good" coverage of the genome.

microarray technologies[39] extract and sequence ~500,000 to ≥ 1-million genetic markers per individual, yielding an [n x k] data matrix **G**[40], of observations, to wit, traditional GWAS designs conduct a series of single-locus tests under the assumptions of *additive*, *dominance*, or *recessive* models of genetic architecture (Zeigler, Konig, & Thompson, 2008; Zeigler, König, & Pahlke, 2010).

However, in light of the phenomena of '*missing heritability*' and its *phantom* counterpart (Lander, 2011; see Zuk et al., 2012), contemporary interest has recently turned to the detection of architectures with the property of epistasis, a task which on a genome-wide scale remains an ongoing challenge. Owing perhaps to the high-dimensional structure of genome-wide data, the detection of epistasis demands both high computational[41] and model[42] complexities, which beget *the curse of dimensionality* and indurate the requirement of a sound test procedure[43] to balance both the P(Type I) and P(Type II) errors[44]. As such, it is clear, epistatic detection on a genome-wide scale

---

[39] Two common microarray sequencing platforms used in GWAS are Illumina and Affymetrix platforms. Differences between each platform include the selection process of tag SNPs (i.e., the 1M BeadChip Illumina selects 950000 tag SNPs from the HapMap project and 100000 non HapMap SNPs, while Affymetrix uses an "unbiased selection of 482 000 SNPs from the SNP Array 5.0" for the SNP Array 6.0, and does not follow the tag SNP approach) (Zeigler, Konig, & Thompson, 2008). The number of genetic markers sequenced is referred to as a tests 'density of coverage' - such that the higher the sequencing density, the greater chance the *causal* variant is included within the 'associated region'.

[40] $\boldsymbol{G}_{n\,x\,k}$ are typical of the order [10^3 x 10^6] - herein, variations between GWAS design matrices are due to test design and the utility of genotype dosage or dummy coding SNPs $X=\begin{Bmatrix}0, & A_1A_1\\ 1, & A_1A_2\\ 2, & A_2A_2\end{Bmatrix}$. Dosage coding treats SNP genotypes as ordered-categorical data (the minor allele increases effect size) (Goudey, 2016). Whereas dummy coding treats SNP genotypes as multiple binary variables without ordinal effects (Goudey, 2016).

[41] As test complexity is linear with n and exponential as the order of interaction increases, an exhaustive test for epistatic effects requires ~$5x10^{11}$ tests for 2-way interactions, $1.7x10^{17}$ tests for 3-way interactions, $4.2x10^{22}$ tests for 4-way interactions, and $8.3x10^{27}$ tests for 5-way interactions (Ritchie, 2015)

[42] As the number of dimensions and categories per dimension increases so too does model complexity. As high parametric complexity is based on the number of orthogonal regression terms required to describe 2-way and m-way interactions. In consideration of 20 SNPs, modeling two dummy variables per bi-allelic locus, 40 parameters are required to model main-effects, 1,560 parameters to model the two-way interactions, 79,040 parameters to model the three-way interactions, and 1,462,240 parameters to model the four-way interactions (Moore, & Hahn, 2002).

[43] See Chapter 4, section 4.3.

[44] While the academic community employs a range of procedures and thresholds for family-wise error control (FWER), it is clear that selection of *stringent P(Type I error) control*, carries in tow the natural consequence of plummeting P(1-Type II error). For a family of single-locus tests (i.e., Bonferroni $a= 0.05$: $k = 10^6$ tests, $a'=5x10^{-8}$) and 2-way interactions (i.e., Bonferroni $a= 0.05$, $m=2$, for $k= 10^6$, $5x10^{11}$ pairwise tests, $a'=10^{-12}$)

comes at both a high computational and statistical cost, a task which contemporary detectors must carefully consider and rectify.

3.2. Epistatic Detectors

Contemporary epistatic detectors are computer algorithms designed to combat the high statistical and computational burden of multiple comparisons by combining the procedures of data generation and data processing. Broadly, data generation procedures tailored for the detection of epistatic effects are categorized by their implementation of either *exhaustive* or *candidate search techniques*.

In the case of the former, exhaustive search algorithms store GWAS data using bitwise data storage[45], parallel processing, multi-CPU cores, cluster super computers, or graphic processing units (GPUs) permit the scalable[46] and sequential testing of the entire parameter search space (R^k) for all *potential* interactions (Culverhouse, Suarez, Lin, & Reich, 2002; Cordell, 2009; Wei, Hemani, & Haley, 2014; Goudey et al., 2015). While the latter reduces the dimension of the parameter search space and tests for the effects of epistasis on a subset of parameters only. Subset selection is based on several techniques, including those guided by previously associated biological pathways and protein-gene-networks[47]; *statistical ranking procedures*; or *stochastic− heuristic− greedy −* search algorithms (Wei, Hemani, & Haley, 2014). While candidate selection procedures boast improvements in processing speed and statistical power, they remain at the whim of publication biases, user-specified significance thresholds, and regrettably omit investigation of genetic loci without statistically significant single-locus effects (Ritchie, 2011; Cordell, 2009; Wei, Hemani, & Haley, 2012).

Coupled with data generation procedures, epistatic detection technologies employ a range of data processors classifiable as parametric regression, data mining machine-learning, and Bayesian model selection, each designed to test for statistical interaction, uncover dependencies between variants, and evaluate model fit all under the guise of 'epistasis detection'. To this end, we will analytically consider a range of contemporary detection technologies available to the empirical scientist, and briefly

---

[45] Each SNP is depicted by three rows for genotype status (0,1,2) and two columns for the grouping variables cases or controls.

[46] Issues in the scalability of exhaustive search algorithms includes the computational costs of storage and efficiency for a large number of candidate solutions.

[47] Typically conducted using queries from public databases for previously reported protein-protein interactions such as IntAct, BioGRID, chEMBL (Niel, Sinoquet, Dina, & Rocheleau, 2015).

explore the technical variations in *how* epistasis is defined and detected, a topic several reviews are dedicated (see Cordell 2002; Phillips, 2008; Cordell 2009; Wei, Hemani, & Haley, 2014).

3.2.1. Parametric Regression

In consideration of the relationship between a quantitative (Z_q) or disease (Z_d) trait, and a fixed set of s[48] genetic variants ($\vec{X}$= {$X_1, X_2 \ldots X_s$}) parametric regression models relevant to our aims, respectively envisage E(Z) as a linear or logistic composite of parameter values $\vec{\theta} = \begin{pmatrix} \alpha \\ \vec{\beta} \end{pmatrix}$ and $\vec{X}$, denoted as $\mathbf{A}\vec{\theta}$. Where $\mathbf{A}$= [$\vec{1}_N, \boldsymbol{X}$] is a design matrix, $\mathbf{X}$ is a sub-matrix (n x (s + m)) whose columns s and m respectively contains a set of scores for the s-genetic variants, and their m- interaction terms (e.g. $x_{i3}x_{i2}$)[49] for n observations; and $\vec{\theta} = \begin{pmatrix} \alpha \\ \vec{\beta} \end{pmatrix}$ is a (1(s+ m)) model parameter vector. Herein each parametric regression model is specified by three elements: 1) the distribution of Z, whose observations are independent and identically distributed (*iid)* along a probability mass or probability density function; 2) the linear predictor $\vec{\eta} = \mathbf{A}\vec{\theta}$ relating model parameters E(Z_i) to $\vec{X}$; and 3) a link functionι^{-1}, relating E(Z) to $\vec{\eta}$, such that $\iota^{-1}[E(Z)] = \mathbf{A}\vec{\theta}$**.** As the aforementioned portrayals envisioned by the linear or logistic regression depict *one* of a family of probability distributions {$\Delta_{\vec{\theta}}$: $\vec{\theta} \in \Theta$}[50] on Z (a family of possible *states of nature*) (Silvey, 1975), it follows that there exist numerous manifestations to which the *shape* ($E(Z) = \mathbf{A}\vec{\theta}$) and *strength* ($V(Z \mid \vec{X})$)[51] of the relationship may respectively assume.

Accordingly, as regression technologies aim to simply *derive* an optimal linear or logistic composite $\mathbf{A}\vec{\theta}$ to predict Z by way of estimating the elements of $\vec{\theta}$ from the observed data, the empirical scientist will construct a test procedure and specify a criterion to make a binary decision regarding the true state of nature extant at the time of

---

[48] Where s is typically a subset of the k loci genotyped at the time of the procedure, $s = 1 \ldots k$.

[49] $m = \sum_{r=2}^{s} \binom{s}{r} = (2^s - s - 1)$ *locus-locus interactions,* there being $\binom{s}{r}$ interactions of the r^{th} order, $r = 2 \ldots s$.

[50] Θ denotes the model parameter space.

[51] The strength of the relationship is contingent on the shape which is decomposed into two parts: 1) primary sense - dispersion around E(Z) and; 2) secondary sense - the sensitivity of Z to changes in $\vec{X}$.

the procedure (Silvey, 1975). While the desired outcome of such a decision is one consonant with nature, the truth remains at all times unknown to the researcher.

As such, linear regression technologies assert the parametric framework: 1) $\vec{Z}_{q\sim} N_n(\mathbf{A}\vec{\theta}, \sigma^2 I)$[52] ; 2) $\vec{\eta} = \mathbf{A}\vec{\theta} = \vec{\beta}'\vec{X} + a\vec{1}$, wherein **A** is an ($n$ x (s+m+1)) design matrix; $\vec{\theta} = \begin{pmatrix} \alpha \\ \vec{\beta} \end{pmatrix}$ a parameter vector, α denotes the intercept and $\vec{\beta}$ the $s + m$ slopes or partial regression coefficients; and 3) the *identity* link function: $\iota^{-1}(\vec{\mu}_{zq}) = \vec{\mu}_{zq}$, wherein $\big(E(Z)\big) = \vec{\beta}'\vec{X} + a\vec{1}$[53]. Following the usual procedure, the empirical scientist estimates $\hat{\vec{\theta}}$[54] from the observed data, and tests the binary hypothesis: [H_0: $\vec{\beta} = 0$ vs H_1: $\vec{\beta} \neq 0$], based on the criterion: if H_0: $\vec{\beta} = 0$, and parametric assumptions are reasonable, then $\frac{MS_{reg}}{MS_{residual}}$ ~$F_{s,(n-s-1)}$. In the event, H_0 is rejected, the researcher may estimate the strength of the relationship based on either $\hat{R}_{xZ}^2 = \frac{SS_{reg}}{SS_{total}}$, or its adjusted counterpart $\hat{R}^2_{xZadj}$ = 1-(1-$R^2_{\vec{x}Z}$)[$\frac{(n-1)}{n-s-1}$)], wherein E($R^2_{\vec{x}Z}$)= $\frac{s}{(n-1)s} > 0$ (see Pedhazur, 1997).

Logistic regression technologies assert the parametric framework: 1) $P(Z_{di} \mid \vec{X}_i = x_i) \sim \prod_{j=1}^{n} p_i(\vec{x})^{Z_i} (1 - p_i((\vec{x}))^{1-Z_i}$, wherein p is the probability of disease status $0 \leq p_i(\vec{x_i}) \leq 1$; $E(Z_i \mid \vec{X}_i = x_i) = p_i(\vec{x})$; $V(Z_i \mid X_i = x_i) = p_i(\vec{x})1 - p_i((\vec{x}))$; 2) $\vec{\eta} = \ln[\frac{P(\vec{x})}{(1-P(\vec{x}))}])\ \mathbf{A}\vec{\theta} = \frac{exp\,(\vec{\beta}'\vec{x}+a\vec{1})}{1+\exp\,(\vec{\beta}'\vec{x}+a\vec{1})}$, where **A** is a ($n$ x (s+m+ 1)) design matrix; $\vec{\theta} = \begin{pmatrix} \alpha \\ \vec{\beta} \end{pmatrix}$ a ((s+m+1)x1) vector of transformed model parameters; and 3) the canonical *logit* link function, $\iota^{-1}(P(\vec{x})) = (\ln[\frac{P(\vec{x})}{(1-P(\vec{x}))}]))\ \mathbf{A}\vec{\theta}$. The empirical scientist estimates $\hat{\vec{\theta}}$[55] from the observed data and tests the binary hypothesis: [H_0: $exp\vec{\beta} = 0$ vs H_1: $exp\vec{\beta} \neq 0$], based on the criterion: *if* H_0: $exp\vec{\beta} = 0$, and assumptions are reasonable[56], *then* according to the

---

[52] Equivalently expressed as $Z_q = \mathbf{A}\vec{\theta} + \vec{\varepsilon}$, and $\vec{\varepsilon} \sim N_s(\vec{0}, \sigma^2 I)$. Asserting multivariate normality, linearity ($\mathbf{A}\vec{\theta} = \vec{\beta}'X + a\vec{1}$); homoscedasticity ($\sigma^2 I$); and independence.

[53] $a\vec{1}$ denotes the mean vector of $\vec{Z}$, when all model predictors = 0.

[54] See Searle (1971); and Agresti (2015) for details on Least Squares estimation for full rank and non-full rank models, respectively.

[55] See Searle (1971) for details on Maximum likelihood estimates (MLE) of a and β.

[56] Rank(**A**) = s, no evidence of influential points or outliers.

Neyman-Person lemma, the likelihood ratio test-statistic, $2ln(\frac{L_{H_0}}{L_{H_1}})\mathbf{A} \sim \chi^2 nH_1 - nH_0$. In the event, H_0 is rejected estimates of the strength of the relationship include its' primary $(1 - \frac{\widehat{E(V(Z|X)}}{\sigma_Z^2})$, and secondary ($\frac{d_{\widehat{\mathrm{E}(\mathrm{Z}1|\vec{X}1=\vec{x}1)}}}{d_{\vec{X}}}$) senses.

Consonant with the definition of epistasis as the departure from the additive combination of loci in their effects on trait variation (Fisher, 1918), the interpretation of regression models of epistasis are bespoke to the scale of Z, with the recovery of epistatic effects dependent on invariance upon transformation (see Cordell 2002; Sverdlov, & Thompson, 2018).

To this end, both linear and logistic regression permits explicit tests for epistatic effects, vis-a-vis, testing model interaction coefficient(s), a family of pairwise contrasts, or comparing model fit between saturated versus reduced linear or log-odd models respectively using the F-ratio or likelihood ratio test statistics (see Goudley, 2015; Agresti, 2015; Searle, 1971; Cordell, 2002; Dunteman & Ho, 2006; Chapman & Clayton, 2007; Cordell, 2009; Wei, Hemani, & Haley, 2014).

Epistatic Detectors - Regression Algorithms

To explore regression-based detection algorithms available to the empirical scientist, we briefly summarize five detectors: 1) *Fast Epistasis;* 2) *GPU-based linear regression for detection of epistasis* (GLIDE); 3) *Multiple Functional Regression Model* (MFRG); 4) *GPU implementation of BOOST* (GBOOST); 5) *Penalized regression - Least Absolute Shrinkage and Selection Operator* (LASSO), and *Smoothly Clipped Absolute Deviation* (SCAD).

Fast Epistasis conducts an exhaustive search employing parallel processing to accommodate up to 500,000 dummy coded SNPs, and a multi-CPU environment to permit QR decomposition to derive least-square estimates, model interaction coefficients, and standard error (see Schüpbach, Xenarios, Bergmann, & Kapur, 2010).

GPU-based linear regression for detection of epistasis (GLIDE) conducts an exhaustive search for all 2-way interactions, accommodating $2.4x10^6$ interaction tests/second conducting a least-squares multiple regression model and t-tests with *n*-4 (df) (see Kam-Thong et al., 2012).

Multiple Functional Regression Model (MFRG) conducts a candidate search for 2-way interactions associated with *several* quantitative phenotypes denoted as the circumstance of pleiotropy. To do so, MFRG selects a subset of SNPs based on genomic

position and functional principal component analysis (fPCA), the output of which is used as model predictors in a classical multivariate regression by eigenfunction expansions (see Zhang, Xie, Liang, & Xiong, 2016).

GPU implementation of BOOST (GBOOST) is an epistatic detection algorithm based on pairing Boolean Operation-based screening and testing (BOOST) algorithm with graphic processing units. The original algorithm BOOST stores genotypic input in bitwise operations to construct *2* x *3* (group x variant) contingency tables for space and computational efficiency (see Wan, Yang, Yang, Xue, Fan, Tang, & Yu, 2010). Next, BOOST conducts a two-step procedure, which begins by approximating the likelihood ratio test-statistic[57] for each SNP pair and then applies an upper-bound threshold to 'prune statistically insignificant interactions' (Wang, Lui, Feng, & Wong, 2012). The second stage is the test phase. Herein, BOOST conducts 2-way interaction tests using the classical likelihood-ratio to test for statistically significant interactions (Yung et al., 2011; Chen & Gou, 2013; Niel, Sinoquet, Dina, & Rocheleau, 2015).

Penalized regression methods include *Least Absolute Shrinkage and Selection Operator* (LASSO) (Tibshirani, 1996) and *Smoothly Clipped Absolute Deviation* (SCAD) (Fan & Li, 2001). Both LASSO and SCAD employ convex optimization to minimize the penalized residual sum of squares by constraining the size of regression coefficients (β) via a tuning parameter (λ). In doing so, by adding a regularization term to be minimized, $\lambda \sum_k \beta_k$ the solution reduces the variance between estimates and their true value (Agresti, 2015). As such, penalized regression methods produce a sequence of models that vary in complexity based on the selection of λ. For model selection, scoring validation, cross-validation, or optimization fit criteria are employed to estimate the lowest prediction error. However, on their own, LASSO and SCAD are not scalable and are reported to inflate false discovery rates with high susceptibility to noise (Niel, Sinoquet, Dina, & Rocheleau, 2015). To ameliorate these effects, stability selection methods are applied to LASSO (sLASSO) and SCAD (sSCAD) algorithms, removing the requirement of cross-validation, and instead bootstrap to randomly sample without replacement from the original data set (Gou et al., 2014).

[57] Tests the deviance between the full versus reduced logistic regression model, and is respectively analogous to the log-linear saturated association and log-linear homogenous association models (Agresti, 2002; as cited by Wang et al., 2012).

3.2.2. Data Mining and Machine Learning Algorithms

In general, data mining and machine learning data processors are a family of computer algorithms designed to extract patterns, anomalies, and dependencies from large data structures, by the respective means of automatic/semi-automatic procedures[58], and learning algorithms[59].

Data mining and machine learning processors step through the space of all *potential* models in a computationally efficient manner. Technical variations between detectors rest on the types of algorithms employed for *attribute* identification and classification (*i.e., feature-selection*, *optimization algorithms*), parameter tuning, model prediction, and fit (i.e., *cross-validati*on, *permutation*, hybrid-methods) (see McKinney, Reif, Ritchie, & Moore, 2006; Cordell, 2009). As we will see, data processors of this class implicitly test of epistatic effects by identifying *dependencies* between attributes which improve model prediction: 1) tree-based classifiers (Jiang, Tang, Wu, & Fu, 2009; Yoshida & Koike, 2011; Wei & Lu, 2014; Basu, Kumbier, Brown, Yu, 2018); 2) clustering algorithms (Zhang, Huang, Zou, & Wang, 2010); 3) linear models (Gao et al., 2014; Park & Hastie, 2008; Wu et al., 2009); and 4) association rules (Wan et al., 2009; Wan et al., 2010).

Epistatic Detectors - Data Mining and Machine Learning

To explore data mining and machine learning detection algorithms available to the empirical scientist, we briefly summarize six detectors: 1) *Tree-based epistasis association mapping* (TEAM); 2) *Cellular automata (*CA); 3) *Random Forests* (RF); 4) *Multi-Factor Dimension Reduction* (MDRD); 5) *ReliefF; 6) Ant-colony optimization* (ACO).

Tree-based epistasis association mapping (TEAM) is a data-mining algorithm, which conducts an exhaustive search for pairwise interactions between SNPs and a disease trait (Zhang et al., 2010). The algorithm inputs a vector of all SNPs and phenotype permutations and approximates a set of double looped minimum spanning trees (MST), where single SNPs (nodes) and weighted SNP pairs[60] (undirected edges) are modelled to

---

[58] (I.e., cluster analysis, association rules, and sequential pattern mining).

[59] In which a program modifies its execution from experience in a *supervised* or *unsupervised* fashion.

[60] The weights for each edge represented by the number of individuals having different genotypes. For an individual genotype differences from two SNPs can be one of six combinations. 0 →1

maximize the computation of contingency tables (Wang et al., 2011). TEAM incrementally updates the observed frequencies in the contingency tables and uses permutation tests to derive a cut-off p-value threshold (Zhang et al., 2010; 2011). TEAM supports both homozygous and heterozygous data and applies to all statistical tests which employ contingency tables (I.e., χ^2, Exact likelihood ratio tests) (McKinney et al., 2006).

*Cellular automata (*CA) is a discrete dynamic state machine learning algorithm employed to simulate and classify real-world dynamic systems (see for e.g., von Neumann, 1951; Wolfram, 2002). CA employs a spatial structure (i.e., an array or grid of cells of any finite dimension), in which the local interaction of a single cell (atoms) and its local neighborhood is modelled by a finite number of states[61] (Wolfram, 2002). A state change occurs in parallel at discrete time steps, either as a change of location or state of the cell in accordance to the rule table, the current state of the cell, and the state of its local neighbourhood (see Wolfram, 1983; Moore & Hahn, 2002). The algorithm uses pattern recognition to build a model that classifies and predicts disease status based on an array of input genotypes (Moore & Hahn, 2002). As an epistatic detector, Moore and Hahn (2002) employed CA along with the parallel *Genetic Algorithm* (GA)[62] for both parameter selection and optimization[63]. CA predictive model aims to identify combinations of SNPs, which interact to influence the global state of disease risk through nearest-neighbour interactions. These predictive models are generated based on cross-validation. Once a predictive model is selected, the null hypothesis of no association is tested using permutations (Moore & Hahn, 2002; McKinney et al., 2009). The benefits of CA include that it is non-parametric and does not require specifications of the disease mode of inheritance. CA also minimizes false positives due to multiple-testing and has the potential to analyze high-dimensional non-linear interactions between SNP markers (see Moore & Hahn, 2002).

(indicating the genotype for each locus),1→ 0, 0→ 2, 2 →0, 1→ 2, 2 →1. Such that the genotype differences connecting two SNPs in the minimum spanning tree (see Zhang et al., 2010).

[61] The state of a cell is a set of discrete characteristics (i.e., gender, political affiliation, location) (Wolfram, 2002).

[62] Genetic Algorithm employs parallel or beam search to generate at random solutions to a particular problem. These solutions are evaluated based on their ability to solve the problem (fitness). The models with the highest fitness undergo exchanges of random model pieces generating variability in the solutions and another phase of model evaluation. The afore noted cycle is re-iterated until the identification of an optimal solution (Moore & Hahn, 2002).

[63] This includes: 1) initiation of CA cell states with the correct combination of genetic variation; 2) an appropriate rule table which specifies the information processing; 3) the number of iterations.

Random Forests (RF) is a machine learning, model-free algorithm for classifying attributes based on aggregative voting of decision-trees[64] (Cordell, 2009). Within the context of GWAS data, RF algorithms use categorical genotypic data as classifiers to discriminate between case and controls and to obtain SNP marker importance. As such, a collection of decision tree classifiers is trained (number specified by user) based on drawing equal-sized bootstrap samples from the original dataset; each sample produces an unpruned classification tree, with a random subset of predictor variables (McKinney et al., 2006; Cordell, 2009). Each tree is constructed using *recursive partitioning* and is a graphical structure, mapping possible values of the predictor variable to its outcome (conducted using a combination of values taken by the predictor variable to reach the binary disease state) (Cordell, 2009). However, RF conditions on main-effects and does not permit a pure test of interaction, testing instead, for the association between SNPs and *allows for a potential interaction* (Cordell, 2009)[65]. RF has strong predictive performance when composed of individually strong and uncorrelated classifier trees (McKinney et al., 2006). Based on the predictions of an array of classification trees, predictor variables are ranked and used in a regression-based search (Cordell, 2009). Estimation of prediction errors, and variable importance[66] are conducted by comparing training data and permutation (Cordell, 2009). Examples of random forest detection algorithms to select marker and tests for interaction include *EpiForest* (Jiang, Tang, Wu, & Fu, 2009), *SNPInterforest* (Yoshida & Koike, 2011), *GWGGI* (Wei & Lu, 2014), and *Iterative Random Forests* (Basu, Kumbier, Brown, Yu, 2018).

EpiForest (Jiang, Tang, Wu, & Fu, 2009), employ an RF algorithm, sliding windows, and sequential forward-selection algorithm to select a subset of SNPs that minimize classification error. Interactions enumerated between the sub-set of SNP markers are conducted, followed by a test for statistical significance for 2-3-way

---

[64] Decision trees classifies samples based on a path of decision points (determining based on a rule, which branch to take, based on one of the features of the sample). The path typically ends at the end or a branch or a leaf, which has a class label (Denisko & Hoffman, 2018).

[65] The test of association while allowing for interaction is analogous to comparing the fit of a linear model with main and interaction effects of both loci, with a model in which all terms involving the second are removed (Cordell, 2009). To this end, the joint test of the association is 'less powerful' than a single locus association test if epistasis is not present (see Cordell, 2009).

[66] Gini importance or mean decrease impurity (MDI) is the average of a variables total decrease in node impurity (weighted by the probability of reaching a particular node), averaged over all trees in the ensemble. Higher the MDI, the higher the variable importance. Gini impurity is a metric regarding the probability of incorrect classification at a given node in a decision tree based on training data.

interactions using a B statistic[67] (see Zhang & Liu, 2007). *SNPInferforest* accommodates SNPs with both large and small marginal effects and identifies possible interactions as a branch[68] on the decision tree. SNPInterforest quantifies interaction strength as a score based on the frequency of SNP combinations in a forest normed by a baseline level[69] (Yoshida & Koike, 2011). As such, a detection threshold of the normalized scores is empirically determined above 25 standard deviations (Yoshida & Koike, 2011). Conversely, *GWGGI* replaces the standard variable selection with a feature-selection forward algorithm to detect joint and higher-order association of SNP markers with the disease. Selected SNP markers are tested for interaction using a likelihood ratio and Mann-Whitney statistic (Wei & Lu, 2014; Niel, Sinoquet, Dina, & Rocheleau, 2015). Finally, *Iterative Random Forests* (Basu, Kumbier, Brown, Yu, 2018), tests for p-way interactions through iteratively refining a weighted random-forest, employing bootstrap selection, and a random-intersection tree algorithm to find subsets of SNPs. The co-occurrence of particular subsets over each iteration signifies a potential interaction that is assessed with a stability score[70] (Denisko & Hoffman, 2018).

Multi-Factor Dimension Reduction (MDRD) is an exhaustive search data-mining algorithm, designed to identify combinations of genetic variants associated with *increased risk* of a multi-factorial common complex disease (see Ritchie et al., 2001; McKinney et al., 2006). Designed to consider every possible combination, MDRD pools N-genetic factors into cells within N-dimensional space, each labeled *high risk* or *low risk* based on a threshold[71] or the ratio of case vs controls within each cell (McKinney et al., 2006; Cordell, 2009). By reducing genetic factors from an N-dimensional contingency table to one dimension, each constructed attribute is a combination of factors (or genetic

---

[67] For L one-way tests, the B statistic tests every candidate SNP and reports all SNPs whose p-values are less than α following Bonferroni corrections. Two-way interaction tests use the B or a *conditional B* statistic and Bonferroni correction for L(L-1)/2 tests. This depends on the: 1) absence (e.g., no marginal effects = B statistic); 2) presence (e.g., both have marginal effects = no test for interaction); 3) or partial presence (e.g., only one SNP of the pair has a marginal effect = conditional B statistic)). Similarly, in the three-way tests, a B or conditional B statistic is applied to all three-way interactions with Bonferroni corrections for L(L-1) (L-2)/6 tests.

[68] A branch is a path from the root node (comprises of 1-2 SNP markers) to a leaf node and indicates a possible interaction amongst SNPs on that branch.

[69] The baseline level is the expected number of simultaneous appearances under the null hypothesis (of no SNP interactions).

[70] The stability score is based on averaging over all bootstrapped selections and describes the fraction of times an interaction occurs. Scores equal to or greater than 0.5 are considered indicative of stable interactions.

[71] T=1.0, high risk > T, low risk <T.

variants) (McKinney et al., 2006; Cordell, 2009; Zeigler, König, & Pahlke, 2010; Evans et al., 2011). Model evaluation and accuracy are respectively conducted using a *naive Bayes classifier*, the prediction of group status (case or control), and cross-validation (McKinney et al., 2006; Cordell, 2009). *cuGWAM*, is one algorithm that applies MDRD using a GPU environment, which scales well with sample size and the number of markers.

ReliefF is a scalable feature-selection filtering algorithm, which detects dependencies between SNP markers (Cordell, 2009). Herein, the nearest-neighbor algorithm selects two attributes and calculates the proximity based on the Manhattan distance. Each neighboring attribute is scored positively or negatively based on their classification as either being in the same or different phenotypic class, and a weight is assigned accordingly. Herein, when the class value differs between pairs, the SNP feature score increases. Whereas, when the class value is the same, the SNP feature score decreases. As such, the SNP score serves as a quality estimate indicating whether or not the marker is involved in the interaction (Cordell, 2009; McKinney et al., 2006). Derivatives of ReliefF include: i) *Regression ReliefF* (RReliefF) – which conducts attribute estimation using regression models (Robnik-Šikonja, & Kononenko, 1997); ii) *Tuned ReliefF* (TuRF) - which utilizes recursive elimination of features and an iterative application of ReliefF to ameliorate noise in large search spaces (Moore & White, 2007; Niel, Sinoquet, Dina, & Rocheleau, 2015); iii) and methods generalizable to multi-class (Kononenko, 1994), and continuous data (Robnik-Šikonja, & Kononenko, 1997).

Ant-colony optimization (ACO) is a machine learning algorithm, which employs a heuristic-search method for disease traits. In this algorithm, an "ant" is a set of SNPs, drawn according to a probability density function. The probability of selecting an SNP is due to its "pheromone concentration"[72]. Following set selection, the algorithm employs a test of joint association between the SNP and the trait using a χ^2. If the test has a $\chi^2 > \tau$, where τ is a particular threshold, the PDF will be updated, and the process restarts. Examples of ACO algorithms include *AntEpiSeeker* (Wang, Robbins, & Rekaya, 2010)), *epiACO* (Sun, Shang, Liu, Li, Zeng, 2017), and *AntMiner* (Shang, Zhang, Lei, Zheng, Chen, 2012). *AntEpiSeeker* (Wang et al., 2010) is a candidate search design, which conducts a parallel search for multiple groups of SNPs associated with a disease trait. The algorithm requires specifications such as the number of iterations, order of

[72] Pheromone concentration depends on the significance level of previous interactions between both the selected set of SNPs and expert knowledge.

interactions, number of SNP in each set, and evaporation rate of pheromones (Niel, Sinoquet, Dina, & Rocheleau, 2015). *epiACO* tests for 'interactions' between SNP combinations and a phenotype based on an *S*-value or fitness function[73]. Here, sets of SNPs are selected using probabilistic and stochastic path-selection while retaining and comparing solutions from previous iterations in the generation of new candidate SNPs (Sun, Shang, Liu, Li, Zeng, 2017). Finally, *AntMiner* (Shang et al., 2012) is a generalized version of AntEpiSeeker, by utilizing ant-decision rules and heuristic search to detect epistatic interactions.

3.2.3. Bayesian Model Selection

Broadly, Bayesian model selection technologies are a range of data processing algorithms (i.e., general linear models (GLM), network learning, and graph theory) employed under the framework of *Bayesian inference*. Herein, the Bayesian inferential approach rests on the assumption that the empirical scientist can describe their *degree* of belief apriori regarding possible parameter values and update this belief following a set of empirical observations (see Silvey, 1975; Kruscheke, 2011; Morey & Rouder, 2011; Kaplan & Depaoli, 2013). In particular, in the empirical setting, one specifies the probability model of all model parameters, and upon stationarity and convergence of the simulated conditional posterior distribution, tests model sensitivity and fit (see Gelman, Carlin, Stern & Rubin, 2014). While summary statistics, posterior intervals, and probabilities from the posterior distribution supplement model interpretation. In the context of hypothesis testing, one may generate and report the posterior probabilities for each hypothesis (rather than employing a criterion set forth to make a binary decision) (Silvey, 1975); or construct a *Bayes Factor* (BF) to summarize the evidence in favour of one statistical model over another (see Kass & Raftery, 1995; Morey & Rouder, 2011). In the context of epistasis detection, as we will see, *Bayesian model selection* detectors employ both implicit and explicit tests for epistastic effects.

Epistatic Detection - Bayesian Model Selection Algorithms

To explore further the nature of Bayesian epistatic detectors, we review four epistatic detection algorithms: 1) *Bayesian Epistasis Association Mapping* (BEAM) (Zhang

[73] Based on information theory and probability theory, the mutual information (MI) between two random variables is a measure of mutual dependence and is typically used in feature selection algorithms (see Sun et al., 2017).

& Liu, 2007); 2) *Epistatic Interaction Detection using Bayesian Network (*EpiBN) (Han, Chen, Talebizaeh, & Xu, 2012); 3) *Detection of Associations, vis-a-vis, Markov Blanket (*Dasso-MB*)* (Han, Park, & Chen, 2010); 4) *Hybrid Bayesian Model Selection* (Yi, Yandell, Churchill, Allison, Eisen, & Pomp, 2005; Yi, Kaklamani, and Pasche, 2012).

Bayesian Epistasis Association Mapping (BEAM) (Zhang and Liu, 2007) identifies single and pairwise associations between genetic loci for quantitative and disease traits in case-control studies. The algorithm tests for 'interaction' based on the between-group difference between inter-locus genotype frequency distributions (Wei, Hemani, & Haley,2012). Sets of SNPs are discretely categorized based on their relationship with the trait: SNPs un-associated to the trait = 0; SNPs with a main effect = 1; and SNPs with pair-wise association = 2. The assignment of SNP markers to each distribution is based on a sampling from the posterior distribution using Markov Chain Monte Carlo (MCMC) sampler and the specification of Dirichlet priors for each group. Computational speed is contingent on both MCMC iteration and sample size, ~ 2-8 minutes for 250,000-100,000 MCMC iterations (Zhang & Liu, 2007). BEAM is a hybrid algorithm conducting a classical statistical significance test for associations between a marker(s) and the disease phenotype by implementing a B-test statistic[74] (Zhang & Liu, 2007).

*Epistatic Interaction Detection using Bayesian Network (*EpiBN) (Han et al., 2012) is a model selection algorithm, which employs both MCMC and a Bayesian score-and-search algorithm to select candidate SNPs and epistatic effects. EpiBN algorithm assumes SNPs are causal genetic variants and graphically depicts the main or interaction effects of SNPs to a trait using the branch-and-bound iterative score and search procedure. Each iteration adds, reverses, or deletes an edge (i.e., interaction) to produce a network structure, which best fits the observed data. The network structure is scored, such that the highest score (EpiScore)[75] is considered the *best fit* between the network structure and the observable data (Han et al., 2012).

[74] $B_M = ln\frac{P_A(D_M, U_M)}{P_0(D_M, U_M)}$; where D_M and U_M denote the genotype data for M in cases and controls, and the numerator and denominator are the Bayes Factor, or marginal probabilities of the data for each hypothesis (Zhang & Liu, 2007). Under the null hypothesis, the B test statistic has an asymptotic χ^2 distribution.

[75] See Han and colleagues (2012) for further details. The epistatic scoring function proposed by the authors is essentially the AIC scoring function, with the substitution of the variance of the G^2 distribution with the true variance of G^2 from the data (where G^2 refers to the test of independence or conditional independence of two variates for discrete variables).

*Detection of Associations using Markov Blanket (*Dasso-MB*)* (Han, Park, & Chen, 2010) employs a *Markov-blanket* variable selection algorithm to detect epistasis. The variable selection algorithm generates, for some variable, a set of variates with the minimal number of either 'direct' or 'conditional effects' to the trait. Forward and backward phases iteratively build a candidate Markov blanket by respectively adding new SNPs under the condition they pass a user-defined threshold of dependency[76] and removing false positives from the model using conditional independence tests[77].

Hybrid Bayesian Model Selection is a detection framework that implements both Bayesian inference and GLM to the task of detecting epistatic effects. Naturally, specification of prior distributions, simulation methods (i.e., MCMC), posterior inference/analysis (i.e., *EM algorithm* (Yi, Kaklamani, and Pasche, 2012), *Bayesian model averaging* and Bayes factors (Yi, Yandell, Churchill, Allison, Eisen, & Pomp, 2005)) effectuate variability in model execution; however, pairing Bayesian inference with GLM permits explicit tests for interaction, considers marginal effects, covariates, and gene-environment interactions while boasting improvements in test power and scalability (see Hoeting, Madigan, Raferty, & Volinsky, 1999; Wei, Hemani, & Haley, 2014).

3.3. Epistasis Detector Pitfalls

While the number of sophisticated epistatic detection technologies has proliferated over the course of several years, there exists, however, a growing disparity between the observed and expected rate[78] in the detection of robust[79] epistatic effects in complex traits for human populations. As such, our aim in this section is to consider a series of limitations in the technical treatment of epistatic detection, categorized as those: 1) general to epistatic detection[80]; 2) bespoke to each data-processing category; and 3) broadly of the quantitative, theoretical and biological sort.

---

[76] Here the dependency threshold is an observed value of a G^2 statistic (log-likelihood test statistic for a multi-nominal model).

[77] SNPs are removed if they are independent of the phenotype given other SNPs within the set (Han, Park, & Chen, 2010).

[78] Given its ubiquitous role for model organisms.

[79] Recall from Chapter 2, robust epistasis refers to scale-invariant interaction effects between the same genetic loci, replicated independently.

[80] See the Introduction and Cordell (2009) for further details.

Regarding the former, there are several areas of confusion in the technical treatment of epistatic detection, originating perhaps in the various working definitions propagated between several academic fields - natural extensions of this sort are manifest in several incongruencies: 1) the definition(s) of epistasis; 2) implementation of explicit and implicit tests for its' effects; and 3) the notable absence of a standardized effect size metric *across* detection technologies, which in aggregate, regrettably leaves both parametric detectors and their non-parametric associates lost in translation.

Of the second, there are numerous technical limitations bespoke to each data-processing methodology the empirical scientist must navigate. In the case of parametric regression, while linear and logarithmic regression technologies generate and evaluate an optimal composite of $\overrightarrow{X}$ to predict Z, incongruences exist between the inferential goals of epistatic detection and its' technical realities. One such incongruence is the inability for linear regression technologies to identify important predictors and a subset of predictors whose population-level effects are *purely* epistatic[81]. Owing to the orthogonal decomposition of Z into two vector-subspaces model and null[82] – one cannot ascertain variant importance vis-à-vis partitioning R^2_{ZX} into the sum of $s + m$ orthogonal subspaces or compare the magnitudes of the partial β coefficient weights, as their transformed[83] and conditional nature[84] relays very little information regarding the real-world importance of a particular variant on trait variation (Pedhauz,1997). Similarly, while one may compare saturated (*epistatic*) versus reduced (*additive*) linear models, the proportion of variance explained by the $\binom{s}{r}$ conditional impacts (should an epistatic model be consonant with nature) remains unknown. Reasonably, it is the case one could test a series of pairwise contrasts to aid in the resolution of whether there exists a linear or non-linear function between a set of predictors 'important' to trait variation. However,

---

[81] Models of epistasis in the absence of main or marginal effects.

[82] Z is decomposed into a model space: $C(\mathbf{A}) = \{\eta: \vec{\theta}, \text{ such that } \eta = \boldsymbol{A}\vec{\theta}\}$, spanned by the columns of the model matrix $\mathbf{A}$; and its orthogonal complement $C(\boldsymbol{A})^{\perp}$ the null space of $\mathbf{A}^{\mathbf{T}}$, denoted as $N(\mathbf{A})$: which contains the differences between possible data vectors and model-fitted values. Of course, $\text{Dim}[C(\mathbf{A})]+\text{Dim}[N(\boldsymbol{A})] = s$.

[83] The residual of the predictor after it is projected into the span of the remaining predictors.

[84] Non-orthogonal by design the weights of a partial coefficient (the average number of standard deviations change in Z associated with a 1-standard deviation increase in a predictor while holding the remaining predictors constant) are both transformed and conditional on the other predictors in the model. As such, comparing predictor weights relays very little information regarding the real-world importance of a particular variant on trait variation. For example, a predictor may be strongly related to Z but have a small β coefficient weight.

given this test scenario effectuates several companions (i.e., the requirement for FWER control, data sparsity, and high model complexity), which regrettably inflate P(Type I error)[85], plummet statistical power P(1-Type II error), and bias $R^2_{\hat{x}Z}$ (see Agresti, 1990; Evans, 2011; Wei, Hemani, & Haley, 2012; Cordell, 2009; Zeigler, König, & Pahlke, 2010). Furthermore, departures of the empirical data-structure from the parametric assumptions[86] required for the majority of parametric test procedures opens the metaphorical door to several non-parametric alternatives including data mining and machine-learning detection algorithms.

While both data mining and machine learning algorithms are capable of implicitly testing for the presence of all m-way 'interactions' within high-dimensional data structures, they too remain sensitive to collinearity amongst predictors, incomplete and unbalanced datasets (McKinney et al., 2006; Cordell, 2009). Furthermore, the aforesaid algorithms often lack generalizability and interpretability as both are stymied by unavoidable computational challenges in test-scalability[87], reliance on user-specified thresholds as evidence of model significance, and the potential for over-fitting requiring further independent replication. In the absence of a universal framework to determine the model significance or quantify the magnitude of an epistatic effect, data mining and machine learning algorithms remain without sound comparability between both frequentist and Bayesian detectors.

While Bayesian model selection methods provide novelty and flexibility to epistatic detection, they remain at the whim of several technical issues: 1) user-specifications in the selection of its probability model and prior distributions; 2) user-

[85] Specifically, under consideration of pairwise association, the χ^2 test-statistic has a poor approximation of *the* χ^2distribution when selected SNP markers have a high single-locus association to the trait of interest (Agresti, 1990). There is an increase in P(Type I error) when testing model fit between the regression of reduced versus saturated models due to test dependencies (Wei, Hemani, & Haley, 2012). As such, potential dependencies between each independence-test, coupled with the risk of inflated or artificially induced pairwise association due to limits of the asymptotic approximation of the χ^2, are potential sources of error (Wei, Hemani, & Haley, 2012; Gouley, 2005).

[86] Presence of multivariate normality; linear independence such that **A**=full rank and $(\mathbf{A'A})^{-1}$ is identifiable; absence of outliers and influential points; homoscedasticity.

[87] RF algorithms computational challenges emerge to ensure that two SNPs jointly selected are present in a sufficient number of trees (Zeigler, Zonig, & Thompson, 2008). Authors report that for a single detection of a 2-way interaction, the same two SNPs must occur in the same tree $2x10^6$, so at least 500,000 trees (700 SNPs per tree) must be grown to ensure interaction representation.

directed diagnostics[88] for model evaluation, sensitivity, and fit; 3) high computational costs required to generate posterior simulations and BF for complex hypothesis tests; and 4) the unfortunate fact BF remain without a consensus on the threshold indicative of model significance (Kass & Raftery, 1995; Zeigler, Zonig, & Thompson, 2008). To this end, it is clear that the vast majority of epistatic detectors reduce un-problematically to an exercise of model-fitting, suggesting the field remains *without* a theoretical basis for epistatic detection.

Lastly, there exist several pitfalls of the quantitative, theoretical, and biological sort an empirical scientist will inevitably confront when undertaking the task of epistatic detection. First, an obscure relationship exists between epistasis and its population-level effect, as there does not exist a predictable relationship between the fact of a particular extant genetic architecture having the property of epistasis and the *magnitude* of σ^2_{EP}. This is not surprising, as the quantity σ^2_{EP} is governed in part by the φ_j, j=1..n (i.e., the proportion of alleles of the second type at each locus), and captures the sum of all interaction effects.

Second, there exist several sources of noise common to the *process* of genomic data-extraction, its' experimental execution, and the nature of genetic architecture, each of which has the potential to obscure and mimic a *true* epistatic signal, should an architecture with the property of epistasis exist. Of the former, tests for epistatic effects are sensitive to genotyping errors due to *batch-effects, the differential bias* in *genotype calling*, low sequencing density, and genomic data extraction process, which impact the quality of genomic sequencing data (Lui et al., 2001; Zeigler, Konig, & Thompson, 2008; Lee et al., 2010). Furthermore, GWAS are riddled with examples of either loosely applied overarching hypotheses that 'a particular trait or pathology has a genetic etiology', or a series of a-posteriori hypotheses postulated from groups independent of those who designed the study and implemented genomic data extraction (Lambert, 2012). To this end, while the former may be ameliorated with improvements in sequencing depth, sample extraction, and post-processing methods (i.e.,. *quality control* and *imputation*), deviations in the processing of genomic data and experimental execution across

[88] Diagnostic tests include:1) chain mixing, convergence, and stationarity; 2) serial dependencies and evidence of an adequate burn-in period for posterior simulations. As such, typical diagnostics include Gelman-Rubin Diagnostics, Geweke, Heidelberger-Welch stationarity, and half-width test, as well as visual inspection of autocorrelation and trace plots (see Gelman, Carlin, Stern, & Rubin, 2004)

empirical studies may obscure the sound detection and replication of epistatic effects, independent of the actual test performance of epistatic detectors (see Lambert, 2012).

Of the latter, there are several sources of structural dependencies between loci, independent of epistasis, engendered by features of genetic architecture such as *linkage disequilibrium* (LD), *haplotype* effects, and *population stratification*. LD refers to the co-inheritance of alleles at distinct genetic loci at a higher rate than expected under independent segregation in a population – its etiology is proposed to stem from population and demographic dynamics, such as population structure and growth[89], genetic drift[90], admixture or migration[91], natural selection[92], variable rates of recombination[93] ,mutation[94], gene conversion[95], and pleiotropy[96] (see Ardlie, Kruglyak, & Seielstad, 2002). Accordingly, following a novel mutation, over each generation recombination changes the sequence of alleles (and thus the spatial proximity of haplotypes neighboring a variant). To this end, while the effect of LD is typically due to

---

89 Rapid population growth decreases LD and reduces genetic drift (Ardlie, Kruglyak, & Seielstad, 2002).

90 Genetic drift refers to generational changes in gene and haplotype frequencies in a population of a finite number of offspring due to the random sampling of gametes. As frequency changes are accentuated in small populations, genetic drift of small stable populations tends to increase LD as haplotypes are lost from the population (Ardlie, Kruglyak, & Seielstad, 2002).

91 Admixture and migration refer to gene flow between populations, which produces spurious LD. In this situation, LD is proportional to the differences in allele frequency between populations and remains unrelated to the distance between markers. However, following subsequent generations, spurious LD, which is generated between unlinked markers quickly disappears, while LD between nearby markers is slowly broken down by recombination events (Ardlie, Kruglyak, & Seielstad, 2002).

92 The phenomenon of natural selection affects the extent of disequilibrium based on either: 1) hitchhiking effect – an entire haplotype which flanks a favored variant is rapidly swept to high frequency or fixation. Or selection against deleterious variants inflate LD, as the deleterious haplotypes are removed from the population; 2) epistatic selection – the combinations of alleles at two or more loci on the same chromosome leads to the association of particular alleles at different loci (studied in drosophila, but not yet been shown to alter LD in humans)(Ardlie, Kruglyak, & Seielstad, 2002).

93 As recombination events break down LD and are variable across the genome, the extent of LD is expected to inversely vary with local recombination rates. To this end, LD may be strong across the non-recombining regions and break down at particular hot spots (Ardlie, Kruglyak, & Seielstad, 2002).

94 Single-nucleotide polymorphisms characterized by CpG dinucleotides are thought to have high mutation rates with little or no LD to markers, even in the absence of historical recombination (Ardlie, Kruglyak, & Seielstad, 2002).

95 Gene conversion refers to the phenomena during meiosis wherein a short stretch of the copied chromosome transfers to the other copy- yielding an effect of two very closely spaced recombination events, which can break down LD like recombination or recurrent mutation. Recently, the rates of gene conversion in humans are reportedly high and important in LD between very tightly linked markers (Ardlie, Kruglyak, & Seielstad, 2002).

96 Pleiotropy is the phenomenon in which a genetic factor influence more then one phenotypic trait outcome.

spatial proximity of two loci, LD may also occur between loci on different chromosomes due to selection or population stratification (Zeigler, Zonig, & Thompson, 2008). While the structure of LD is characterized within model organisms; however, less is known about LD structure in humans, perhaps owing to the variability in the rate of LD decay[97], pattern and proportion of LD between ethnic groups, and regional variability[98] between both local and distal polymorphisms (see Ardlie, Kruglyak, & Seielstad, 2002). While high LD (r^2=.8)[99] and a low rate of decay[100] are required in GWAS designs between a *casual variant* and a *tag SNP marker* to capture common variation in the genome, several corollary relationships exist. Firstly, the proportion of variance explained by a *tag* SNP is *smaller* than the variance explained by a *true* causal variant. As such, the rate of decay in LD between a genetic effect and a observed marker is linear (r^2) for the detection of additive effects; r^4 for dominance effects; r^4 for *additive x additive*; r^6 for *additive x*

---

[97] LD decay is a function of the number of generations of random mating (t), and recombination distance (r) of the loci: $D_t = D_0(1 - r)t$. Here D_t is the amount of remaining LD between two loci after *t* generations of random mating, and D_o is the original LD (Zhu, Gore, Buckler, & Yu, 2004). Genome-wide LD is presented graphically as a decay plot of estimated D' or r^2 over distance or physical linear arrangement of LD between polymorphic sites within a gene or loci along a chromosome.

[98] Regional variability in LD due to gene conversion or differences in allele frequency also present issues in quantifying or comparing populations based on an *average* level of LD. As even a region with high LD, may have some pairs of loci will not show levels of LD (Ardlie, Kruglyak, & Seielstad, 2002).

[99] Quantified as the dependence of two genetic loci (metrics of LD include D (Lewontin, 1964), normalized *D'* (Lewontin, 1964), and r^2 (Hill and Robertson, 1968)). D quantifies the difference between observed haplotype frequencies and expected allele frequencies under random segregation (Ardlie,2002). Here the expected haplotype frequency = allele frequency of both alleles (PAPB) – as such normalized D' is often used for interpretability and is rescaled to take into account cell count. $D'_{AB} = \begin{cases} \frac{D_{AB}}{\max(-pApB,-papb)}, if\ D_{AB} < 0 \\ \frac{D_{AB}}{\min(papB,pApb)}, \quad if\ D_{AB} > 0 \end{cases}$ (Zhu, Gore, Buckler, & Yu, 2004).

While values of D'<1 suggest disrupted ancestral LD, the relative magnitude of values of D' has no clear interpretation (Ardlie, 2002). $r^2 = \frac{D2}{P(A)P(B)P(a)P(b)} = \frac{\chi_1^2}{N}$, or the squared Pearson product-moment correlation, with an expectation of $\frac{1}{1+4Nc}$; (N is the population size, and c is the recombination rate) (Hill and Robertson, 1987; as cited by Zhu, Gore, Buckler, & Yu, 2004). D=1, suggests "complete LD"; and r^2= 1 suggests perfect LD. Wherein the former refers to the circumstance where three out of the four possible haplotypes in the population, two loci are not separated by recombination. The latter refers to a state where two of the four possible haplotypes have the same allele frequencies.

[100] High LD decay suggests a shorter distance of LD, which provides higher mapping resolution, and requires a large number of markers (Zhu, Gore, Buckler, & Yu, 2004). Additionally, LD decay (r^2=0.1, 0.2) has an impact on the mapping resolution and marker density in which higher LD decay results in lower mapping resolution and requires increased marker density; while lower LD decay permits increased mapping resolution and requires lower marker density (Ardlie, Kruglyak, & Seielstad, 2002).

dominance; and r^8 for *dominance x dominance* epistatic effects[101] (Wei, Hemani, & Haley, 2014). Secondly, the presence of unknown structural dependencies *between* tag SNP markers or a *pair* of SNP markers with an *unknown or unlinked* causal variant serves as potential sources of spurious associations. Akin to LD structure, the impact of haplotype effects due to the co-inheritance of a *group* of genes, *combination* of alleles, or *cluster* of SNPs from a *single parent* has the potential to yield structural dependencies, which inflate test-statistics in a pairwise scan (Wei, Hemani, & Haley, 2014; Zeigler, Konig, & Thompson, 2004). Comparably, owing perhaps to Simpson's paradox, another source of structural dependency which mimics the effect of epistasis and inflates P(Type I error) is population stratification or population substructure (Zeigler, Konig, & Thompson, 2004). Here *shared ancestry* between cases (rather than genes associated with disease) accounts for systemic differences in allele frequencies between cases and controls, requiring its' effects deemed negligible or statistically adjusted for[102] before the investigation of single locus or epistatic effects (Pearl, 2013; Zeigler, Konig, & Thompson, 2004). While the implementation of higher sequencing density and modeling covariates using permutation, GLM, or fine-fit mapping techniques[103] to identify and ameliorate sources of spurious association (Wei, Hemani, & Haley, 2014). It is clear that the deconvolution of empirical and biological artifacts from epistatic signal *if* an architecture with the property of epistasis is indeed present, remains an ongoing challenge. As such, in light of the aforenamed pitfalls, it is apparent that the adjudication of epistatic detectors based on empirical data alone remains problematic at best, as the true engendering architecture (and its constituent parts) extant in nature remain at all times *unknown* to the researcher.

---

[101] As such, the coverage of the genome is greater when searching for additive effects versus interaction effects (Wei, Hemani, & Haley, 2014).

[102] When geological information is available stratified analysis are typically employed. However, in its' absence, procedures such as genomic control (GC, Devlin and Roeder, 1999), structured association (Pritchard et al., 2000), and eigenstrat (Price et al., 2006) are typically used (see Zeigler, Konig, & Thompson, 2008).

[103] Fine-fit mapping refers to the sequencing of all variants in an associated region or dense coverage. Naturally, the ideal test scenario is one in which the two SNPs are not in LD with each other or with a third unobserved variant. Wei and colleagues (2014) suggest fitting fine-mapped additive SNPs as covariates with the interacting SNPs to evaluate SNP independence, in addition to ensuring that interacting SNPs have an LD $r^2 < 0.1$ between the causal variant and the observed SNP, and a normalized disequilibrium be $D' < 0.1$ to reduce the possibility of haplotypes effects.

Chapter 4. Epistasis and its Detection: Technical Foundations

Introduction

As demonstrated in Chapter 3, whatever sophistications are inherent to their technical details, in a broad stroke, an epistasis detector is simply a tool of detection and, accordingly, must answer to the logic of detection theory. It follows, then, that its success as a detector of epistasis will rest on a) the extent to which the class of objects the elements of which are its targets of detection is consonant with the normative definition of the concept epistasis and b) the inferential soundness of the detector itself. Our aim in this chapter is to lay forth in broad terms: 1) a technical definition of the property of epistasis and its engendering architecture; 2) the notion of genotype-specific epistatic effects; 3) and the technical foundations of the epistatic detection problem.

4.1. Definition of Epistasis Revisited

For s >1, recall that an architecture has the property of epistasis when, for at least 2 of the 3^S genotypes, $\boldsymbol{g}^*$,

$$\Psi'(\boldsymbol{g}^*) \neq \Psi'(\boldsymbol{g}^*)_{\text{Main.}} \tag{4.1}$$

In Chapter 2, $\Psi'(\boldsymbol{g}^*)_{\text{Main}}$ was defined as: $[\mu_{\Psi'(\boldsymbol{g})} + \sum \beta(\boldsymbol{g}_j^*) + \sum \delta(\boldsymbol{g}_j^*)]$. In preparation for the simulation studies to be undertaken, we now elucidate in a bit more detail, the nature of $\Psi'(\boldsymbol{g}^*)_{\text{Main}}$, and, in consequence, so too epistasis. To do so, we begin by defining: $\boldsymbol{g}_v$ to be the x 3^S element vector of genotypic values ($\Psi'(\boldsymbol{g}^*)$); **D**, the 3^Sx 3^S diagonal matrix, the elements of which are the probabilities $P(\boldsymbol{g}^*)$, in the same lexicographic order as $\boldsymbol{g}_v$; **A** to be the 3^Sx[1+3^S] design matrix; and $\mathbf{I_3}$ the [3x3] identity matrix. Examples of **A** include:

for s = 2,

$$\mathbf{A} = [\vec{1}_3 \otimes \vec{1}_3 : \mathbf{I_3} \otimes \vec{1}_3 : \vec{1}_3 \otimes \mathbf{I_3}] \tag{4.2}$$

$$= [\vec{1}_9 : \mathbf{A_1} : \mathbf{A_2}];$$

and for $s = 3$, (4.3)

$$\mathbf{A} = [\vec{1}_3 \otimes \vec{1}_3 \otimes \vec{1}_3 : \vec{1}_3 \otimes \vec{1}_3 \otimes \mathbf{I}_3 : \mathbf{I}_3 \otimes \vec{1}_3 \otimes \vec{1}_3 : \vec{1}_3 \otimes \mathbf{I}_3 \otimes \vec{1}_3]$$

$$= [\vec{1}_{27} : \mathbf{A_1} : \mathbf{A_2} : \mathbf{A_3}].$$

Let $\mathbf{A}^*$ be the reduced design matrix, with first column identical to $\mathbf{A}$, but in which the final column of each $\mathbf{A}_J$ is discarded [$\mathbf{A}_J \rightarrow \mathbf{A}_J^*$]: i.e., $\mathbf{A}^* = [\mathbf{A}\ [\ ,1], \mathbf{A}_1^*, \mathbf{A}_2^*, \ldots]$. Then, the [1x 3^S] vector of main effects fitted values is,

$$\Psi'(\boldsymbol{g}_\mathbf{v})_{\text{Main}} = \mathbf{A}^* \vec{\theta} \tag{4.4}$$

in which,

$$\vec{\theta} = (\mathbf{A}^{*\prime} \boldsymbol{D} \mathbf{A}^*)^{-1} \mathbf{A}^{*\prime} \boldsymbol{D} \boldsymbol{g}_v. \tag{4.5}$$

Evidently,

$$\sigma_{EP}^2 = (\boldsymbol{g}_\mathbf{v} - \mathbf{A}^* \vec{\theta})' \ \boldsymbol{D} (\boldsymbol{g}_\mathbf{v} - \mathbf{A}^* \vec{\theta})$$

$$\sigma_{EP}^2 = \boldsymbol{g}_\mathbf{v}\,' \boldsymbol{D}\, \boldsymbol{g}_\mathbf{v} - \boldsymbol{g}_\mathbf{v}' \boldsymbol{D} \mathbf{A}^* (\mathbf{A}^{*\prime} \boldsymbol{D} \mathbf{A}^*)^{-1} \mathbf{A}^{*\prime} \boldsymbol{D}\, \boldsymbol{g}_\mathbf{v}. \tag{4.6}$$

Letting i signify gene content at locus 1, j at locus 2, etc., it can be shown that the element of $\Psi'(\boldsymbol{g}_\mathbf{v})_{\text{Main}}$ corresponding to any $\boldsymbol{g}^*$, is equal to:

for $s = 2$,

$$\Psi'(\boldsymbol{g}^*)_{\text{Main}} = [\ \hat{\mu}_{ij} = \mu_{i.} + \mu_{.j} - \mu_{\Psi\prime(g)}]; \tag{4.7}$$

for $s = 3$,

$$\Psi'(\boldsymbol{g}^*)_{\text{Main}} = [\ \hat{\mu}_{ijk} = \mu_{i..} + \mu_{.j.} + \mu_{..k} - 2\mu_{\Psi\prime(g)}]; \tag{4.8}$$

and, finally, for the general case of s loci:

$$\Psi'(\boldsymbol{g}^*)_{\text{Main}} = \hat{\mu}_{ijkl..} = [\ \mu_{i..} + \mu_{.j.} + \mu_{..k} + \cdots - (k-1)\mu_{\Psi'(g)}]. \tag{4.9}$$

In other words, the *main effect fitted values* contained in $\boldsymbol{A}^*(\boldsymbol{A}^{*\prime}\boldsymbol{D}\boldsymbol{A}^*)^{-1}\boldsymbol{A}^{*\prime}\boldsymbol{D}\boldsymbol{g}_\mathbf{v}$ is equivalent to those yielded by a regular s-way ANOVA on $\Psi'(\boldsymbol{g}^*)$. We will find it convenient to

employ this last expression, $\Psi'(\boldsymbol{g}^*)_{\text{Main}}$, hereafter, and define epistasis as that property of an architecture wherein for at least 2 of the 3^S genotypes,

$$\Psi'(\boldsymbol{g}) \neq \Psi'(\boldsymbol{g}^*)_{\text{Main,}} \tag{4.10}$$

or equivalently, the circumstance in which $\sigma^2_{EP} \neq 0$.

4.2. Genotype-Specific Epistatic Effects

For a particular genotype $\boldsymbol{g}^*$, the *genotype-specific epistatic effect* is defined as

$$\tau(\boldsymbol{g}^*) = \Psi'(\boldsymbol{g}^*) - \Psi'(\boldsymbol{g}^*)_{\text{Main}}.^{104} \tag{4.11}$$

Naturally, there are 3^S of these effects, and it can be proven that

$$\text{E}(\tau(\boldsymbol{g})) = 0^{105} \text{ and } \text{V}(\tau(\boldsymbol{g})) = \sigma^2_{EP}. \tag{4.12}$$

In the case in which $s = 2$, for example,

$$\begin{aligned} \text{E}(\tau(\boldsymbol{g})) &= \text{E}(\Psi'(\boldsymbol{g}^*) - \Psi'(\boldsymbol{g}^*)_{\text{Main}}) \\ &= \text{E}(\Psi'(\boldsymbol{g})) - \text{E}(\mu_{i.} + \mu_{.j} - \mu_{\Psi\prime(g)}) \\ &= \mu_{\Psi\prime(\boldsymbol{g})} - \left[\mu_{\Psi'(\boldsymbol{g})} + \mu_{\Psi'(\boldsymbol{g})} - \mu_{\Psi'(\boldsymbol{g})}\right] = 0, \end{aligned} \tag{4.13}$$

and

$$\begin{aligned} \text{V}(\tau(\boldsymbol{g})) &= E[\tau(\boldsymbol{g}) - \text{E}(\tau(\boldsymbol{g}))]^2 \\ &= \left[\sum_{i=1}^{3}\sum_{j=1}^{3} P(g_{ij})\left(\tau(g_{ij})\right)^2\right] \\ &= \sigma^2_{EP}. \end{aligned} \tag{4.14}$$

---

[104] Please see the works of Cockerham & Kempthorne (1954); Falconer & Mackay, (1996); Lynch & Walsh (1998); Templeton (2000) for further details and definitions on epistatic *genic effects* or *interaction deviations*.

[105] $E(\tau(\boldsymbol{g}) - E(\tau(\boldsymbol{g})) = E(\tau(\boldsymbol{g}) - E(E(\tau(\boldsymbol{g}))) = E(\tau(\boldsymbol{g})) - E(\tau(\boldsymbol{g})) = 0$.

4.3. Technical Foundations of Detection

An architecture with the property of epistasis is one yielding a non-zero epistatic variance component. As such, the detection problem as related to epistasis reduces to that of making a binary decision vis-a-vis the hypothesis pair: [H_0: σ^2_{EP}=0, or H_1: $\sigma^2_{EP} \neq 0$]. Broadly, let there be a statistical procedure *P* designed to yield a binary decision respecting this pair. *P* features a test statistic *T*, the distribution of which is $\Delta[n, \phi'^*]$, wherein *n* is the sample size; ϕ'^* the effect size measure (a quantity which captures the degree of departure from H_0, or equivalently, how far from zero is the parameter (σ^2_{EP})). Recall that under the condition H_0 is true, the distribution of T is $\Delta[n, \phi'^*= 0]$, called *the null distribution*, and, under the condition that H_0 is false, by $\phi'^* > 0$, it's distribution is $\Delta[n, \phi'^* > 0]$, called *an alternative distribution*[106]. Partition the real line into two disjoint regions R (the rejection region), and A (the acceptance region), such that $R \cup A = \mathbb{R}$. The decision rule of P has, then, the following form:

If $T \subset A$, decide in favour of H_0,

If $T \subset R$, decide in favour of H_1.

Region A is selected such that $P(T \subset A | \phi'^* = 0)$ = P(Type I error) is equal to an antecedent selected, typically low, value, α. To this end, the probability of detecting epistasis is simply the probability of deciding in favour of H_1, when $\sigma^2_{EP} \neq 0$. Formally, this probability is $P(T \subset R | \phi'^* > 0) = \int_R \Delta[n, \phi'^* > 0]$, and is recognizable as the power function of procedure P. A procedure *P* is *sound* vis-a-vis its role as a detector of epistasis only if α is set acceptably low, and, for values of $\phi'^* > 0$ likely to be encountered in those empirical contexts, $P(T \subset R | \phi'^* > 0)$ is large[107]. While the researcher may select a detection technology with the inferential aim of rendering decisions in regards to the pair [H_0: $\sigma^2_{EP} = 0$ and H_1: $\sigma^2_{EP} \neq 0$] unless the detection technology is *sound*, the inferences

[106] As such, there exist innumerable realizations of $\Delta[n, \phi'^* > 0]$, each one coded to a particular standardized departure from σ^2_{EP}=0. Of course, only one will be extant at the time of the test procedure.

[107] All told, a sound test procedure is one that delivers correct decisions with high probability (i.e., signaling in favor of H_0 when σ^2_{EP}= 0 and in favor of H_1 when $\sigma^2_{EP} \neq 0$).

it yields are likely to misportray the empirical state of affairs, and, in so doing, subvert the scientific progress.

Chapter 5. Issues Affecting the Probability of Detection

Introduction

As witnessed in Chapter 4, the detection of epistasis reduces un-problematically to a technical issue bearing on the *soundness* of a statistical procedure employed in the service of yielding decisions about the hypothesis pair [H_0: σ^2_{EP}=0, or H_1: $\sigma^2_{EP} \neq 0$]. In particular, the empirical scientist requires a test procedure *P*, wherein both α is set low and, for values of $\phi'^* > 0$ likely to be yielded by extant architectures, P(T$\subset$ R $|\phi'^*$) is large. Given that researchers have had little success in detecting epistasis even though theory points strongly to its existence, it would seem reasonable to entertain the possibility that the procedures heretofore employed have not been sound; in particular, that for the $\phi'^* > 0$ occurring in nature, P(T$\subset$ R $|\phi'^*$) frequently turns out to be too small. Because the preeminent aim of the thesis is to investigate why it is that epistasis appears to be difficult to detect, it will be fruitful to elucidate in more detail some of the factors determining the numerical value of P(T$\subset$ R $|\phi'^*$), a task to which, in this chapter, we turn.

5.1. The parameters of P(T$\subset$ R $|\phi'^* > 0$)

Let there be, as in Chapter 4, a procedure *P*, the purpose of which is to yield decisions about the hypothesis pair [H_0: σ^2_{EP}=0, or H_1: $\sigma^2_{EP} \neq 0$], and let *T* be its test statistic. In the general case wherein a particular architecture has the property of epistasis (i.e., $\sigma^2_{EP} \neq 0$), it follows that H_0 is false by some particular amount ϕ'^*, $\phi'^* > 0$, unknown to the researcher, and the distribution of *T* is $\Delta[n, \phi'^*]$. Under this state of nature, the adjudication of the performance of *P* as a detector of epistasis is in terms of the *power* P(T$\subset$ R $|\phi'^* > 0$) it delivers. In general, the probability P(T$\subset$ R $|\phi'^* > 0$) is a function of three parameters, α, ϕ'^*, and n. Let us review these parameters.

The first parameter α stands for the probability P($T \subset$ R $|\phi'^* = 0$) = P(Type I error), i.e., the Type I error rate, the antecedent selection of which sets the critical values demarcating the acceptance and rejection regions which form the test-statistic *T*'s decision rule. The second parameter ϕ', called the *effect size measure*, quantifies the

degree of departure from H_0. Power will be an increasing function of ϕ'. In the conceptions of detection theory, all things being equal, the smaller the object to be detected, the smaller will be the probability of detection. Naturally, as with any tool of detection, it will not, in general, be possible to design *P* to ensure that it performs at a high level for *all* possible values of ϕ'. A given detector of epistasis will, under standard circumstances, deliver adequate sensitivity only within a certain range of ϕ'. What this implies is that, in sculpting a procedure for optimal employment in a given research context, the researcher must specify one or more candidate values of ϕ', say ϕ'^{*}[108], which are deemed integral to the scientific aims of the test-procedure. Once selected, the aim turns to muster the resources, typically sufficient sample size necessary to achieve for the particular focal ϕ'^{*} under consideration, a level of power deemed sufficiently high (e.g., greater than or equal to .90). As previously implied, the final parameter *n* represents the resources applied to a given problem of epistatic detection. Naturally, the optimal choice of *n* is intimately related to the design of the instrument of detection, and, accordingly, depends upon several factors: 1) the values of α and $P(T \subset R \mid \phi'^{*} > 0)$ deemed acceptable by the researcher; 2) [corollary to the former point] the candidate ϕ'^{*}, or the range of ϕ' of scientific interest, likely to be extant when *P* is employed; 3) other technical details bearing on the optimal performance of *P*, an example being, the desirability of equal *n* over the 3^s genotypes, when T is the F-test statistic, yielded by ANOVA based approaches to epistatic detection[109].

All told, a test procedure *P* designed for detecting epistasis is *sound,* if before its employment *a* has been set to a reasonably low value and is *n* specified such that $P(T \subset R \mid \phi'^{*} > 0)$ is satisfactory for the set of candidate departures from H_0 (ϕ'^{*}). Evidently, as $P(T \subset R \mid \phi'^{*} > 0)$ is tied intimately to ϕ'^{*}, so too is any judgment of soundness. Of course, it is open to question precisely how accurate extant scientific knowledge is in its speculations about the sorts of ϕ'^{*} engendered by architectures arising in empirical contexts. To this end, it is plausible a potential catalyst behind the lacunae of support for epistasis is that values of $\sigma^2_{EP} \neq 0$ are smaller than generally appreciated. Naturally, such a scenario suggests that unbeknownst to the researchers, the test procedures employed for epistatic detection are *uniformly unsound* (concerning the values of ϕ'^{*}). If

---

[108] should any of these be extant when the procedure is employed.

[109] Equal *n* ensuring orthogonality of the 2^s-1 effects defined under such approaches (Iversen & Norpoth, 1987).

this were the case, the proper remedy would be to increase the resources- i.e., sample size- brought to bear on the epistatic detection problem.

5.2. Assumptions Inherent to T

The optimal performance of many statistical procedures depends upon the satisfaction of a set of assumptions. The assumptions attendant to a particular procedure *P*, are a set of riders or side-conditions, the satisfaction of which is necessary so that the distribution of *T* accord with its theoretical distribution, $\Delta[n, \phi'^*]$. If, in a particular domain of application, *T*'s assumptions are violated, those probabilities employed to characterize *P*'s performance - notably, the nominal Type I error rate, α, and the power function $P(T \subset R \mid \phi'^*)$ - will be, to some extent, in error. It is a possibility that procedures employed in the service of detecting epistasis rest on assumptions, the satisfaction of which is made unlikely by the empirical phenomenon itself. Consider, for example, the employment of the standard F-test of interaction, featuring MS_{EP} and $MS_{U \mid EP}$, in the testing of the hypothesis pair [H_0: $\sigma^2_{EP}=0$, or H_1: $\sigma^2_{EP} \neq 0$]. As is well known, the assumptions on which the standard F-test rests are normality of each of the 3^s populations of phenotypic values (one for each genotype) and homogeneity of variance. However, the very nature of epistasis may well induce of violation of these assumptions. To this end, let a given architecture have the properties of Hardy Weinberg Equilibrium (HWE)[110],

$$P(\Psi'(g_1=0)) = (1-\varphi)^2 \text{ , } P(\Psi'(g_1=1)) = 2\varphi(1-\varphi), \text{ and } P(\Psi'(g_1=2)) = \varphi^2, \qquad (5.1)$$

and Linkage Equilibrium (LE),

$$P(\boldsymbol{g} = \boldsymbol{g}^*) = \prod_{j=1}^{s} P(g_j = \boldsymbol{g}_j^*). \qquad (5.2)$$

[110] From Chapter 2, recall that the proportion of alleles in *P* of type A_2 are - φ. For any number of alleles, one can calculate the frequency proportions in a randomly mating infinite sized populations, vis-à-vis the multiplicative expansion of $(\delta+\varphi)^2$. In the scenario of HWE, allele counts are sufficient statistics, and the probabilities of the genotype counts conditional on the allele counts permit computation of parameter values for the phenotypic distribution (Lynch & Walsh, 1998). However, the properties of HWE vary for sex-linked genes. Give males are the heterogametic sex, for each mating pair, there are three X-chromosomes, and the frequency 1- $\varphi = [\, 1 - \varphi\, M(0) + 2(1 - \varphi F(0))]/3$ (Lynch & Walsh, 2008).

[111] See Searle, 1971 pg. 270; Iversen & Norpoth, 1987; Lynch & Walsh, 1998.

All told when an architecture is in keeping with both properties the 3^s distributions of phenotypic values are characterized by allele and genotype frequencies with generational stability[112] (5.1), and statistical independence (5.2)[113], permitting the sound orthogonal decomposition of σ_Z^2 (2.18) into its constituent parts in both the single locus (2.19) and multi-locus (2.20) case (Lynch & Walsh, 1998; Templeton, 2000).

5.3. A Hidden Factor: Genetic-Environment Association

In the case in which an architecture has the properties of epistasis ($\sigma_{EP}^2 \neq 0$) and gene-environmental association, it follows that,

$$E(Z \mid \boldsymbol{g}) = \Psi'(\boldsymbol{g}) + \varepsilon(\boldsymbol{g}),$$

and,

$$V(E(Z \mid \boldsymbol{g})) = \sigma_A^2 + \sigma_D^2 + \sigma_{EP}^2 + 2\sigma_{\Psi'(\boldsymbol{g}),\varepsilon(\boldsymbol{g})} + \sigma_{\varepsilon(\boldsymbol{g})}^2.$$

Evidently, in the empirical setting, the researcher will not have access to the genotypic values $\Psi'(\boldsymbol{g})$, but, rather, estimates of the conditional means, $E(Z \mid \boldsymbol{g})$. As the presence of $\varepsilon(\boldsymbol{g})$ effectuates 3^s departures between $E(Z \mid \boldsymbol{g})$ and $\Psi'(\boldsymbol{g})$ in a magnitude and direction unknown, a bias of this sort evinces departures between the Fisherian decomposition of both respective quantities. The implication is that estimates of the variance components [$\sigma_{A(c)}^2, \sigma_{D(c)}^2, \sigma_{EP(c)}^2$] recovered by decomposition of $E(Z \mid \boldsymbol{g})$ in the empirical setting will be 'contaminated' by gene-environmental association. All told, at the population level, unless $\sigma_{\varepsilon(\boldsymbol{g})}^2 = 0$: 1) the epistatic variance yielded under a decomposition of $E(Z \mid \boldsymbol{g})$ is not the target quantity σ_{EP}^2, but rather, its contaminated

---

[112] Violations of HWE introduce a non-probabilistic sampling of a population's allele frequencies (typically a function of the forces of selection and mutation on heterozygosity).

[113] Violations of linkage equilibrium (LE), referred to as Linkage disequilibrium (LD) or dependencies between loci obstructs the orthogonal decomposition of genetic variance components. The effects of LD quantified as *the covariance of the frequency of 'non-alleles' of the same gamete*, are either positive (coupling-over representation) or negative (repulsion-underrepresentation) in direction (Lynch & Walsh, 1998). In particular, if genetic loci with a positive influence on Z are associated with each other on a chromosome, the observed genetic variation is inflated relative to is an expectation under random assortment. Naturally, the observed genetic variation deflates relatively to its expectation under random assortment when loci of positive and negative impact on Z are associated with one another on a chromosome (Lynch & Walsh, 1998). To this end, LD structure may also obscure the observed epistatic genetic variance from its expected value. See the works of Gallais (1974), Weir & Cockerham (1977).

counterpart, $\sigma^2_{EP(c)}$; and 2) $\sigma^2_{EP(c)}$ will differ from σ^2_{EP} to a degree - and in a direction - unknown.

In light of (2.1), (2.2), and the previous observations, it is apparent that, in a given empirical context, a standard F-test featuring MS_{EP} and $MS_{U|EP}$ is not a test purely of the focal hypothesis pair [H_0: σ^2_{EP}=0, or H_1: $\sigma^2_{EP} \neq 0$][114], but, rather, a test of its contaminated counterpart [H_0: $\sigma^2_{EP(c)}$=0, or H_1: $\sigma^2_{EP(c)} \neq 0$][115]. There is, of course, no reason to suppose that a procedure performing optimally *vis a vis* the contaminated pair [H_0: $\sigma^2_{EP(c)}$=0, or H_1: $\sigma^2_{EP(c)} \neq 0$], will do so, also, *vis-a-vis* the pair of scientific import. To this end, we conclude by observing that it is a possibility the difficulties in detecting epistasis derive from collateral effects of contamination by gene-environmental association upon epistatic tools of detection, such as the F-test.

[114] $F_{(n,\ n\text{-}1(ab))} \sim \frac{MS_{EP}}{MS_{U/EP}}$; $E(MS_{EP}) = [\sigma^2_R + \left(\frac{n(ab)}{(a-1)(b-1)}\right)\sigma^2_{EP}]$, and $E(MS_{U|EP}) = \sigma^2_R$.

[115] $\sigma^2_{EP(C)} = \sum(\tau_{(g(c))})^2$; $F_{(n,\ n\text{-}1(ab))} \sim \frac{MS_{EP}}{MS_{U/EP}}$; $E(MS_{EP}) = [\sigma^2_R + \left(\frac{n(ab)}{(a-1)(b-1)}\right)\sigma^2_{EP(c)}]$, and $E(MS_{U|EP}) = \sigma^2_R$.

Chapter 6. General Overview of Simulation Studies I and II

Introduction

In the remainder of the thesis we investigate two explanations for the difficulties encountered in detecting epistasis. The first relates to the possibility that the σ^2_{EP} (or equivalently the ϕ'^*) produced by epistatic architectures are *simply small*; the consequence being that, for the sorts of sample sizes employed in research, the power delivered by commonly employed detection tools is disadvantageously small. The second relates to the possibility that the presence of gene-environment association generates bias in the estimation of genotypic values, and, in so doing, alters in unfavourable ways the performance of tools of detection. In adjudicating the merit of each of these candidate explanations, the problem, of course, is that the architectures for which these difficulties ostensibly hold, are precisely those for which epistasis is not detectable. Accordingly, there would appear to be no empirical means of verifying whether these possibilities occur empirically. We attempt to overcome this obstacle through the undertaking of two simulation studies, hereafter referred to as simulation studies I and II.

The two simulation studies rest on four constructed di-genic epistatic architectures, engendered by crossing two genotypic functions with two levels of gene-environment association (absent/present). By sampling over its parameter space, under each architecture, we generate the empirical distribution of a variety of focal quantities. In simulation I, the empirical distributions of σ^2_{EP}, ϕ'^*, and ω^2_{EP} are approximated, and for architectures featuring gene-environment association, the contaminated counterparts, $\sigma^2_{EP(c)}$, $\phi'^*_{(c)}$, and $\omega^2_{EP(c)}$, and the associated biases $(\phi'^*_{(c)} - \phi'^*)$ and $(\omega^2_{EP(c)} - \omega^2_{EP})$. The general aim in undertaking this first simulation study is to provide a glimpse of the expected empirical range of $\sigma^2_{EP}(\phi')$, and, for those architectures featuring gene-environment association, *how far off the mark* the recovered epistatic effect sizes, $\phi'_{(c)}$ are from their true counterparts ϕ'. In the second study, we evaluate the *detection performance* of a paradigm-case detector of epistasis - the classical F-test of omnibus interaction -, by assembling the empirical distribution of power values corresponding to the distribution of ϕ' and $\phi'_{(c)}$ generated in study I. Nuance is brought to the picture

painted by the distribution of power values, through reporting: 1) the *median* power profile; 2) *proportion of architectures* which yield satisfactory power (say ≥ .90); and 3) the *magnitude and direction* of *bias* engendered by the former two criteria.

In the remainder of the chapter, we will: 1) elucidate in detail the method of construction of the four architectures; 2) describe the approach taken to sampling the parameter space; 3) provide two fully worked examples illustrative of the construction methodology described in (1), along with the computational basis for the resulting population-level variance components; 4) elucidate, in full, the set of focal quantities and criteria that will stand as the output of the two simulation studies; and, finally, 5) delineate the software and packages employed for data simulation.

6.1. Construction of the Four Architectures

At the core of each of the four constructed architectures is the crossing of genotypic function, $\Psi'(\boldsymbol{g})$, and level of gene-environmental association. The two genotypic functions employed herein are: 1) the *max* function, $\Psi'(\boldsymbol{g}) = max\{\Psi'(\boldsymbol{g_j})\}_{j=1,}^{\boldsymbol{N}}$, previously used in the works of Zuk and colleagues (2010)[116], and symbolized herein as $\Psi'(\boldsymbol{g})_{\mathbf{Max}}$; and 2) the *min* function, $\Psi'(\boldsymbol{g}) = min\{\Psi'(\boldsymbol{g_j})\}_{j=1}^{\boldsymbol{N}}$, symbolized as $\Psi'(\boldsymbol{g})_{\mathbf{Min}}$. Once again, the level of gene-environment association is either absent ($\boldsymbol{\varepsilon} = [0]$) or present ($\boldsymbol{\varepsilon} \neq [0]$). The situation can be depicted with reference to the fourfold table of Figure 6.1.

[116] According to Zuk et. al. (2010), $max\{\Psi'(\boldsymbol{g_j})\}_{j=1}^{\boldsymbol{N}}$ is a desirable choice as a generator of epistasis, in consequence of the fact that it captures various *gateway processes* known to be operative in animal biology, and so possesses of a certain degree of ecological validity.

Figure 6.1 Four Architectures – Crossing of Genotypic Function and Gene-environmental Association

$\Psi'(\boldsymbol{g})_{\mathbf{Max}}$	$\Psi'(\boldsymbol{g})_{\mathbf{Min}}$	
$\Psi'(\boldsymbol{g})_{\mathbf{Max}}$ $[s{=}2, \Psi'(\boldsymbol{g})_{\mathbf{Max}}, \vec{\theta}, \boldsymbol{\varepsilon} = [\mathbf{0}], H^2]$	$\Psi'(\boldsymbol{g})_{\mathbf{Min}}$ $[s{=}2, \Psi'(\boldsymbol{g})_{\mathbf{Min}}, \vec{\theta}, \boldsymbol{\varepsilon} = [\mathbf{0}], H^2]$	$\boldsymbol{\varepsilon} = [\mathbf{0}]$
$\Psi'(\boldsymbol{g})_{\mathbf{Max,GE}}$ $[s{=}2, \Psi'(\boldsymbol{g})_{\mathbf{Max}}, \vec{\theta}, \boldsymbol{\varepsilon} \neq [\mathbf{0}], H^2]$	$\Psi'(\boldsymbol{g})_{\mathbf{Min,GE}}$ $[s{=}2, \Psi'(\boldsymbol{g})_{\mathbf{Min}}, \vec{\theta}, \boldsymbol{\varepsilon} \neq [\mathbf{0}], H^2]$	$\boldsymbol{\varepsilon} \neq [\mathbf{0}]$

Hence forth we will tie our results and discussion to the designations of the four architectures as manifest in the table. Thus, for example, architectures featuring $\Psi'(\boldsymbol{g})_{\mathbf{Max}}$ and gene-environment association ($\boldsymbol{\varepsilon} \neq [\mathbf{0}]$) will be designated as $\Psi'(\boldsymbol{g})_{\mathbf{Max,GE}}$.

Each complete, numerically instantiated, architecture, yielding of population-level variance components, is built up from the level of locus-specific genotypic values expressed in terms of *ak* parameterization (see Chapter 2), and features the properties of HWE (5.1) and LE (5.2). The basic idea may be elucidated for the general *polygenic* case for $s > 1$ loci, as follows*:*

1. Specify s and $\Psi'(\boldsymbol{g})$.

2. Specify the genetic parameter vector $\vec{\theta}$, which contains the parameters $[a_1, a_2, \ldots, a_s, k_1, k_2, \ldots, k_s, \varphi_1, \varphi_2, \ldots, \varphi_s]$ (see chapter 2)[117], and which, in conjunction with $\Psi'(\boldsymbol{g})$, yields the 3^s genotypic values and the population genetic variance components, σ_A^2, σ_D^2, and σ_{EP}^2.

3. Specify a 3^s element vector $\boldsymbol{\varepsilon}$ containing gene-environment association parameters, under which $\mathrm{E}(\mathrm{Z} \mid g) = \Psi'(\boldsymbol{g}) + \boldsymbol{\varepsilon}(\boldsymbol{g})$, and which yields the quantities $\sigma^2_{\varepsilon(\boldsymbol{g})}$ and $2\sigma_{\Psi'(\boldsymbol{g}),\varepsilon(\boldsymbol{g})}$:

[117] for s=3, $\{a_j, k_j, d_j\}$ where j=1...3; etc.

3.1. for architectures in which gene-environmental association is absent, specify $\boldsymbol{\varepsilon}$ to be the null vector, $\boldsymbol{\varepsilon} = [\mathbf{0}]$;

3.2. for architectures in which gene-environmental association is present, specify the non-null value of $\boldsymbol{\varepsilon} \neq [\mathbf{0}]$.

4. Construct σ_R^2:

4.1.1. for architectures in which $\boldsymbol{\varepsilon} = [\mathbf{0}]$, from (2.15), $\sigma_R^2 = \sigma_E^2$. Because $H^2 = \frac{\sigma_A^2+\sigma_D^2+\sigma_{EP}^2}{\sigma_Z^2}$, it follows that specifying H^2 determines σ_R^2 in accordance with the formula,

$$\sigma_R^2 = \sigma_Z^2 - [\sigma_A^2 + \sigma_D^2 + \sigma_{EP}^2] = [\frac{1}{H^2} - 1][\sigma_A^2 + \sigma_D^2 + \sigma_{EP}^2]; \quad (6.1)$$

4.1.2. for architectures in which, $\boldsymbol{\varepsilon} \neq [\mathbf{0}]$; from (2.15), $\sigma_E^2 = \sigma_{\varepsilon(g)}^2 + \sigma_R^2$, specifying H^2 determines σ_R^2 in accordance with the formula,

$$\sigma_R^2 = [\frac{1}{H^2} - 1][\sigma_A^2 + \sigma_D^2 + \sigma_{EP}^2] - 2\sigma_{\Psi'(g),\varepsilon(g)} - \sigma_{\varepsilon(g)}^2. \quad (6.2)$$

A complete architecture can be represented as a 5-tuple [s, $\Psi'(\boldsymbol{g})$, $\vec{\theta}$, $\boldsymbol{\varepsilon}$, H^2], for which any particular realization, [s^*, $\Psi'(\boldsymbol{g})^*$, $\vec{\theta}^*$, $\boldsymbol{\varepsilon}^*$, H^{2*}] yields a set of population variance components[118]. Accordingly, by sampling over the parameter space of [$\vec{\theta}$,H^2] and generating the empirical distributions of key focal quantities, one is afforded opportunity to gain insight, "*in vacuo*," into both the empirical range of an architectures focal quantities, and establish associations between the values assumed by these quantities and the numerical realizations that yielded them. Under such an approach, the candidate explanations can be evaluated, free from the noise imparted by the empirical setting of epistatic detection (described at length in Chapter 3, section 3.3).

[118] For architectures in which, $\boldsymbol{\varepsilon} = [\mathbf{0}]$: [σ_A^2, σ_D^2, $\sigma_{EP}^2, \sigma_E^2$], and for architectures in which, $\boldsymbol{\varepsilon} \neq [\mathbf{0}]$: [σ_A^2, σ_D^2, $\sigma_{EP}^2, \sigma_{\varepsilon(g)}^2, \sigma_R^2$].

6.2. Sampling over the parameter space

In this section, we present the theoretical basis for the selection of parameter values, in terms of numerical realizations of the architectures are produced.

6.2.1. Sampling of the a parameter

For all four architectures and each of the two loci, the same three values of a were sampled. As will be recalled, parameter a is the linear rate of change in $\Psi'(\boldsymbol{g}_j)$, and, as such, is equal to $\frac{(\mu_{Z|g_{1=2}} - \mu_{Z|g1=0})}{2}$ (Lynch and Walsh, 1998). Low, medium, and high values of a were selected by means of the formulas $\frac{b}{3}$, $2\frac{b}{3}$, $3\frac{b}{3} - j$, respectively, wherein, j and b were sampled from a random uniform distribution. All told, the three sampled values were 16, 32, and 44.

6.2.2. Sampling of the k parameter

For all four architectures and each of the two loci, five unique values of k were sampled. As it will be recalled, parameter k controls the non-linearity inherent to $\Psi'(\boldsymbol{g_j})$. It is commonly said that: 1) $k = 0$ signifies complete *additive* gene action; 2) $k = 1$, complete dominance of the A_1 allele; 3) $k = -1$, complete dominance of the A_2 allele; 4) $k > 1$, over-dominance, such that the phenotypic expression of the heterozygote (A_1A_2) which exceeds both homozygotes (A_1A_1; A_2A_2); 5) and $k > -1$, under-dominance where the phenotypic expression of the heterozygote is lower than both homozygotes. The two elements corresponding to the circumstance in which $k > 1$, $k > -1$, were randomly selected from two uniform distributions. All told, the sample values for locus 1 were 0, 1, -1, 2, -6, and for locus 2, 0,1 -1,5,-7.

6.2.3. Sampling of φ and H^2 parameters

For all four architectures and each of the two loci, the same three values of φ and H^2 were sampled. Recall, of course, that φ and H^2, respectively, refer to locus-specific recessive allele frequency and broad-sense heritability. As both parameters are bounded between 0 and 1, element selection was fixed to examine the impact of small, medium,

and large magnitudes. All told the sample values for φ, and H^2 were respectively, 0.1, 0.5, 0.9, and 0.2, 0.5, 0.8.

6.2.4. Sampling of $\boldsymbol{\varepsilon_{3x3}}$

For architectures in which, $\boldsymbol{\varepsilon} \neq [0]$, we specified two unique matrices, $\boldsymbol{\varepsilon}_{3x3}$, and randomly sampled, for each, 9 gene-environmental parameters $\varepsilon(\boldsymbol{g})$ elements from a normal distribution N(3^S, $SD = 1$). As it will be recalled, $\varepsilon(\boldsymbol{g})$ quantifies the mean environmental impact conditional on genotype. All told, the two matrices for architectures $\Psi'(\boldsymbol{g})_{\mathbf{Max,GE}}$ and $\Psi'(\boldsymbol{g})_{\mathbf{Min,GE}}$ were respectively:

$$\boldsymbol{\varepsilon}_{3x3} = \begin{bmatrix} -0.360 & -0.202 & -0.029 \\ 0.090 & 0.740 & -0.389 \\ 0.096 & 0.123 & 0.511 \end{bmatrix}, \tag{6.3}$$

and,

$$\boldsymbol{\varepsilon}_{3x3} = \begin{bmatrix} -0.502 & 0.886 & -0.581 \\ 0.131 & 0.116 & 0.714 \\ -0.078 & 0.318 & -0.825 \end{bmatrix}. \tag{6.4}$$

6.2.5. Legitimate Architectures

Crossing the 3, 3, 5, 5, 3, 3, and 3, values selected for the parameters a_1, a_2, k_1, k_2, φ_1, φ_2, and H^2, respectively, generates a total of 6075 unique architectures, and for each, potentially, a set of focal quantities. However, for admissibility of a given architecture into the first simulation study, it must the case that $\sigma_R^2 \geq 0$[119]. For admissibility into the second simulation study, a given architecture must additionally have the property of epistasis; i.e., $\sigma_{EP}^2 > 0$[120]. All told, for $\Psi'(\boldsymbol{g})_{\mathbf{Max}}$ and $\Psi'(\boldsymbol{g})_{\mathbf{Min}}$ there were 6075 architectures

---

[119] As the environmental variance is set in the units of broad-sense heritability H^2, bespoke to architectures in which, $\boldsymbol{\varepsilon} \neq [0]$, the numerical realization of σ_R^2 may assume either positive or negative values (see formula 6.1). In light of this, we set forth the restriction that, for any *legitimate* architecture $\sigma_R^2 \geq 0$; else, the architecture is *illegitimate* and excluded from analysis in simulation study I.

[120] Following the definitions presented in (4.1), and (4.10) it is clear, while a particular architecture may be *ostensibly* epistatic (based on construction), an architecture has the *property of epistasis* only under the condition it yields a non-zero σ_{EP}^2. As our aims in the second simulation study are to adjudicate the *performance of detection* of a tool of detection over the empirical distribution of epistatic effect sizes, we set forth the second restriction, that only architectures which engender the *property of epistasis*, are admissible to simulation study II.

admitted into both simulation studies I and II. A total of 5832 architectures of type $\Psi'(\boldsymbol{g})_{\mathbf{Max,GE}}$ were admitted into simulation study I, and 5075 of type $\Psi'(\boldsymbol{g})_{\mathbf{Min,GE}}$. A total of 5238 of the former type, and 4482 of the latter, were admitted into simulation study II.

6.3. Architectures in which $\boldsymbol{\varepsilon = [0]}$: detailed description for the case of $\boldsymbol{\Psi'(g)}$Max

Following the general survey of architecture construction and sampling of its parameter space, our aims in the following section are to provide a detailed description of a single $\Psi'(\boldsymbol{g})_{\mathbf{Max}}$ architecture of the quantitative form: $[s = 2, \Psi'(\boldsymbol{g}) = \Psi'(\boldsymbol{g})_{\mathbf{Max}}, \vec{\theta}^* = \begin{bmatrix} a_1^* \\ a_2^* \\ k_1^* \\ k_2^* \\ \varphi_1^* \\ \varphi_2^* \end{bmatrix} \boldsymbol{\varepsilon}^*{}_{3x3} = [0], H^{2*}]$[121]. A complete architecture of this sort is built up from 6 locus-specific genotypic values expressed in terms of *ak* parameterization and the properties of HWE (5.1) and LE (5.2). Following section 6.1, it is the case, $\Psi'(\boldsymbol{g})_{\mathbf{Max}}$, and $\vec{\theta}^*$, specifies its joint distribution, genotypic frequencies, and population-level genetic variance components.

[121] Recall, φ = P(allele$_2$), δ = P(allele$_1$).

Figure 6.2 Digenic Architecture $\Psi'(\boldsymbol{g})_{\text{Max}}$ Construction

A_1A_1 $\Psi'(g_{.}=0) = 0$ $P(g_{.}=0) = \delta_1^2$ **0**	**A_1A_2** $\Psi'(g_{.}=1) = (k_{.}+1)a_{.}$ $P(g_{.}=1) = 2(\varphi_1\delta_1)$ **1**	**A_2A_2** $\Psi'(g_{.}=2) = 2a_{.}$ $P(g_{.}=2) = \varphi_1^2$ **2**	
$\text{Max}(\Psi'(g_{0,0}))$ $P(0,0) = \varphi_1^2\varphi_2^2$	$\text{Max}(\Psi'(g_{0,1}))$ $P(0,1) = 2(\varphi_1\delta_1)\,\varphi_2^2$	$\text{Max}(\Psi'(g_{0,2}))$ $P(0,2) = (\delta_1^2\varphi_2^2)$	**B_1B_1** $\Psi'(g_{.}=0) = 0$ $P(g_{.}=0) = \delta_2^2$ **0**
$\text{Max}(\Psi'(g_{1,0}))$ $P(0,1) = \varphi_1^2(2(\varphi_2\delta_2))$	$\text{Max}(\Psi'(g_{1,1}))$ $P(1,1) = 2(\varphi_1\delta_1)2(\varphi_2\delta_2)$	$\text{Max}(\Psi'(g_{1,2}))$ $P(1,2) = \delta_1^2(2(\varphi_2\delta_2))$	**B_1B_2** $\Psi'(g_{.}=1) = (k_{.}+1)a_{.}$ $P(g_{.}=1) = 2(\varphi_2\delta_2)$ **1**
$\text{Max}(\Psi'(g_{2,0}))$ $P(0,2) = \varphi_1^2\delta_2^2$	$\text{Max}(\Psi(g_{2,1}))$ $P(1,2) = (2(\varphi_1\delta_1)\delta_2^2)$	$\text{Max}(\Psi'(g_{2,2}))$ $P(2,2) = \delta_1^2\delta_2^2$	**B_2B_2** $\Psi'(g_{.}=2) = 2a_{.}$ $P(g_{.}=2) = \varphi_2^2$ **2**

And so, the Fisherian decomposition of $\Psi'(\boldsymbol{g})$[122] yields the following genetic variance components.

$$\sigma^{2*}_{\Psi'(\boldsymbol{g})} = +\sigma_A^2 + \sigma_D^2 + \sigma_{EP}^2.$$

$$\sigma_A^{2*} = \sigma_{A_1}^2 + \sigma_{A_2}^2;$$

$$\sigma_{A_1}^{2*} = 2\,\varphi_1\delta_1[a_1[1+k_1(2\varphi_1 - 1)]]^2;$$

$$\sigma_{A_2}^{2*} = 2\,\varphi_2\delta_2[a_2[1+k_2(2\varphi_2 - 1)]]^2;$$

$$\sigma_D^{2*} = \sigma_{D_1}^2 + \sigma_{D_2}^2;$$

$$\sigma_{D_1}^{2*} = \sigma_{L_1}^2 - \sigma_{A_1}^2 = 2\varphi_1\delta_1\, a_1\, k_1]^2;$$

$$\sigma_{D_2}^{2*} = [2\varphi_2\delta_2\, a_2\, k_2]^2\,;$$

---

[122] Wherein, $\mu_{\Psi'(\boldsymbol{g})} = \varphi_1^2\,\mu_{s2} + 2(\varphi_1\delta_1)(\mu_{s2} + (k_1+1)a_1) + \delta_1^2\,(\mu_{s2} + 2a_1) = \mu_{s2} + \mu_{s1}$.
$\mu_{\Psi'(g_1)} = 2(1-\varphi_1) = 2\delta_1$; $\sigma^2_{\Psi'(g_1)} = 2\varphi_1(1-\varphi_1)$, and $\mu_{.1} = \frac{1}{\varphi^2}\varphi_1^2[\delta_2{}^2.0 + 2(\varphi_2\delta_2)(k_2+1)a_2 + \delta_2^2.\,2a_2] = \mu_{s2}$; $\mu_{.2} = \mu_{s2} + (k_1+1)a_1$; $\mu_{.3} = \mu_{s2} + 2a_1$, and $\sigma^2_{L_1} = 2\delta_1 a_1^2[2\delta_1(1 - k_1\varphi_1 + 1)^2] + \varphi_1(k_1+1)^2$.
$\mu_{\Psi'(g_2)} = 2\delta_2$; $\sigma^2_{\Psi'(g_2)} = 2\varphi_2(1-\varphi_1)$; $\mu_{1.} = \mu_{s1}$; $\mu_{2.} = \mu_{s1} + (k_1+1)a_2$; $\mu_{3.} = \mu_{s1} + 2a_2$; and $\sigma^2_{L_2} = 2\delta_2 a_2^2[2\delta_2(1 - k_2\varphi_2 + 1)^2] + \varphi_2(k_2+1)^2$.

$$\sigma_{EP}^{2*} = \sigma_{\Psi'(\boldsymbol{g})}^{2*} - \sigma_A^{2*} - \sigma_D^{2*}. \quad (6.5)$$

6.4. Architectures in which ε ≠ [0]: detailed description for the case of $\Psi'(\boldsymbol{g})$Max

Next, we provide a detailed description of a single digenic $\Psi'(\boldsymbol{g})_{\mathbf{Max,GE}}$ architecture of the quantitative form: $[s = 2, \Psi'(\boldsymbol{g}) = \Psi'(\boldsymbol{g})_{\mathbf{Max}}, \boldsymbol{\varepsilon}_{\boldsymbol{3x3}}^{*} = \begin{bmatrix} \varepsilon_{00} & \varepsilon_{10} & \varepsilon_{20} \\ \varepsilon_{01} & \varepsilon_{11} & \varepsilon_{21} \\ \varepsilon_{02} & \varepsilon_{12} & \varepsilon_{22} \end{bmatrix}, \vec{\theta}^{*} = \begin{bmatrix} a_1^* \\ a_2^* \\ k_1^* \\ k_2^* \\ \varphi_1^* \\ \varphi_2^* \end{bmatrix}, H^{2*}]$. A complete architecture of this sort is built up from 6 locus-specific genotypic values expressed in terms of *ak* parameterization and the properties of HWE (5.1) and LE (5.2). Following section 6.1, it is the case, $\Psi'(\boldsymbol{g})_{\mathbf{Max}}$, $\vec{\theta}^{*}$, and $\boldsymbol{\varepsilon}_{\boldsymbol{3x3}}^{*}$ specifies its joint distribution, genotypic frequencies, and population-level genetic variance components.

Figure 6.3 Digenic Architecture $\Psi'(\boldsymbol{g})_{\text{MaxGE}}$ Construction

A_1A_1 $\Psi'(g_1{=}0) = 0$ $P(g_1{=}0) = \delta_1^2$ **0**	**A_1A_2** $\Psi'(g_1{=}1) = (k_1{+}1)a_1$ $P(g_1{=}1) = 2(\varphi_1\delta_1)$ **1**	**A_2A_2** $\Psi'(g_1{=}2) = 2a_1$ $P(g_1{=}2) = \varphi_1^2$ **2**	
$E(Z \mid \boldsymbol{g} = g_{0,0})$ $\text{Max}(\Psi'(g_{0,0}))+\varepsilon_{0,0}$ $P(0,0) = \varphi_1^2\varphi_2^2$	$E(Z\|\boldsymbol{g} = g_{0,1})$ $\text{Max}(\Psi'(g_{0,1}))+\varepsilon_{0,1}$ $P(0,1) = 2(\varphi_1\delta_1)\,\varphi_2^2$	$E(Z\|\boldsymbol{g} = g_{0,2})$ $\text{Max}(\Psi'(g_{0,2}))+\varepsilon_{0,2}$ $P(0,2) = (\delta_1^2\varphi_2^2)$	**B_1B_1** $\Psi'(g_2{=}0) = 0$ $P(g_2{=}0) = \delta_2^2$ **0**
$E(Z\|\boldsymbol{g} = g_{1,0})$ $\text{Max}(\Psi'(g_{1,0})))+\varepsilon_{1,0}$ $P(1,0) = \varphi_1^2(2(\varphi_2\delta_2))$	$E(Z\|\boldsymbol{g} = g_{1,1})$ $\text{Max}(\Psi'(g_{1,1}))+\varepsilon_{1,1}$ $P(1,1) = 2(\varphi_1\delta_1)2(\varphi_2\delta_2)$	$E(Z\|\boldsymbol{g} = g_{1,2})$ $\text{Max}(\Psi'(g_{1,2}))+\varepsilon_{1,2}$ $P(1,2) = \delta_1^2(2(\varphi_2\delta_2))$	**B_1B_2** $\Psi'(g_2{=}1) = (k_1{+}1)a_1$ $P(g_2{=}1) = 2(\varphi_2\delta_2)$ **1**
$E(Z\|\boldsymbol{g} = g_{2,0})$ $\text{Max}(\Psi'(g_{2,0}))+\varepsilon_{2,0}$ $P(2,0) = \varphi_1^2\delta_2^2$	$E(Z\|\boldsymbol{g} = g_{2,1})$ $\text{Max}(\Psi'(g_{2,1}))+\varepsilon_{2,1}$ $P(2,1) = (2(\varphi_1\delta_1)\delta_2^2)$	$E(Z\|\boldsymbol{g} = g_{2,2})$ $\text{Max}(\Psi'(g_{2,2}))+\varepsilon_{2,2}$ $P(2,2) = \delta_1^2\delta_2^2$	**B_2B_2** $\Psi'(g_2{=}2) = 2a_2$ $P(g_2{=}2) = \varphi_2^2$ **2**

Following Chapter 5, the Fisherian decomposition of $E(Z \mid \boldsymbol{g})$[123] yields the following genetic variance components:

$$\sigma^{2*}_{\Psi'(\boldsymbol{g})(c)} = +\sigma^{2*}_{A(c)} + \sigma^{2*}_{D(c)} + \sigma^{2*}_{EP(c)};$$

$$\sigma^{2*}_{A(c)} = \sigma^{2*}_{A_{1(c)}} + \sigma^{2*}_{A_{2(c)}};$$

$$\sigma^{2*}_{A_{1(c)}} = \frac{\sigma^2_{E(Z|g),g_1}}{2\varphi_1(1-\varphi_1)};$$

$$\sigma^{2*}_{A_{2(c)}} = \frac{\sigma^2_{E(Z|g),g_2}}{2\varphi_2(1-\varphi_2)};$$

$$\sigma^{2*}_{D(c)} = \sigma^{2*}_{D_1} + \sigma^{2*}_{D_2};$$

[123] Wherein $\mu_{E(Z|\boldsymbol{g})} = \varphi_1^2\,\mu_{s2} + 2(\varphi_1\delta_1)(\mu_{s2}+(k_1+1)a_1) + \delta_1^2\,(\mu_{s2}+2a_1) = \mu_{s2}+\mu_{s1}$. $\mu_{E(Z|\boldsymbol{g}=g_1)}=2(1-\varphi_1)=2\delta_1$; $\sigma^2_{\mu_{E(Z|\boldsymbol{g}=g_1)}} = 2\varphi_1(1-\varphi_1)$, and $\mu_{.1}=\frac{1}{\varphi^2}\varphi_1^2[{\delta_2}^2.0+2(\varphi_2\delta_2)(k_2+1)a_2+\delta_2^2.\,2a_2]$ $=\mu_{s2}$; $\mu_{.2}=\mu_{s2}+(k_1+1)a_1$; $\mu_{.3}=\mu_{s2}+2a_1$. $\sigma^2_{L_1}=2\delta_1a_1^2[2\delta_1(1-k_1\varphi_1+1)^2]+\varphi_1(k_1+1)^2$. $\mu_{E(Z|\boldsymbol{g}=g_2)}=2\delta_2$; $\sigma^2_{E(Z|\boldsymbol{g}=g_2)} = 2\varphi_2(1-\varphi_1)$; $\mu_{1.}=\mu_{s1}$; $\mu_{2.}=\mu_{s1}+(k_1+1)a_2$; $\mu_{3.}=\mu_{s1}+2a_2$; and $\sigma^2_{L_2}=$ $2\delta_2a_2^2[2\delta_2(1-k_2\varphi_2+1)^2]+\varphi_2(k_2+1)^2$.

$$\sigma^{2*}_{D_{1(c)}} = \sigma^{2*}_{L_{1(C)}} - \sigma^{2*}_{A_{1(c)}};$$

$$\sigma^{2*}_{D_{2(c)}} = \sigma^{2*}_{L_{2(C)}} - \sigma^{2*}_{A_{2(c)}};$$

$$\sigma^{2*}_{EP(c)} = \sigma^{2*}_{\Psi'(\boldsymbol{g})(c)} - \sigma^{2*}_{A(c)} - \sigma^{2*}_{D(c)}. \tag{6.6}$$

Please see Appendices A and B for numerical examples of a single architecture generated in R.

6.5. Focal Quantities and Criteria

Following the detailed descriptions of the four constructed architectures, we now lay forth the general aims of simulation studies I and II, their focal quantities, and the set of criteria employed to adjudicate the merits of both candidate explanations.

6.5.1. Simulation Study I: General Aims

To evaluate the tenability of both candidate explanations, the first simulation study was curated to adjudicate in quantitative terms: 1) the *degree* to which epistasis is manifest for architectures in which, $\varepsilon = [\mathbf{0}]$; 2) and *how far off the mark* the recovered epistatic effect sizes, are from their true value for architectures in which, $\varepsilon \neq [\mathbf{0}]$**.** In doing so, we will approximate a set of empirical distributions engendered by sampling over the parameter spaces of:

$$\Psi'(\boldsymbol{g})_{\mathbf{Max}}\text{: } [s\text{=}2,\ \Psi'(\boldsymbol{g})_{\mathbf{Max}},\ \vec{\theta},\ \boldsymbol{\varepsilon}_{3x3} = [0], H^2]; \tag{6.7}$$

$$\Psi'(\boldsymbol{g})_{\mathbf{Min}}\text{ : } [s\text{=}2,\ \Psi'(\boldsymbol{g})_{\mathbf{Min}},\ \vec{\theta},\ \boldsymbol{\varepsilon}_{3x3} = [0], H^2]; \tag{6.8}$$

$$\Psi'(\boldsymbol{g})_{\mathbf{Max,GE}}\text{: } [s\text{=}2,\ \Psi'(\boldsymbol{g})_{\mathbf{Max}},\ \vec{\theta},\ \boldsymbol{\varepsilon}_{3x3} = \begin{bmatrix} -0.360 & -0.202 & -0.029 \\ 0.090 & 0.740 & -0.389 \\ 0.096 & 0.123 & 0.511 \end{bmatrix}, H^2]; \tag{6.9}$$

$$\Psi'(\boldsymbol{g})_{\mathbf{Min,GE}}\text{: } [s\text{=}2,\ \Psi'(\boldsymbol{g})_{\mathbf{Min}},\ \vec{\theta},\ \boldsymbol{\varepsilon}_{3x3} = \begin{bmatrix} -0.502 & 0.886 & -0.581 \\ 0.131 & 0.116 & 0.714 \\ -0.078 & 0.318 & -0.825 \end{bmatrix}, H^2]. \tag{6.10}$$

Simulation Study I: Focal Quantities

Following the general aims of simulation study I, it is the case for each of the four legitimate architectures under consideration, we will approximate several empirical distributions of the derived population-level variance components (Λ_{σ^2}), standardized effects (Λ_{ω^2}), and associated biases ($\Lambda_{\phi'_{(c)}-\phi'}$). To this end, in the care of the 6075 legitimate architectures in which, $\varepsilon = [\mathbf{0}]$, the focal quantities of interest include, the epistatic population-level variance component,

$$\sigma^2_{EP} = E(\Psi'(\boldsymbol{g}) - \Psi'(\boldsymbol{g})_{\mathbf{Main}})^2; \tag{6.11}$$

its standardized effect,

$$\omega^2_{EP} = \frac{\sigma^2_{EP}}{\sigma^2_Z}; \tag{6.12}$$

and effect size,

$$\phi'^{*} = \sqrt{\frac{\sigma^2_{EP}}{\sigma^2_R}}. \tag{6.13}$$

Naturally, concomitant to the population-level effects of epistasis, we will also derive the population level genetic-variance components: σ^2_{A}, σ^2_{D} and report the empirical distributions of their standardized effects, $\omega^2_A = \frac{\sigma^2_A}{\sigma^2_Z}$, $\omega^2_D = \frac{\sigma^2_D}{\sigma^2_Z}$.

Next, for all legitimate architectures in which, $\varepsilon \neq [\mathbf{0}]$, the focal quantities include both the true and *contaminated* epistatic population level variance components[124],

$$\sigma^2_{EP} = E(\Psi'(\boldsymbol{g}) - \Psi'(\boldsymbol{g})_{\mathbf{Main}})^2;$$

$$\sigma^2_{EP(c)} = E(E(Z|\boldsymbol{g}) - E(Z|\boldsymbol{g})_{Main})^2; \tag{6.14}$$

standardized effects,

$$\omega^2_{EP} = \frac{\sigma^2_{EP}}{\sigma^2_Z};$$

[124] For the sake of brevity, only the contaminated effects will be reported, as true effects are listed (6.10, 6.11, 6.12).

$$\omega^2_{EP(c)} = \frac{\sigma^2_{EP(c)}}{\sigma^2_Z}; \tag{6.15}$$

effect sizes,

$$\phi'^* = \sqrt{\frac{\sigma^2_{EP}}{\sigma^2_R}};$$

$$\phi'^*_{(c)} = \sqrt{\frac{\sigma^2_{EP(C)}}{\sigma^2_R}}; \tag{6.16}$$

and associated biases,

$$\phi'^*_{(c)} - \phi'^*; \tag{6.17}$$

$$|\phi'^*_{(c)} - \phi'^*|; \tag{6.18}$$

$$\omega^2_{EP(c)} - \omega^2_{EP.} \tag{6.19}$$

Naturally, for architectures of this sort, we will also derive the quantities: $\sigma^2_{\mathrm{A(c)}}, \sigma^2_{\mathrm{D(c)}}, \sigma^2_R, \sigma^2_{\varepsilon(g)}$, and report the empirical distributions of their standardized effects, $\omega^2_{A(c)} = \frac{\sigma^2_{A(c)}}{\sigma^2_{Z(c)}}$, $\omega^2_D = \frac{\sigma^2_{D(c)}}{\sigma^2_{Z(c)}}$, $\omega^2_{\varepsilon(g)} = \frac{\sigma^2_{\varepsilon(g)}}{\sigma^2_Z}$, $\omega^2_R = \frac{\sigma^2_R}{\sigma^2_Z}$, $\rho_{\Psi'(g),\gamma(\mathrm{E})}$[125].

Simulation Study I: Adjudication of Candidate Explanations

To adjudicate the *degree* to which epistasis is manifest over the 6075 *legitimate* architectures of $\Psi'(\boldsymbol{g})_{\mathbf{Max}}$ (6.7) and $\Psi'(\boldsymbol{g})_{\mathbf{Min}}$ (6.8) construction, first, we will report numerical summaries[126] for the approximated empirical distributions, and the proportion of epistatic effect sizes classified under Cohens' guidelines (1988)[127]. In doing so, our aims are to address whether, on aggregate, epistatic effect sizes ϕ'^*arising under

---

[125] $\rho_{\Psi'(g),\mathrm{E}}$ refers to the *degree of variability* of the impact of environment on Z, conditional on subpopulations of individuals with the same genotype. Classified under Cohens guidelines (1988), as small ($\rho = 0.10$; $R^2 = 0.01$), medium ($\rho = 0.3$, ; $R^2 = 0.9$) , or large (ρ =0.5, $R^2 = 0.25$).

[126] For each empirical distribution we report the mean, standard deviation, minimum, maximum, and every 10^{th} percentile point.

[127] i.e., small ($\phi'^* = 0.10$; $\omega^2 = 0.01$,), medium ($\phi'^* = 0.25$, ; $\omega^2 = 0.058$) , and large ($\phi'^* = 0.4$, $\omega^2 = 0.137$).

architectures of epistatic construction are generally small. Second, to delineate the relationship between the empirical distribution of epistatic effects ($\Lambda_{\phi'}$) and its engendering architectures, we will analytically consider: 1) which architectures (and derived focal quantities) are associated with small, medium, and large epistatic effects, by sub-setting the empirical distribution $\Lambda_{\phi'}$ into its 1^{st}, 2^{nd}, and 3^{rd}quantiles and reporting the partitioned empirical distributions of each focal quantity; 2) the kinds of architectures which engender the three largest nominal values of ϕ'^{*}, by reporting the parametric construction $[\vec{\theta}^{*}, H^2]$ of the three architectures and its associated population variance components; 3) the role of genetic parameters in the variability of $\Lambda_{\phi'}$, by conducting a full-factorial ANOVA decomposition of $\Lambda_{\phi'}$ in terms of 127 estimable effects, which include pooled genetic main effects and interaction effects[128].

For the 5832 and 5076 *legitimate* architectures of $\Psi'(\boldsymbol{g})_{\mathbf{Max,GE}}$ (6.9) and $\Psi'(\boldsymbol{g})_{\mathbf{Min,GE}}$ (6.10) construction an additional aim is to evaluate *how far off the mark* the recovered epistatic effect sizes, are from their true value ($\phi'^{*}_{(c)}$-ϕ'^{*}). First, we will report both graphical and numerical summaries of their approximate empirical distributions for each focal quantity. Second, to delineate the relationship between the parametric construction of the engendering architectures and the manifest distribution of bias ($\Lambda_{\phi'_{(C)}-\phi'}$) we will analytically consider: 1) which architectures (and derived focal quantities) are associated with small, medium, and large bias by sub-setting $\Lambda_{\phi'_{(C)}-\phi'}$ into its 1^{st}, 2^{nd}, and 3^{rd} quantiles and reporting the partitioned empirical distributions of each focal quantity; 2) the kinds of architectures which engender the three largest nominal values of $|\phi'^{*}_{(c)} - \phi'^{*}|$, by reporting the parametric construction $[\vec{\theta}^{*}, H^2]$ of the three architectures and its associated population variance components; 3) the role of genetic parameters in the variability of $\Lambda_{\phi'_{(c)}-\phi'}$ by performing a full-factorial ANOVA decomposition of $\Lambda_{\phi'_{(c)}-\phi'}$, in terms of the 127 estimable genetic effects.

---

[128] 3 pooled genetic main-effects and H^2, $\binom{7}{2}$) = 21, 2-way interaction effects, with all others interaction effects collapsed into the category 'higher order effects' (i.e., the ($\binom{7}{3}$)= 35, 3-way interaction effects, ($\binom{7}{4}$)= 35, 4-way interaction effects, ($\binom{7}{5}$)= 21, 5-way interaction effects, ($\binom{7}{6}$)=7, 6-way interaction effects, and ($\binom{7}{7}$)=1, 7 way interaction effects).

6.5.2. Simulation Study II - General Aims

To adjudicate the tenability of both candidate explanations the second simulation study was curated to settle in quantitative terms: 1) the *performance of detection*[129] of a test procedure, over the empirical range of $\Lambda_{\phi'>0}$ for all admissible architectures in which, $\boldsymbol{\varepsilon} = [\mathbf{0}]$; 2) the *performance of detection* of the test procedure(s) over the empirical range of $\Lambda_{\phi'>0}$and $\Lambda_{\phi'_{(c)}>0}$, and the *magnitude/direction* of its departure, for all admissible architectures in which, $\boldsymbol{\varepsilon} \neq [\mathbf{0}]$. As the *performance of detection* is a function of ϕ'^*, n, a, for each architecture, we will approximate a set of unique distributions of power each coded to $\Lambda_{\phi'>0}(\Lambda_{\phi'_{(c)}>0})$ and the values selected for both $\boldsymbol{n}$ and $\boldsymbol{a}$. To this end, we now introduce the following components of simulation study II: 1) the tool of detection; 2) the special parameters $\boldsymbol{n}$ and $\boldsymbol{a}$; 3) the focal quantities; 4) and criteria of detection.

Tool of Detection

As we saw in Chapter 3, there exist manifold ways to test for the presence of epistasis, or equivalently, the circumstances in which $\sigma^2_{EP} > 0$. Naturally, to adjudicate a test procedure curated to render a sound decision regarding the hypothesis pair: $[H_0: \sigma^2_{EP} = 0;$ or $H_1: \sigma^2_{EP} \neq 0]$, an ideal scenario is one unabridged by reductions in power effectuated by family-wise corrections (concomitant to the sound testing of a family of component hypotheses) (Ramsey, 1978; Einot & Gabriel, 1975; Shaffer, 1995; Lehman & Romano, 2005). To this end, we selected the omnibus F-test statistic of interaction, constructed as follows:

$$F = \frac{(\vec{Z}-\boldsymbol{A}^*\hat{\vec{\theta}})' (\vec{Z}-\left(\boldsymbol{A}^*\hat{\vec{\theta}}\right)-\left(\vec{Z}-\boldsymbol{A}\hat{\vec{\theta}}_F\right)'\left(\vec{Z}-\boldsymbol{A}\hat{\vec{\theta}}_F\right)/\, df_{Int}}{\left(\vec{Z}-\boldsymbol{A}\hat{\vec{\theta}}_F\right)'\left(\vec{Z}-\boldsymbol{A}\hat{\vec{\theta}}_F\right)/\, df_{Resid}}\,^{130}. \tag{6.20}$$

---

[129] Recall for a tool of detection, its *performance* of detection is, in fact, the *power function*, $(1-\beta(\phi'^*, n, a)$ =P(T⊂ $R|\phi'^* > 0))$. Recall, of course, the power function takes as input a single realization of ϕ'^*, sample size (n), and Type I error rate (a) (see Chapter 5). As the selection of a delineates both the A and R on $\Delta[n, \phi'^* > 0]$, and the selection of n, a test procedures degrees of freedom, it follows, that for a particular test its power of detection is a function of all three parameters $[\phi'^*, n, a]$.

[130] Recall from (4.2) and (4.3), $\boldsymbol{A}$ is the 3^Sx$[1+3^S]$ design matrix of the *full* model, and $\boldsymbol{A}^*$ its *reduced* counterpart, while $\boldsymbol{A}\vec{\theta}$ and $\boldsymbol{A}^*\vec{\theta}$ denote the respective model fitted values. As before, s denotes the number of loci, and $\vec{Z}$, the $[1x3^s]$ vector of cell-means. As such, one may respectively derive the residual Sum of Squares (SS) and degrees of freedom (df) for both the *full* and *reduced* models: 1)

It is known that, if $\sigma_{EP}^2 = 0$, the distribution of the test-statistic is,

$$F \sim [2^s, 3^S(n\text{-}1)], \tag{6.21}$$

else,

$$ncF \sim [2^s, 3^S(n\text{-}1), \delta]^{131}. \tag{6.22}$$

Special Parameters n and a

The parameter values for both sample-size per genotype (n) and Type I error (a) were selected to encompass a range of empirically reasonable values to evaluate the functional relationship between power, n, and a. To this end, the two selected parameter vectors were:

$$\boldsymbol{n} = [10, 20, 50, 100, 500, 1000], \tag{6.23}$$

$$\boldsymbol{a} = [\,0.01, 0.05, 0.10, 0.20, 0.30, 0.40]. \tag{6.24}$$

Simulation Study II: Focal Quantities

Following the general aims of simulation study II, to adjudicate on aggregate the omnibus F-test of interactions performance of detection for each of the four admissible architectures under consideration, we will approximate 36 empirical distributions of power, the particulars of wit, we now elucidate in further detail. It is the case, for architectures in which, $\boldsymbol{\varepsilon} = [\mathbf{0}]$, each of the 6075 *admissible* $\Psi'(\boldsymbol{g})_{\mathbf{Max}}$ and $\Psi'(\boldsymbol{g})_{\mathbf{Min}}$ architectures generate a unique power function,

$$1 - \beta(\phi'^*, n, a) = \mathrm{P}(\mathrm{T} \sqsubset R \left| \phi'^* > 0 \right.) \tag{6.25}$$

coded to a particular nominal realization of ϕ'^* (drawn from $\Lambda_{\phi'>0}$) and a unique $[\boldsymbol{n},\boldsymbol{a}]$ pair. Accordingly, by sampling overall empirical realizations of $\Lambda_{\phi'>0}$, we are afforded an approximation of its empirical distribution,

---

$SS_{ResidF} = (\vec{Z} - \boldsymbol{A}^*\vec{\theta})'\,(\vec{Z} - (\boldsymbol{A}^*\vec{\theta})$; $df_{Int} = \binom{S}{2}.4 + \binom{S}{3}.8 + \cdots)$; 2) $SS_{ResidR} = (\vec{Z} - \boldsymbol{A}_F^*\vec{\theta}_F)'(\vec{Z} - \boldsymbol{A}_F^*\vec{\theta}_F)$; $df_{\text{residl}} = ([3^s\text{n}]\text{-}1)\text{-}2\text{s-}\ df_{Int}$).

131 $\delta = 3^S\, n\phi'^{*2}$.

$$\Lambda_{1-\beta(\phi',n,a)}. \tag{6.26}$$

To this end, we generate 36 distributions of power each coded to the empirical range of $\Lambda_{\phi'>0}$ and $\boldsymbol{n}$ and $\boldsymbol{a}$. Next, to evaluate the performance of detection on aggregate, we will derive and report two focal quantities: its *median value*,

$$\widetilde{\Lambda}_{1-\beta(\phi',n,a);} \tag{6.27}$$

and the *proportion of architectures wherein the performance of detection is deemed satisfactory* (say $\geq .90$),

$$\Lambda_{\mathrm{P}(1-\beta(\phi',n,a)\geq .90)}. \tag{6.28}$$

Now, for architectures in which, $\boldsymbol{\varepsilon} \neq [\mathbf{0}]$, for each of the 5238 and 4482 admissible $\Psi'(\boldsymbol{g})_{\mathbf{MaxGE}}$, and $\Psi'(\boldsymbol{g})_{\mathbf{Min,GE}}$ architectures, we generate *two* unique power functions,

$$1-\beta(\phi'^{*}, n, a) = P(\mathrm{T}\subset R\left|\phi'^{*}>0\right.),$$

$$1-\beta(\phi'^{*}_{(c)}, n, a) = P(T\subset R\left|\phi'^{*}_{(c)}>0\right.). \tag{6.29}$$

As before, each respective power function is coined to a nominal realization of $\phi'^{*}(\phi'^{*}_{(c)})$ and the unique $[\boldsymbol{n}, \boldsymbol{a}]$ pair. By sampling overall empirical realizations of $\Lambda_{\phi'>0}$, and $\Lambda_{\phi'_{(c)}>0}$, for each architecture, we are afforded an approximation of its true and contaminated empirical distributions of power,

$$\Lambda_{1-\beta(\phi',n,a);}$$

$$\Lambda_{1-\beta(\phi'_{(c)},n,a);} \tag{6.30}$$

and from the 36 distributions coded to the crossings of $\boldsymbol{n}$ and $\boldsymbol{a}$, we derive the focal quantities,

$$\widetilde{\Lambda}_{1-\beta(\phi',n,a)},$$

$$\widetilde{\Lambda}_{1-\beta(\phi'_{(c)},n,a);} \tag{6.31}$$

and

$\Lambda_{\mathrm{P}(1-\beta(\phi',n,a)\geq.90)},$

$\Lambda_{P(1-\beta(\phi'_{(c)},n,a)\geq.90)}.$ (6.32)

Naturally, bespoke to architectures of this sort, we will also quantify their magnitude and degree of departure, in its general sense,

$$[\Lambda_{1-\beta(\phi'_{(c)},n,a)} - \Lambda_{1-\beta(\phi',n,a)}] = [1\text{-}\,\beta(\phi'^{*}_{(c)}, n, a) - 1\text{-}\beta(\phi'^{*}, n, a)]. \quad (6.33)$$

in terms of its *median bias*,

$$[\widetilde{\Lambda}_{\,1-\beta(\phi'_{(c)},n,a)} - \widetilde{\Lambda}_{\,1-\beta(\phi',n,a)}]. \quad (6.34)$$

and finally, the bias engendered between the *proportion of architectures with satisfactory power*,

$$[\Lambda_{P(1-\beta(\phi'_{(c)},n,a)\geq.90)} - \Lambda_{\mathrm{P}(1-\beta(\phi',n,a)\geq.90)}]. \quad (6.35)$$

Detection Performance Criteria

All told, to adjudicate on aggregate the performance of detection of the omnibus F- test-statistic of interaction, we employ three *criteria of detection*: 1) the *median power profile* $\left(\widetilde{\Lambda}_{1-\,\beta(\phi'^{*},n,a)}\right)$, to assess what one can expect of the power of a particular test over the 36 unique combinations of $\boldsymbol{n}$, and $\boldsymbol{a}$; 2) the *proportion of architectures which yield power >0.90,* ($P(\Lambda_{1-\beta(\phi'^{*},n,a)} \geq 0.90)$, as indices of *how common* one may encounter an architecture where detection of epistasis is deemed satisfactory; and 3) finally bespoke to architectures in which, $\boldsymbol{\varepsilon} \neq [0]$, we evaluate further, the *magnitude and direction* of *bias* engendered by the former two criteria ($[\widetilde{\Lambda}_{\,1-\beta(\phi'_{(c)},n,a)} - \widetilde{\Lambda}_{\,1-\beta(\phi',n,a)}]$; $[\Lambda_{P(1-\beta(\phi'_{(c)},n,a)\geq.90)} - \Lambda_{\mathrm{P}(1-\beta(\phi',n,a)\geq.90)}]$). Naturally, possession of the latter criteria permits us the quantitative tools to quantify the kinds of departures present *if* architectures with the properties of epistasis *and* gene-environmental association do indeed alter in some *unfavourable* way the performance of the omnibus F test-statistic of interaction to detect epistasis.

6.6. Data Simulation

Both simulation study I and II were conducted and analyzed using R (R Core Team, 2016) and the following packages:

1) Dplyr ; Hadley Wickham, Romain François, Lionel Henry and Kirill Müller (2020). dplyr: A Grammar of Data Manipulation. R package version 0.8.5. https://CRAN.R-project.org/package=dplyr.

2) Knitr; Xie Y (2020). *knitr: A General-Purpose Package for Dynamic Report Generation in R*. R package version 1.28, https://yihui.org/knitr/.

3) Xtable; David B. Dahl, David Scott, Charles Roosen, Arni Magnusson and Jonathan Swinton (2019). xtable: Export Tables to LaTeX or HTML. R package version 1.8-4. https://CRAN.R-project.org/package=xtable.

4) Plotly; C. Sievert. Interactive Web-Based Data Visualization with R, plotly, and shiny.Chapman and Hall/CRC Florida, 2020.

5) Sjstats; Lüdecke D (2020). _sjstats: Statistical Functions for Regression Models (Version0.17.9)_. doi: 10.5281/zenodo.1284472 (URL: https://doi.org/10.5281/zenodo.1284472),<URL: https://CRAN.R-project.org/package=sjstats>.

6) Fmsb; Minato Nakazawa (2019). fmsb: Functions for Medical Statistics Book with some Demographic Data. R package version 0.7.0. https://CRAN.R-project.org/package=fmsb.

R-code for both simulations are included in the Appendices D-I.

Chapter 7. Results - Simulation Study I

Introduction

Recall, of course, our aims herein are to gain insight into the empirical range of $\Lambda_{\phi'}$ and $\Lambda_{\phi'_{(C)}-\phi'}$ to respectively resolve: 1) the degree to which epistasis is manifest for architectures in which, $\varepsilon = [\mathbf{0}]$; and 2) how far off the mark the recovered epistatic effect sizes, are from their true value for architectures in which, $\varepsilon \neq [\mathbf{0}]$**.** To this end, the results of the first simulation study are organized into four sections, in accordance with both architecture nomenclature and the terms of adjudication outlined in Chapter 6.

7.1. $\Psi'(g)_{\text{Max}}$ Architectures

7.1.1. Empirical Distributions

Table 7.1, and Table 7.2 respectively present the summary statistics and every 10th percentile points of the empirical distributions of standardized genetic effects. In Figure 7.1, the empirical distribution of epistatic effect sizes faceted by small, medium, and large departures, according to Cohen's guidelines (1988).

Table 7.1 Summary Statistics of Standardized Effects

	Mean	Median	SD	Min	Max
Additive	0.305	0.244	0.221	2.48e-05	0.799
Dominance	0.149	0.078	0.172	9.53e-07	0.798
Epistasis	0.046	0.012	0.089	4.27e-06	0.784
Effect Size	0.272	0.173	0.298	0.002	1.980

Table 7.2 Empirical Distributions of Standardized Effects

	.10	.20	.30	.40	.50	.60	.70	.80	.90
Additive	0.040	0.111	0.142	0.173	0.244	0.344	0.437	0.517	0.656
Dominance	0.009	0.022	0.037	0.055	0.078	0.129	0.163	0.246	0.407
Epistasis	0.001	0.002	0.004	0.007	0.012	0.022	0.037	0.062	0.128
Effect Size	0.037	0.058	0.096	0.124	0.173	0.213	0.300	0.424	0.654

Figure 7.1 Empirical Distribution of $\Psi'(\boldsymbol{g})_{\text{Max}}$ Effect Size

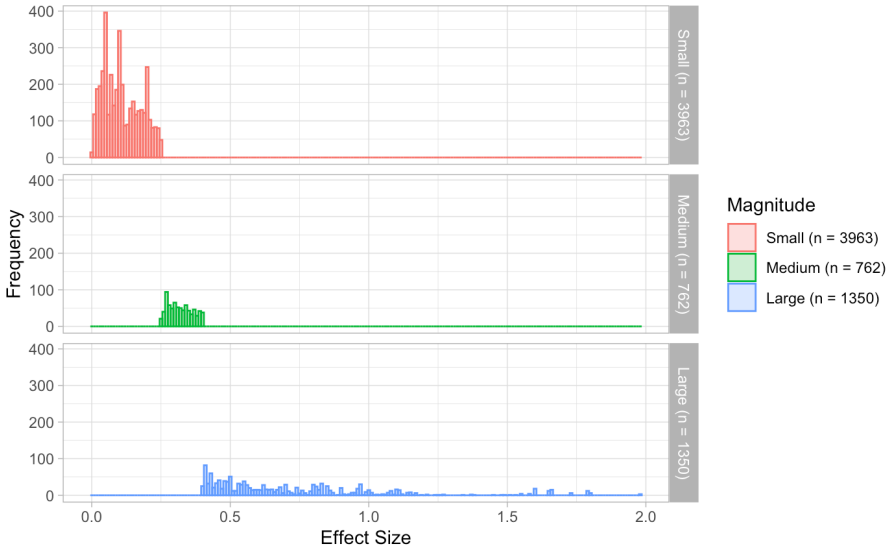

Do $\Psi'(\boldsymbol{g})_{\text{Max}}$ *architectures generate on aggregate small epistatic effect sizes* (ϕ'_{Max})*?*

Based upon an examination of Table 7.1, Table 7.2, and Figure 7.1, there is preliminary support for the first candidate hypothesis. While all 6075 architectures of $\Psi'(\boldsymbol{g})_{\text{Max}}$ construction, have the property of epistasis ($\sigma^2_{EP} > 0$), upon further inspection, it is clear the *average* magnitude of $\Lambda_{\phi'_{Max}}$ is small [median = 0.17, SD=0.30, min=0.002, max=1.98] according to Cohen's (1988) guidelines. Furthermore, it appears the *majority* of $\Lambda_{\phi'_{Max}}$ are classifiable as *small* [60^{th} percentile = 0.21], while the *minority* of $\Lambda_{\phi'_{Max}}$ are classifiable as medium [70th to 80th percentiles= 0.300-0.42] to large [90th to 100th percentiles=0.654-1.980].

7.1.2. Which Architectures go with which Effect Size

To evaluate which architectures and derived focal quantities are associated with different magnitudes of ϕ'_{Max} , we partitioned the empirical distribution of $\Lambda_{\phi'_{Max}}$, into its 1st, 2nd, and 3rd quantiles, respectively denoted as small, medium, and large[132], and summarize the magnitudes of $\Lambda'_{\omega^2_{\Psi'(g)}}$.

[132] Recall this particular distinction deviates from Cohen's guidelines and is based on the quantiles of the empirical distribution of ϕ'^*(small = 25th; medium = 50th; and large = 75th).

Architectures with Small Effect Sizes

Table 7.3 and Table 7.4 respectively present the summary statistics and every 10th percentile points for the empirical distributions of standardized genetic effects associated with the 1st quantile of the empirical distribution of epistatic effects.

Table 7.3 Summary Statistics of Standardized Effects – Small

Small Effect Size	Mean	Median	SD	Min	Max
Additive	0.218	0.168	0.174	2.48e-05	0.799
Dominance	0.129	0.069	0.148	9.53e-07	0.792
Epistasis	0.001	0.001	0.001	4.27e-06	0.005
Effect Size	0.043	0.045	0.019	0.002	0.076

Table 7.4 Empirical Distributions of Standardized Effects – Small

Small Effect Size	.10	.20	.30	.40	.50	.60	.70	.80	.90
Additive	0.0362	0.0904	0.1317	0.1456	0.1683	0.1872	0.1990	0.3618	0.4909
Dominance	0.0067	0.0196	0.0346	0.0607	0.0688	0.1235	0.1626	0.1853	0.3330
Epistasis	0.0001	0.0004	0.0006	0.0009	0.0011	0.0015	0.0019	0.0020	0.0026
Effect Size	0.0169	0.0249	0.0325	0.0366	0.0454	0.0493	0.0504	0.0583	0.0709

Architectures with Medium Effect Sizes

Table 7.5 and Table 7.6 respectively present the summary statistics and every 10th percentile points for the empirical distributions of standardized genetic effects associated with the 2nd quantile of the empirical distribution of epistatic effects.

Table 7.5 Summary Statistics of Standardized Effects – Medium

Medium Effect Size	Mean	Median	SD	Min	Max
Additive	0.314	0.302	0.222	9.926e-05	0.798
Dominance	0.151	0.080	0.181	8.729e-05	0.798
Epistasis	0.018	0.012	0.016	0.001	0.095
Effect Size	0.181	0.172	0.075	0.076	0.360

Table 7.6 Empirical Distributions of Standardized Effects – Medium

Medium Effect Size	.10	.20	.30	.40	.50	.60	.70	.80	.90
Additive	0.019	0.061	0.128	0.145	0.186	0.344	0.433	0.517	0.642
Dominance	0.007	0.015	0.038	0.055	0.096	0.136	0.172	0.265	0.488
Epistasis	0.003	0.005	0.007	0.008	0.010	0.020	0.030	0.047	0.069
Effect Size	0.083	0.100	0.114	0.161	0.197	0.211	0.240	0.274	0.393

Architectures with Large Epistatic Effect Sizes

Table 7.7 and Table 7.8 respectively present the summary statistics and every 10th percentile points for the empirical distributions of standardized genetic effects associated with the 3rd quantile of the empirical distribution of epistatic effects.

Table 7.7 Summary Statistics of Standardized Effects – Large

Large Effect Size	Mean	Median	SD	Min	Max
Additive	0.372	0.377	0.232	0.0007	0.770
Dominance	0.162	0.0924	0.1749	0.0003	0.759
Epistasis	0.147	0.1097	0.1308	0.026	0.78
Effect Size	0.682	0.568	0.325	0.360	1.98

Table 7.8 Empirical Distributions of Standardized Effects – Large

Large Effect Size	.10	.20	.30	.40	.50	.60	.70	.80	.90
Additive	0.060	0.119	0.199	0.286	0.377	0.480	0.545	0.611	0.692
Dominance	0.012	0.027	0.039	0.053	0.092	0.139	0.211	0.258	0.464
Epistasis	0.036	0.056	0.074	0.089	0.110	0.129	0.151	0.195	0.319
Effect Size	0.398	0.424	0.459	0.506	0.569	0.654	0.789	0.872	1.090

7.1.3. The Architectures yielding the Three Largest Epistatic Effect sizes

The three largest nominal values of ϕ'^{*}_{Max} were all equal to 1.98 and were generated by three distinct architectures of $\Psi'(\boldsymbol{g})_{\mathbf{Max}}$ construction:

$$\phi'^{*}_{Max1} = 1.98;\ \vec{\theta}^{*} = \begin{bmatrix} \alpha_1 = 44 \\ \alpha_2 = 44 \\ k_1 = 1 \\ k_2 = 1 \\ \varphi_1 = 0.1 \\ \varphi_2 = 0.1 \end{bmatrix};\ H^2 = 0.8;\ \omega^{2*}_{\Psi'_{(g)}} = \begin{bmatrix} \omega^{2*}_{A} = 0.002 \\ \omega^{2*}_{D} = 0.013 \\ \omega^{2*}_{EP} = 0.780 \end{bmatrix} \omega^{2*}_{E} = 0.20;$$

$$\phi'^{*}_{Max2} = 1.98;\ \vec{\theta}^{*} = \begin{bmatrix} \alpha_1 = 16 \\ \alpha_2 = 16 \\ k_1 = 1 \\ k_2 = 1 \\ \varphi_1 = 0.1 \\ \varphi_2 = 0.1 \end{bmatrix};\ H^2 = 0.8;\ \omega^{2*}_{\Psi'_{(g)}} = \begin{bmatrix} \omega^{2*}_{A} = 0.002 \\ \omega^{2*}_{D} = 0.013 \\ \omega^{2*}_{EP} = 0.780 \end{bmatrix} \omega^{2*}_{E} = 0.20;$$

$$\phi'^{*}_{Max3} = 1.98; \vec{\theta}^{*} = \begin{bmatrix} \alpha_1 = 32 \\ \alpha_2 = 32 \\ k_1 = 1 \\ k_2 = 1 \\ \varphi_1 = 0.1 \\ \varphi_2 = 0.1 \end{bmatrix}; H^2 = 0.8; \omega^{2*}_{\Psi'(g)} = \begin{bmatrix} \omega^{2*}_{A} = 0.002 \\ \omega^{2*}_{D} = 0.013 \\ \omega^{2*}_{EP} = 0.780 \end{bmatrix} \omega^{2*}_{E} = 0.20. \tag{7.1}$$

From (7.1), all three architectures which engendered the largest ϕ'^{*}_{Max} are characterized by: 1) *equal* additive effects between loci ($\alpha_1 = [44, 16, 32], \alpha_1 = [44, 16, 32]$); 2) *complete dominance* of the first allele[133] ($k_1 = 1, k_2 = 1$); 3) *small* recessive allele frequencies ($\varphi_1 = 0.1, \varphi_2 = 0.1$); and 4) *large* broad-sense heritability ($H^2 = 0.8$).

7.1.4. The Role of Genetic Parameters in Determining the Distribution of Epistatic Effect sizes

To quantitatively evaluate the dependency of $\Lambda_{\phi'_{Max}}$ on the set of genetic parameters $\vec{\theta}$ and H^2 we employ a full-factorial 7-way ANOVA decomposition of $\Lambda_{\phi'_{Max}}$ in in terms of the 127 estimable effects[134]. It turned out that 38.2% of the variability in $\Lambda_{\phi'_{Max}}$ was attributable to the pooled genetic main effects; 27.6% to 2-way interactions; and 33.1% to higher order interactions. The top five effects yield 48.7% of the variability in $\Lambda_{\phi'_{Max}}$, and include: 1) the main effect $H^2 = 0.23$; 2) pooled-main effect $\varphi_{\cdot} = 0.076$; 3) pooled main effect $k_{\cdot} = 0.062$; 4) 2-way interactions of $\alpha_1 : \alpha_2 = 0.059$; and 5) 2-way interactions $k_1 : k_2 = 0.051$.

7.2. $\Psi'(g)_{\text{Min}}$ Architectures

7.2.1. Empirical Distributions

Table 7.9 and Table 7.10 respectively present the summary statistics and every 10th percentile points of the empirical distributions of standardized genetic effects. In

[133] or equivalently, complete dominance of the homozygous genotype.

[134] 2^7-1 estimable genetic effects.

Figure 7.2, the empirical distribution of epistatic effect size is faceted by small, medium, and large departures, according to Cohen's guidelines (1988).

Table 7.9 Summary Statistics of Standardized Effects

	Mean	Median	SD	Min	Max
Additive	0.2739	0.1833	0.2212	1.467e-06	0.7906
Dominance	0.1535	0.0867	0.1872	0.0004	0.7999
Epistasis	0.0725	0.0104	0.1290	1.944e-06	0.7842
Effect Size	0.3253	0.1971	0.3849	0.0016	1.9801

Table 7.10 Empirical Distributions of Standardized Effects

	.10	.20	.30	.40	.50	.60	.70	.80	.90
Additive	0.0110	0.0602	0.1317	0.1514	0.1833	0.3292	0.3936	0.4941	0.6164
Dominance	0.0088	0.0230	0.0382	0.0522	0.0867	0.1282	0.1644	0.2090	0.4741
Epistasis	0.0003	0.0016	0.0034	0.0068	0.0104	0.0299	0.0605	0.1247	0.1906
Effect Size	0.0257	0.0499	0.0825	0.1140	0.1971	0.2402	0.3881	0.4867	0.8628

Figure 7.2 Empirical Distribution of $\Psi'(\boldsymbol{g})_{\text{Min}}$ Effect Sizes

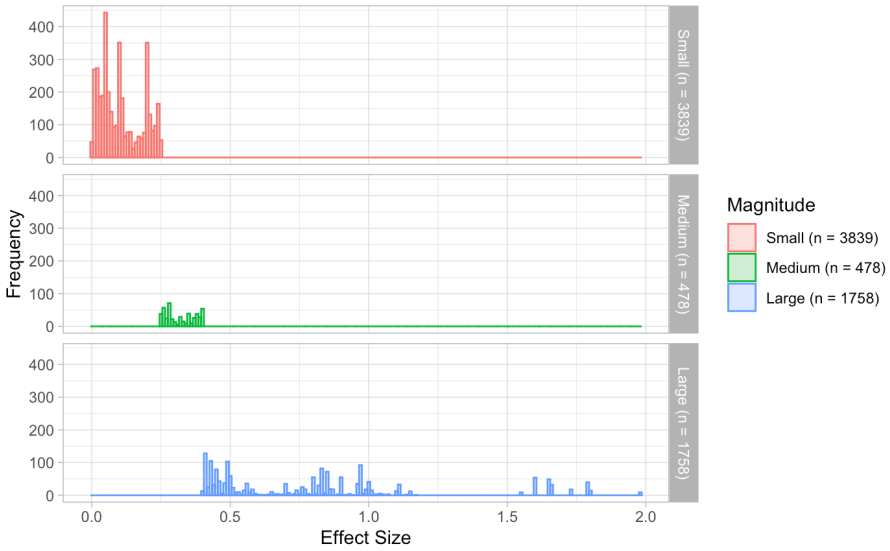

Do $\Psi'(\boldsymbol{g})_{Min}$ architectures generate small epistatic effect sizes, ϕ'_{Min}?

Based upon an examination of Tables 7.9, Table 7.10, and Figure 7.2 there is preliminary support for the first candidate hypothesis. While all 6075 architectures of $\Psi'(\boldsymbol{g})_{\text{Min}}$ epistatic construction, have the property of epistasis, upon further inspection, it is clear the *average* magnitude of $\Lambda_{\phi'_{Min}}$ is small [median $= 0.21$, SD $= 0.38$, min $= 0.0016$, max$= 1.98$], according to Cohen's (1988) guidelines. Furthermore, it appears the *majority*

of $\Lambda_{\phi'_{Min}}$ are classifiable as small [60^{th} percentile= 0.24], while the *minority* of $\Lambda_{\phi'_{Min}}$ are classifiable as medium [70th percentile =0.39] to large [80th to 90th percentiles, 0.49-0.86].

7.2.2. Which Architectures go with which Effect sizes

To evaluate which architectures and derived focal quantities are associated with different magnitudes of ϕ'_{Min} , we partitioned the empirical distribution of $\Lambda_{\phi'_{Min}}$, into its 1st, 2nd, and 3rd quantiles $\Lambda'_{\phi'_{Min}}$, respectively denoted as small, medium and large, and summarize the magnitudes of $\Lambda'_{\omega^2_{\Psi'(g)}}$.

Architectures with Small Effect Sizes

Table 7.11 and Table 7.12 respectively present the summary statistics and every 10th percentile points for the empirical distributions of standardized genetic effects associated with the 1st quantile of the empirical distribution of epistatic effects.

Table 7.11 Summary Statistics of Standardized Effects – Small

Small Effect Size	Mean	Median	SD	Min	Max
Additive	0.212	0.158	0.185	1.467e-06	0.668
Dominance	0.148	0.111	0.164	0.0004	0.799
Epistasis	0.0009	0.0005	0.0008	1.944e-06	0.003
Effect Size	0.033	0.034	0.017	0.0016	0.060

Table 7.12 Empirical Distributions of Standardized Effects – Small

Small Effect Size	.10	.20	.30	.40	.50	.60	.70	.80	.90
Additive	0.0032	0.0309	0.1317	0.1514	0.1582	0.1804	0.3456	0.3830	0.5529
Dominance	0.0192	0.0398	0.0486	0.0663	0.1112	0.1363	0.1628	0.1956	0.2470
Epistasis	5.207e-05	0.0001	0.0002	0.0003	0.0005	0.0008	0.0016	0.0019	0.0020
Effect Size	0.0093	0.0145	0.0202	0.0259	0.0344	0.0430	0.0490	0.0499	0.0540

Architectures with Medium Effect Sizes

Table 7.13 and 7.14 respectively present the summary statistics and every 10th percentile points for the empirical distributions of focal quantities associated with the 2nd quantile of the empirical distribution of epistatic effects.

Table 7.13 Summary Statistics of Standardized Effects – Medium

Medium Effect Size	Mean	Median	SD	Min	Max
Additive	0.292	0.185	0.234	6.364e-05	0.790
Dominance	0.169	0.095	0.209	0.0004	0.799
Epistasis	0.026	0.010	0.032	0.0007	0.137
Effect Size	0.200	0.197	0.104	0.060	0.430

Table 7.14 Empirical Distributions of Standardized Effects – Medium

Medium Effect Size	.10	.20	.30	.40	.50	.60	.70	.80	.90
Additive	0.0190	0.0611	0.1276	0.1447	0.1857	0.3439	0.4334	0.5169	0.6418
Dominance	0.0072	0.0148	0.0375	0.0545	0.0955	0.1364	0.1721	0.2653	0.4877
Epistasis	0.0034	0.0050	0.0068	0.0080	0.0104	0.0198	0.0301	0.0472	0.0690
Effect Size	0.0834	0.0999	0.1140	0.1614	0.1971	0.2114	0.2402	0.2739	0.3935

Architectures with Large Effect Sizes

Table 7.15 and Table 7.16 respectively present the summary statistics and every 10th percentile points for the empirical distributions of standardized genetic effects associated with the 3rd quantile of the empirical distribution of epistatic effects.

Table 7.15 Summary Statistics of Standardized Effects – Large

Large Effect Size	Mean	Median	SD	Min	Max
Additive	0.298	0.250	0.217	0.001	0.744
Dominance	0.127	0.049	0.155	0.002	0.740
Epistasis	0.237	0.164	0.168	0.037	0.784
Effect Size	0.871	0.825	0.398	0.430	1.980

Table 7.16 Empirical Distributions of Standardized Effects – Large

Large Effect Size	.10	.20	.30	.40	.50	.60	.70	.80	.90
Additive	0.021	0.069	0.144	0.221	0.250	0.354	0.439	0.550	0.596
Dominance	0.009	0.016	0.030	0.038	0.049	0.089	0.130	0.206	0.336
Epistasis	0.095	0.115	0.125	0.146	0.164	0.192	0.266	0.372	0.545
Effect Size	0.456	0.487	0.556	0.756	0.825	0.863	0.972	1.017	1.650

7.2.3. The Architectures Yielding the Three Largest Epistatic Effect Sizes

The three largest nominal values of ϕ'^{*}_{Min} were all equal to 1.98 and were generated by three distinct architectures of $\Psi'(\boldsymbol{g})_{\mathbf{Min}}$ construction:

$$\phi'^{*}_{Min1} = 1.98;\ \vec{\theta}^{*} = \begin{bmatrix} \alpha_1 = 16 \\ \alpha_2 = 16 \\ k_1 = -1 \\ k_2 = -1 \\ \varphi_1 = 0.9 \\ \varphi_2 = 0.9 \end{bmatrix};\ H^2 = 0.8;\ \omega^2_{\Psi'(g)} = \begin{bmatrix} \omega^2_A = 0.003 \\ \omega^2_D = 0.013 \\ \omega^2_{EP} = 0.784 \end{bmatrix};\ \omega^2_E = 0.20$$

$$\phi'^{*}_{Min2} = 1.98;\ \vec{\theta}^{*} = \begin{bmatrix} \alpha_1 = 16 \\ \alpha_2 = 32 \\ k_1 = -1 \\ k_2 = -1 \\ \varphi_1 = 0.9 \\ \varphi_2 = 0.9 \end{bmatrix};\ H^2 = 0.8;\ \omega^2_{\Psi'_{(g)}} = \begin{bmatrix} \omega^2_A = 0.003 \\ \omega^2_D = 0.013 \\ \omega^2_{EP} = 0.784 \end{bmatrix};\ \omega^2_E = 0.20$$

$$\phi'^{*}_{Min3} = 1.98;\ \vec{\theta}^{*} = \begin{bmatrix} \alpha_1 = 16 \\ \alpha_2 = 44 \\ k_1 = -1 \\ k_2 = -1 \\ \varphi_1 = 0.9 \\ \varphi_2 = 0.9 \end{bmatrix};\ H^2 = 0.8;\ \omega^2_{\Psi'_{(g)}} = \begin{bmatrix} \omega^2_A = 0.003 \\ \omega^2_D = 0.013 \\ \omega^2_{EP} = 0.784 \end{bmatrix} \omega^2_E = 0.20 \qquad (7.2)$$

From (7.2), the three architectures which engender the largest ϕ'^{*}_{Min} are characterized by: 1) *equal* additive effects for the first locus ($\alpha_1 = [16,16,16]$), while additive effects *vary* over $\boldsymbol{a}$ for the second ($\alpha_2 = [16,32,44]$); 2) *complete dominance* of the second allele[135] for both loci ($k_1 = -1, k_2 = -1$); 3) *large* recessive allele frequencies for both loci ($\varphi_1 = 0.9, \varphi_2 = 0.9$); and 4) *large* broad-sense heritability ($H^2 = 0.8$).

7.2.4. The Role of Genetic Parameters in Determining the Distribution of Epistatic Effect Sizes

To quantitatively evaluate the variability of $\Lambda_{\phi'_{\mathrm{Min}}}$ on the set of genetic parameters $\vec{\theta}$ and H^2 we employ a full-factorial 7-way ANOVA decomposition of $\Lambda_{\phi'_{Min}}$ in terms of the 127 estimable effects. It turned out that, 54% of the variability in $\Lambda_{\phi'_{Min}}$ is attributed to pooled genetic main effects; 32% 2-way interactions, and 14% to higher-order interactions. The top five effects yield 65.5% of the variability in $\Lambda_{\phi'_{Min}}$ are: 1) main effect $H^2 = 0.20$; 2) pooled main-effect $k_{\cdot} = 0.17$; 3) pooled main effect $\varphi_{\cdot} = 0.16$; 4) 2-way interaction $k_1 : k_2 = 0.077$; and 5) 2-way interaction $k_1 : \varphi_1 = 0.036$.

[135] Or equivalently, complete dominance of the homozygous genotype.

7.3. $\Psi'(g)_{\text{Max,GE}}$ Architectures

7.3.1. Empirical Distributions

Empirical Distributions of Bias

Table 7.17 and Table 7.18 respectively present the summary statistics and every 10th percentiles point of the empirical distributions of bias.

Table 7.17 Empirical Distribution of Bias

.10	.20	.30	.40	.50	.60	.70	.80	.90
-0.0105	-0.0053	-0.0028	-0.0011	0.0023	0.0047	0.0082	0.0149	0.0345

Table 7.18 Summary Statistics of Absolute Bias

Mean	Median	SD	Min	Max
0.034	0.007	0.126	0.000306	1.761

How far off the mark are the recovered $\phi'_{MaxGE(c)}$ *from* ϕ'_{MaxGE}?

Based on examination of Tables 7. 17 and Table 7.18, it appears the departure between contaminated and true ϕ' are *minimal* on aggregate for $\Lambda_{|\phi'_{MaxGE(c)} - \phi'_{MaxGE|}}$ [median=0.007, SD=0.12, min=0.0004, max=1.76], and the circumstances in which $\phi'_{MaxGE(c)} > \phi'_{MaxGE}$ and $\phi'_{MaxGE(c)} < \phi'_{MaxGE}$ are relatively *equal* in proportion over $\Lambda_{\phi'_{MaxGE(c)} - \phi'_{MaxGE}}$.

Empirical Distributions of Standardized Effects

Table 7.19, Table 7.20, Table 7.21, and Table 7.22 respectively present the summary statistics and every 10th percentile points of the empirical distributions of standardized genetic effects and genetic bias. In Figure 7.3 and Figure 7.4, the empirical distributions of true and contaminated epistatic effect sizes were faceted by small, medium, and large departures. And finally, in Figure 7.5, the empirical distributions of bias associated with each standardized genetic effect.

Table 7.19 Summary Statistics -Standardized Effects

	Mean	Median	SD	Min	Max
Additive	0.242	0.156	0.225	0.000e+00	0.726
Dominance	0.227	0.165	0.221	0.009	0.800
Epistasis	0.026	1.018e-05	0.064	0.000e+00	0.555
Effect Size	0.156	0.003	0.263	0.000e+00	1.637
Additive.C	0.238	0.157	0.224	3.357e-06	0.671
Dominance.C	0.230	0.167	0.222	0.006	0.841
Epistasis.C	0.032	0.001	0.081	1.266e-07	0.776
Effect Size.C	0.179	0.038	0.310	0.000	2.444
G.E Association	0.013	4.954e-05	0.061	3.254e-07	0.672
Residual	0.500	0.499	0.246	0.044	0.886
G.E Correlation	0.109	0.255	0.440	-0.889	0.867
Effect Size Bias	0.023	0.002	0.128	-0.301	1.761

Table 7.20 Empirical Distributions- Standardized Effects

	.10	.20	.30	.40	.50	.60	.70	.80	.90
Additive	0.0001	0.0015	0.0477	0.1475	0.1561	0.2821	0.3869	0.4084	0.6188
Dominance	0.0426	0.0468	0.1053	0.1132	0.1646	0.1756	0.1996	0.4192	0.5644
Epistasis	0.000e+00	1.174e-33	3.854e-33	1.590e-32	1.018e-05	0.0047	0.0137	0.0317	0.0782
Effect Size	0.000e+00	5.733e-17	1.089e-16	1.920e-16	0.0025	0.0923	0.1680	0.2728	0.4778
Additive.C	0.0002	0.0016	0.0334	0.1453	0.1569	0.2523	0.3853	0.4047	0.6178
Dominance.C	0.0428	0.0473	0.1049	0.1138	0.1667	0.1791	0.2000	0.4309	0.5800
Epistasis.C	4.808e-06	1.643e-05	3.697e-05	0.0001	0.0007	0.0055	0.0154	0.0339	0.0819
Effect Size.C	0.0031	0.0059	0.0097	0.0170	0.0383	0.0932	0.1728	0.2893	0.5268
G.E Association	4.647e-06	9.850e-06	1.889e-05	3.109e-05	4.954e-05	7.702e-05	0.0001	0.0003	0.0012
Residual	0.1936	0.1990	0.2135	0.4940	0.4985	0.5037	0.7950	0.7990	0.8002
G.E Correlation	-0.6150	-0.2743	-0.1263	0.0481	0.2551	0.3128	0.3987	0.4966	0.5859
Effect Size Bias	-0.0105	-0.0053	-0.0028	-0.0011	0.0023	0.0047	0.0082	0.0149	0.0345

Table 7.21 Summary Statistic - Genetic Bias

	Mean	Median	SD	Min	Max
Additive Bias	-0.0117	-0.1100	0.3768	-0.6839	0.8405
Dominance Bias	0.0028	0.0006	0.0293	-0.2367	0.3191
Epistatic Bias	0.0059	2.922e-06	0.0430	-0.1082	0.5424
Effect Size Bias	0.0229	0.0023	0.1280	-0.3014	1.7612

Table 7.22 Empirical Distribution - Genetic Bias

	.10	.20	.30	.40	.50	.60	.70	.80	.90
Additive Bias	-0.4396	-0.2962	-0.2732	-0.1435	-0.1100	-0.0640	0.1815	0.3641	0.5185
Dominance Bias	-0.0021	-0.0004	6.513e-05	0.0003	0.0006	0.0010	0.0018	0.0034	0.0077
Epistatic Bias	-0.0026	-0.0011	-0.0004	-8.037e-05	2.922e-06	1.111e-05	3.046e-05	7.573e-05	0.0003
Effect Size Bias	-0.0105	-0.0053	-0.0028	-0.0011	0.0023	0.0047	0.0082	0.0149	0.0345

Figure 7.3 Empirical Distribution of $\Psi'(g)_{Max,GE}$ True Effect Sizes

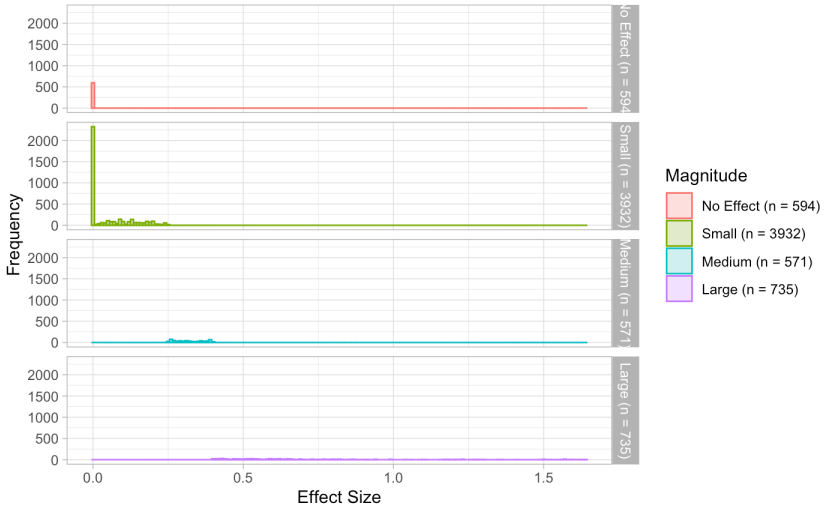

Figure 7.4 Empirical Distributions of $\Psi'(g)_{Max,GE}$ Contaminated Effect Sizes

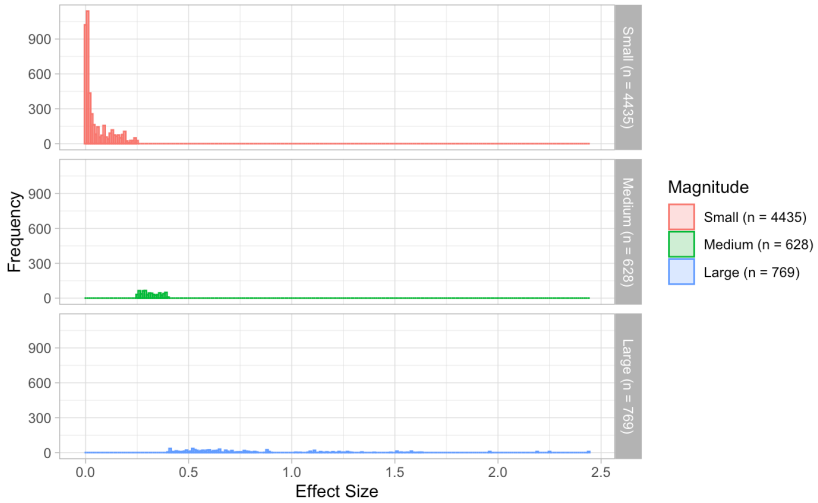

Figure 7.5 Empirical Distribution of Genetic Bias

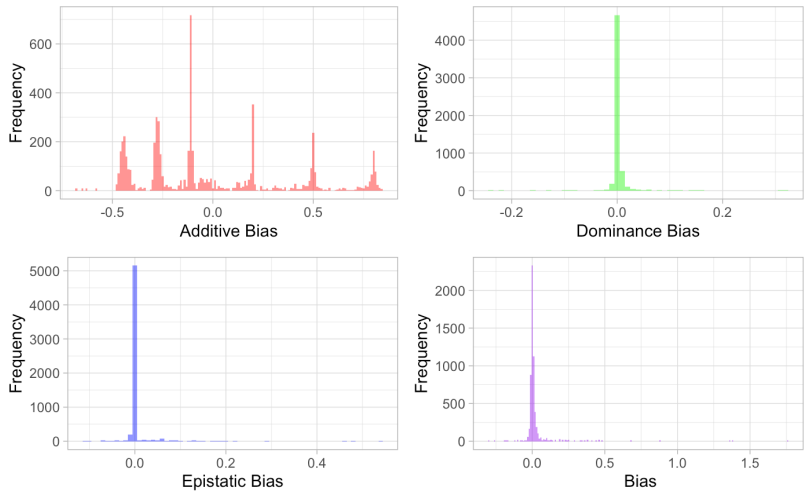

How far off the mark are the recovered values, $\omega^2_{\Psi'(\boldsymbol{g})(\boldsymbol{c})}$ from their true counterpart $\omega^2_{\Psi'(\boldsymbol{g})}$?

Based on the examination of Table 7.19, Table 7.20, Table 7.21, Table 7.22, and Figure 7.5 the departure between contaminated and true standardized genetic effects[136] are unique in both magnitude and direction across the 5382 empirical distributions. Upon further inspection, it is evident for $\Lambda_{\omega^2_{A(c)}-\omega^2_A}$ the departure between contaminated and true additive standardized effects are large on aggregate [median=-0.11, SD=0.37, min=-0.68, max=0.84], and the majority of bias in $\Lambda_{\omega^2_{A(c)}-\omega^2_A}$ occurs in the circumstance $\omega^2_{A(c)} < \omega^2_A$. Whereas for $\Lambda_{\omega^2_{D(c)}-\omega^2_D}$ the departure between contaminated and true standardized dominance effects are minimal on aggregate [median=0.0006, SD=0.02, min=-0.24, max=0.31], and the *majority* of cases occur in the circumstance $\omega^2_{D(c)} > \omega^2_D$. Finally, for $\Lambda_{\omega^2_{EP(c)}-\omega^2_{EP}}$ the departure between contaminated and true epistatic standardized effects are small on aggregate [median=2.9x10^{-6}, SD=0.04, min= -0.11, max=0.54], and the circumstances in which $\omega^2_{EP(c)} < \omega^2_{EP}$, and $\omega^2_{EP(c)} > \omega^2_{EP}$ occur are relatively equally over $\Lambda_{\omega^2_{EP(c)}-\omega^2_{EP}}$. Furthermore, in contrast to architectures in which, $\boldsymbol{\varepsilon} = [0]$, from Figures 6 and 7, there are 594 $\Psi'(\boldsymbol{g})_{\text{Max,GE}}$ architectures, which *do*

[136] Recall that $\omega^2_{\varepsilon(g)}$ is the proportion of variance in Z attributed to the dependency (or association) between the environmental effects and genotypic-values; ω^2_R – the proportion of variance in Z attributed to environment, *independent* of genetics; and $\rho_{\Psi'_{(g)},E}$ – the sensitivity or strength of the dependencies between environment and the genotypic-values (in a linear sense). As such, afore noted quantities will be respectively referred to (in the Tables and figures hereafter) as '*G.E Association*,' '*Residual*,' and '*G.E.Correlation.*'

not engender a *true* population-level effect of epistasis. To this end, only 5238 architectures have the property of epistasis and will be admitted into simulation study II.

7.3.2. Which Architectures go with which Magnitude of Bias

To gain insight into the sorts of architectures associated with particular magnitudes of $\Lambda_{\phi'_{MaxGE(c)} - \phi'_{MaxGE}}$, we partition the empirical distribution $\Lambda_{\phi'_{MaxGE(c)} - \phi'_{MaxGE}}$ into its 1st, 2nd, and 3rd quantiles (respectively denoted as small, medium, and large), and summarize the partitioned empirical distributions of both the standardized genetic effects and associated biases.

Architectures with Small Bias

Table 7.23, Table 7.24, Table 7.25, and Table 7.26 respectively present the summary statistics and every 10th percentile points of the empirical distributions of standardized genetic effects and genetic bias associated with the 1st quantile of the distribution of bias.

Table 7.23 Summary Statistics – Small Bias

Small Bias	Mean	Median	SD	Min	Max
Additive	0.2555	0.2019	0.2231	0.000e+00	0.6783
Dominance	0.2716	0.1737	0.2199	0.0094	0.7972
Epistasis	0.0719	0.0343	0.0986	0.0001	0.5544
Effect Size	0.4059	0.3152	0.3115	0.0266	1.6371
Additive.C	0.2501	0.1990	0.2205	1.186e-05	0.6419
Dominance.C	0.2741	0.1741	0.2214	0.0063	0.8017
Epistasis.C	0.0657	0.0300	0.0957	9.577e-05	0.5516
Effect Size.C	0.3859	0.2934	0.3102	0.0220	1.6272
G.E Association	0.0077	7.203e-05	0.0370	3.713e-06	0.3540
Residual	0.4102	0.4900	0.2237	0.1619	0.8861
G.E Correlation	-0.1050	-0.1471	0.4651	-0.8894	0.8672
Effect Size Bias	-0.0200	-0.0087	0.0407	-0.3014	-0.0039

Table 7.24 Empirical Distributions of Standardized Effects – Small Bias

Small Bias	.10	.20	.30	.40	.50	.60	.70	.80	.90
Additive	0.0007	0.0208	0.0595	0.1294	0.2019	0.3357	0.3780	0.5598	0.6021
Dominance	0.0514	0.1030	0.1285	0.1628	0.1737	0.2056	0.3527	0.4748	0.6739
Epistasis	0.0064	0.0128	0.0179	0.0274	0.0343	0.0495	0.0710	0.0912	0.1886
Effect Size	0.1225	0.1633	0.2020	0.2637	0.3152	0.3849	0.4828	0.5994	0.7875
Additive.C	0.0009	0.0218	0.0606	0.1156	0.1990	0.3184	0.3734	0.5401	0.6009
Dominance.C	0.0538	0.1034	0.1375	0.1634	0.1741	0.2152	0.3583	0.4743	0.6779
Epistasis.C	0.0053	0.0100	0.0154	0.0231	0.0300	0.0447	0.0602	0.0802	0.1831
Effect Size.C	0.1011	0.1445	0.1861	0.2494	0.2934	0.3615	0.4454	0.5827	0.7706
G.E Association	1.942e-05	3.053e-05	3.883e-05	5.247e-05	7.203e-05	9.323e-05	0.0001	0.0002	0.0005
Residual	0.1931	0.1979	0.2027	0.2101	0.4900	0.4982	0.5035	0.5122	0.8005
G.E Correlation	-0.7693	-0.5559	-0.4610	-0.2705	-0.1471	0.0344	0.2562	0.3370	0.5464
Effect Size Bias	-0.0290	-0.0174	-0.0128	-0.0105	-0.0087	-0.0071	-0.0062	-0.0053	-0.0045

Table 7.25 Genetic Bias Summary Statistics – Small Bias

Small Bias	Mean	Median	SD	Min	Max
Additive Bias	0.0186	-0.0800	0.3865	-0.6532	0.8012
Dominance Bias	0.0025	0.0005	0.0294	-0.1283	0.3113
Epistatic Bias	-0.0062	-0.0020	0.0153	-0.1082	-4.426e-05
Effect Size Bias	-0.0200	-0.0087	0.0407	-0.3014	-0.0039

Table 7.26 Genetic Bias Empirical Distribution – Small Bias

Small Bias	.10	.20	.30	.40	.50	.60	.70	.80	.90
Additive Bias	-0.4290	-0.3933	-0.2606	-0.1668	-0.0800	0.0064	0.2185	0.4523	0.6425
Dominance Bias	-0.0041	-0.0014	-0.0007	-9.976e-05	0.0005	0.0012	0.0020	0.0041	0.0082
Epistatic Bias	-0.0095	-0.0050	-0.0036	-0.0026	-0.0020	-0.0015	-0.0012	-0.0009	-0.0006
Effect Size Bias	-0.0290	-0.0174	-0.0128	-0.0105	-0.0087	-0.0071	-0.0062	-0.0053	-0.0045

Architectures with Medium Bias

Table 7.27, Table 7.28, Table 7.29, and Table 7.30 respectively present the summary statistics and every 10th percentile points of the empirical distributions of standardized genetic effects and genetic bias associated with the 2nd quantile of the distribution of bias.

Table 7.27 Summary Statistics – Medium Bias

Medium Bias	Mean	Median	SD	Min	Max
Additive	0.2009	0.1547	0.1985	0.000e+00	0.6419
Dominance	0.1826	0.1125	0.1923	0.0114	0.8000
Epistasis	0.0082	1.493e-32	0.0300	0.000e+00	0.5546
Effect Size	0.0569	1.750e-16	0.1163	0.000e+00	1.6359
Additive.C	0.2019	0.1548	0.1995	3.357e-06	0.6540
Dominance.C	0.1834	0.1130	0.1931	0.0110	0.8115
Epistasis.C	0.0081	2.628e-05	0.0297	1.266e-07	0.5521
Effect Size.C	0.0592	0.0076	0.1140	0.0004	1.6322
G.E Association	3.361e-05	1.594e-05	4.930e-05	3.254e-07	0.0004
Residual	0.6066	0.7938	0.2220	0.1807	0.8080
G.E Correlation	0.2402	0.3609	0.4008	-0.8894	0.8672
Effect Size Bias	0.0023	0.0023	0.0041	-0.0039	0.0112

Table 7.28 Empirical Distributions of Standardized Effects – Medium Bias

Medium Bias	.10	.20	.30	.40	.50	.60	.70	.80	.90
Additive	0.0001	0.0007	0.0131	0.1500	0.1547	0.1571	0.3710	0.3902	0.5689
Dominance	0.0423	0.0439	0.0468	0.1053	0.1125	0.1668	0.1864	0.1999	0.4995
Epistasis	0.000e+00	7.067e-34	1.921e-33	5.627e-33	1.493e-32	4.194e-32	0.0016	0.0068	0.0179
Effect Size	0.000e+00	3.270e-17	6.296e-17	9.220e-17	1.750e-16	3.651e-16	0.0488	0.0984	0.1815
Additive.C	0.0002	0.0007	0.0135	0.1495	0.1548	0.1587	0.3741	0.3917	0.5716
Dominance.C	0.0424	0.0445	0.0472	0.1055	0.1130	0.1670	0.1876	0.2014	0.5001
Epistasis.C	2.062e-06	4.808e-06	8.772e-06	1.643e-05	2.628e-05	5.564e-05	0.0015	0.0065	0.0175
Effect Size.C	0.0020	0.0031	0.0043	0.0059	0.0076	0.0097	0.0470	0.0957	0.1789
G.E Association	2.461e-06	4.669e-06	7.654e-06	1.038e-05	1.594e-05	2.178e-05	3.161e-05	5.054e-05	8.358e-05
Residual	0.1986	0.4944	0.4978	0.4996	0.7938	0.7979	0.7991	0.7997	0.8006
G.E Correlation	-0.4232	-0.0954	0.1149	0.2714	0.3609	0.3987	0.4863	0.5529	0.6297
Effect Size Bias	-0.0028	-0.0020	-0.0011	0.0011	0.0023	0.0033	0.0048	0.0064	0.0082

Table 7.29 Genetic Bias Summary Statistics – Medium Bias

Medium Bias	Mean	Median	SD	Min	Max
Additive Bias	-0.0175	-0.1098	0.3220	-0.4838	0.8115
Dominance Bias	0.0008	0.0004	0.0018	-0.0058	0.0115
Epistatic Bias	-0.0001	2.922e-06	0.0003	-0.0025	9.908e-05
Effect Size Bias	0.0023	0.0023	0.0041	-0.0039	0.0112

Table 7.30 Genetic Bias Empirical Distribution – Medium Bias

Medium Bias	.10	.20	.30	.40	.50	.60	.70	.80	.90
Additive Bias	-0.3531	-0.2789	-0.2554	-0.1138	-0.1098	-0.1036	0.1698	0.2009	0.4997
Dominance Bias	-0.0004	2.143e-05	9.392e-05	0.0002	0.0004	0.0006	0.0009	0.0014	0.0025
Epistatic Bias	-0.0005	-0.0002	-8.206e-05	7.877e-07	2.922e-06	6.188e-06	1.122e-05	1.840e-05	3.445e-05
Effect Size Bias	-0.0028	-0.0020	-0.0011	0.0011	0.0023	0.0033	0.0048	0.0064	0.0082

Architectures with Large Bias

Table 7.31, Table 7.32, Table 7.33, and Table 7.34 respectively present the summary statistics and every 10th percentile points of the empirical distributions of standardized genetic effects and genetic bias associated with the 3rd quantile of the distribution of bias.

Table 7.31 Summary Statistics – Large Bias

Large Effect	Mean	Median	SD	Min	Max
Additive	0.3103	0.3830	0.2578	0.000e+00	0.7256
Dominance	0.2728	0.1756	0.2543	0.0086	0.8000
Epistasis	0.0165	1.203e-32	0.0475	0.000e+00	0.3189
Effect Size	0.1034	1.745e-16	0.2589	0.000e+00	1.5669
Additive.C	0.2967	0.3257	0.2587	1.343e-05	0.6710
Dominance.C	0.2800	0.1779	0.2564	0.0104	0.8405
Epistasis.C	0.0465	0.0002	0.1147	2.475e-05	0.7760
Effect Size.C	0.2104	0.0270	0.4350	0.0112	2.4443
G.E Association	0.0429	0.0004	0.1116	3.024e-05	0.6718
Residual	0.3768	0.2318	0.2200	0.0440	0.8860
G.E Correlation	0.0607	0.1142	0.3926	-0.7240	0.8396
Effect Size Bias	0.1070	0.0270	0.2328	0.0112	1.7612

Table 7.32 Empirical Distributions of Standardized Effects – Large Bias

Large Bias	.10	.20	.30	.40	.50	.60	.70	.80	.90
Additive	1.775e-33	0.0010	0.0602	0.1550	0.3830	0.3902	0.6041	0.6244	0.6244
Dominance	0.0439	0.1098	0.1170	0.1650	0.1756	0.1796	0.2000	0.5000	0.7996
Epistasis	0.000e+00	5.547e-34	1.777e-33	3.662e-33	1.203e-32	2.455e-32	1.018e-31	0.0050	0.0499
Effect Size	0.000e+00	3.261e-17	6.699e-17	1.269e-16	1.745e-16	2.770e-16	7.099e-16	0.1114	0.4264
Additive.C	0.0002	0.0013	0.0134	0.1431	0.3257	0.3919	0.5211	0.6197	0.6351
Dominance.C	0.0463	0.1051	0.1141	0.1683	0.1779	0.1826	0.2101	0.5066	0.8007
Epistasis.C	3.926e-05	7.111e-05	0.0001	0.0001	0.0002	0.0003	0.0009	0.0588	0.1722
Effect Size.C	0.0131	0.0149	0.0169	0.0194	0.0270	0.0345	0.0632	0.2854	0.6530
G.E Association	8.102e-05	0.0001	0.0002	0.0003	0.0004	0.0007	0.0017	0.0414	0.1362
Residual	0.1796	0.1916	0.1966	0.2047	0.2318	0.4844	0.4971	0.5136	0.7704
G.E Correlation	-0.4506	-0.2568	-0.1609	-0.0833	0.1142	0.2551	0.3532	0.3988	0.5378
Effect Size Bias	0.0131	0.0149	0.0169	0.0194	0.0270	0.0345	0.0586	0.1083	0.2528

Table 7.33 Genetic Bias Summary Statistics – Large Bias

Large Bias	Mean	Median	SD	Min	Max
Additive Bias	-0.0303	-0.2626	0.4585	-0.6839	0.8405
Dominance Bias	0.0072	0.0023	0.0504	-0.2367	0.3191
Epistatic Bias	0.0300	0.0002	0.0799	2.475e-05	0.5424
Effect Size Bias	0.1070	0.0270	0.2328	0.0112	1.7612

Table 7.34 Genetic Bias Empirical Distribution – Large Bias

Large Bias	.10	.20	.30	.40	.50	.60	.70	.80	.90
Additive Bias	-0.4487	-0.4419	-0.4202	-0.2802	-0.2626	-0.0970	0.1282	0.5066	0.8005
Dominance Bias	-0.0083	-0.0020	0.0004	0.0014	0.0023	0.0039	0.0070	0.0125	0.0389
Epistatic Bias	3.926e-05	7.111e-05	0.0001	0.0001	0.0002	0.0003	0.0009	0.0369	0.0865
Effect Size Bias	0.0131	0.0149	0.0169	0.0194	0.0270	0.0345	0.0586	0.1083	0.2528

7.3.3. Architectures yielding the Three Largest Values of Absolute Bias

The three largest nominal values of $|\phi'_{MaxGE(c)} - \phi'_{MaxGE}|$ were all equal to 1.76, and were generated by three distinct architectures of $\Psi'(\boldsymbol{g})_{\mathbf{Max,GE}}$ epistatic construction, characterized by the following quantitative expressions and standardized genetic effects:

$$|\phi'^{*}_{MaxGE(c)} - \phi'^{*}_{MaxGE}| = 1.76,\ \vec{\theta}* = \begin{bmatrix} \alpha_1 = 16 \\ \alpha_2 = 16 \\ k_1 = -6 \\ k_2 = -1 \\ \varphi_1 = 0.1 \\ \varphi_2 = 0.9 \end{bmatrix};\ H^2 = 0.8;\ \omega^2_{\Psi'_{(g)}} = \begin{bmatrix} \omega^2_A = 0.144 \\ \omega^2_D = 0.648 \\ \omega^2_{EP} = 0.079 \end{bmatrix};$$

$$\omega^2_{\Psi'_{(g)C}} = \begin{bmatrix} \omega^2_{Ac} = 0.018 \\ \omega^2_{DC} = 0.727 \\ \omega^2_{EPC} = 0.210 \end{bmatrix};\ \begin{bmatrix} \omega^2_{\varepsilon(g)} = 0.34 \\ \omega^2_R = 0.044 \end{bmatrix};\ \rho_{\Psi'(g),\gamma(\mathrm{E})} = \text{-}0.177.$$

$$|\phi'^{*}_{MaxGE(c)} - \phi'^{*}_{MaxGE}|\ 1.76, \vec{\theta}* = \begin{bmatrix} \alpha_1 = 16 \\ \alpha_2 = 32 \\ k_1 = -6 \\ k_2 = -1 \\ \varphi_1 = 0.1 \\ \varphi_2 = 0.9 \end{bmatrix};\ H^2 = 0.8;\ \omega^2_{\Psi'_{(g)}} = \begin{bmatrix} \omega^2_A = 0.144 \\ \omega^2_D = 0.648 \\ \omega^2_{EP} = 0.079 \end{bmatrix};$$

$$\omega^2_{\Psi'_{(g)C}} = \begin{bmatrix} \omega^2_{Ac} = 0.018 \\ \omega^2_{DC} = 0.727 \\ \omega^2_{EPC} = 0.210 \end{bmatrix};\ \begin{bmatrix} \omega^2_{\varepsilon(g)} = 0.34 \\ \omega^2_R = 0.044 \end{bmatrix};\ \rho_{\Psi'(g),\gamma(\mathrm{E})} = \text{-}0.177.$$

$$|\phi'^{*}_{MaxGE(c)} - \phi'^{*}_{MaxGE}| = 1.76, \vec{\theta}* = \begin{bmatrix} \alpha_1 = 16 \\ \alpha_2 = 44 \\ k_1 = -6 \\ k_2 = -1 \\ \varphi_1 = 0.1 \\ \varphi_2 = 0.9 \end{bmatrix};\ H^2 = 0.8;\ \omega^2_{\Psi'_{(g)}} = \begin{bmatrix} \omega^2_A = 0.144 \\ \omega^2_D = 0.648 \\ \omega^2_{EP} = 0.079 \end{bmatrix};$$

$$\omega^2_{\Psi'_{(g)C}} = \begin{bmatrix} \omega^2_{Ac} = 0.018 \\ \omega^2_{DC} = 0.727 \\ \omega^2_{EPC} = 0.210 \end{bmatrix};\ \begin{bmatrix} \omega^2_{\varepsilon(g)} = 0.34 \\ \omega^2_R = 0.044 \end{bmatrix};\ \rho_{\Psi'(g),\gamma(\mathrm{E})} = \text{-}0.177. \tag{7.3}$$

From (7.3), the three architectures which engender the largest bias are characterized by: 1) *equal* additive effects for the first locus, while additive effects *vary* over $\boldsymbol{a}$ for the second ($\alpha_1 = [16,16,16], \alpha_2 = [16,32,44]$); 2) *under dominance* for the first locus, and *complete dominance* of the second allele for the second ($k_1 = -6, k_2 = -1$); 3) *small* recessive allele frequencies for the first locus, and *large* recessive allele frequencies

for the second ($\varphi_1 = 0.1, \varphi_2 = 0.9$); 4) *large* broad-sense heritability (H^2 = 0.8); and 5) *small* gene-environmental correlation ($\rho_{\Psi'(g),\gamma(\mathrm{E})}$= -0.117). Notably, the departure of 1.76 for all three architectures was engendered by the deviation between the contaminated epistatic effect $\phi'^{*}_{MinGE(C)}$ =2.19, and its true counterpart ϕ'^{*}_{MinGE} =0.426.

7.3.4. Role of Genetic Parameters in Determining the Distribution of Bias

To quantitatively evaluate the dependency of $\Lambda_{\phi'_{MaxGE(c)} - \phi'_{MaxGE}}$, on the set of genetic parameters $\vec{\theta}$ and H^2, we employ a full-factorial 7-way ANOVA decomposition of $\Lambda_{\phi'_{MaxGE(c)} - \phi'_{MaxGE}}$ in terms of the 127 estimable effects. It turned out that 12.2 % of the total variability in $\Lambda_{\phi'_{MaxGE(c)} - \phi'_{MaxGE}}$ is accounted for by pooled-genetic main effects 37.5% by 2-way interactions, and 50.3% by higher-order interactions. Of the 127 effects the top five effects sum to account for 65.1% of the total variability, and are as follows: 1) 2-way interaction k_1: k_2 = 24.6%; 2) 3-way interaction 3-way interaction k_1: φ_1: k_2= 19.4%; 3) 3-way interaction k_1: k_2: H_2 = 8.5%; 4) pooled main-effect k =11.2%; and 5) 3-way interaction k_1: φ_1: k_2= 6.3%.

7.4. $\Psi'(g)_{\mathrm{Min,GE}}$ Architectures

7.4.1. Empirical Distributions

Empirical Distributions of Bias

Table 7.35 and 7.36 respectively present the summary statistics and every 10th percentile points of the empirical distributions of bias.

Table 7.35 Summary Statistics of Absolute Bias

Mean	Median	SD	Min	Max
0.0660	0.0117	0.1506	0.0002	0.9914

Table 7.36 Empirical Distribution of Bias

.10	.20	.30	.40	.50	.60	.70	.80	.90
-0.0514	-0.0269	-0.0164	-0.0072	0.0006	0.0023	0.0044	0.0082	0.1853

How far off the mark are the recovered $\phi'^{*}_{MinGE(c)}$ *from* ϕ'^{*}_{MinGE}?

Based on an examination of Table 7.35 and Table 7.36 it appears the departure between contaminated and true ϕ' are *minimal* on aggregate. Furthermore, over $\Lambda_{|\phi'_{MinGE(c)} - \phi'_{MinGE|}}$ [median=0.011, SD=0.15, min=0.0002, max=0.99] it appears the circumstances in which $\phi'_{MinGE(c)} > \phi'_{MinGE}$ and $\phi'_{MinGE(c)} < \phi'_{MinGE}$ are relatively equal in proportion.

Empirical Distributions of Standardized Effects

Table 7.37, Table 7.38, Table 7.39, and Table 7.40 respectively present the summary statistics and every 10th percentile points of the empirical distributions of standardized genetic effects and genetic bias. In Figure 7.6 and Figure 7.7, respectively, the empirical distributions of true and contaminated effect sizes faceted by small, medium, and large departures according to Cohen's guidelines (1988). And finally, in Figure 7.8, the empirical distributions of bias associated with each standardized genetic effects.

Table 7.37 Summary Statistics of Standardized Effects

	Mean	Median	SD	Min	Max
Additive	0.2086	0.1584	0.1899	0.000e+00	0.7579
Dominance	0.1615	0.1018	0.1871	0.0034	0.7991
Epistasis	0.1070	0.0020	0.1521	0.000e+00	0.5559
Effect	0.3820	0.0596	0.5235	0.000e+00	2.9348
Additive.C	0.2258	0.1676	0.1972	4.432e-06	0.8507
Dominance.C	0.1812	0.1155	0.1877	0.0135	0.8957
Epistasis.C	0.1037	0.0365	0.1378	1.597e-07	0.5449
Effect.C	0.4088	0.2702	0.4863	0.0004	2.5776
G.E Association	0.0189	0.0003	0.0633	5.229e-07	0.6510
Residual	0.4894	0.5006	0.2444	0.0256	0.8070
G.E Correlation	-0.1392	-0.0207	0.4010	-0.9789	0.7334
Effect Size Bias	0.0268	0.0006	0.1617	-0.6970	0.9888

Table 7.38 Empirical Distributions of Standardized Effects

	.10	.20	.30	.40	.50	.60	.70	.80	.90
Additive	0.0015	0.0364	0.0743	0.1333	0.1584	0.1895	0.2768	0.3810	0.5677
Dominance	0.0263	0.0396	0.0473	0.0667	0.1018	0.1357	0.1636	0.1977	0.4939
Epistasis	0.000e+00	2.218e-33	1.407e-32	1.226e-08	0.0020	0.0778	0.1385	0.2251	0.3465
Effect Size	0.000e+00	6.624e-17	1.965e-16	0.0001	0.0596	0.3254	0.4732	0.7500	1.3081
Additive.C	0.0015	0.0465	0.0808	0.1499	0.1676	0.2220	0.3101	0.3922	0.5831
Dominance.C	0.0383	0.0461	0.0587	0.1004	0.1155	0.1499	0.1851	0.2352	0.4906
Epistasis.C	3.674e-06	9.496e-06	2.541e-05	0.0067	0.0365	0.0762	0.1270	0.2122	0.3183
Effect Size.C	0.0025	0.0049	0.0092	0.1066	0.2702	0.3265	0.5515	0.7772	1.2539
G.E Association	8.860e-06	2.092e-05	4.284e-05	0.0001	0.0003	0.0008	0.0022	0.0063	0.0624
Residual	0.1914	0.2025	0.2156	0.4869	0.5006	0.5047	0.7630	0.7981	0.8009
G.E Correlation	-0.7450	-0.5620	-0.4115	-0.2033	-0.0207	0.0822	0.1169	0.1691	0.2829
Effect Size Bias	-0.0514	-0.0269	-0.0164	-0.0072	0.0006	0.0023	0.0044	0.0082	0.1853

Table 7.39 Genetic Bias Summary Statistics

	Mean	Median	SD	Min	Max
Additive Bias	0.0172	0.0002	0.0557	-0.1122	0.6946
Dominance Bias	0.0197	0.0034	0.0470	-0.0229	0.3344
Epistatic Bias	-0.0034	6.325e-07	0.0326	-0.1334	0.2628
Effect Size Bias	0.0268	0.0006	0.1617	-0.6970	0.9888

Table 7.40 Genetic Bias Empirical Distribution

	.10	.20	.30	.40	.50	.60	.70	.80	.90
Additive Bias	-0.0051	-0.0019	-0.0005	-1.455e-05	0.0002	0.0029	0.0083	0.0222	0.0580
Dominance Bias	-0.0026	-0.0012	-0.0005	-0.0002	0.0034	0.0070	0.0122	0.0233	0.0482
Epistatic Bias	-0.0292	-0.0157	-0.0090	-0.0037	6.325e-07	3.736e-06	9.496e-06	2.608e-05	0.0139
Effect Size Bias	-0.0514	-0.0269	-0.0164	-0.0072	0.0006	0.0023	0.0044	0.0082	0.1853

Figure 7.6 **Empirical Distribution of True $\Psi'(g)_{\text{Min,GE}}$ Effect Sizes**

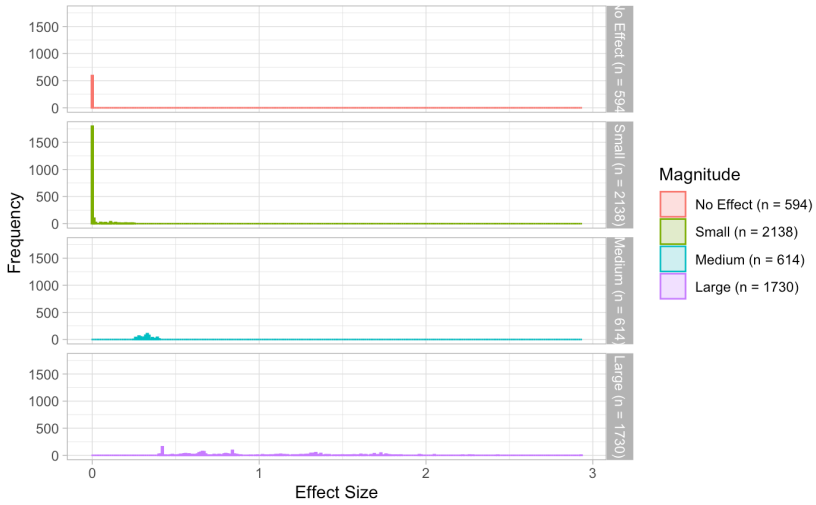

Figure 7.7 **Empirical Distribution of Contaminated $\Psi'(g)_{\text{Min,GE}}$ Effect Sizes**

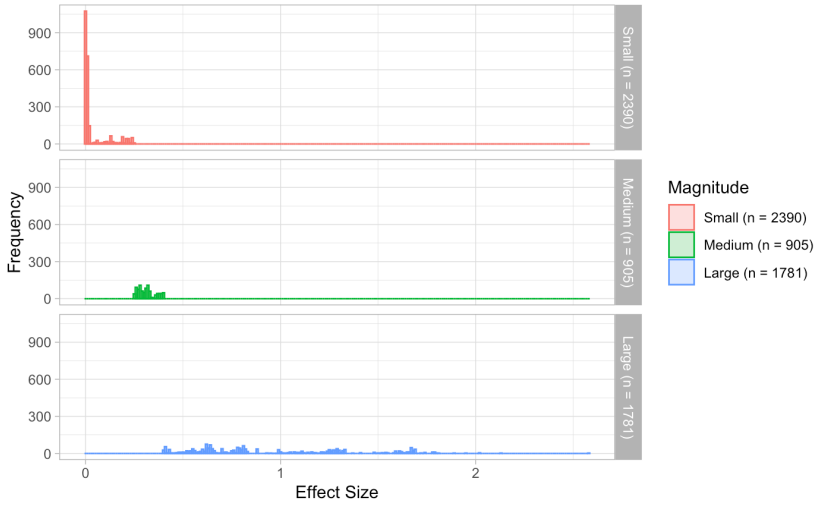

Figure 7.8 Empirical Distribution of Genetic Bias

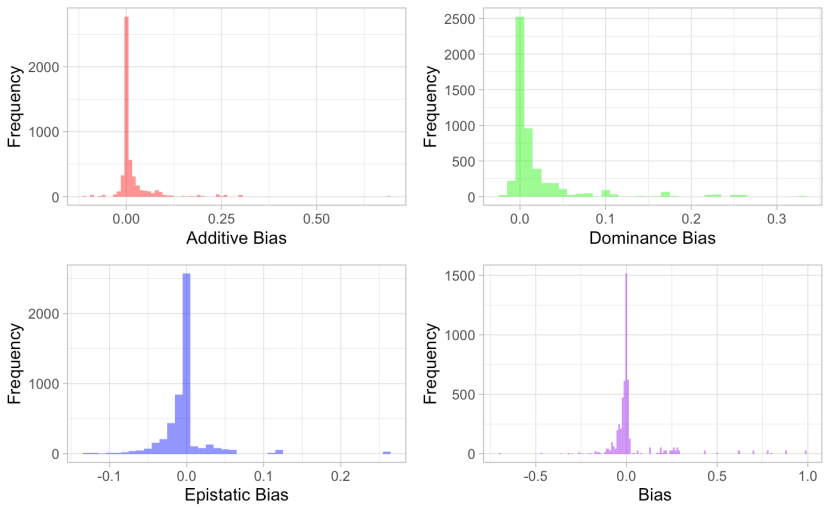

How far off the mark are the recovered values of $\omega^2_{\Psi'(g(C))}$ *from their true counterpart* $\omega^2_{\Psi'(g)}$?

Based on the examination of Table 7.37, Table 7.38, Table 7.39, Table 7.40, and Figure 7.8, it appears the departure between contaminated and true standardized genetic effects are unique in magnitude and direction across the 5072 empirical distributions. Upon further inspection, it is evident for $\Lambda_{\omega^2_{A(c)}-\omega^2_A}$ the departure between contaminated and true additive standardized effects are minimal on aggregate [median=0.0002, SD=0.05, min=-0.11, max=0.70], and the manifest bias $\Lambda_{\omega^2_{A(c)}-\omega^2_A}$ occurs relatively equal in proportion for the circumstances in which, $\omega^2_{A(c)} < \omega^2_A$ and $\omega^2_{A(c)} > \omega^2_A$. Similarly, for $\Lambda_{\omega^2_{D(c)}-\omega^2_D}$ the departure between contaminated and true standardized dominance effects are minimal on aggregate [median=0.03, SD=0.04, min=-0.02, max=0.33], and the proportion of $\Lambda_{\omega^2_{D(c)}-\omega^2_D}$, in which, $\omega^2_{D(c)} < \omega^2_D$ and $\omega^2_{D(c)} > \omega^2_D$ are relatively equal. Finally, for $\Lambda_{\omega^2_{EP(c)}-\omega^2_{EP}}$ the departure between contaminated and true epistatic standardized effects is considerably small on aggregate [median=6.3x10^{-7}, SD=0.03, min=-0.13, max=0.26]. However, it appears for the majority of $\Lambda_{\omega^2_{EP(c)}-\omega^2_{EP}}$, $\omega^2_{EP(c)} = \omega^2_{EP}$. Finally, from Figures 9 and 10, it is clear, there are 594 $\Psi'(\boldsymbol{g})_{\text{Min,GE}}$ architectures without the true population-level effect of epistasis, and thus only 4482 architectures were admitted into the second simulation study.

7.4.2. Which Focal Quantities go with which Magnitudes of Bias

We now turn to report the recovery of the focal values under various magnitudes of $\Lambda_{\phi'_{MinGE(c)} - \phi'_{MinGE}}$. As such, we partition the empirical distribution $\Lambda_{\phi'_{MinGE(c)} - \phi'_{MinGE}}$ into its 1st, 2nd, and 3rd quantiles respectively denoted as small, medium, and large, and summarize the magnitude of the empirical distributions of standardized effects and genetic biases.

Architectures with Small Bias

Table 7.41, Table 7.42, Table 7.43, and Table 7.44 respectively present the summary statistics and every 10th percentile points of the empirical distributions of standardized genetic effects and genetic bias associated with the 1st quantile of the distribution of bias.

Table 7.41 Summary Statistics - Small Bias

Small Bias	Mean	Median	SD	Min	Max
Additive	0.1839	0.1905	0.1094	0.000e+00	0.5893
Dominance	0.1319	0.0934	0.1358	0.0034	0.7454
Epistasis	0.2927	0.2967	0.1449	0.0098	0.5559
Effect	1.0432	1.0234	0.5050	0.1129	2.9348
Additive.C	0.2207	0.2193	0.1337	1.773e-05	0.7551
Dominance.C	0.1549	0.1128	0.1424	0.0159	0.8957
Epistasis.C	0.2602	0.2655	0.1375	0.0056	0.5409
Effect.C	0.9747	0.9328	0.4877	0.0852	2.5776
G.E Association	0.0116	0.0031	0.0503	0.0002	0.5571
Residual	0.3643	0.2017	0.2183	0.0256	0.8005
G.E Correlation	0.1286	0.1102	0.1395	-0.0537	0.6924
Effect Size Bias	-0.0685	-0.0448	0.0806	-0.6970	-0.0213

Table 7.42 Empirical Distributions - Small Bias

Small Bias	.10	.20	.30	.40	.50	.60	.70	.80	.90
Additive	0.0156	0.0739	0.1217	0.1653	0.1905	0.1997	0.2433	0.2847	0.3125
Dominance	0.0296	0.0389	0.0507	0.0623	0.0934	0.1087	0.1527	0.1595	0.3345
Epistasis	0.1162	0.1528	0.2106	0.2434	0.2967	0.3401	0.3470	0.3604	0.5529
Effect Size	0.3946	0.5805	0.6709	0.8170	1.0234	1.2607	1.3380	1.5001	1.7309
Additive.C	0.0186	0.0954	0.1602	0.1934	0.2193	0.2503	0.2875	0.3141	0.3471
Dominance.C	0.0403	0.0553	0.0660	0.0856	0.1128	0.1437	0.1722	0.2038	0.3532
Epistasis.C	0.0786	0.1283	0.1793	0.2079	0.2655	0.3005	0.3189	0.3406	0.4771
Effect Size.C	0.3419	0.5270	0.6170	0.7608	0.9328	1.1935	1.2760	1.4133	1.6708
G.E Association	0.0008	0.0012	0.0020	0.0025	0.0031	0.0041	0.0061	0.0094	0.0164
Residual	0.1633	0.1823	0.1907	0.1953	0.2017	0.4725	0.4880	0.4976	0.7832
G.E Correlation	-0.0338	0.0052	0.0787	0.1078	0.1102	0.1251	0.1489	0.2078	0.3275
Effect Size Bias	-0.1140	-0.0816	-0.0716	-0.0514	-0.0448	-0.0379	-0.0349	-0.0269	-0.0238

Table 7.43 Genetic Bias Summary Statistics- Small Bias

Small Bias	Mean	Median	SD	Min	Max
Additive Bias	0.0367	0.0193	0.0685	-0.0019	0.6946
Dominance Bias	0.0230	0.0164	0.0216	0.0041	0.1557
Epistatic Bias	-0.0326	-0.0243	0.0235	-0.1334	-0.0037
Effect Size Bias	-0.0685	-0.0448	0.0806	-0.6970	-0.0213

Table 7.44 Genetic Bias Empirical Distributions- Small Bias

Small Bias	.10	.20	.30	.40	.50	.60	.70	.80	.90
Additive Bias	0.0009	0.0029	0.0068	0.0130	0.0193	0.0266	0.0359	0.0521	0.0834
Dominance Bias	0.0074	0.0097	0.0115	0.0137	0.0164	0.0203	0.0231	0.0298	0.0460
Epistatic Bias	-0.0647	-0.0438	-0.0362	-0.0292	-0.0243	-0.0218	-0.0184	-0.0157	-0.0137
Effect Size Bias	-0.1140	-0.0816	-0.0716	-0.0514	-0.0448	-0.0379	-0.0349	-0.0269	-0.0238

Architectures with Medium Bias

Table 7.45, Table 7.46, Table 7.47, and Table 7.48 respectively present the summary statistics and every 10th percentile points of the empirical distributions of standardized genetic effects and genetic bias associated with the 2nd quantile of the distribution of bias.

Table 7.45 Summary Statistics- Medium Bias

Medium Bias	Mean	Median	SD	Min	Max
Additive	0.1751	0.1483	0.1801	0.000e+00	0.7489
Dominance	0.1496	0.1018	0.1722	0.0101	0.7991
Epistasis	0.0671	1.298e-05	0.1063	0.000e+00	0.5559
Effect	0.2362	0.0054	0.3331	0.000e+00	1.6859
Additive.C	0.1767	0.1468	0.1799	4.432e-06	0.8377
Dominance.C	0.1508	0.1016	0.1703	0.0135	0.7972
Epistasis.C	0.0645	2.905e-05	0.1033	1.597e-07	0.5449
Effect.C	0.2329	0.0088	0.3273	0.0004	1.6691
G.E Association	0.0005	3.372e-05	0.0030	5.229e-07	0.0412
Residual	0.6080	0.7882	0.2180	0.0619	0.8070
G.E Correlation	-0.3041	-0.2937	0.3854	-0.9789	0.5322
Effect Size Bias	-0.0033	0.0006	0.0077	-0.0209	0.0057

Table 7.46 Empirical Distributions - Medium Bias

Medium Bias	.10	.20	.30	.40	.50	.60	.70	.80	.90
Additive	0.0007	0.0026	0.0546	0.0760	0.1483	0.1583	0.1840	0.3815	0.3982
Dominance	0.0314	0.0396	0.0433	0.0516	0.1018	0.1160	0.1588	0.1976	0.4945
Epistasis	4.236e-34	5.188e-33	1.869e-32	2.497e-07	1.298e-05	0.0437	0.0847	0.1311	0.2160
Effect Size	2.299e-17	9.656e-17	1.925e-16	0.0006	0.0054	0.2793	0.3292	0.4170	0.6615
Additive.C	0.0007	0.0025	0.0621	0.0794	0.1468	0.1577	0.1892	0.3770	0.3961
Dominance.C	0.0357	0.0412	0.0461	0.0548	0.1016	0.1158	0.1608	0.1963	0.4899
Epistasis.C	2.025e-06	3.674e-06	5.972e-06	1.152e-05	2.905e-05	0.0406	0.0790	0.1261	0.2071
Effect Size.C	0.0017	0.0025	0.0035	0.0049	0.0088	0.2702	0.3176	0.4042	0.6509
G.E Association	4.640e-06	8.860e-06	1.367e-05	2.142e-05	3.372e-05	6.302e-05	0.0001	0.0003	0.0007
Residual	0.2055	0.4958	0.5013	0.5041	0.7882	0.7980	0.8002	0.8008	0.8019
G.E Correlation	-0.8459	-0.7270	-0.5930	-0.4391	-0.2937	-0.0581	0.0350	0.1142	0.1511
Effect Size Bias	-0.0164	-0.0113	-0.0072	-0.0035	0.0006	0.0015	0.0023	0.0031	0.0044

Table 7.47 Genetic Bias Summary Statistics- Medium Bias

Medium Bias	Mean	Median	SD	Min	Max
Additive Bias	0.0016	-1.206e-05	0.0078	-0.0190	0.0888
Dominance Bias	0.0012	-0.0003	0.0052	-0.0191	0.0493
Epistatic Bias	-0.0027	6.325e-07	0.0039	-0.0157	6.322e-05
Effect Size Bias	-0.0033	0.0006	0.0077	-0.0209	0.0057

Table 7.48 Genetic Bias Empirical Distribution- Medium Bias

Medium Bias	.10	.20	.30	.40	.50	.60	.70	.80	.90
Additive Bias	-0.0034	-0.0016	-0.0008	-0.0002	-1.206e-05	3.161e-05	0.0009	0.0035	0.0083
Dominance Bias	-0.0024	-0.0014	-0.0009	-0.0005	-0.0003	-0.0001	0.0025	0.0041	0.0066
Epistatic Bias	-0.0092	-0.0062	-0.0037	-0.0010	6.325e-07	2.115e-06	3.733e-06	5.927e-06	1.152e-05
Effect Size Bias	-0.0164	-0.0113	-0.0072	-0.0035	0.0006	0.0015	0.0023	0.0031	0.0044

Architectures with Large Bias

Table 7.49, Table 7.50, Table 7.51, and Table 7.52 respectively present the summary statistics and every 10^{th} percentile points of the empirical distributions of standardized genetic effects and their genetic bias associated with the 3^{rd} quantile of the distribution of bias.

Table 7.49 Summary Statistics - Large Bias

Large Bias	Mean	Median	SD	Min	Max
Additive	0.3002	0.1895	0.2371	0.0012	0.7579
Dominance	0.2149	0.1628	0.2416	0.0105	0.7988
Epistasis	0.0012	2.465e-33	0.0076	0.000e+00	0.0714
Effect	0.0122	7.843e-17	0.0569	0.000e+00	0.4787
Additive.C	0.3290	0.3191	0.2397	0.0012	0.8507
Dominance.C	0.2682	0.1837	0.2293	0.0205	0.7971
Epistasis.C	0.0256	0.0027	0.0456	7.000e-06	0.2628
Effect.C	0.1945	0.0591	0.2565	0.0058	0.9888
G.E Association	0.0629	0.0102	0.1039	1.131e-05	0.6510
Residual	0.3773	0.3118	0.1998	0.0567	0.8016
G.E Correlation	-0.0773	-0.0016	0.4439	-0.8576	0.7334
Effect Size Bias	0.1823	0.0230	0.2508	0.0057	0.9888

Table 7.50 Empirical Distributions - Large Bias

Large Bias	.10	.20	.30	.40	.50	.60	.70	.80	.90
Additive	0.0065	0.0364	0.1333	0.1895	0.1895	0.3708	0.4737	0.5976	0.6337
Dominance	0.0105	0.0421	0.0667	0.1278	0.1628	0.1667	0.1869	0.2667	0.7896
Epistasis	0.000e+00	0.000e+00	0.000e+00	1.109e-34	2.465e-33	9.861e-33	2.990e-32	1.727e-31	8.651e-06
Effect Size	0.000e+00	0.000e+00	0.000e+00	1.895e-17	7.843e-17	1.968e-16	3.899e-16	5.814e-16	0.0065
Additive.C	0.0066	0.0591	0.1364	0.2383	0.3191	0.4184	0.4883	0.6033	0.6338
Dominance.C	0.0512	0.1078	0.1249	0.1500	0.1837	0.2040	0.2921	0.4340	0.7799
Epistasis.C	1.186e-05	2.353e-05	4.640e-05	7.425e-05	0.0027	0.0206	0.0320	0.0414	0.0555
Effect Size.C	0.0069	0.0093	0.0112	0.0183	0.0591	0.1942	0.2544	0.2800	0.6189
G.E Association	3.895e-05	6.617e-05	0.0001	0.0002	0.0102	0.0561	0.0703	0.1260	0.1559
Residual	0.2006	0.2035	0.2074	0.2180	0.3118	0.4652	0.5098	0.5421	0.6769
G.E Correlation	-0.7428	-0.5423	-0.4115	-0.2034	-0.0016	0.0257	0.2719	0.2831	0.5137
Effect Size Bias	0.0069	0.0082	0.0100	0.0148	0.0230	0.1853	0.2428	0.2751	0.6189

Table 7.51 Genetic Bias Summary Statistics- Large Bias

Large Bias	Mean	Median	SD	Min	Max
Additive Bias	0.0288	-0.0004	0.0812	-0.1122	0.2988
Dominance Bias	0.0533	0.0100	0.0806	-0.0229	0.3344
Epistatic Bias	0.0244	0.0027	0.0453	0.000007	0.2628
Effect Size Bias	0.1823	0.0230	0.2508	0.0057	0.9888

Table 7.52 Genetic Bias Empirical Distribution- Large Bias

Large Bias	.10	.20	.30	.40	.50	.60	.70	.80	.90
Additive Bias	-0.0237	-0.0100	-0.0059	-0.0030	-0.0004	0.0001	0.0232	0.0657	0.0928
Dominance Bias	-0.0057	-0.0028	-0.0016	-0.0007	0.0100	0.0398	0.0570	0.1046	0.1828
Epistatic Bias	1.186e-05	2.353e-05	4.362e-05	6.979e-05	0.0027	0.0139	0.0301	0.0414	0.0555
Effect Size Bias	0.0069	0.0082	0.0100	0.0148	0.0230	0.1853	0.2428	0.2751	0.6189

7.4.3. Architectures yielding the Largest Values of Absolute Bias

The three largest nominal values of $|\phi'_{MinGE(c)} - \phi'_{MinGE}|$ were all equal to 0.99, and were generated by three distinct architectures of $\Psi'(\boldsymbol{g})_{\mathbf{Min,GE}}$ characterized by the following quantitative expressions and standardized genetic effects:

$$|\phi'^{*}_{MinGE(C)} - \phi'^{*}_{MinGE}| = 0.99; \vec{\theta}^{*} = \begin{bmatrix} \alpha_1 = 16 \\ \alpha_2 = 16 \\ k_1 = 0.0 \\ k_2 = -1 \\ \varphi_1 = 0.5 \\ \varphi_2 = 0.9 \end{bmatrix}; H^2 = 0.2; \ \omega^2_{\Psi'_{(g)}} = \begin{bmatrix} \omega^2_A = 0.036 \\ \omega^2_D = 0.163 \\ \omega^2_{EP} = 0.00 \end{bmatrix};$$

$$\omega^2_{\Psi'_{(g)C}} = \begin{bmatrix} \omega^2_{A(C)} = 0.059 \\ \omega^2_{D(C)} = 0.410 \\ \omega^2_{EP(C)} = 0.262 \end{bmatrix}; \omega^2_E = \begin{bmatrix} \omega^2_{\varepsilon(g)} = 0.533 \\ \omega^2_R = 0.267 \end{bmatrix}; \rho_{\Psi'(g),\gamma(\mathrm{E})} = -0.001.$$

$$|\phi'^{*}_{MinGE(C)} - \phi'^{*}_{MinGE}| = 0.99; \vec{\theta}^{*} = \begin{bmatrix} \alpha_1 = 16 \\ \alpha_2 = 16 \\ k_1 = 0.0 \\ k_2 = -1 \\ \varphi_1 = 0.5 \\ \varphi_2 = 0.9 \end{bmatrix}; H^2 = 0.2; \ \omega^2_{\Psi'_{(g)}} = \begin{bmatrix} \omega^2_A = 0.036 \\ \omega^2_D = 0.163 \\ \omega^2_{EP} = 0.00 \end{bmatrix};$$

$$\omega^2_{\Psi'_{(g)C}} = \begin{bmatrix} \omega^2_{A(C)} = 0.059 \\ \omega^2_{D(C)} = 0.410 \\ \omega^2_{EP(C)} = 0.262 \end{bmatrix}; \omega^2_E = \begin{bmatrix} \omega^2_{\varepsilon(g)} = 0.533 \\ \omega^2_R = 0.267 \end{bmatrix}; \rho_{\Psi'(g),\gamma(\mathrm{E})} = -0.001.$$

$$|\phi'^{*}_{MinGE(C)} - \phi'^{*}_{MinGE}| \ 0.99; \vec{\theta}^{*} = \begin{bmatrix} \alpha_1 = 16 \\ \alpha_2 = 16 \\ k_1 = 0.0 \\ k_2 = -1 \\ \varphi_1 = 0.5 \\ \varphi_2 = 0.9 \end{bmatrix}; H^2 = 0.2; \ \omega^2_{\Psi'_{(g)}} = \begin{bmatrix} \omega^2_A = 0.036 \\ \omega^2_D = 0.163 \\ \omega^2_{EP} = 0.00 \end{bmatrix};$$

$$\omega^2_{\Psi'_{(g)C}} = \begin{bmatrix} \omega^2_{A(C)} = 0.059 \\ \omega^2_{D(C)} = 0.410 \\ \omega^2_{EP(C)} = 0.262 \end{bmatrix}; \omega^2_E = \begin{bmatrix} \omega^2_{\varepsilon(g)} = 0.533 \\ \omega^2_R = 0.267 \end{bmatrix}; \rho_{\Psi'(g),\gamma(\mathrm{E})} = -0.001.$$

$$|\phi'^{*}_{MinGE(C)} - \phi'^{*}_{MinGE}| = 0.99; \vec{\theta}^{*} = \begin{bmatrix} \alpha_1 = 16 \\ \alpha_2 = 16 \\ k_1 = 0.0 \\ k_2 = -1 \\ \varphi_1 = 0.5 \\ \varphi_2 = 0.9 \end{bmatrix}; H^2 = 0.2; \ \omega^2_{\Psi'_{(g)}} = \begin{bmatrix} \omega^2_A = 0.036 \\ \omega^2_D = 0.163 \\ \omega^2_{EP} = 0.00 \end{bmatrix};$$

$$\omega^2_{\Psi'_{(g)C}} = \begin{bmatrix} \omega^2_{A(C)} = 0.059 \\ \omega^2_{D(C)} = 0.410 \\ \omega^2_{EP(C)} = 0.262 \end{bmatrix}; \omega^2_E = \begin{bmatrix} \omega^2_{\varepsilon(g)} = 0.533 \\ \omega^2_R = 0.267 \end{bmatrix}; \rho_{\Psi'(g),\gamma(\mathrm{E})} = -0.001. \quad (7.4)$$

From (7.4), the three architectures which engender the largest bias are characterized by: 1) *constant* additive effects for the first locus, while additive effects *vary* over $\boldsymbol{a}$ for the second ($\alpha_1 = [16,16,16], \alpha_2 = [16,32,44]$); 2) *no dominance* for the first locus, and *complete dominance* of the second allele for the second ($k_1 = 0.0, k_2 = -1$)); 3) *moderate* recessive allele frequencies for the first locus, and *large* recessive allele frequencies for the second ($\varphi_1 = 0.5, \varphi_2 = 0.9$); 4) *small* broad-sense heritability ($H^2 = 0.2$); and 5) a *small* gene-environmental correlation ($\rho_{\Psi'(g),\gamma(\mathrm{E})} = -0.001$). Notably, the departure of 0.99 for all three architectures was engendered by the deviation between the contaminated epistatic effect $\phi'^{*}_{MinGE(C)}$ =0.99, and its true counterpart ϕ'^{*}_{MinGE} =0.00.

7.4.4. Role of Genetic Parameters in Determining the Distribution of Bias

To quantitatively evaluate the dependency of $\Lambda_{\phi'_{MinGE(C)}-\phi'_{MinGE}}$ on the set of genetic parameters $\vec{\theta}$ and H^2, we employ a full-factorial 7-way ANOVA decomposition of $\Lambda_{\phi'_{MinGE(C)}-\phi'_{MinGE}}$ in terms of the 127 estimable effects. It turned out that, 25.5% of the variability in bias is attributed to pooled-genetic main effects, 51.1 % to pairwise-interactions, and 23.3% to higher-order interactions. The top 5 effects yield 72.3% of the variability in $\Lambda_{\phi'_{MinGE(C)}-\phi'_{MinGE}}$. Presented in order of magnitude, they include: 1) 2-way interaction k_1: k_2 = 35%; 2) main effect $k_{\cdot}$ = 21.3% ; 3) 3-way interaction between k_1: k_2: H^2 = 6.6% 4) 3-way interaction between k_1: φ_1: k_2 = 5.4% ; and 5) 2-way interaction k_2: φ_2 = 4.0%.

Chapter 8. Results Simulation Study II

Introduction

Recall, of course, our aims herein are to adjudicate the omnibus F-test statistic of interaction's performance of detection for all admissible architectures. To this end, consonant with the first simulation study, simulation study two is organized into four sections, in accordance with both architecture nomenclature and the criteria of detection outlined in Chapter 6.

8.1. $\Psi'(g)_{\text{Max}}$ Architectures

8.1.1. Median Power Profile for $\Psi'(g)_{\text{Max}}$

In Table 8.1, the median power profile $\widetilde{\Lambda}_{1-\beta(\phi',n,a)}$ generated over the empirical distribution $\Lambda_{\phi'>0}$ and 36 combinations of $\boldsymbol{n}$ and $\boldsymbol{a}$.

Table 8.1 Median Power $\Psi'(g)_{\text{Max}}$

	.01	.05	.10	.20	.30	.40
10	0.014	0.064	0.122	0.232	0.337	0.438
20	0.020	0.081	0.147	0.266	0.374	0.476
50	0.041	0.136	0.224	0.363	0.477	0.577
100	0.092	0.241	0.355	0.510	0.622	0.709
500	0.732	0.889	0.937	0.972	0.985	0.992
1000	0.984	0.997	0.999	1.000	1.000	1.000

What one can expect of a particular tests power over unique combinations of $\boldsymbol{n}$ *and* $\boldsymbol{a}$?

Based on the examination of Table 8.1, the median power profiles generated over various pairings of $[\boldsymbol{n},\boldsymbol{a}]$ are *unsatisfactory* for the majority of the 36 $\Lambda_{1-\beta(\phi'^{*}_{Max},n^{*},a^{*})}$. Upon closer inspection, for the *majority* of $\Lambda_{1-\beta(\phi'^{*}_{Max},n^{*},a^{*})}$, each coded to a unique pairings of $[\boldsymbol{n},\boldsymbol{a}]$ (N=25, min: [n=10, a=0.01]; max: [n=500, a=0.01]), the omnibus F-test-statistic yields *unsatisfactory* power of detection, ranging from $[0.14 \leq (1-\beta(\phi'_{Max},n,a) \geq 0.90) \geq 0.70]$, in the case of ~50% of the engendering architectures. Whereas, for the *minority* of $\Lambda_{1-\beta(\phi'^{*}_{Max},n^{*},a^{*})}$, each coded to a unique pairings of $[\boldsymbol{n},\boldsymbol{a}]$ (N=11, min: [n=500, a=0.05]; max: [n=1000, a=0.40]), the test statistic yields *satisfactory*

power profile ranging from, [0.90≤ $(1-\beta(\phi'_{Max},n,a)\geq 0.90)\geq 1.00$] in the case of ~50% of the engendering architectures. As such, the empirical scientist, on test day, can expect to have *satisfactory power to detect epistasis* in the case of ~50% of the engendering architectures under consideration for test-procedures coded to either [n= 500, a= 0.05 to 0.40] or any pairing of n=1000, with any reasonable Type I error rate.

8.1.2. Proportion of $\Psi'(\boldsymbol{g})_{\mathbf{Max}}$ with Power ≥ 0.90

In Table 8.2, the proportion of $\Psi'(\boldsymbol{g})_{\text{Max}}$ architectures with satisfactory power (≥ 0.90).

Table 8.2 Proportion of $\Psi'(\boldsymbol{g})_{\text{Max}}$ Architectures ≥ 0.90

	.01	.05	.10	.20	.30	.40
10	0.013	0.015	0.017	0.030	0.046	0.057
20	0.029	0.050	0.067	0.085	0.101	0.118
50	0.101	0.127	0.148	0.183	0.212	0.243
100	0.178	0.232	0.251	0.282	0.310	0.341
500	0.415	0.494	0.525	0.567	0.593	0.610
1000	0.564	0.600	0.620	0.654	0.713	0.736

How common may one encounter an $\Psi'(\boldsymbol{g})_{Max}$ where detection of epistasis is deemed 'satisfactory'?

Based on examination of Table 8.2, it appears that an acceptable power of detection is generally *uncommon* for all omnibus F-test-procedures considered. Upon closer inspection, for 20 $\Lambda_{1-\beta(\phi'_{Max},n,a)}$ (min: [n=10, a =0.01]; max: [n=100, a =0.05]), the proportion of $\Psi'(\boldsymbol{g})_{\mathbf{Max}}$ architectures with *satisfactory nominal power* are below the 25th percentile, and range from [$0.013 \leq P(1-\beta(\phi'_{Max},n,a)\geq 0.90)\geq 0.232$]. For 6 $\Lambda_{1-\beta(\phi'_{Max},n,a)}$ (min [n=100, a=0.10], max: [n=500, a=0.05]), the proportion of $\Psi'(\boldsymbol{g})_{\mathbf{Max}}$ architectures with *satisfactory nominal power* are between the 25th and 50th percentile, and range from [$0.251 \leq P(1-\beta(\phi'_{Max},n,a)\geq 0.90)\geq 0.49$]. Finally, for the remaining 10 $\Lambda_{1-\beta(\phi'_{Max},n,a)}$(min: [$n$=500, a =0.10], max: [n=1000, a =0.40]), the proportion of $\Psi'(\boldsymbol{g})_{\mathbf{Max}}$ architectures with *satisfactory nominal power* are between 50th and 75th percentile, and range from [$0.52 \leq P(1-\beta(\phi'_{Max},n,a)\geq 0.90)\geq 0.75$]. All told, it appears that on average, satisfactory *power to detect epistasis* is relatively *uncommon*, and unsurprisingly improves for test procedures in the care of relatively high per-genotype sample size, and relaxed Type I error rate.

8.2. $\Psi'(g)_{\text{Min}}$ Architectures

8.2.1. Median Power Profile for $\Psi'(g)_{\text{Min}}$

In Table 8.3, the median power profile $\widetilde{\Lambda}_{1-\beta(\phi',n,a)}$ generated over the empirical distributions of $\Lambda_{\phi'>0}$ and 36 combinations of $\boldsymbol{n}$ and $\boldsymbol{a}$.

Table 8.3 Median Power $\Psi'(g)_{\text{Min}}$

	.01	.05	.10	.20	.30	.40
10	0.016	0.069	0.129	0.242	0.348	0.450
20	0.023	0.091	0.162	0.285	0.396	0.497
50	0.054	0.166	0.263	0.409	0.524	0.621
100	0.132	0.310	0.433	0.588	0.693	0.771
500	0.872	0.959	0.980	0.992	0.996	0.998
1000	0.998	1.000	1.000	1.000	1.000	1.000

What one can expect of a particular tests power over unique combinations of n *and* a?

Based on the examination of Table 8.3, it appears that for the majority of [$\boldsymbol{n}$, $\boldsymbol{a}$] pairing, $\Lambda_{1-\beta(\phi'_{Min},n,a)}$ yields, on average, *unsatisfactory* power to detect epistasis. Upon closer inspection, for the *majority* of $\Lambda_{1-\beta(\phi'_{Min},n,a)}$, each coded to a unique pairing of [$\boldsymbol{n}$, $\boldsymbol{a}$] (N=25,min: [n=10, a =0.01]; max: [n=500, a=0.01]), the omnibus F-test-statistic will yield *unsatisfactory* power of detection, ranging from $[0.016 \leq (1-\beta(\phi'_{Min},n,a) \geq 0.90) \geq 0.87]$, in the case of ~50% of the engendering architectures. In contrast, for the *minority* of $\Lambda_{1-\beta(\phi'_{Min},n,a)}$, each coded to a unique pairing of [$\boldsymbol{n}$, $\boldsymbol{a}$] (N=11 ,min: [n=500, a=0.05]; max: [n=1000, a=0.40]), the test-statistic will yield *satisfactory* power, ranging from $[0.96 \leq (1-\beta(\phi'_{Min},n,a) \geq 0.90) \geq 1.00]$ in the case of ~50% of the engendering architectures. As such, the empirical scientist, on test day, may expect to have *satisfactory power to detect epistasis* in the case of ~50% of the engendering architectures, if for example, they have selected a sample size per-genotype of n= 500, and any reasonable Type I error rate. If, however, n=100, Type I error rate would need to be around 0.4 for the test statistic to yield roughly the same power of detection performance.

8.2.2. Proportion of $\Psi'(\boldsymbol{g})_{\text{Min}}$ with Power ≥.90

In Table 8.4, the proportion of $\Psi'(\boldsymbol{g})_{\text{Min}}$ architectures with satisfactory power (≥ 0.90).

Table 8.4 Proportion of $\Psi'(\boldsymbol{g})_{\text{Min}}$ Architectures over 0.90

	.01	.05	.10	.20	.30	.40
10	0.037	0.037	0.037	0.050	0.085	0.113
20	0.049	0.095	0.133	0.154	0.162	0.166
50	0.162	0.171	0.183	0.229	0.282	0.310
100	0.222	0.298	0.314	0.329	0.334	0.354
500	0.461	0.534	0.549	0.558	0.579	0.591
1000	0.557	0.583	0.606	0.628	0.689	0.700

How common may one encounter an $\Psi'(\boldsymbol{g})_{\text{Min}}$ where detection of epistasis is deemed 'satisfactory'?

From Table 8.4, it appears that the satisfactory power of detection is generally *uncommon*. Upon closer inspection, for 16 $\Lambda_{1-\beta(\phi'_{Min},n,a)}$ (min: [n=10, a=0.01]; max: [n=50, a=0.20]), the proportion of $\Psi'(\boldsymbol{g})_{\text{Min}}$ architectures with *satisfactory nominal power* are below the 25th percentile, and range from [0.037 ≤ P(1-$\beta(\phi'^{*}_{Min}, n, a)$ ≥0.90) ≥0.229]. For 9 $\Lambda_{1-\beta(\phi'_{Min},n,a)}$ (min: [n=50, a=0.30], max: [n=500, a=0.01]), the proportion of $\Psi'(\boldsymbol{g})_{\text{Min}}$ architectures with *satisfactory nominal power* are between the 25th and 50th percentile, and range from [0.298 ≤ P(1-$\beta(\phi'^{*}_{Min}, n, a)$ ≥0.90) ≥0.461]. Finally, for the 11 remaining $\Lambda_{1-\beta(\phi'_{Min},n,a)}$ (min: [n=500, a=0.05], max: [n=1000, a=0.40]), the proportion of $\Psi'(\boldsymbol{g})_{\text{Min}}$ architectures with *satisfactory nominal power* are between the 50th and 75th percentile, and range from [0.534 ≤ P(1-$\beta(\phi'^{*}_{Min}, n, a)$ ≥0.90) ≥0.70]. All told, it appears that on average, the satisfactory power to detect epistasis is relatively uncommon, naturally improving in circumstances of relatively high per-genotype sample size and relaxed Type I error rate.

8.3. $\Psi'(g)_{\text{Max,GE}}$ Architectures

8.3.1. Median Power $\Psi'(g)_{\text{Max,GE}}$

In Table 8.5 and Table 8.6 is presented, respectively the median power for the 36 empirical distributions of true $\widetilde{\Lambda}_{1-\beta(\phi'_{MaxGE},n,a)}$ and contaminated $\widetilde{\Lambda}_{1-\beta(\phi'_{MaxGE(c)},n,a)}$ epistatic effects.

Table 8.5 Median Power $\Psi'(g)_{\text{Max,GE}}$

	.01	.05	.10	.20	.30	.40
10	0.015	0.068	0.127	0.239	0.343	0.444
20	0.023	0.088	0.154	0.272	0.380	0.481
50	0.052	0.144	0.220	0.339	0.449	0.547
100	0.105	0.204	0.281	0.406	0.513	0.603
500	0.309	0.387	0.473	0.579	0.663	0.735
1000	0.393	0.480	0.530	0.616	0.690	0.755

Table 8.6 Median Power $\Psi'(g)_{\text{Max,GE}}$ - Contaminated

	.01	.05	.10	.20	.30	.40
10	0.015	0.068	0.129	0.243	0.350	0.451
20	0.023	0.099	0.176	0.283	0.383	0.483
50	0.075	0.134	0.198	0.332	0.444	0.541
100	0.094	0.203	0.309	0.450	0.550	0.637
500	0.272	0.467	0.517	0.617	0.691	0.750
1000	0.427	0.476	0.529	0.623	0.718	0.784

What one may expect of true and contaminated statistical power with different combinations of n and a?

Based on examination of Tables 8.6 and 8.6, the median power profiles generated over various pairing of [$\boldsymbol{n}$, $\boldsymbol{a}$] yields an *unsatisfactory power* profile, in the case of ~50% of the engendering architectures for both the 36 $\Lambda_{1-\beta(\phi'^{*}_{MaxGE},n^{*},a^{*})}$, and 36 $\Lambda_{1-\beta(\phi'^{*}_{MaxGE(c)},n^{*},a^{*})}$. As Tables 1.1.57, and 1.1.58 suggest, the aforementioned empirical distributions of power respectively range between [$0.015 \leq (1-\beta(\phi'_{MaxGE},n,a)) \geq 0.755$] and [$0.015 \leq (1-\beta(\phi'_{MaxGE(C)},n,a)) \geq 0.784$], for ~50% of all engendering architectures.

8.3.2. Proportion of $\Psi'(\boldsymbol{g})_{\text{Max,GE}}$ with Power ≥0.90

Table 8.7 and Table 8.8 respectively present the proportion of $\Psi'(\boldsymbol{g})_{\text{Max,GE}}$ with satisfactory power of detection for both $\Lambda_{\text{P}(1-\beta(\phi'_{MaxGE},n,a)\geq 0.90)}$ and $\Lambda_{\text{P}(1-\beta(\phi'_{MaxGE(c)},n,a)\geq 0.90)}$.

Table 8.7 Proportion of $\Psi'(\boldsymbol{g})_{\text{Max,GE}}$ Architectures ≥ 0.90

	.01	.05	.10	.20	.30	.40
10	0.008	0.012	0.020	0.023	0.026	0.032
20	0.022	0.028	0.036	0.048	0.060	0.078
50	0.060	0.085	0.102	0.119	0.135	0.165
100	0.116	0.145	0.173	0.193	0.215	0.234
500	0.279	0.323	0.339	0.363	0.386	0.412
1000	0.360	0.399	0.415	0.422	0.450	0.465

Table 8.8 Proportion of Contaminated $\Psi'(\boldsymbol{g})_{\text{Max,GE}}$ Architecture ≥ 0.90

	.01	.05	.10	.20	.30	.40
10	0.015	0.018	0.025	0.034	0.035	0.042
20	0.034	0.035	0.044	0.057	0.073	0.092
50	0.073	0.101	0.119	0.133	0.145	0.167
100	0.131	0.149	0.176	0.202	0.223	0.252
500	0.293	0.331	0.345	0.371	0.393	0.420
1000	0.369	0.406	0.424	0.434	0.452	0.472

How common it is that one may encounter an $\Psi'(\boldsymbol{g})_{Max,GE}$ architecture where the detection of epistasis is deemed satisfactory?

Overall, it appears the proportion of $\Psi'(\boldsymbol{g})_{\text{Max,GE}}$ architectures which yield satisfactory power are generally *uncommon* for both true and contaminated epistatic effects. Based on examination of Table 8.7,it appears for all 36 $\Lambda_{1-\beta(\phi'_{MaxGE},n,a)}$ (min: [n=10, a =0.01] and max: [n=1000, a=0.40]), the proportion of $\Psi'(\boldsymbol{g})_{\text{Max,GE}}$ architectures which yield *satisfactory* nominal power are below the 50th percentile, ranging from [0.008≤ $P(1-\beta(\phi'^{*}_{MaxGE}, n, a) \geq 0.90) \geq 0.465$]. Upon further inspection, it appears for 24 $\Lambda_{1-\beta(\phi'_{MaxGE(c)},n,a)}$(min: [$n$=10, a=0.01] and max: [n=100, a=0.40]), the proportion of $\Psi'(\boldsymbol{g})_{\text{Max,GE}}$ architectures with *satisfactory nominal power* are below the 25th percentile, ranging from [0.015≤ $(1-\beta(\phi'^{*}_{MaxGE(c)}, n, a) \geq 0.90) \geq 0.234$]. While for 12 $\Lambda_{1-\beta(\phi'_{MaxGE(c)},n,a)}$(min: [$n$=500, a=0.01] and max: [n=1000, a=0.40]), the proportion of

$\Psi'(\boldsymbol{g})_{\mathbf{Max,GE}}$ architectures producing *satisfactory nominal power* are between 25th and 50th percentile, ranging from [0.279≤ $P(1-\beta(\phi'^{*}_{MaxGE(c)}, n, a) \geq 0.90) \geq 0.465$].

Similarly, based on examination of Table 8.8, it appears for all 36 $\Lambda_{1-\beta(\phi'_{MaxGE(c)},n,a)}$ the proportion of $\Psi'(\boldsymbol{g})_{\mathbf{Max,GE}}$ architectures which yield *satisfactory* nominal power are below the 50th percentile, ranging from [0.015≤ (1-$\beta(\phi'^{*}_{MaxGE(c)}, n, a)$ ≥ 0.90) ≥0.472]. Upon further inspection, it appears for 23 $\Lambda_{1-\beta(\phi'_{MaxGE(c)},n,a)}$(min: [$n$=10, a=0.01] and max: [n=100, a =0.30]), the proportion of $\Psi'(\boldsymbol{g})_{\mathbf{Max,GE}}$ architectures with *satisfactory nominal power* are below the 25th percentile, ranging from [0.015≤ (1 − $\beta(\phi'^{*}_{MaxGE(c)}, n, a) \geq 0.90) \geq 0.223$]. While for 13 $\Lambda_{1-\beta(\phi'_{MaxGE(c)},n,a)}$(min: [$n$=100, a=0.40] and max: [n=1000, a=0.40]), the proportion of $\Psi'(\boldsymbol{g})_{\mathbf{Max,GE}}$ architectures with *satisfactory nominal power* are between 25th and 50th percentile, ranging from [0.252≤ $P(1-\beta(\phi'^{*}_{MaxGE(c)}, n, a) \geq 0.90) \geq 0.472$].

8.3.3. Associated Biases $\Psi'(\boldsymbol{g})_{\mathbf{Max,GE}}$

Table 8.9 and Table 8.10 respectively present the departures in median power between contaminated and true distributions [$\widetilde{\Lambda}_{1-\beta(\phi'_{MaxGE(c)},n,a)} - \widetilde{\Lambda}_{1-\beta(\phi'_{MaxGE},n,a)}$] and the proportion of $\Psi'(\boldsymbol{g})_{\mathbf{Max,GE}}$ architectures with satisfactory power [$\Lambda_{P(1-\beta(\phi'_{MaxGE(c)},n,a)\geq.90)} - \Lambda_{\mathrm{P}(1-\beta(\phi'_{MaxGE},n,a)\geq.90)}$].

Table 8.9 **Bias Median Power - $\Psi'(\boldsymbol{g})_{\text{Max,GE}}$**

	.01	.05	.10	.20	.30	.40
10	-2.189e-05	0.0007	0.0019	0.0047	0.0067	0.0065
20	0.0003	0.0118	0.0214	0.0109	0.0033	0.0024
50	0.0229	-0.0103	-0.0212	-0.0075	-0.0049	-0.0063
100	-0.0116	-0.0012	0.0278	0.0445	0.0374	0.0341
500	-0.0369	0.0795	0.0434	0.0374	0.0281	0.0146
1000	0.0342	-0.0043	-0.0011	0.0072	0.0281	0.0289

Table 8.10 **Bias Proportion Power - $\Psi'(\boldsymbol{g})_{\text{Max,GE}}$**

	.01	.05	.10	.20	.30	.40
10	0.007	0.006	0.005	0.011	0.009	0.010
20	0.012	0.007	0.008	0.009	0.013	0.014
50	0.013	0.017	0.018	0.014	0.010	0.002
100	0.015	0.004	0.002	0.010	0.008	0.018
500	0.014	0.007	0.006	0.008	0.007	0.008
1000	0.008	0.008	0.009	0.012	0.003	0.007

Is it the case the property of gene-environmental association alters in some unfavourable way the performance of the test procedure to detect epistasis?

Based on an examination of Table 8.9 and Table 8.10, there is evidence that the property of gene-environmental association engenders bias for both criteria of detection. Upon closer inspection of Table 8.9, it appears the departures in median power between contaminated and true distributions [$\widetilde{\Lambda}_{1-\beta(\phi'_{MaxGE(c)},n,a)} - \widetilde{\Lambda}_{1-\beta(\phi'_{MaxGE},n,a)}$] are *minimal* in absolute magnitude [min: 2.18x10^{-5}, max: 0.079], and *variable* in direction. Upon closer review, for the majority of $\widetilde{\Lambda}_{1-\beta(\phi'_{MaxGE(c)},n,a)} - \widetilde{\Lambda}_{1-\beta(\phi'_{MaxGE},n,a)}$ (N=25) the departures are *positive* in direction, suggesting inflation in median power for empirical distributions of *contaminated* epistatic effects, in comparison to their *true* counterparts. Conversely, for the minority of $\widetilde{\Lambda}_{1-\beta(\phi'_{MaxGE(c)},n,a)} - \widetilde{\Lambda}_{1-\beta(\phi'_{MaxGE},n,a)}$ (N=11) the departures are *negative* in direction, suggesting deflation in median power for empirical distributions of *contaminated* epistatic effects, in comparison to their true counterparts. However, it is clear overall 36 $\widetilde{\Lambda}_{1-\beta(\phi'_{MaxGE(c)},n,a)} - \widetilde{\Lambda}_{1-\beta(\phi'_{MaxGE},n,a)}$ the magnitude and direction of such departures are *without* a discernable pattern between sample-size per genotype and Type I error. Similarly, an inspection of Table 8.10 suggests the departures between the proportion of $\Psi'(\boldsymbol{g})_{\text{Max,GE}}$ architectures with satisfactory power [$\Lambda_{P(1-\beta(\phi'_{MaxGE(c)},n,a)\geq.90)} - \Lambda_{\text{P}(1-\beta(\phi'_{MaxGE},n,a)\geq.90)}$] are *minimal* in absolute magnitude [min: 0.002, max: 0.018] and *positive* in direction for all 36 departures, suggesting *inflation* in the proportion of

$\Psi'(\boldsymbol{g})_{\text{Max,GE}}$ architectures with a satisfactory power for empirical distributions of *contaminated* epistatic effects, in comparison to their *true* counterparts. As before, it appears there is no discernable pattern between the magnitude of departure and the magnitude of sample-size per genotype and Type I error rate.

8.4. $\Psi'(\boldsymbol{g})_{\text{Min,GE}}$ Architectures

8.4.1. Median Power for $\Psi'(\boldsymbol{g})_{\text{Min,GE}}$

Table 8.11 and Table 8.12 respectively present the median power for the 36 empirical distributions of true $\tilde{\Lambda}_{1-\beta(\phi'_{MinGE},n,a)}$ and contaminated $\tilde{\Lambda}_{1-\beta(\phi'_{MinGE(c)},n,a)}$ epistatic effects.

Table 8.11 Median Power $\Psi'(\boldsymbol{g})_{\text{Min,GE}}$

	.01	.05	.10	.20	.30	.40
10	0.112	0.209	0.290	0.409	0.507	0.599
20	0.209	0.303	0.393	0.507	0.593	0.652
50	0.343	0.390	0.468	0.579	0.636	0.695
100	0.412	0.512	0.564	0.624	0.664	0.732
500	0.605	0.625	0.625	0.665	0.673	0.735
1000	0.617	0.625	0.625	0.659	0.687	0.737

Table 8.12 Median Power $\Psi'(\boldsymbol{g})_{\text{Min,GE}}$ - Contaminated

	.01	.05	.10	.20	.30	.40
10	0.121	0.206	0.301	0.422	0.522	0.618
20	0.221	0.294	0.402	0.533	0.619	0.654
50	0.343	0.389	0.500	0.600	0.645	0.733
100	0.454	0.549	0.599	0.646	0.667	0.734
500	0.667	0.674	0.685	0.703	0.745	0.760
1000	0.691	0.706	0.709	0.718	0.747	0.778

What one may expect of true and contaminated statistical power with different combinations of n and α?

Based on examination of Table 8.11 and Table 8.12, it appears that for all 36 $\Lambda_{1-\beta(\phi'_{MinGE},n,a)}$ and $\Lambda_{1-\beta(\phi'_{MinGE(c)}}$ the omnibus F-test-statistic yields *unacceptable* power to detect *true* epistatic effects in ~50% of the architectures, even in the care of high sample size per genotype and Type I error control. As Tables 8.11 and 8.12 suggest, the aforementioned empirical distributions of power respectively range between [0.112

$\leq(1-\beta(\phi'_{MinGE},n,a))\geq$ 0.737] and [0.121 $\leq(1-\beta(\phi'_{MinGE(C)},n,a))\geq$ 0.778], for ~50% of all engendering architectures.

8.4.2. Proportion of $\Psi'(\boldsymbol{g})_{\text{Min,GE}}$ architectures with Power ≥.90

Table 8.13 and Table 8.14 respectively present the proportion of $\Psi'(\boldsymbol{g})_{\text{Min,GE}}$ architectures with a satisfactory power for $\Lambda_{\text{P}(1-\beta(\phi'_{MinGE},n,a)\geq 0.90)}$ and $\Lambda_{\text{P}(1-\beta(\phi'_{MinGE(c)},n,a)\geq 0.90)}$.

Table 8.13 Proportion of $\Psi'(\boldsymbol{g})_{\text{Min,GE}}$ Architectures ≥ 0.90

	.01	.05	.10	.20	.30	.40
10	0.065	0.127	0.141	0.161	0.164	0.190
20	0.160	0.164	0.204	0.233	0.277	0.305
50	0.277	0.319	0.335	0.340	0.378	0.401
100	0.340	0.392	0.409	0.462	0.494	0.517
500	0.532	0.536	0.539	0.544	0.546	0.547
1000	0.542	0.546	0.549	0.557	0.558	0.558

Table 8.14 Proportion of Contaminated $\Psi'(\boldsymbol{g})_{\text{Min,GE}}$ Architectures ≥ 0.90

	.01	.05	.10	.20	.30	.40
10	0.062	0.099	0.134	0.155	0.162	0.170
20	0.153	0.162	0.186	0.232	0.251	0.302
50	0.251	0.311	0.336	0.345	0.361	0.405
100	0.345	0.386	0.414	0.445	0.497	0.539
500	0.585	0.596	0.599	0.603	0.614	0.621
1000	0.602	0.620	0.622	0.629	0.631	0.632

How common it is that one may encounter an $\Psi'(\boldsymbol{g})_{\text{Min,GE}}$ *where the detection of epistasis is deemed satisfactory*?

Overall it appears an acceptable power of detection is *uncommon* for both $\Lambda_{1-\beta(\phi'_{MinGE(c)},n,a)}$, and $\Lambda_{1-\beta(\phi'_{MinGE(c)},n,a)}$. Firstly, according to Table 8.13, we can see that for *all* of the 36 $\Lambda_{1-\beta(\phi'_{MinGE(c)},n,a)}$, the proportion of $\Psi'(\boldsymbol{g})_{\text{Min,GE}}$ architectures which yield *satisfactory nominal power* are well below the 75th percentile, ranging between [0.065 ≤ P(1-$\beta(\phi'_{Min,GE(c)},n,a)$)≥0.90)≥ 0.558]. Secondly, according to Table 8.14, it is apparent that for *all* 36 $\Lambda_{1-\beta(\phi'_{Min,GE(c)},n,a)}$ the proportion of $\Psi'(\boldsymbol{g})_{\text{Min,GE}}$ architectures which yield satisfactory nominal power are also, well below the 75th percentile, ranging from [0.062≤ P(1-$\beta(\phi'_{MinGE(c)},n, a)$ ≥0.90)≥ 0.632]. All told, it appears that the *acceptable power to detect*

epistasis is *uncommon* for $\Psi'(\boldsymbol{g})_{\text{Min,GE}}$ architectures with the properties of epistasis, even in the care of relatively high per-genotype sample size, and relaxed Type I error rate.

8.4.3. Associated Bias $\Psi'(\boldsymbol{g})_{\text{Min,GE}}$

Table 8.15 and Table 8.16 respectively present the departures in median power between contaminated and true distributions $[\widetilde{\Lambda}_{1-\beta(\phi'_{MinGE(c)},n,a)} - \widetilde{\Lambda}_{1-\beta(\phi'_{MinGE},n,a)}]$ and the proportion of $\Psi'(\boldsymbol{g})_{\text{Min,GE}}$ architectures with satisfactory power $[\Lambda_{P(1-\beta(\phi'_{MinGE(c)},n,a)\geq.90)} - \Lambda_{\text{P}(1-\beta(\phi'_{MinGE},n,a)\geq.90)}]$.

Table 8.15 Bias Median Power - $\Psi'(\boldsymbol{g})_{\text{Min,GE}}$

	.01	.05	.10	.20	.30	.40
10	0.0095	-0.0036	0.0114	0.0136	0.0151	0.0195
20	0.0125	-0.0093	0.0089	0.0260	0.0259	0.0015
50	9.967e-06	-0.0016	0.0314	0.0210	0.0090	0.0386
100	0.0428	0.0370	0.0352	0.0214	0.0028	0.0022
500	0.0614	0.0485	0.0599	0.0375	0.0720	0.0249
1000	0.0736	0.0811	0.0845	0.0596	0.0604	0.0405

Table 8.16 Bias Proportion Power - $\Psi'(\boldsymbol{g})_{\text{Min,GE}}$

	.01	.05	.10	.20	.30	.40
10	-0.003	-0.028	-0.007	-0.005	-0.002	-0.020
20	-0.007	-0.002	-0.018	-0.000	-0.026	-0.003
50	-0.026	-0.008	0.001	0.005	-0.017	0.004
100	0.005	-0.006	0.005	-0.017	0.003	0.023
500	0.054	0.060	0.060	0.060	0.068	0.074
1000	0.060	0.074	0.072	0.072	0.073	0.074

Is it the case an engendering $\Psi'(\boldsymbol{g})_{Min,GE}$ architecture with the properties of epistasis and gene-environmental association alters in some unfavourable way the performance of the test procedure to detect epistasis?

Based on an examination of Table 8.15 and Table 8.16, there is evidence that the property of gene-environmental association engenders bias for both criteria of detection. Upon closer inspection of Table 8.15 it appears the departures in median power between the 36 contaminated and true distributions $[\widetilde{\Lambda}_{1-\beta(\phi'_{MinGE(c)},n,a)} - \widetilde{\Lambda}_{1-\beta(\phi'_{MinGE},n,a)}]$ are *minimal* in absolute magnitude [min: $9.97\text{x}10^{-6}$, max: 0.084], and *variable* in direction. For all *but* $3\,\widetilde{\Lambda}_{1-\beta(\phi'_{MinGE(c)},n,a)} - \widetilde{\Lambda}_{1-\beta(\phi'_{MinGE},n,a)}$ (n= [10,20,50], a=0.05) the median power of *true* epistatic effects are *inflated* in comparison to their *contaminated* counterparts, while

there is no discernable pattern between the magnitude or direction of median biases with sample-size per genotype and type I error control. Similarly, an inspection of Table 8.16, suggests the departures between the proportion of $\Psi'(\boldsymbol{g})_{\mathbf{Min,GE}}$ architectures with satisfactory power [$\Lambda_{P(1-\beta(\phi'_{MinGE(c)},n,a)\geq.90)} - \Lambda_{\mathrm{P}(1-\beta(\phi'_{MinGE},n,a)\geq.90)}$] are also *minimal* in absolute magnitude [min: 0.002, max: 0.074] and *variable* in direction. Upon closer review, for all *but* 17 $\Lambda_{P(1-\beta(\phi'_{MinGE(c)},n,a)\geq.90)} - \Lambda_{\mathrm{P}(1-\beta(\phi'_{MinGE},n,a)\geq.90)}$ (N=19) the departures are *positive* in direction, suggesting the empirical distributions of *contaminated* epistatic effects are inflated in comparison to their *true* counterparts. Once more, no discernable pattern exists between the magnitude or direction of biases in the proportion of architectures with satisfactory power with sample-size per genotype and Type I error rate.

Chapter 9. Discussion

Introduction

For the empirical scientist interested in unpacking the relative contributions of genetics (G) and environment (E) on quantitative trait (Z) variation, of scientific import, of course, is the extant form of the architecture and its constituent parts: s, $\Psi'(\boldsymbol{g})$, and *f*. Indeed, scientific details regarding the extant nature of s – the number of causal loci-, $\Psi'(\boldsymbol{g})$ - the genotypic scalar function-, and *f* - the function that maps $\Psi'(\boldsymbol{g})$ and $\gamma(E)_i$ into Z – remain a central focus of scientific debate. While historic accounts respectively envisage $\Psi'(\boldsymbol{g})$ and *f* as a linear function of *s* loci with the property of additive separability, ushering empirical and inferential focus onto additive, dominance, or recessive models of genetic architecture[137], departures from this narrative are seemingly ubiquitous for complex traits across the extant literature evaluating model organisms. While the phenomenon of epistasis and the joint impact of genetics and environment onto Z[138] are now a centrepiece of the contemporary story, translation of the afore noted findings in model organisms onto human populations suffers on *both* empirical and inferential fronts. While the genome-wide study of human populations remains within its infancy, a great deal of effort has gone into the detection of epistasis. However, despite the sophistication of technologies and the putative ubiquity of epistatic architectures, the successful detection of epistasis within human populations remains a rarity. To this end, the goals of the thesis were to elucidate the quantitative issues involved in the inferential aims of epistatic detection. To do so, we adjudicated the merits of two candidate explanations.

The first relates to the possibility the population-level manifestations of epistasis, notably, σ^2_{EP} (ϕ'^*), are by their nature, *small*. As such, if the inferential tools employed to adjudicate the pair [H_0: $\sigma^2_{EP} = 0$; or H_1: $\sigma^2_{EP} \neq 0$] have machinations with disadvantageously small sample sizes, the consequence, of course, is that the power delivered is also disadvantageously small. Naturally, detector insensitivity of this sort is ameliorated by increasing sample size. The second relates to whether the presence of a

[137] A notion based upon Mendelian inheritance and diseases.

[138] Also, notably the way in which the field viewed genes, from that of a 'blueprint' to a 'dynamic system' (Lewontin, 1974; Alberch, 1991; Pigliucci, 2010; Svedolv & Thompson, 2018).

gene-environmental association generates a bias in estimates of genotypic values and, in so doing, systematically diminishes the detection power of the inferential tools employed to adjudicate the pair [H_0: $\sigma^2_{EP} = 0$; or H_1: $\sigma^2_{EP} \neq 0$]. To evaluate the merits of each candidate explanation two simulation studies were conducted, resting upon the construction of four digenic epistatic architectures. The architectures were created by crossing two genotypic functions $\Psi'(\boldsymbol{g})_{\mathbf{Max}}$ and $\Psi'(\boldsymbol{g})_{\mathbf{Min}}$, with the two-levels of gene-environment association, $\boldsymbol{\varepsilon} = [0]$, and $\boldsymbol{\varepsilon} \neq [0]$. By sampling over their parameter space, we generated 6075 unique architectures of $\Psi'(\boldsymbol{g})_{\mathbf{Max}}$, $\Psi'(\boldsymbol{g})_{\mathbf{Min}}$, $\Psi'(\boldsymbol{g})_{\mathbf{MaxGE}}$, and $\Psi'(\boldsymbol{g})_{\mathbf{MinGE}}$ construction. Notably, only *admissible* architectures were included in both simulation studies I and II (see Chapter 6).

In simulation study I, we aimed to assess: 1) whether epistatic effect sizes ϕ'^{*} arising under architectures in which $\boldsymbol{\varepsilon} = [0]$, were generally small; and 2) to gain insight into *how far off the mark* the recovered contaminated epistatic effect sizes were from their true counterparts, for architectures in which $\boldsymbol{\varepsilon} \neq [0]$. To this end, for all admissible architecture of each nomenclature, we evaluated the empirical range of $\Lambda_{\phi'}$, $\Lambda_{\phi'_{(c)}}$ and $\Lambda_{\phi'_{(c)} - \phi'}$; 2) reported the parametric construction of the three architecture(s) yielding the highest three nominal ϕ'^{*} and $|\phi'_{(c)} - \phi'|$; and 3) the role of genetic parameters in the variance of $\Lambda_{\phi'}$ $\left(\Lambda_{\phi'_{(c)} - \phi'}\right)$, by decomposing its variability into 2^7-1 estimable effects. In simulation study II, we aimed to assess what one may expect of statistical power under different combinations of sample size per genotype ($\boldsymbol{n}$) and Type I error rate ($\boldsymbol{\alpha}$). To adjudicate the omnibus F-test statistic of interactions[139] performance of detection over the empirical range of $\Lambda_{\phi'}$, we generated 36 unique empirical power coded to the combinations of $\boldsymbol{n}$ and $\boldsymbol{\alpha}$, and employed two criteria of detection: 1) the *median power* over all architectures to detect: $\sigma^2_{\mathrm{EP}} > 0$; and 2) the *proportion* of all architectures wherein the P(detection $\sigma^2_{\mathrm{EP}} > 0$) is greater or equal to 0.90. Additionally, for all admissible architectures in which $\boldsymbol{\varepsilon} \neq [0]$, we evaluated whether the presence of gene-environmental association altered in some un-favorable way the performance of

[139] Of note –there are numerous methodologies utilized to test the presence of epistasis (Chapter 3). As the omnibus F-test statistic of interaction is equivalent to testing for all interactions it is one that consolidates statistical power and works to reconcile issues such as FWER. However, the topic of whether this is the best method to deal with FWER is one we do not explore here (as it is a vast area and not the focus of this thesis). Rather, the motivation is to get a *sense* of what power is like for *one* sensible approach under various plausible architectures.

the test procedure to detect epistasis, vis-a-vis, the *magnitude* and *direction* of the departures between both afore noted criteria.

9.1. Main and Corollary Findings

All told, results from both simulation studies I and II provided preliminary support for both candidate explanations. In line with the first explanation, the empirical range of $\Lambda_{\phi'}$ suggests that on aggregate, the epistatic effect sizes ϕ'^{*}arising under architectures of $\Psi'(\boldsymbol{g})_{\mathbf{Max}}$ and $\Psi'(\boldsymbol{g})_{\mathbf{Min}}$ construction were generally *small* according to Cohen's guidelines (1988). Indeed, all 6075 architectures of $\Psi'(\boldsymbol{g})_{\mathbf{Max}}$ and $\Psi'(\boldsymbol{g})_{\mathbf{Min}}$ construction had the property of epistasis and engendered a non-zero population-level effect; and, in keeping with expectations, the omnibus F-test statistic yielded *satisfactory power* in the case of ~50% of the engendering architectures for test procedures coded to [$\boldsymbol{n}$,$\boldsymbol{a}$] pairing of large magnitude[140]. However, the proportion of architectures with satisfactory power to detect epistasis remained small, irrespective of sample size per genotype or Type I error rate. In line with the second candidate explanation, the empirical range of $\Lambda_{\phi'_{(c)}-\phi'}$ under the admissible architectures of $\Psi'(\boldsymbol{g})_{\mathbf{Max,GE}}$ and $\Psi'(\boldsymbol{g})_{\mathbf{Min,GE}}$ construction were also relatively *small* on aggregate[141]. In keeping with expectations, the property of the gene-environmental association obscured the performance of the omnibus F-test statistic of interaction to detect a true epistatic population-level effect in a magnitude and direction idiomatic to architecture nomenclature, the criteria employed, and without a discernable relationship to the crossings of $\boldsymbol{n}$ and $\boldsymbol{a}$.

Supplementary to the main findings, an inspection of simulation study I yielded several corollary relationships between an architecture's parametric construction and $\Lambda_{\phi'}$ ($\Lambda_{\phi'_{C}-\phi'}$), conditional on architecture nomenclature. First, there was a non-injective relationship between the genetic parameter vectors and the focal quantities of interest. That is to say, of the 6075 unique architectures in which, $\boldsymbol{\varepsilon} = [0]$, $\Psi'(\boldsymbol{g})_{\mathbf{Max}}$ and $\Psi'(\boldsymbol{g})_{\mathbf{Min}}$ architectures with the property of epistasis, respectively generated only 2568 and 1933

---

[140] From sections 8.4.1, and 8.4.2, the *minority* of $\Lambda_{1-\beta(\phi'^{*}_{Max},n^{*},a^{*})}$, each coded to a unique pairing of [$\boldsymbol{n}$, $\boldsymbol{a}$] (N=11, min: [n=500, a=0.05]; max: [n=1000, a=0.40]), and the *minority* of $\Lambda_{1-\beta(\phi'_{Min},n,a)}$, each coded to a unique pairing of [$\boldsymbol{n}$, $\boldsymbol{a}$] (N=11 ,min: [n=500, a=0.05]; max: [n=1000, a=0.40]), respectively.

[141] Although there were no formal criteria as a metric of the size of bias.

unique epistatic effect sizes. Additionally, of the 5238 and 4482 legitimate $\Psi'(\boldsymbol{g})_{\mathbf{Max,GE}}$ and $\Psi'(\boldsymbol{g})_{\mathbf{Min,GE}}$ architectures with the property of epistasis only 2764 (2862) and 1312 (1359) unique true(contaminated) epistatic effect sizes were respectively generated. Second, there were 594 $\Psi'(\boldsymbol{g})_{\mathbf{Max,GE}}$ and $\Psi'(\boldsymbol{g})_{\mathbf{Min,GE}}$ architectures *without* the property of epistasis[142]. Third, bespoke to architecture nomenclature there was a unique combination of parameters *k*, φ, H^2 associated to the empirical distributions of $\Lambda_{\phi'}$ ($\Lambda_{\phi'_C-\phi'}$), in particular: 1) the three largest nominal values of $\phi'^*(|\phi'^*_{(C)} - \phi'^*|)$; 2) the largest proportion of variance in $\Lambda_{\phi'}$ ($\Lambda_{\phi'_C-\phi'}$); 3) and the parametric construction of architectures which yield small, medium, and large magnitudes of ϕ'^* and $\phi'^*_{(C)}$(see Appendix C for details).

Concerning the former, for architectures in which, $\boldsymbol{\varepsilon} = [0]$, the three largest nominal epistatic effect sizes were engendered by both $\Psi'(\boldsymbol{g})_{\mathbf{Max}}$ and $\Psi'(\boldsymbol{g})_{\mathbf{Min}}$ architectures under slightly different parameterizations[143]. Herein the three $\Psi'(\boldsymbol{g})_{\mathbf{Max}}$ architectures were characterized by complete dominance of the homozygous recessive alleles for both loci, equally rare recessive allele frequencies, and large broad-sense heritability. In contrast, the three $\Psi'(\boldsymbol{g})_{\mathbf{Min}}$ architectures were characterized by complete dominance of the homozygous dominant allele, equally large recessive allele frequencies, and large broad-sense heritability. Notably, based upon the utility of the *max* and *min* $\Psi'(\boldsymbol{g})$, the construction of these particular architectures mirror (to a certain extent) categories of epistasis (e.g., duplicate dominant and duplicate recessive epistasis) encountered in the study of diallelic crosses[144]. While the disparities between the

---

[142] Naturally, architectures without the property of epistasis also yield a population level epistatic variance component of zero. While decomposition of the *kinds* of architectures that engender a zero epistatic variance component is beyond the scope of this particular thesis, this is a topic for further consideration at a later time.

[143] Notably, while additive genetic parameters (α_1,α_2) were *equal* between loci for $\Psi'(\boldsymbol{g})_{\mathbf{Max}}$[143]($\alpha_1 = [44, 16, 32], \alpha_2 = [44, 16, 32]$)and *variable* for $\Psi'(\boldsymbol{g})_{\mathbf{Min}}$ architectures ($\alpha_1 = [16,16,16]$), ($\alpha_2 = [16,32,44]$).

[144] While the consensus of classifying epistasis according to the divergence of digenic phenotypic ratios from (9:3:31) remains a remnant of the past (Bateson 1908; Cordell, 2002; Miko, 2008) its prominence in the characterization of model organisms provides a unique point of reference. Notably, all six classifications of digenic epistasis rest upon the circumstance *both* causal loci have *complete dominance* and implicates *interaction*, *masking*, and *modification* of phenotypic expression due to the interaction of the alleles of two or more loci (Miko, 2008). The six classifications are as follows: 1) *recessive epistasis* – a recessive allele masks both the dominant and recessive alleles at a second locus (9:3:4). An empirical example is the grain colour of maize; 2) *duplicate recessive epistasis* - a recessive allele at either of the two loci, masks the expression of the dominant alleles at both loci (9:7). An empirical example is the colour of the pea flower. Also referred to as complementary gene

definition of epistasis as departures from the phenotypic ratio of 9:3:31, and deviations from additive gene-effects on a quantitative phenotype remains a well-documented topic (see e.g., Cheverud & Routman, 1995; Cordell 2002; Templeton, 2000; Mackay, 2004; Phillips, 2008; Wei, Hemani, & Haley, 2014), it is interesting to note that epistatic gene-action of this sort, is echoed within our simulation and arises in the circumstance when both $\Psi'(\boldsymbol{g})_{\mathbf{Max}}$ and $\Psi'(\boldsymbol{g})_{\mathbf{Min}}$ architectures have the property of epistasis and the magnitude of its population-level effect is maximal.

In contrast, for architectures in which $\boldsymbol{\varepsilon} \neq [0]$ the three highest values of absolute bias constructed by $\Psi'(\boldsymbol{g})_{\mathbf{Max,GE}}$ and $\Psi'(\boldsymbol{g})_{\mathbf{Min,GE}}$ architectures had unique locus-specific effects. For $\Psi'(\boldsymbol{g})_{\mathbf{Max,GE}}$ architectures the three largest absolute bias was characterized by large broad-sense heritability, and for the first locus, under-dominance and rare recessive allele frequency in the population. For the second, complete dominance of the homozygous dominant allele, and large recessive allele frequency in the population. For all three $\Psi'(\boldsymbol{g})_{\mathbf{Min,GE}}$ architectures were characterized by large broad-sense heritability. The first locus was characterized by complete additivity and intermediate frequency for the recessive allele in the population. In contrast, the second locus was characterized by under dominance and large allele frequency of the recessive allele in the population.

Regarding the second, upon investigating the role of genetic parameters in the variability of both $\Lambda_{\phi'}$ ($\Lambda_{\phi'_C - \phi'}$), it is the case, the same genetic parameters (i.e., k, φ, H^2) accounted for the largest proportion of variance across architecture nomenclature. For architectures in which, $\boldsymbol{\varepsilon} = [0]$ it is the case main effect H^2 accounted for the majority of the variability in $\Lambda_{\phi'}$; followed by pooled-main effects $\varphi.$ and $k.$ for architectures $\Psi'(\boldsymbol{g})_{\mathbf{Max}}$ and $\Psi'(\boldsymbol{g})_{\mathbf{Min}}$, respectively; and finally, pooled main effects $k.$ for $\Psi'(\boldsymbol{g})_{\mathbf{Max}}$ and $\varphi.$ for $\Psi'(\boldsymbol{g})_{\mathbf{Min}}$ architectures. For architectures in which, $\boldsymbol{\varepsilon} \neq [0]$, it is the case, 2-way

action as both genes are required for phenotypic expression; 3) *dominant epistasis* – a dominant allele at one locus masks the phenotypic effect of the dominant and recessive alleles at a second (12:3:1). Empirical examples include skin color in mice, seed coat colour in barley, and the colour of summer squash; 4) *duplicate dominant epistasis* - a dominant allele at either locus masks the recessive alleles at either locus (15:1). Empirical examples include awn in rice and nodulation in peanuts; 5) *dominant and recessive epistasis* - the dominant allele at either locus masks the effect of the other (13:3); and 6) *polymeric gene-action* - when the individual action of dominant alleles produce a similar phenotypic effect, but the presence of both alleles produces an enhanced phenotype (9:6:1). Empirical examples are the shape of summer squash and awn length (Miko, 2008). While a full examination of *all* simulated architectures is beyond the scope of the thesis, these observations provide an interesting point of reference.

interactions 2-way interactions k_1: k_2 accounted for the majority of the variability in $\Lambda_{\phi'_C - \phi'}$ [145]; followed by a 3-way interaction (k_1: φ_1: k_2) for $\Psi'(\boldsymbol{g})_{\text{Max.GE}}$ architectures, and pooled main effect *k.* for $\Psi'(\boldsymbol{g})_{\text{Min.GE}}$ architectures[146]; and finally, a 3-way interactions for both $\Psi'(\boldsymbol{g})_{\text{Max.GE}}$ (k_1: k_2: H^2), and $\Psi'(\boldsymbol{g})_{\text{Min.GE}}$ architectures (k_1: φ_1: k_2)[147].

Concerning the latter, the production of the small, medium, and large magnitudes of ϕ'^* ($\phi'^*_{(C)}$) appeared to vary over the unique combinations of joint parameter values faceted by the levels of H^2 [148]. For the 6075 $\Psi'(\boldsymbol{g})_{\text{Max}}$ architectures with the property of epistasis, upon visual inspection of Figures C.1 to C.7[149] (Appendix C) the distributions of $\Lambda_{\phi'_{\text{Small}}}$, $\Lambda_{\phi'_{\text{Medium}}}$, and $\Lambda_{\phi'_{\text{Large}}}$ varied *relatively* equally over the joint combinations of a, φ, and k. However, while distributions of $\Lambda_{\phi'_{\text{Small}}}$, and $\Lambda_{\phi'_{\text{Medium}}}$ were present across all levels H^2, the distribution $\Lambda_{\phi'_{\text{Large}}}$ increased in variability and magnitude as the magnitude of H^2 increased (with several notable outliers).

Next, upon visual inspection of Figures C.8 to C.14 (Appendix C) for the 6075 $\Psi'(\boldsymbol{g})_{\text{Min}}$ architectures[150] with the property of epistasis, the distributions of $\Lambda_{\phi'_{\text{Small}}}\Lambda_{\phi'_{\text{Medium}}}$, and $\Lambda_{\phi'_{\text{Large}}}$ varied *relatively* equally over the joint combinations of a, φ; and analogous to the afore noted $\Psi'(\boldsymbol{g})_{\text{Max}}$ architectures, $\Lambda_{\phi'_{\text{Large}}}$ increased in variability and magnitude as the magnitude of H^2 increased. However, the three distributions of ϕ' varied considerably over the joint combinations of *k.* Herein, any pairwise parameter combinations which *included under dominance* ($k < 0$) produced $\Lambda_{\phi'_{\text{Small}}}$ across all levels H^2. Finally, for the 5238 and 4482

---

[145] $\Psi'(\boldsymbol{g})_{\text{Max.GE}}$ (k_1: k_2 =0.246), and $\Psi'(\boldsymbol{g})_{\text{Min.GE}}$ architectures (k_1: k_2 =0.35).

[146] $\Psi'(\boldsymbol{g})_{\text{Max.GE}}$ (k_1: φ_1: k_2= 0.194), and $\Psi'(\boldsymbol{g})_{\text{Min.GE}}$ architectures (k = 0.213%).

[147] $\Psi'(\boldsymbol{g})_{\text{Max.GE}}$ (k_1: k_2: H^2 = 0.085), and $\Psi'(\boldsymbol{g})_{\text{Min.GE}}$ architectures (k_1: φ_1: k_2 = 0.054).

[148] We evaluated the nine joint combinations: 1) rare (0.1), intermediate (0.5), and large (0.9) allele frequencies (φ_1, φ_2) of the recessive allele (A_2) for two causal loci in a population; 2) the linear contribution of both loci to trait variation (α_1, α_2); and 3) of course, the twenty-five combinations of the joint combination of the non-linear contribution of both loci to trait variation (k_1, k_2). For each of the analyses, all other parameters were held constant.

[149] Notably, all Figures herein present the crossing of the joint parameters, and the distributions of ϕ'^*, $\phi'^*_{(C)}$, and $\phi'^*_{(C)} - \phi'^*$, faceted by H^2.

[150] [Small ϕ': n=3839; Medium ϕ': n=478; Large ϕ': n=1758].

architectures of $\Psi'(\boldsymbol{g})_{\mathbf{Max,GE}}$[151] and $\Psi'(\boldsymbol{g})_{\mathbf{Min.GE}}$[152] construction with the property of epistasis, visual inspection of Figures C.15 to C.32 (Appendix C) suggested slight divergences between $\Lambda_{\phi'_{(c)}}$ and $\Lambda_{\phi'}$ over the joint parameter combinations of *a*, φ, and moderate too large for *k,* particularly so for parameter combinations (k_1=-6 k_2 =-1) and (k_1=-1 k_2 =0; k_1=-1 k_2 =1; k_1=-1 k_2 =5).

9.2. Reconciling Results with Extant Literature

As converging empirical evidence portrays epistasis as a ubiquitous property of genetic architectures and a protagonist in complex trait variability, it is no wonder the study of epistasis at its most rudimentary form is of interest (*s*=*2*). Naturally, consideration of architectures of this sort in an experimental setting is typically conducted with model organisms (i.e., chickens, plants, drosophila), as its experimental design affords control over genetic architecture[153], breeding structure, and environmental conditions[154]. However, as experimental designs for human populations remain without dominion over both genetic and environmental factors, epistatic detection often relies upon population-level estimates; accordingly, the empirical scientists often turn to simulation studies to unpack and adjudicate the functional roles of genetics and environment on complex trait variability.

While our simulation study is not the first to consider simulating digenic architectures with the property of epistasis, contemporary accounts in the literature focus on several scenarios: 1) *disease traits* (see Li & Reich, 2000[155]; Evans, Marchini,

---

[151] [Small ϕ': n=3963; Medium ϕ': n=762; Large ϕ': n=3839].

[152] [Small ϕ': n=3839; Medium ϕ': n=478; Large ϕ': n=1758].

[153] Genetically tractable studies which permit empirical researchers to the study of epistasis vis-à-vis: 1) natural and induced mutations on both homozygous genetic background and for segregating variants; 2) inbred lines and outbred populations; 3) chromosome substitution, introgression, near-isogenic lines. (Mackay, 2014).

[154] Naturally, experimental designs on model organisms partial out covariation between genetics and environment – a notable feature which often remains absent in procedures involving human populations.

[155] The authors characterize the space of all nonredundant two-locus penetrance models, which restrict disease probabilities to 0 and 1, and a series of classifications which supplement or expand upon disease models such as *multiplicative, heterogeneity, threshold,* and *interference*.

Morris, & Cardon, 2006[156]; Hallgrímsdóttir &Yuster, 2008[157]; Moore, Hahn, Ritchie, Thornton, & White, 2004[158]); 2) *complex traits* with linkage structure and allele-frequency distributions which vary from the assumptions of HWE and LE (Kao & Zeng, 2002; Hill, Goddard, & Visscher, 2008); and 3) the simulation of genome-wide data[159] to adjudicate novel tools of epistatic detection according to algorithm scalability, FWER[160], and statistical power (Purcell, 2007; Zhang, Huang, Zou, Wang, 2010[161]; Wang et al., 2011; Zhang, Xie, Liang, & Xiong, 2016; Tuo, Zhang, Yuan, He, Liu, Liu, 2017). All told, it appears our study is one of the first to analytically consider the range of ϕ' produced by four unique architectures with the properties of epistasis and gene-environmental association, and the performance of detection of the omnibus F test of interaction over a pre-selected range of *n* and *a*. To this end, while the ability to contextualize our findings within the extant literature remains somewhat limited, we are afforded the unique opportunity to explore the extent to which our findings map onto theoretical expectations of epistasis.

As afore noted, several prominent authors distinguish *functional* and *statistical* epistasis, suggesting both: 1) inconsonance between the strength of architectures underlying gene-action and the magnitude of its population-level effects[162]; and 2) the

---

[156] The authors evaluated 50 di-genic epistatic models for disease traits (after removing redundant models generated from $2^9 = 512$ possibilities yielded by binary genotypic means (0,1)) and calculating both single locus and interaction variance components.

[157] Authors derive a series of two-locus models for continuous penetrance values and evaluate the triangulation of the nine genotypic values. Their work suggests there are sixty-nine symmetry classes for the shape of a two-locus model.

[158] Authors construct a series of 10^6 penetrance models with nine penetrance values to simulate a series of disease models (i.e., autosomal recessive pathologies such as cystic fibrosis).

[159] Simulated data which mimics the structure of genome-wide association or quantitative trait-loci analyses (i.e., implementation of algorithms such as *Hapsample* (Wright et al., 2007)).

[160] Authors herein vary in how they define Type I error rate and the types of family-wise error control used. Wang et al., 2011 define Type I error rate of a detection tool as the proportion of data-sets false discovery of epistasis. See Becker, Herold, Meesters, Mattheisen, Baur (2011) for a discussion on significance levels in GWAS interaction analyses.

[161] Herein, the authors tested the algorithm TEAM using simulated human GWAS data (112036 SNPs, 250 cases, 250 controls) and employed the false discovery rate (FDR) threshold of 0.005.

[162] Several prominent authors suggest that small magnitudes of $\sigma^2_{EP}(\phi')$ are not incompatible with substantial epistatic gene-action, as epistatic genotypic effects contribute to additive, dominant and epistatic gene-effects and their population-level genetic variance components (Cheverud, Routman, 1994; Lynch & Walsh, 1998; Templeton, 2000; Mackay, 2014). To this end, authors propose epistatic effects have the potential to *bias* σ^2_A and σ^2_D, referring to a distinction between *real* and *apparent* genetic variance. (e.g., *real* additive genetic variance is due to *additive gene action* between causal loci, whereas *apparent* additive genetic variance is due to non-zero main effects that arise from epistatic gene-action *across* causal loci (Mackay, 2014)). Recall, of course, when *s=2*,

expectation that the population-level effect of epistasis is *maximal* when recessive allele-frequencies in a population are *intermediate* (0.5)[163] (Cheverud & Routman, 1994; Falconer & Mackay, 1996; Lynch & Walsh, 1998; Templeton, 2000; Mackay, 2014; Huang & Mackay, 2016). Indeed, within our own simulation, architectures of epistatic construction engendered distributions of population-level effects which ranged from complete absence, to small, medium, and large departures (in accordance to Cohen's guidelines (1988)); however, our findings diverged from contemporary expectations to suggest, rather, a unique combination of parameters (i.e., k φ, H^2) were not only implicated in the largest nominal values ϕ' ($|\phi'_{(C)} - \phi'|$), but also the largest *proportion of variance in* $\Lambda_{\phi'}$ ($\Lambda_{\phi'_C - \phi'}$), and the manifest distributions of small, medium or large magnitudes of ϕ' ($|\phi'_{(C)} - \phi'|$)[164]. While the role of genetics and environment on phenotypic expression is a well-documented phenomenon (Lewontin, 1974; Alberch, 1991; Pigliucci, 2010; Svedolv & Thompson, 2018), we were unable to find contemporary expectations regarding the impact of the gene-environmental association on the detection of epistasis (and the magnitude/direction of its distortion). To this end, it is with due circumspection our simulations present a preliminary account of *one* potential way gene-environmental association may impact the empirical detection of epistasis.

---

epistatic effects can be characterized by the following categories: 1) additive x additive; 2) additive x dominance; 3) dominance x additive; 4) dominance x dominance interactions (see Lynch & Walsh, 1998; Templeton 2000). To this end, when minor allele-frequencies in a population depart from 0.5, epistatic effects are proposed to contribute to *both* additive and dominance variance components (Templeton, 2002). While it is the case the obscure relationship between functional and statistical epistasis remains a well-documented topic in both theoretical and empirical literature, a full review and analysis of this sort is beyond the scope of the thesis. Please see the works of Cheverud & Routman, (1994); Lynch & Walsh, (1998); Templeton, (2000); Cordell (2002); Miko (2008); Hill, Goddard, & Visscher, (2008); Phillips (2008); Moore & Williams, (2009); Mackay, (2014); Wei, Hemani, & Haley, (2014) for further detail.

[163] While only a sample of the allele frequency spectrum was considered in our simulation, it was the case, both $\Psi'(\boldsymbol{g})_{\mathbf{Max}}$ and $\Psi'(\boldsymbol{g})_{\mathbf{Min}}$ architectures yielded the largest three magnitudes of ϕ'^* in the circumstance the proportion of phenotypic variance attributable to genetics was *large* (H^2=0.8)[163] and both allele frequencies were *extreme* (0.1, 0.9), rather than intermediate (0.5). As our corollary results suggest the magnitude of ϕ' varies over the levels of H^2, our findings are in line with the theoretical expectations that genetic variance attributed to epistasis will increase or decrease concomitant to the magnitude of total genetic variability (i.e., whether the trait is *rare* or c*ommon* within a population). As Zuk and colleagues (2012) suggest, when a trait is rare versus common in a population the genetic variability is lower, and so too, the population effect of epistasis.

[164] Herein the unique impact of the sampled parameters k, φ, H^2 on $\Lambda_{\phi'}$ were not overtly unsurprising given: 1) all genetic effects are population specific and specified by parameters a, k, and φ (Lynch & Walsh, 1994); 2) the definition and magntidue of population-level genetic effects are a function weighted by φ and k (see Lynch & Walsh, 1998); and 3) the proportion of phenotypic variability attributed to environmental variance was set to the units of broad-sense heritability.

9.3. Limitations and Future Directions

In consideration of the thesis, there are several natural limitations inherent to both the general construction of any simulation study and those bespoke to our aims. Of the former, it is clear the realism of such a simulation is conditional upon the presence of *all* elements genetic and environmental, which impact trait variation. To this end, while it is reasonable there are omitted elements that inform trait variation in natural populations, we aimed to generate four *rudimentary* digenic architectures, which in its simplest form permit us the opportunity to consider the empirical range of its population-level effects without the impact of both biological and experimental noise. As the study of epistatic architectures in natural populations remains in its infancy, it is with due circumspection we contextualize our results, given both the scale of the design and upon reflection that there exist potentially innumerable functional forms architectures of epistatic construction may manifest.

In light of the afore noted limitations, we now present several natural extensions of our work and potential areas of further exploration: 1) the relationships between the architecture of epistatic construction and the population-level effect of epistasis across architecture nomenclature. In particular, a full characterization of the parametric structure of the 594 $\Psi'(\boldsymbol{g})_{\mathbf{Max,GE}}$ and $\Psi'(\boldsymbol{g})_{\mathbf{Min,GE}}$ architectures wherein σ^2_{EP}=0; 2) investigation into the relationship between the magnitude and direction of mean environmental impacts conditional on genotype on the distribution of bias engendered for architectures in which, $\boldsymbol{\varepsilon} \neq [0]$; 3) investigation into the orthogonal decomposition of σ^2_{EP} (i.e., $\sigma^2_{AxA}, \sigma^2_{AxD}, \sigma^2_{DxA}, \sigma^2_{DxD}$) and assess the purposed contribution of epistatic genotypic-effects to both σ^2_A and σ^2_D over varying allele distributions and the entire allele-spectrum[165]; 4) whether our current findings are generalizable to other polygenic architectures of complex traits, $s \leq 3$; and 5) whether the presence of gene-environmental interaction (e.g., *epigenetics*) plays an independent or associated role to epistasis in quantitative trait variation, and if its presence obscures in some manner the performance of epistatic detection.

[165] Based on the definitions laid forth by Cheverud & Routman, (1994).

9.4 Conclusion

All told, by way of analysis and simulation study, our aims to shed light on the quantitative issues of why epistasis is so hard to detect led us to characterize the *statistical detection* problem, elucidate *two candidate explanations*, and formally assess the *performance of detection* for the omnibus F-test statistic of interaction. In so doing, it is the case simulation studies I and II afford to us in concert, the unique vantage to evaluate the merits of both candidate explanations, unabridged by the restrictions effectuated in the empirical setting of epistatic detection. To this end, not only do our findings support both candidate explanations, but they also provide preliminary insight into the range of epistatic effect sizes and the parametric construction of architectures which yield the property of epistasis. Naturally, it is with due circumspection that our findings are offered into the unfolding narrative around the relationship between a digenic architecture of epistatic construction and its role in the functional mapping from genotype to phenotype.

References

Alberch, P. (1991). From genes to phenotype: dynamical systems and evolvability. *Genetica*, *84*(1), 5-11.

Anderson, D. W., McKeown, A. N., & Thornton, J. W. (2015). Intermolecular epistasis shaped the function and evolution of an ancient transcription factor and its DNA binding sites. *Elife*, *4*, e07864.

Assareh, Volkert, & Jing Li. (2012). Interaction Trees: Optimizing Ensembles of DecisionTrees for Gene Gene Interaction Detections. *Machine Learning and Applications (ICMLA),2012 11thInternational Conference on, 1*, 616-621.

Aylor, D., Zeng, Z., & Allison, D. (2008). From Classical Genetics to QuantitativeGeneticsto Systems Biology: Modeling Epistasis (Modeling Epistasis). *PLoS Genetics, 4*(3),E1000029.

Burch, C. L., & Chao, L. (2004). Epistasis and its relationship to canalization in the RNA virus φ 6. Genetics, 167(2), 559-567.

Bateman, A. J. (1959). The viability of near-normal irradiated chromosomes. *International Journal of Radiation Biology and Related Studies in Physics, Chemistry and Medicine*, *1*(2),170-180.

Bateson, W., & Mendel, G. (1913). *Mendel's principles of heredity*. University press.

Bergboer, Zeeuwen, & Schalkwijk. (2012). Genetics of Psoriasis: Evidence for Epistatic Interaction between Skin Barrier Abnormalities and Immune Deviation. *Journal of Investigative Dermatology, 132*(10), 2320-2331.

Burdick, K., Kamiya, A., Hodgkinson, C., Lencz, T., DeRosse, P., Ishizuka, K., . . .Malhotra, A. (2008). Elucidating the relationship between DISC1, NDEL1 and NDE1 and the risk for schizophrenia: Evidence of epistasis and competitive binding. *Human Molecular Genetics, 17*(16), 2462-2473.

Bush WS, Moore JH. Chapter 11: Genome-Wide Association Studies. Lewitter F, Kann M,eds. *PLoS Computational Biology*. 2012;8(12):e1002822.doi:10.1371/journal.pcbi.1002822.

Cattaert, T., Calle, M. L., Dudek, S. M., Mahachie John, J. M., Van Lishout, F., Urrea,V.,Ritchie, M,D.,VanSteen,K. (2011). Model-Based Multifactor Dimensionality Reduction for detecting epistasis in case–control data in the presence of noise. *Annals of human genetics*, *75*(1), 78-89.

Cheverud, J. (1988). A COMPARISON OF GENETIC AND PHENOTYPICCORRELATIONS. *Evolution*, *42*(5), 958-968.

Cheverud, J. M., & Routman, E. J. (1995). Epistasis and its contribution to genetic variance components. *Genetics*, *139*(3), 1455-1461.

Cross-Disorder Group of the Psychiatric Genomics Consortium. (2013). Identification of riskloci with shared effects on five major psychiatric disorders: a genome-wide analysis. *Lancet*. *381*(9875), 1371-1379.Doi:10.1016/S01406736(12)62129-1.

Cross-Disorder Group of the Psychiatric Genomics Consortium (2013). Genetic relationship between five psychiatric disorders estimated from genome-wide SNPs. *Nature genetics*. *45*(9):984-994. Doi:10.1038/ng.2711.

Cockerham, C. C. (1954). An extension of the concept of partitioning hereditary variance for analysis of covariances among relatives when epistasis is present. *Genetics*, *39*(6), 859-882.

Cordell, H. J. (2009). Detecting gene–gene interactions that underlie human diseases. *Nature Reviews Genetics*, *10*(6), 392-404.

Cortes, A., Pulit, S. L., Leo, P. J., Pointon, J. J., Robinson, P. C., Weisman, M. H., ... & Chiocchia, G. (2015). Major histocompatibility complex associations of ankylosing spondylitis are complex and involve further epistasis with ERAP1. *Nature communications*, *6*, 7146.

Costanzo, M., Baryshnikova, A., Bellay, J., Kim, Y., Spear, E. D., Sevier, C. S., ... & Prinz,J. (2010). The genetic landscape of a cell. *science*, *327*(5964), 425-431.

Coutinho, A., Sousa, M., Martins, I., Correia, M., Morgadinho, C., Bento, T., . . . Vicente, H. (2007). Evidence for epistasis between SLC6A4 and ITGB3 in autism etiology and in the determination of platelet serotonin levels. *Human Genetics, 121*(2), 243-256.

Culverhouse R, Suarez BK, Lin J, Reich T. A Perspective on Epistasis: Limits of Models Displaying NoMain Effect. *American Journal of Human Genetics*. 2002;70(2):461-471.

Dillmann, C., & Foulley, J. L. (1998). Another look at multiplicative models in quantitative genetics. *Genetics Selection Evolution*, *30*(6), 543.

Dudoit S, van der Laan MJ. (2008). Multiple testing procedures with applications to genomics: *Springer genetics*, *70*(6), 726-737.

De Visser, J., & Hoekstra, R. (1998). Synergistic epistasis between loci affecting fitness: Evidence in plants and fungi. *Genetical Research, 71*(1), 39-49.

De Visser, J. A. G., Park, S. C., & Krug, J. (2009). Exploring the effect of sex on empirical fitness landscapes. *the american naturalist*, *174*(S1), S15-S30.

Elena, S., Solé, & Sardanyés. (2010). Simple genomes, complex interactions: Epistasis in RNA virus. *Chaos: An Interdisciplinary Journal of Nonlinear Science, 20*(2), 026106.

Einot, I., & Gabriel, K. R. (1975). A study of the powers of several methods of multiple comparisons. *Journal of the American Statistical Association*, *70*(351a), 574-583.

Evans, D. (2011). Gene-Gene Interaction and Epistasis-Chapter 12. In *Analysis of ComplexDisease Association Studies,*197-213.

Evans, D. M., Spencer, C. C. A., Pointon, J. J., Su, Z., Harvey, D., Kochan, G., … the WellcomeTrust Case Control Consortium 2 (WTCCC2). (2011). Interaction between *ERAP1* and HLA-B27 in ankylosing spondylitis implicates peptide handling in the mechanism for HLA-B27 in disease susceptibility. *Nature Genetics*, *43*(8), 761–767.http://doi.org/10.1038/ng.873

Evans, D., Marchini, J., Morris, A., Cardon, L., MacKay, T., & Mackay, Trudy. (2006). Two Stage Two-Locus Models in Genome-Wide Association (Epistasis inGenome-Wide Association). *PLoS Genetics, 2*(9), E157.

Everts, R, E., Rothuizen, J., van Oost, B,A. (2000). Identification of a premature stop codon inthe melanocyte stimulating hormone receptor gene (MC1R) in Labrador and Golden retrievers with yellow coat color, *Animal Genetics*.

Flatt, T. (2005). The evolutionary genetics of canalization. *The Quarterly review of biology*, *80*(3), 287-316.

Gao H, Granka JM, Feldman MW. (2010). On the Classification of Epistatic Interactions. *Genetics*. *184*(3), 827837. Doi:10.1534/genetics.109.111120.

Gratten, J., Wray, N. R., Keller, M. C., & Visscher, P. M. (2014). Large-scale genomics unveils the genetic architecture of psychiatric disorders. *Nature neuroscience*, *17*(6), 782.

Grigorenko, E. (2003). *Epistasis and the genetics of complex traits.* (pp. 247-266). American Psychological Association.

Gyenesei, A., Moody, J., Semple, C, M., Haley, C,S.,m Wei, W. (2012). High-throughput analysis of epistasis in genome-wide association studies with BiForce, *Bioinformatics*,28(15), 1957–1964.

Hansen TF. (2006). The evolution of genetic architecture. Annu Rev Ecol Evol Syst. 37(1):123– 157.

Halligan, D., & Keightley, P. (n.d.). Spontaneous Mutation Accumulation Studies in Evolutionary Genetics. *Annual Review of Ecology, Evolution, and Systematics, 40*(1), 151-172.

Hallgrimsdottir, I., & Yuster, D. (2006). A complete classification of epistatic two-locus models. *BMC Genet. 9*(17). [PubMed: 18284682]

Heun, Reinhard, Kölsch, Heike, Ibrahim-Verbaas, Carla A, Combarros, Onofre, Aulchenko, Yurii S, Breteler, Monique, . . . Lehmann, Donald J. (2012). Interactions between PPAR-α and inflammation-related cytokine genes on the development of Alzheimer's disease, observed by the Epistasis Project. *International Journal of Molecular Epidemiology and Genetics*, *3*(1), 39-47.

Hu, T., Sinnott-Armstrong, N. A., Kiralis, J. W., Andrew, A. S., Karagas, M. R., & Moore, J. H.(2011). Characterizing genetic interactions in human disease association studies usingstatistical epistasis networks. *BMC bioinformatics*, *12*(1), 364.

Huang, W., & Mackay, T. F. (2016). The Genetic Architecture of Quantitative Traits Cannot Be Inferred from Variance Component Analysis. *PLoS genetics*, *12*(11), e1006421. https://doi.org/10.1371/journal.pgen.1006421

Holzinger, K. J. (1929). The relative effect of nature and nurture influences on twin differences. *Journal of Educational Psychology*, *20*(4), 241.

Ileena Mitra, Alinoë Lavillaureix, Erika Yeh, Michela Traglia, Kathryn Tsang, Carrie E Bearden, . . . Lauren A Weiss. (2017). Reverse Pathway Genetic Approach Identifies Epistasis in Autism Spectrum Disorders. *PLoS Genetics*,*13*(1), E1006516.

Iqbal, M., Khan, K., Rahman, H., & Sher, H. (2010). Detection of epistasis for plant height and leaf area per plant in maize (Zea mays L.) from generation means analysis. *Maydica*, *55*(1), 33-39. (additive x additive interaction)

Falconer, D. S. (1975). Introduction to quantitative genetics. *Pearson Education India*.

Falconer, D. S. (1989). Introduction to quantitative genetics. New York, NY: *Longman Essex*.

Falconer, D. S. (1967). The inheritance of liability to diseases with variable age of onset, withparticular reference to diabetes mellitus.

Falconer, D.S., & Mackay, T.F.C. (1996). Heritability. *Introduction to quantitative genetics*,160183.

Fisher, R. A. (1918). 009: The Correlation Between Relatives on the Supposition of MendelianInheritance.

Fisher, R. A., Immer, F. R., & Tedin, O. (1932). The genetical interpretation of statistics of thethird degree in the study of quantitative inheritance. *Genetics*, *17*(2), 107-124.

Gandon, S., & Otto, S. P. (2007). The evolution of sex and recombination in response to abiotic or coevolutionary fluctuations in epistasis. *Genetics*, *175*(4), 1835-1853.

Geiringer, H. (1944). On the probability theory of linkage in Mendelian heredity. *The Annals of Mathematical Statistics*, *15*(1), 25-57.

Gregersen, J. W., Kranc, KR., Ke, X., Svendsen, P., Madsen, L.S., Thomsen, A.R., & Fugger, L. (2006). Functional epistasis on a common MHC haplotype associated with multiple sclerosis. *Nature,* 443(7111), 574.

Guillaume, F., & Otto, S. P. (2012). Gene functional trade-offs and the evolution of pleiotropy. *Genetics*, *192*(4), 1389-1409.

Hall, D. W., Agan, M., & Pope, S. C. (2010). Fitness epistasis among 6 biosynthetic loci in the budding yeast Saccharomyces cerevisiae. *Journal of heredity*, *101*(suppl_1), S75-S84.

Hill, W. G., Goddard, M. E., & Visscher, P. M. (2008). Data and theory point to mainly additive genetic variance for complex traits. *PLoS Genet*, *4*(2), e1000008.

Horner, T. W., Comstock, R. E., & Robinson, H. F. (1955). *Non-allelic gene interactions and the interpretation of quantitative genetic data*.

Holzinger, K.J. (1929). The relative effect of nature and nurture influences on twin differences. *Journal of Educational Psychology, 20*(4),241.

Jinks, J. & Fulker, D. (1970). Comparison of the biometrical genetical, MAVA, and classical approaches to the analysis of the human behavior. *Psychological Bulletin, 73*(5), 311-349

Johannsen, W. (2014). The genotype conception of heredity. *International journal of epidemiology*, *43*(4),9891000.

Kam-Thong, T., Azencott, C. A., Cayton, L., Pütz, B., Altmann, A., Karbalai, N., …& Borgwardt, K. M. (2012). GLIDE: GPU-based linear regression for detection of epistasis. *Human heredity*, *73*(4), 220-236.

Kendler, K,S., Gardner, C, O. (2010). "Interpretation of interactions: Guide for the perplexed".*British Journal ofPsychiatry*, *197*(3), pp. 170–171.

Kempthorne, O. (1997). Heritability: Uses and abuses. *Genetica*, *99*(2), 109-112.

Kempthorne, O. (1978). A BIOMETRICS INVITED PAPER: Logical, epistemological and statistical aspects of nature-nurture data interpretation. *Biometrics*, 1-23.

Khan, A. I., Dinh, D. M., Schneider, D., Lenski, R. E., & Cooper, T. F. (2011). Negative epistasis between beneficial mutations in an evolving bacterial population. *Science*, *332*(6034), 1193-1196.

Kölsch, Heike, Lehmann, Donald, Ibrahim-Verbaas, Carla, Combarros, Onofre, Duijn, Cornelia, Hammond, Naomi, . . . Heun, Reinhard. (2012). Interaction of insulin and PPAR-α genes in Alzheimer's disease: The Epistasis Project. *Journal of NeuralTransmission, 119*(4), 473-479.

Kirino, Y., Bertsias, G., Ishigatsubo, Y., Mizuki, N., Tugal-Tutkun, I., Seyahi, E., ... & Emrence, Z. (2013). Genome-wide association analysis identifies new susceptibility loci for Behcet's disease and epistasis between HLA-B* 51 and ERAP1. *Nature genetics*, *45*(2), 202.

Kira, K., & Rendell, L. A. (1992). A practical approach to feature selection. In *MachineLearning Proceedings*, 249-256.

Kononenko, I.: 1994, 'Estimating attributes: analysis and extensions of Relief'. In: L.De Raedt and F. Bergadano (eds.): Machine Learning: ECML-94. *Springer,* 171–182

Lander, Eric S. (1996). "The New Genomics: Global Views of Biology." *Science*, *274*(5287), 53653.

Lehmann, Donald J., Schuur, Maaike, Warden, Donald R., Hammond, Naomi, Belbin, Olivia, Kölsch, Heike, . . . Smith, A. David. (2012). Transferrin and HFE genes interact in Alzheimer's disease risk: The Epistasis Project. *Neurobiology of Aging*, *33*(1), 202.e1 202.e13.

Lehmann, E. L., & Romano, J. P. (2012). Generalizations of the familywise error rate. In *Selected Works of EL Lehmann*(pp. 719-735). Springer, Boston, MA.

Le Rouzic, A., Álvarez-Castro, J. M., & Carlborg, Ö. (2008). Dissection of the Genetic Architecture of Body Weight in Chicken Reveals the Impact of Epistasis on Domestication Traits. *Genetics*, *179*(3), 1591–1599.http://doi.org/10.1534/genetics.108.089300

Li, W., & Reich, J. (2000). A complete enumeration and classification of two-locus disease models. *Human heredity*, *50*(6), 334-349.

Lin, H. X., Yamamoto, T., Sasaki, T., & Yano, M. (2000). Characterization and detection of epistatic interactions of 3 QTLs, Hd1, Hd2, and Hd3, controlling heading date in rice using nearly isogenic lines. *Theoretical and Applied Genetics*, *101*(7), 1021-1028.

Lin, H., Lei, Y., Zhang, B., Dai, Z., & Lu, X. (2015). Common variants of HTR1A and SLC6A4 confer the increasing risk of Schizophrenia susceptibility: A population based association and epistasis analysis. *American Journal of Medical Genetics Part B:Neuropsychiatric Genetics, 168*(8), 749-755.

Liu, Yao-Zhong, Guo, Yan-Fang, Xiao, Peng, Xiong, Dong-Hai, Zhao, Lan-Juan, Shen,Hui, . .Deng, Hong-Wen. (2006). Epistasis between Loci on Chromosomes 2 and 6 Influences Human Height. *The Journal of Clinical Endocrinology &Metabolism, 91*(10), 3821-3825.

Li, W., & Reich, J. (1999). A Complete Enumeration and Classification of Two-Locus Disease Models. Human Heredity, 50(6):334-349 (2000).

Loïc de Pontual, Norann A. Zaghloul, Sophie Thomas, Erica E. Davis, David M.Mcgaughey,Hélène Dollfus, . . . Jeanne Amiel. (2009). Epistasis between RET andBBS mutations modulates enteric innervation and causes syndromic Hirschsprungdisease. *Proceedings of the National Academy of Sciences, 106*(33), 13921-13926.

Lynch, M., & Walsh, B. (1998). *Genetics and Analysis of Quantitative Traits*. Dunerland, MA: Sinauer.

Maruyama, T. (1966). The mutational load with epistatic gene interactions in fitness. *Genetics*, *54*(6),1337-1351.

Mather (1949). *Biometrical Genetics - The Study of Continuous Variation*. Methuen and Co.Ltd; London.

Matthew A. Brown, Tony Kenna, & B. Paul Wordsworth. (2015). Genetics of ankylosing spondylitis—insights into pathogenesis. *Nature Reviews Rheumatology, 12*(2), 81 91.

Mayr, E. (1961). Cause and effect in biology. *Science*, *134*(3489), 1501-1506.

McArdle, J. J., & Prescott, C. A. (2005). Mixed-effects variance components models for biometric family analyses. *Behavior genetics*, *35*(5), 631-652.

McGuffin, P., Rijsdijk, F., Andrew, M., Sham, P., Katz, R., & Cardno, A. (2003). The heritability of bipolar affective disorder and the genetic relationship to unipolar depression. *Archives of general psychiatry*, *60*(5), 497-502.

McKinney, B. A., Reif, D.M., Ritchie, M.D., Moore, J.H. (2006). Machine Learning for Detecting Gene-Gene Interactions: A Review. *Applied bioinformatics*, *5*(2), 77-88.

Miko, I. (2008) Epistasis: Gene interaction and phenotype effects. *Nature Education* 1(1):197

Morrison, M. (2002). Modelling populations: Pearson and Fisher on Mendelism and biometry. *The British journal for the philosophy of science*, *53*(1), 39-68.

Molla, A., Korneyeva, M., Gao, Q., Vasavanonda, S., Schipper, P. J., Mo, H. M., ... & Hsu, A.(1996). Ordered accumulation of mutations in HIV protease confers resistance to ritonavir. *Nature medicine*, *2*(7), 760-766.

Mõttus, R., Kandler, C., Bleidorn, W., Riemann, R., & McCrae, R. R. (2017). Personality traits below facets: The consensual validity, longitudinal stability, heritability, and utility of personality nuances. Journal of Personality and Social Psychology, 112(3), 474.

Moore, J. H., & Hahn, L. W. (2002, September). Cellular automata and genetic algorithms for parallel problem solving in human genetics. In *International Conference on Parallel Problem Solving from Nature* (pp. 821-830). Springer, Berlin, Heidelberg.

Moore JH, Hahn LW., Ritchie MD., Thornton TA., White BC. Application of Genetic Algorithms to the Discovery of Complex Models for Simulation Studies in Human Genetics. *Proceedings of the Genetic and Evolutionary Computation Conference / GECCO Genetic and Evolutionary Computation Conference*. 1150-1155.

Moore, JH., Hahn, LW., Ritchie, MD., Thornton, TA., & White, BC. (2004). Routine discovery of complex genetic models using genetic algorithms. *Applied soft computing*, *4*(1), 79-86.

Neuman, R., Rice, J., & Chakravarti, A. (1992). Two-Locus models of disease. *Genetic Epidemiology*, *9*(5),347-365.

Otto, S. P., & Gerstein, A. C. (2006). Why have sex? The population genetics of sex and recombination.

Pang, X., LZ., Yap, J. S., Wang, J., Zhu, J., Bo, W., ... & Shen, D. (2012). A statistical procedure to map high-order epistasis for complex traits. Briefings in bioinformatics, 14(3), 302-314.

Pavlicev, M., & Wagner, G. P. (2012). A model of developmental evolution: selection, pleiotropy and compensation. *Trends in Ecology & Evolution*, *27*(6), 316-322.

Phillips PC. Epistasis—the essential role of gene interactions in the structure and evolution of genetic systems. *Naturereviews Genetics*. 2008;9(11):855-867. Doi:10.1038/nrg2452

Pigliucci, M. (2010). Genotype–phenotype mapping and the end of the 'genes as blueprint'metaphor. *Philosophical Transactions of the Royal Society B: Biological Sciences*, *365*(1540), 557-566.

Purcell, S., Neale, B., Todd-Brown, K., Thomas, L., Ferreira, M. A., Bender, D., ... & Sham, P. C. (2007). PLINK: a tool set for whole-genome association and population-based linkage analyses. *The American Journal of Human Genetics*, *81*(3), 559-575

Polderman, T. J., Benyamin, B., De Leeuw, C. A., Sullivan, P. F., Van Bochoven, A., Visscher,P. M., & Posthuma,D. (2015). Meta-analysis of the heritability of human traits based on fifty years of twin studies. *Nature genetics*, *47*(7), 702-709

Ramsey, P. H. (1978). Power differences between pairwise multiple comparisons. *Journal of the American Statistical Association*, *73*(363), 479-485.

Ritchie, M,D., Hahn, L,W., Roodi, N., Bailey, L,R., Dupont, W,D., Parl, F,F., Moore, J,H.(2001). Multifactor dimensionality reduction reveals high-order interactions among estrogen metabolism genes in sporadic breast cancer, *Am. J. Hum. Genet, 69*(1).

Rijsdijk, F. V., & Sham, P. C. (2002). Analytic approaches to twin data using structural equation models. *Briefings in bioinformatics*, *3*(2), 119-133

Robnik ˇ Sikonja, M. and I. Kononenko, (1997), 'An adaptation of Relief for attribute estimation in regression'. In: D. H. Fisher (ed.): Machine Learning: Proceedings of the Fourteenth International Conference (ICML'97). 296–304, Morgan Kaufmann.

Robnik-Šikonja, M., & Kononenko, I. (2003). Theoretical and empirical analysis of ReliefF and RreliefF. *Machine learning*, *53*(1-2), 23-69.

Ramanan, V. K., & Saykin, A. J. (2013). Pathways to neurodegeneration: mechanistic insights from GWAS in Alzheimer's disease, Parkinson's disease, and related disorders. *American journal of neurodegenerative disease*, *2*(3), 145.

Rhinn, H., Fujita, R., Qiang, L., Cheng, R., Lee, J.H., & Abeliovich, A. (2013). Integrative genomics identifies APOEε4 effectors in Alzhiemer's disease. *Nature, 500*(74600), 45.

Rueffler, C., Hermisson, J., & Wagner, G. P. (2012). Evolution of functional specialization and division of labor. *Proceedings of the National Academy of Sciences*, *109*(6), E326-E335.

Sailer, Z. R., & Harms, M. J. (2017). Detecting *High-Order Epistasis* in Nonlinear Genotype Phenotype Maps. *Genetics*, *205*(3), 1079-1088.

Schüpbach, T., Xenarios, I., Bergmann, S., & Kapur, K. (2010). FastEpistasis: a high performance computing solution for quantitative trait epistasis. *Bioinformatics*, *26*(11),1468–1469.

Schönemann, P. H. (1997). On models and muddles of heritability. *Genetica*, *99*(2), 97-108

Schönemann (1989). New questions about old heritability estimates. *Bulletin of the Psychonomic Society,27*(2),175-178.

Shalizi, C. (2007, September 27). Yet More on the Heritability and Malleability of IQ. Three Toed Sloth:Retrieved from http://bactra.org/weblog/520.html.

Simón-Sánchez, J., & Singleton, A. (2008). Genome-wide association studies in neurological disorders. *The Lancet Neurology*, *7*(11), 1067-1072.

Strange, A., Capon, F., Spencer, C.C., Knght, J., Weale, M, E., Allen, M.H., & Blackwell, JM. (2010). A genome-wide association study identifies new psoriasis suspceptibility loci and an interaction between HLA-C and ERAP1. *Nature genetics, 42*(11), 985.

Takahashi, Y., Seki, N., Ishiura, H., Mitsui, J., Matsukawa, T., Kishino, A., Itoyama, Y. (2008). Development of a high-throughput microarray-based resequencing system for neurological disorders and its application to molecular genetics of amyotrophic lateral sclerosis. *Archives of neurology*, *65*(10), 1326-1332.

Telford, M. J. (2007). Phylogenomics. *Current Biology*, *17*(22), R945-R946.

Templeton, A. R., Wade, M., Brodie, B., & Wolf, J. (2000). Epistasis and the evolutionary process. In *Epistasis complex trait* (pp. 41-57). Oxford Univ. Press.

The Psychiatric GWAS Consortium. (2009). Genome-wide association studies: History, rationale and prospects for psychiatric disorders. *The American journal of psychiatry*. *166*(5), 540- 556. Doi:10.1176/appi.ajp.2008.08091354.

Tinbergen, N. (1963). On aims and methods of ethology. *Zeitschrift für tierpsychologie*, *20*(4), 410- 433.

Tuo, S., Zhang, J., Yuan, X., He, Z., Liu, Y., & Liu, Z. (2017). Niche harmony search algorithm for detecting complex disease associated high-order SNP combinations. *Scientific reports*, *7*(1), 1-18.

Ueki, M., & Cordell, H. J. (2012). Improved Statistics for Genome-Wide Interaction Analysis. *PloS Genetics*, *8*(4), e1002625.

Waddington, C. H. (1942). Canalization of development and the inheritance of acquired characters. *Nature*, *150*(3811), 563.

Wade, M. J. (2002). A gene's eye view of epistasis, selection and speciation. *Journal of Evolutionary Biology*, *15*(3), 337-346.

Wagner, G. P., & Altenberg, L. (1996). Perspective: complex adaptations and the evolution of evolvability. *Evolution*, *50*(3), 967-976.

Wagner, G. P., Pavlicev, M., & Cheverud, J. M. (2007). The road to modularity. *Nature Reviews Genetics*, *8*(12), 921-931.

Wang, Y., Liu, G., Feng, M., & Wong, L. (2011). An empirical comparison of several recent epistatic interaction detection methods. *Bioinformatics (Oxford, England)*, *27*(21), 2936–2943. https://doi.org/10.1093/bioinformatics/btr512

Weinreich, D. M., Delaney, N. F., DePristo, M. A., & Hartl, D. L. (2006). Darwinian evolution can follow only very few mutational paths to fitter proteins. *science*, *312*(5770), 111-114.

Wei, W., Hemani, G., Haley, C.S. (2014). Detecting epistasis in human complex traits. *NatureReviewsGenetics.15()*,722-733.

Weinberger, D. (2014). Epistasis in schizophrenia genetics: What's missing is not heritability. *Schizophrenia Research, 160*(1-3), E2-E3.

Wright, S. (1923). The theory of Path Coefficients a Reply to Niles Criticism. *Genetics*, *8*(3), 239-255.

Wray, N. R., & Gottesman, I. I. (2012). Using summary data from the 125anish national registers to estimate heritabilities for schizophrenia, bipolar disorder, and major depressivedisorder. *Frontiers ingenetics*, *3*, 118.

Wagner, Laubichler, and Bagheri-Chaichian. (1998). Genetic measurement theory of epistatic effects. Genetica 102, 569–580 (1998). https://doi.org/10.1023/A:1017088321094

Whitlock, M. C., Phillips, P. C., & Wade, M. J. (1993). Gene interaction affects the additive genetic variance in subdivided populations with migration and extinction. *Evolution*, *47*(6), 1758-1769.

Wiltshire, S., Bell, J. T., Groves, C. J., Dina, C., Hattersley, A. T., Frayling, T. M., ... & Froguel, P. (2006). Epistasis Between Type 2 Diabetes Susceptibility Loci on Chromosomes 1q21-25 and 10q23-26 in Northern Europeans. *Annals of human* effects.*Genetica,102/103*, 569–580.

Wolfram, S., 1983, "Statistical Mechanics of Cellular Automata", *Reviews of Modern Physics*, 55(3): 601–644. doi:10.1103/RevModPhys.55.601

Wu, R., & Li, B. (1999). A Multiplicative-Epistatic Model for Analyzing Interspecific Differences in Outcrossing Species. *Biometrics, 55*(2), 355-365.

VanderWeele, T. (2015). *Explanation in causal inference: methods for mediation and interaction*. Oxford University Press.

Vitzthum, V. J. (2003). A number no greater than the sum of its parts: the use and abuse of heritability. *Human biology*, *75*(4), 539-558.

Yu, Z., Li, C. F., Mkhikian, H., Zhou, R. W., Newton, B. L., & Demetriou, M. (2014). Family studies of Type 1 diabetes reveal additive and epistatic effects between *MGAT1* andthree other polymorphisms. *Genes and Immunity*, *15*(4), 218–223.

Yung, L. S., Yang, C., Wan, X., & Yu, W. (2011). GBOOST: a GPU-based tool for detecting gene gene interactions in genome–wide case control studies. *Bioinformatics*, *27*(9),1309-1310.

Ziegler, A., König, I. R., & Pahlke, F. (2010). *A Statistical Approach to Genetic Epidemiology: Concepts and Applications, with an E-learning platform*. John Wiley & Sons.

Zhang, F., Boerwinkle, E., Xiong, M. (2014). Epistasis analysis for quantitative traits by functional regression model. *Genome Res,* 24, 989-998

Zhang Y, Liu JS. (2007) Bayesian inference of epistatic interactions in case-control studies. Nat Genet(39),1167-1173.

Zhang, X., Huang, S., Zou, F., & Wang, W. (2010). TEAM: Efficient two-locus epistasis tests in humangenome-wide association study. *Bioinformatics, 26*(12), I217-I227.

Zhang X, Huang S, Zou F, Wang W. (2011). Tools for efficient epistasis detection in genome wide association study. *Source Code for Biology and Medicine*, *6*(1). Doi:10.1186/1751 0473-6-1.

Zhang, F., Xie, D., Liang, M., & Xiong, M. (2016). Functional Regression Models for Epistasis Analysis of Multiple Quantitative Traits. *PloS Genetics, 12*(4), E1005965.

Zheng, H., Van Hulle, C. A., & Rathouz, P. J. (2015). Comparing Alternative Biometric Models with and without Gene-by-Measured Environment Interaction in Behavior Genetic Designs: Statistical Operating Characteristics. *Behavior Genetics*, *45*(4), 480–491.

Zuk, O., Hechter, E., Sunyaev, S. & Lander, E. (2012). The mystery of missing heritability: Genetic interactions create phantom heritability. *Proceedings of the National Academy of Science of the United States of America,109*(4): 1193-1198

.

Appendix A Numerical Example of Architectures in which $\boldsymbol{\varepsilon = [0]}$: detailed description for the case of $\boldsymbol{\Psi'(g)_{Max}}$

Herein we provide a detailed description of a single digenic $\Psi'(\boldsymbol{g})_{\mathbf{Max}}$ architecture of the quantitative form: $[s = 2, \Psi'(\boldsymbol{g}) = \Psi'(\boldsymbol{g})_{\mathbf{Max}}, \boldsymbol{\varepsilon}^*_{\boldsymbol{3x3}} = [0], \vec{\theta}^* = \begin{bmatrix} \alpha_1 = 16 \\ \alpha_2 = 16 \\ k_1 = 1 \\ k_2 = 1 \\ \varphi_1 = 0.1 \\ \varphi_2 = 0.1 \end{bmatrix}, \boldsymbol{H^2} = .\mathbf{8}]$. A complete architecture of this sort is built up from 6 locus-specific genotypic values expressed in terms of *ak* parameterization and the properties of HWE (5.1) and LE (5.2). Following section 6.1, it is the case, $\Psi'(\boldsymbol{g})_{\mathbf{Max}}$ and $\vec{\theta}^*$specifies its joint distribution, genotypic frequencies, and population-level genetic variance components. In Figure A.1, we present the joint distribution, genotypic frequencies, and nine genotypic values which arise from the afore noted parameter values.

Figure A.1 Two Locus Max Epistatic Architecture

A_1A_1 **$\Psi'(g_i=0) = 0$** **$P(g_i=0) = 0.01$** **0**	**A_1A_2** **$\Psi'(g_i=1) = 32$** **$P(g_i=1) = 0.18$** **1**	**A_2A_2** **$\Psi'(g_i=2) = 32$** **$P(g_i=2) = 0.81$** **2**	
Max($\Psi'(0,0)$) $P(0,0) = 0.0001$ $\Psi'(0,0)) = \mathbf{0}$	Max($\Psi'(0,1)$) $P(1,0) = 0.0018$ $\Psi'(0,1))$=**32**	Max($\Psi'(0,2)$) $P(2,0) = 0.0081$ $\Psi'(0,2)) = \mathbf{32}$	**B_1B_1** **$\Psi'(g_i=0) = 0$** **$P(g_i=0) = 0.01$** **0**
Max($\Psi'(1,0)$) $P(0,1) = 0.1458$ $\Psi'(1,0)) = \mathbf{32}$	Max($\Psi'(1,1)$) $P(1,1) = 0.0324$ $\Psi'(1,1)$=**32**	Max($\Psi'(1,2)$) $P(2,1) = 0.0018$ $\Psi'(1,2) = \mathbf{32}$	**B_1B_2** **$\Psi'(g_i=1) = 32$** **$P(g_i=1) = 0.18$** **1**
Max($\Psi'(2,0)$) $P(0,2) = 0.6561$ $\Psi'(2,0) = \mathbf{32}$	Max($\Psi'(1,2)$ $P(1,2)$=0.1458 $\Psi'(2,1) =)\mathbf{32}$	Max($\Psi'(2,2)$ $P(2,2) = 0.0081$ $\Psi'(2,2)) = \mathbf{32}$	**B_2B_2** **$\Psi'(g_i=2) = 32$** **$P(g_i=2) = 0.81$** **2**

From Figure A.1, we may derive the following quantities:

1. $\Psi'(\boldsymbol{g})_{\mathbf{Main}} = \begin{bmatrix} 31.3632 & 31.6832 & 31.6832 \\ 31.6832 & 32.0032 & 32.0032 \\ 31.6832 & 32.0032 & 32.0032 \end{bmatrix}$;
2. $\tau_{(g)} = \begin{bmatrix} -0.00313632 & 0.00057024 & 0.00256608 \\ 0.00057024 & -0.00010368 & -0.00046656 \\ 0.00256608 & -0.00046656 & -0.00209952 \end{bmatrix}$;
3. $\sigma_A^2 = 0.0003$;
4. $\omega_A^2 = 0.002$;
5. $\sigma_D^2 = 0.0016$;
6. $\omega_D^2 = 0.012$;
7. $\sigma_{EP}^2 = 0.100$, $\phi'^* = 1.98$
8. $\omega_{EP}^2 = 0.784$.

Appendix B Numerical Example of Architectures in which ε ≠ [0]: detailed description for the case of $\Psi'(\boldsymbol{g})_{\mathbf{Max,GE}}$

Herein we provide a detailed description of a single digenic $\Psi'(\boldsymbol{g})_{\mathbf{Max,GE}}$ architecture of the quantitative form: $[s = 2, \Psi'(\boldsymbol{g}) = \Psi'(\boldsymbol{g})_{\mathbf{Max}}, \boldsymbol{\varepsilon}^{*}_{3x3} = \begin{bmatrix} -0.360 & -0.202 & -0.029 \\ 0.090 & 0.740 & -0.389 \\ 0.096 & 0.123 & 0.511 \end{bmatrix}, \vec{\theta}^{*} = \begin{bmatrix} \alpha_1 = 16 \\ \alpha_2 = 16 \\ k_1 = -6 \\ k_2 = -1 \\ \varphi_1 = 0.1 \\ \varphi_2 = 0.9 \end{bmatrix}, \boldsymbol{H^2} = .\mathbf{8}]$. A complete architecture of this sort is built up from 6 locus-specific genotypic values expressed in terms of *ak* parameterization and the properties of HWE (5.1) and LE (5.2). Following section 6.1, it is the case, $\Psi'(\boldsymbol{g})_{\mathbf{Max}}$, and $\vec{\theta}^{*}$ specifies its joint distribution, genotypic frequencies, genotypic values, and population-level genetic variance components. However, given $\boldsymbol{\varepsilon}^{*}_{3x3} = \begin{bmatrix} -0.360 & -0.202 & -0.029 \\ 0.090 & 0.740 & -0.389 \\ 0.096 & 0.123 & 0.511 \end{bmatrix}$, it is the case, the true genetic architecture is distorted by the elements of $\boldsymbol{\varepsilon}^{*}_{3x3}$, yielding nine E(Z | $\boldsymbol{g}$) and a set of contaminated population-level genetic variance components. To this end, in Figure B.1, we present the joint distribution, genotypic frequencies, and E(Z | $\boldsymbol{g}$), which arise from the afore noted parameter values.

Figure B.1 Digenic Architecture $\Psi'(\boldsymbol{g})_{\mathbf{MaxGE}}$ Construction

A_1A_1 **$\Psi'(g_i=0) = 0$** **$P(g_i=0) = 0.01$** **0**	**A_1A_2** **$\Psi'(g_i=1) = -80$** **$P(g_i=1) = 0.18$** **1**	**A_2A_2** **$\Psi'(g_i=2) = -12$** **$P(g_i=2) = 0.81$** **2**	
Max($\Psi'(0,0)$) $P(0,0) = 0.0081$ $\mathbf{0} + (-0.360)$ E(Z | $\boldsymbol{g}$ =0,0)=-0.360	Max($\Psi'(0,1)$) $P(1,0) = 0.0018$ $\mathbf{0} + (-0.202) =$ E(Z | $\boldsymbol{g}$ =0,1)=-0.202	Max($\Psi'(0,2)$) $P(2,0) = 0.0001$ $\mathbf{0} + (-0.029) =$ E(Z | $\boldsymbol{g}$ =0,2)=-0.029	**B_1B_1** **$\Psi'(g_i=0) = 0$** **$P(g_i=0) = 0.81$** **0**
Max($\Psi'(1,0)$) $P(0,1) = 0.1458$ $\mathbf{0} + 0.090$ E(Z | $\boldsymbol{g}$ =1,0) = 0.090	Max($\Psi'(1,1)$) $P(1,1) = 0.0324$ $\mathbf{0} + 0.740 =$ E(Z | $\boldsymbol{g}$ =1,1)=0.740	Max($\Psi'(1,2)$) $P(2,1) = 0.0018$ $\mathbf{0} + (-0.389) =$ E(Z | $\boldsymbol{g}$ =1,2)=-2.389	**B_1B_2** **$\Psi'(g_i=1) = 0$** **$P(g_i=1) = 0.18$** **1**
Max($\Psi'(2,0)$) $P(0,2) = 0.6561$ $\mathbf{0} + 0.096 =$ E(Z | $\boldsymbol{g}$ =2,0)=0.096	Max($\Psi'(2, 1)$) $P(1,2)$=0.1458 $-\mathbf{2} + 0.123 =$ E(Z | $\boldsymbol{g}$=2,1)=0.123	Max($\Psi'(2,2)$) $P(2,2) = 0.0081$ $-\mathbf{2} + 0.511 =$ E(Z | $\boldsymbol{g}$ =2,2)=-1.489	**B_2B_2** **$\Psi'(g_i=2) = -2$** **$P(g_i=2) = 0.01$** **2**

From Figure B.1, we may derive the following quantities:

9. $\Psi'(\boldsymbol{g})_{\text{Main}} = \begin{bmatrix} 0.0198 & 0.0198 & -1.9602 \\ -0.0002 & -0.0002 & -1.9802 \\ -0.0002 & -0.0002 & -1.9802 \end{bmatrix}$;
10. $\tau_{(\boldsymbol{g})} = \begin{bmatrix} -0.00016038 & -3.564\text{e}-05 & 0.00019602 \\ 0.00002916 & 6.480\text{e}-06 & -0.00003564 \\ 0.00013122 & 2.916\text{e}-05 & -0.00016038 \end{bmatrix}$;
11. $\Psi'(\boldsymbol{g})_{\text{Main(c)}} = \begin{bmatrix} -0.3362634 & -0.1958134 & -2.063023 \\ 0.1741966 & 0.3146466 & -1.552563 \\ 0.0769966 & 0.2174466 & -1.649763 \end{bmatrix}$;
12. $\tau_{(\boldsymbol{g})(C)} = \begin{bmatrix} 0.00016038 & -3.564\text{e}-05 & 0.00019602 \\ 0.00002916 & 6.480\text{e}-06 & -0.00003564 \\ 0.00013122 & 2.916\text{e}-05 & -0.00016038 \end{bmatrix}$;
13. $\sigma_A^2 = 0.007$;
14. $\omega_A^2 = 0.144$;
15. $\sigma_D^2 = 0.031$;
16. $\omega_D^2 = 0.64$;
17. $\sigma_{EP}^2 = 0.000392$;
18. $\omega_{EP}^2 = 0.0079$;
19. $\sigma_{A(c)}^2 = 0.00089$;
20. $\omega_{A(c)}^2 = 0.018$;
21. $\sigma_{D(c)}^2 = 0.0356$;
22. $\omega_{D(c)}^2 = 0.727$;
23. $\sigma_{EP(c)}^2 = 0.0103$;
24. $\omega_{EP(c)}^2 = 0.210$;
25. $\sigma_{\varepsilon(\boldsymbol{g})}^{2*} = 0.016$;
26. $\omega_{\varepsilon(\boldsymbol{g})}^{2*} = 0.34$;
27. $\sigma_{\Psi'(\boldsymbol{g}),\varepsilon(\boldsymbol{g})}{}^{*} = -0.0045$;
28. $\rho_{\Psi'(\boldsymbol{g}),\varepsilon(\boldsymbol{g})} = -0.177$;
29. $\sigma_R^{2*} = 0.0021$;
30. $\omega_R^{2*} = 0.044$.

Appendix C Joint Parameter combinations and the Magnitude of ϕ'^{*} and $\phi'^{*}_{(C)}$.

Herein, we present the distributions of ϕ'^{*}, $\phi'^{*}_{(C)}$ faceted by H^2. For each, we present the joint combinations of each parameter, while holding all others constant. To begin, for the *6075* $\Psi'(\boldsymbol{g})_{\mathbf{Max}}$ *architectures,* we present Figures C.1 to C.7.

Figure C.1 Joint Allele Frequencies, Effect Size, and Broadsense Heritability

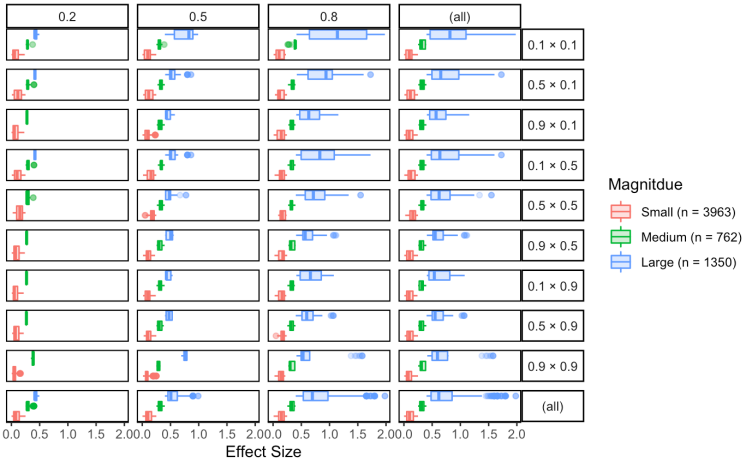

Figure C.2 Joint Dominance Parameters Locus A=1, Effect Size and Broad-sense Heritability

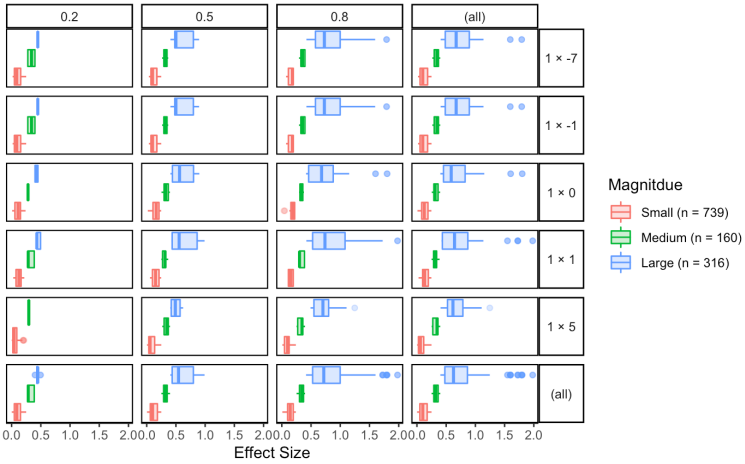

Figure C.3 **Joint Dominance Parameters Locus A=-1, Effect Size and Broad-sense Heritability**

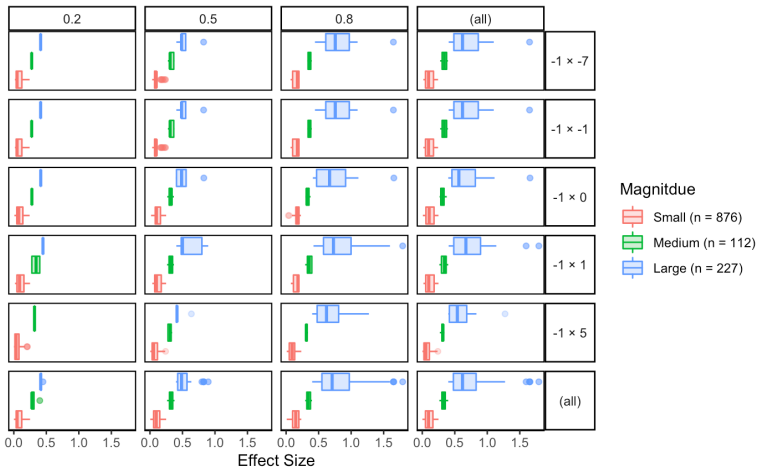

Figure C.4 **Joint Dominance Parameters Locus A=0, Effect Size and Broad-sense Heritability**

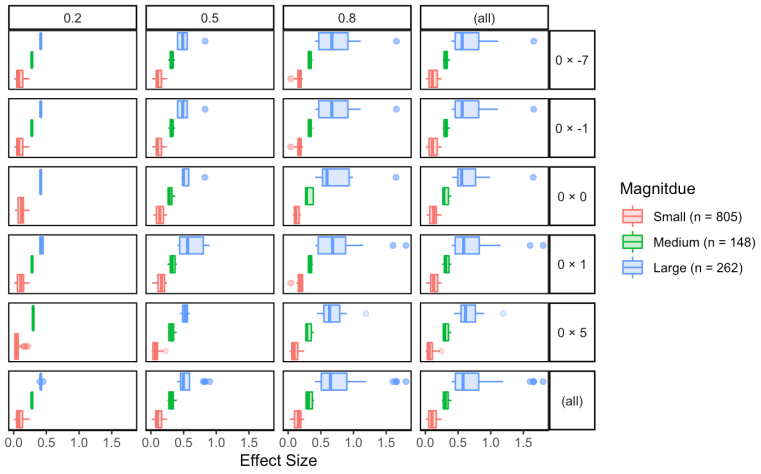

Figure C.5 **Joint Dominance Parameters Locus A=2, Effect Size and Broad-sense Heritability**

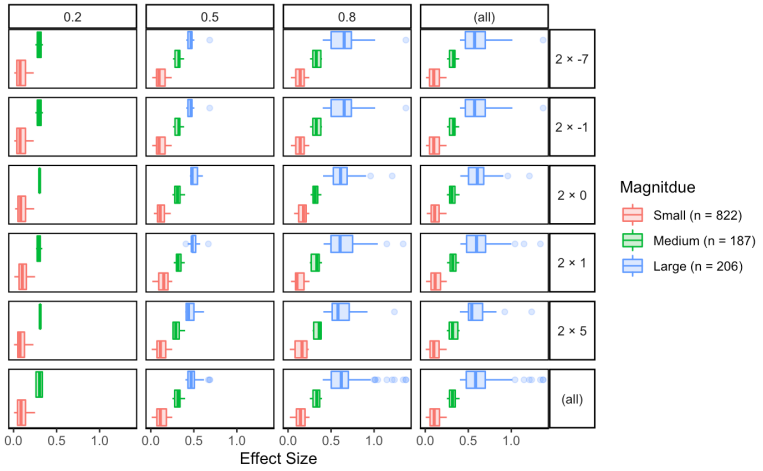

Figure C.6 **Joint Dominance Parameters Locus A=-6, Effect Size and Broad-sense Heritability**

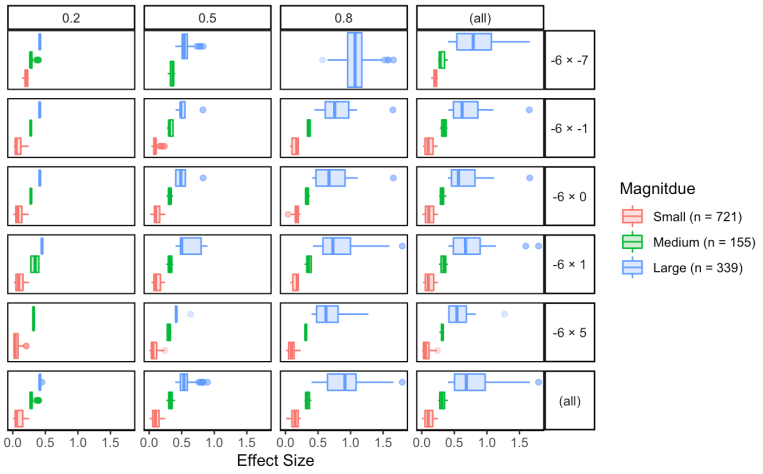

Figure C.7 Joint Additive Parameters, Effect Size and Broadsense Heritability

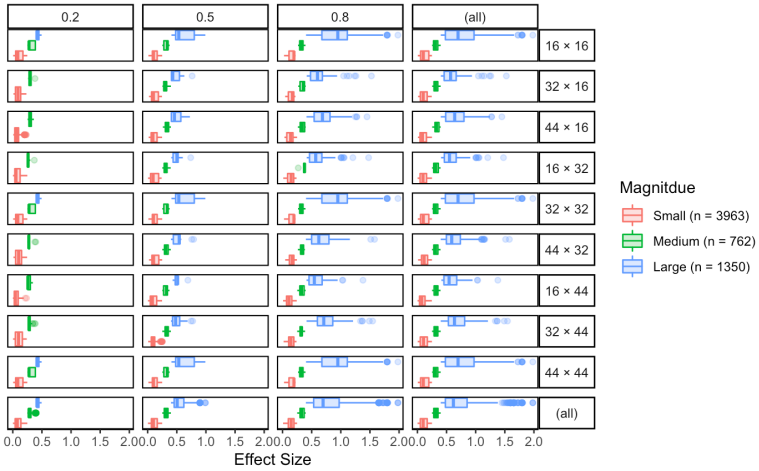

Next, for the 6075 $\Psi'(\boldsymbol{g})_{\text{Min}}$ architectures we present Figures C.8 to C.14

Figure C.8 Joint Allele Frequencies, Effect Size, and Broadsense Heritability

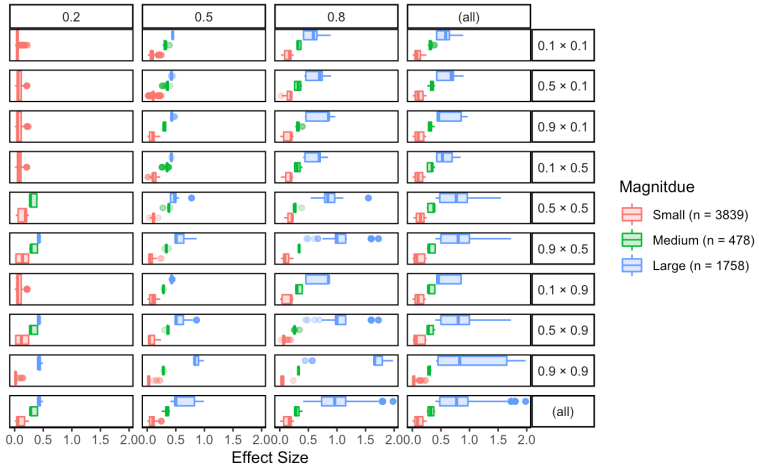

FigureC.9 **Joint Dominance Parameters Locus A=1, Effect Size and Broadsense Heritability**

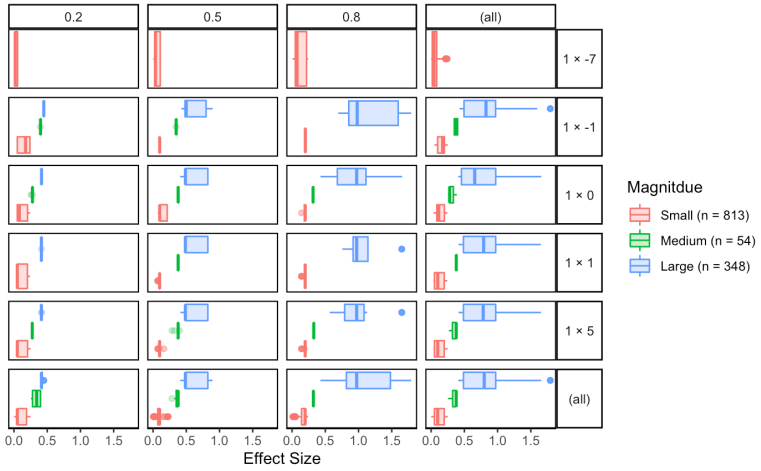

Figure C.10 **Joint Dominance Parameters Locus A=-1, Effect Size and Broadsense Heritability**

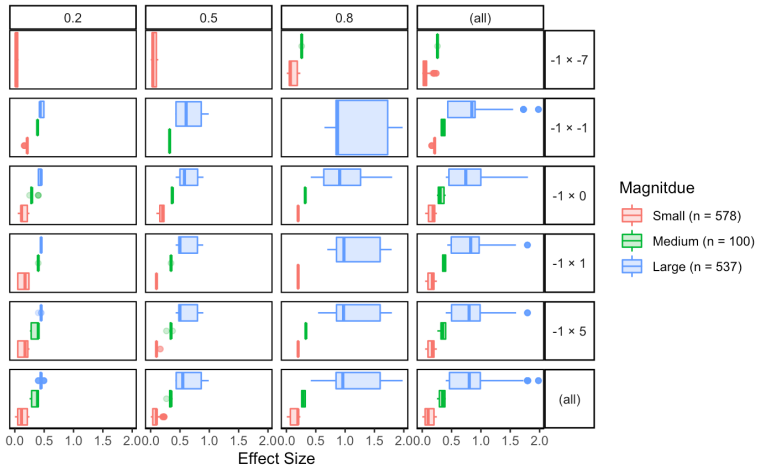

Figure C.11 **Joint Dominance Parameters Locus A=0, Effect Size and Broadsense Heritability**

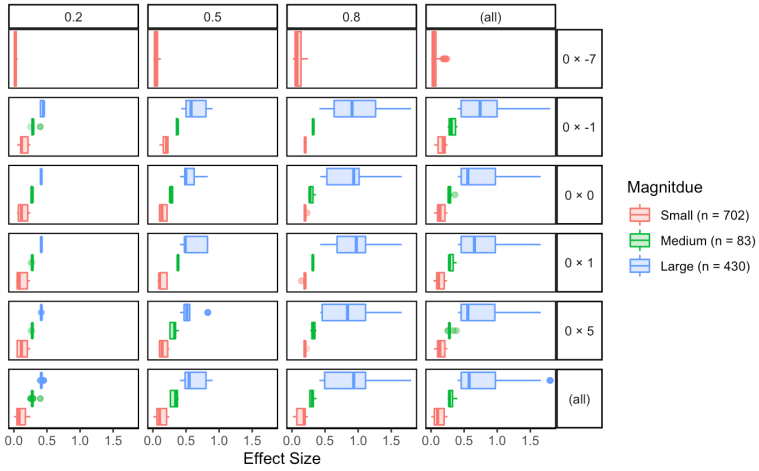

Figure C.12 **Joint Dominance Parameters Locus A=2, Effect Size and Broadsense Heritability**

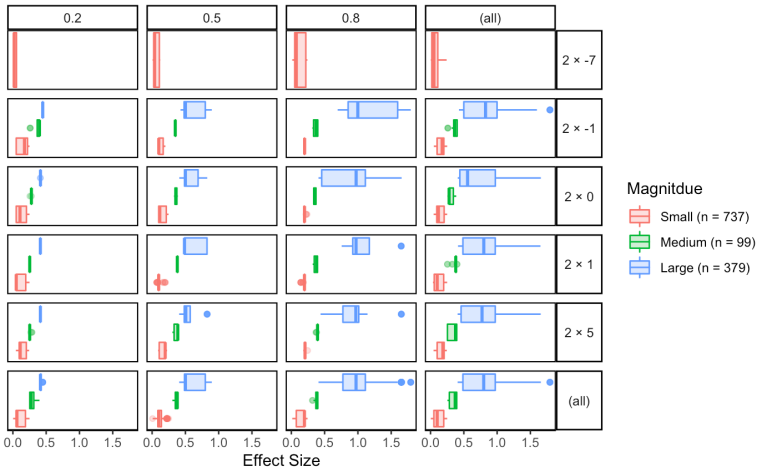

Figure C.13 **Joint Dominance Parameters Locus A=-6, Effect Size and Broadsense Heritability**

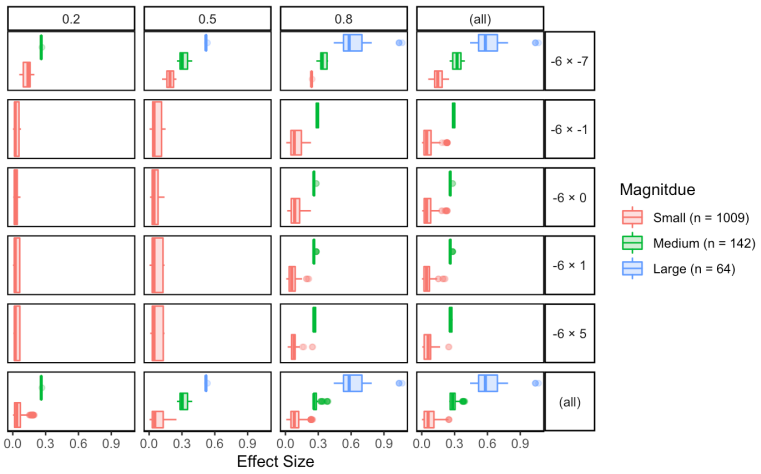

Figure C.14 **Joint Additive Parameters, Effect Size and Broadsense Heritability**

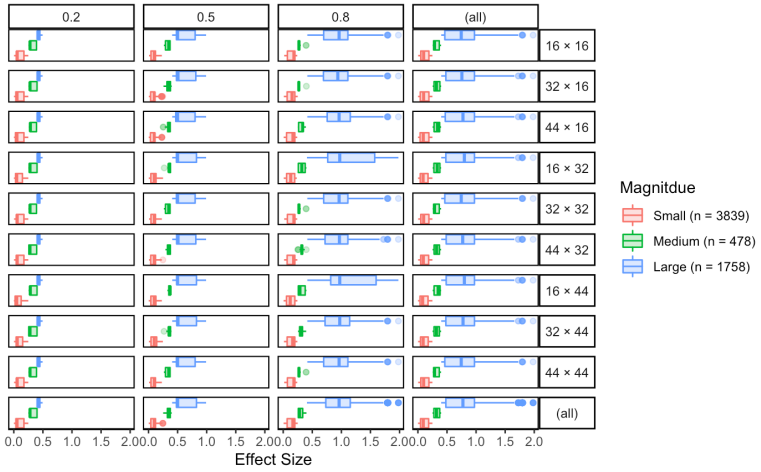

For the 5238 $\Psi'(\boldsymbol{g})_{\mathbf{MaxGE}}$ architectures, we now present Figures C.15 to C.23.

Figure C.15 Joint Allele Frequencies, True Effect Size, and Broadsense Heritability

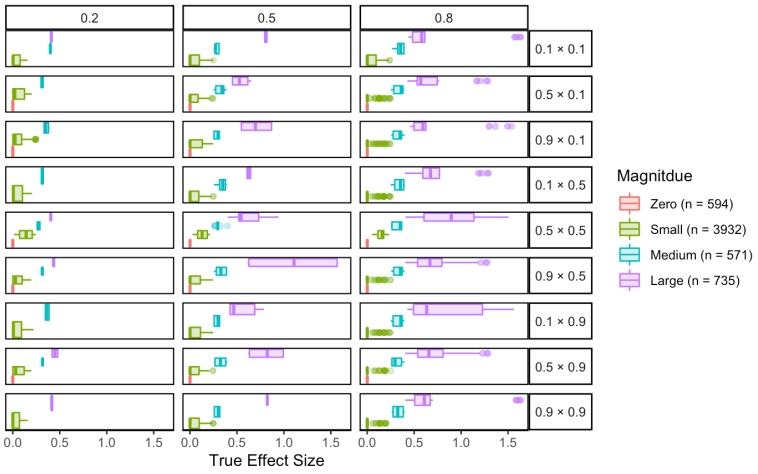

Figure C.16 Joint Allele Frequencies, Contaminated Effect Size, and Broad-sense Heritability

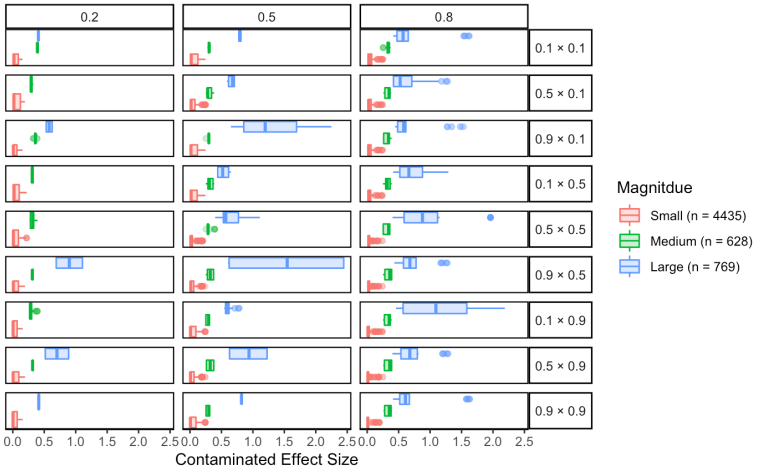

Figure C.17 **Joint dominance parameters Locus A=1, Effect Size and Broad-sense Heritability**

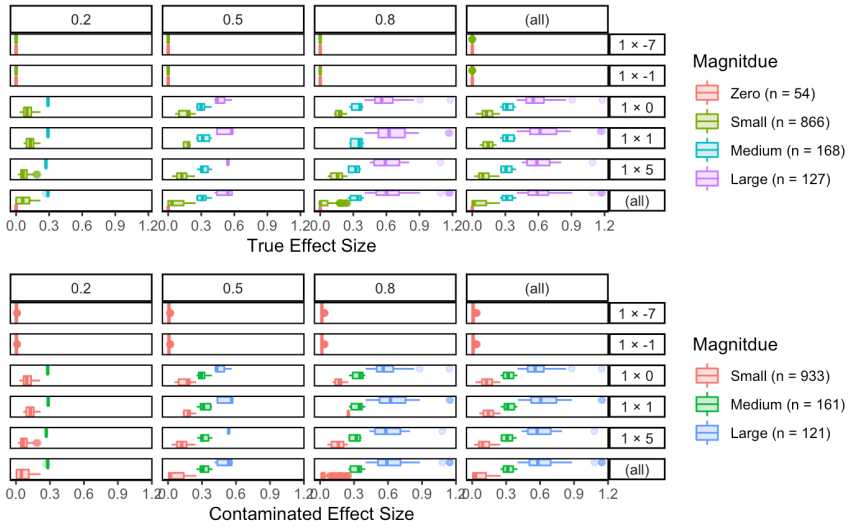

Figure C.18 **Joint dominance parameters Locus A=-1, Effect Size and Broad-sense Heritability**

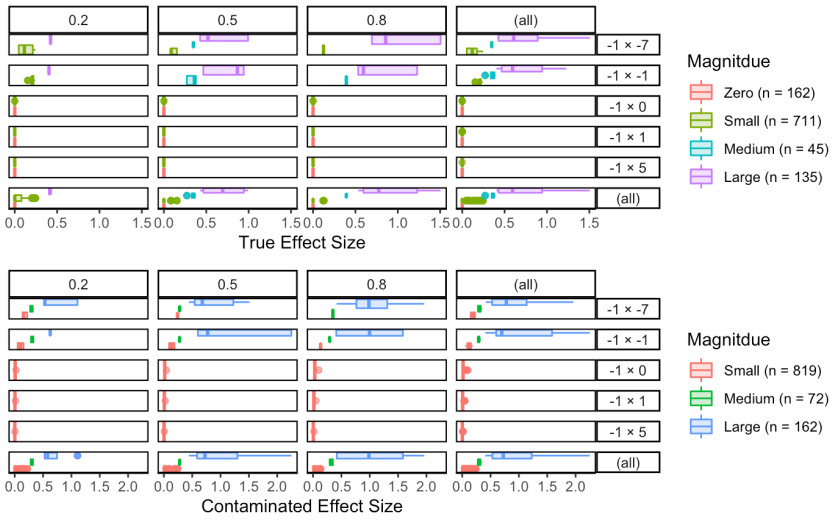

Figure C.19 **Joint dominance parameters Locus A=0, Effect Size and Broad-sense Heritability**

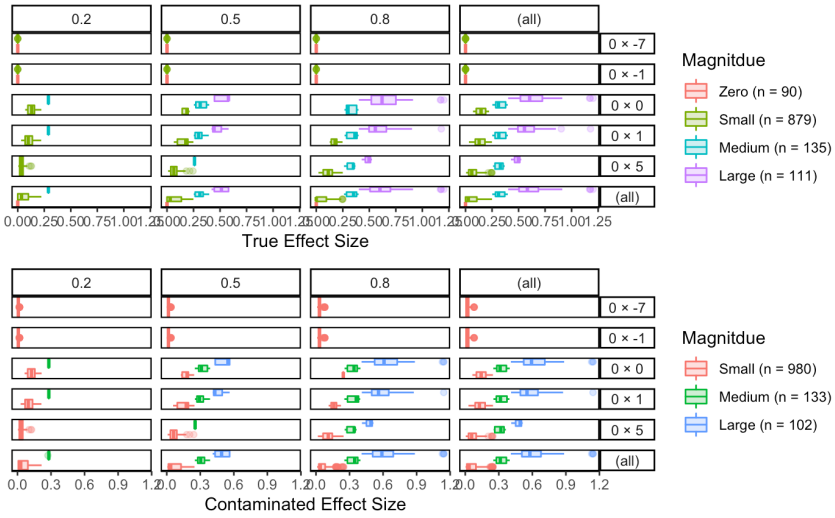

Figure C.20 **Joint dominance parameters Locus A=2, Effect Size and Broad-sense Heritability**

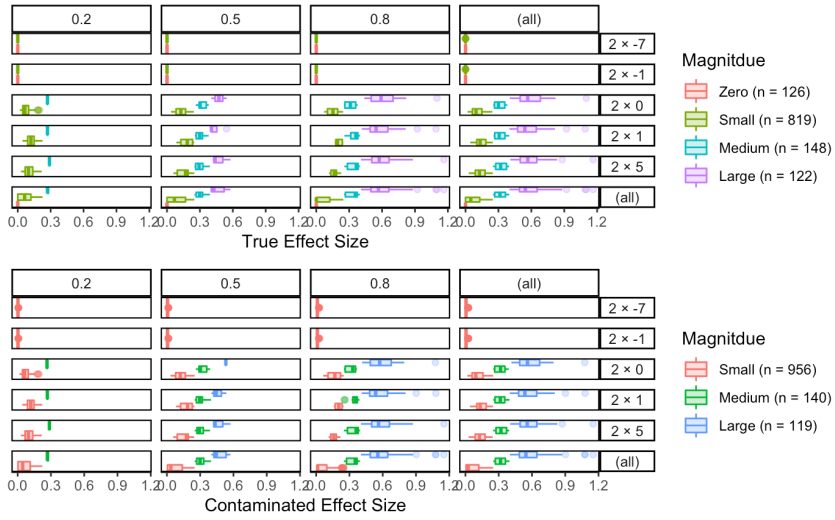

Figure C.21 **Joint dominance parameters Locus A=-6, Effect Size and Broad-sense Heritability**

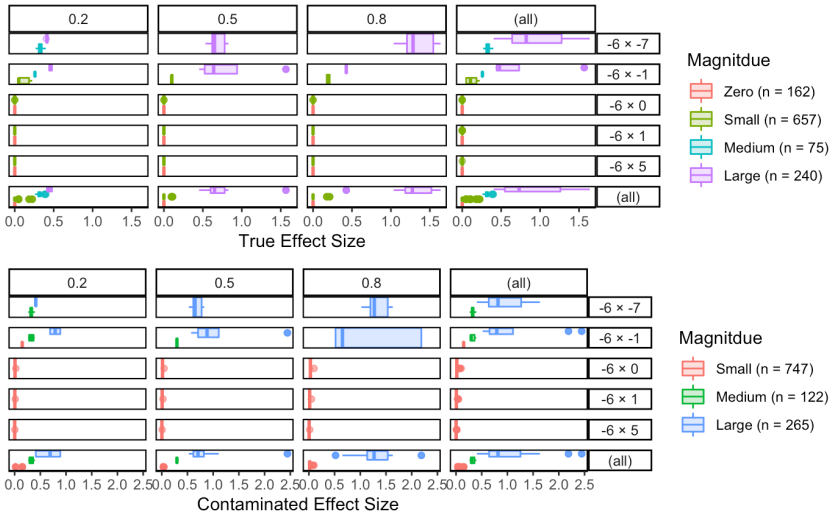

Figure C.22 **Joint Additive parameters,True Effect Size and Broad-sense Heritability**

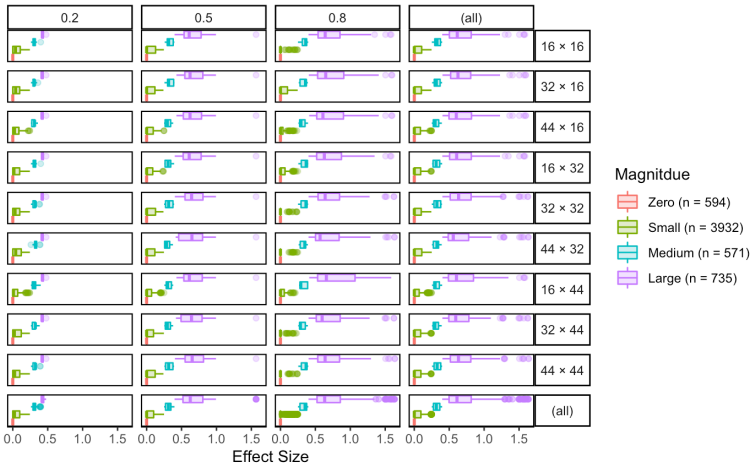

Figure C.23 **Joint Additive Parameters, Contaminated Effect Size and Broadsense Heritability**

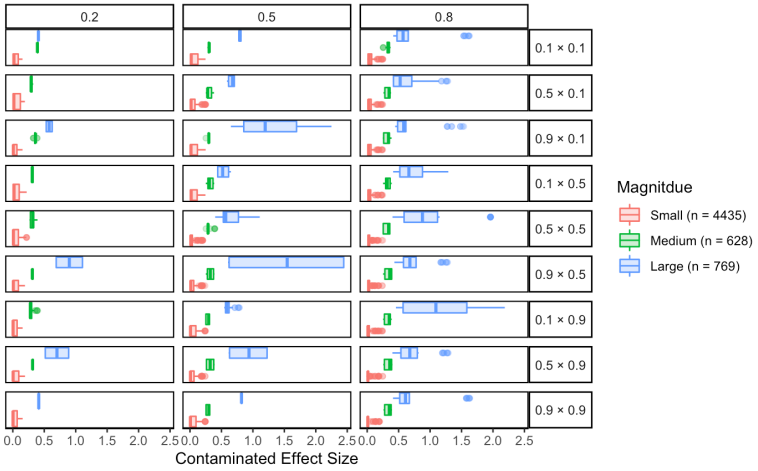

Finally, for the 4482 $\Psi'(\boldsymbol{g})_{\text{Min,GE}}$ architectures we present Figures C.24 to C.32.

Figure C.24 **Joint Allele Frequencies, True Effect Size and Broadsense Heritability**

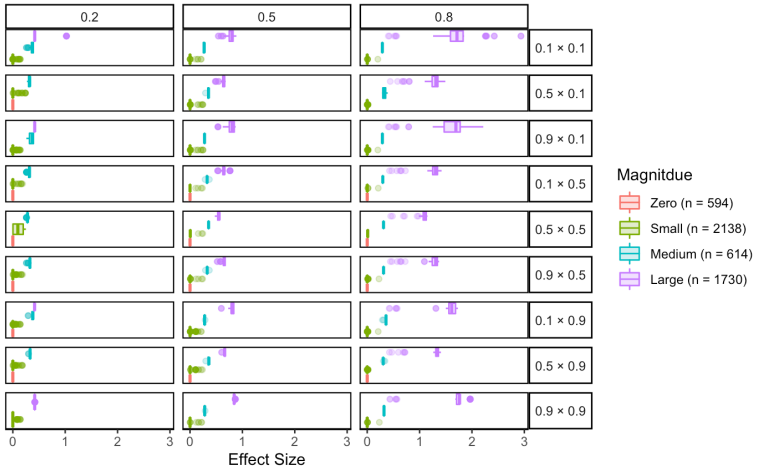

Figure C.25 **Joint Allele Frequencies, Contaminated Effect Size and Broadsense Heritability**

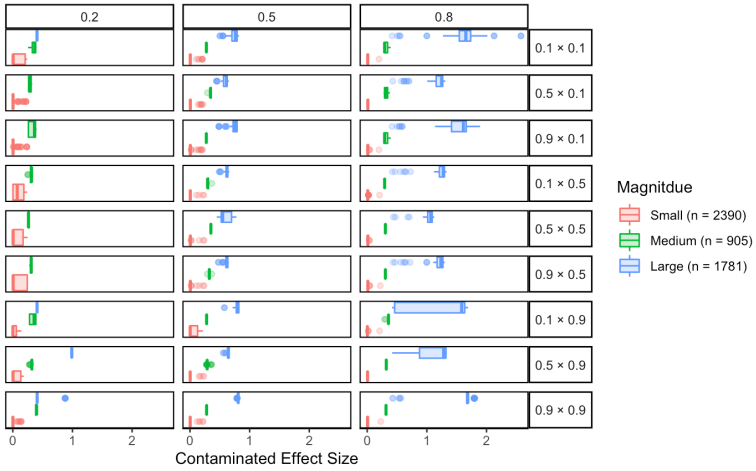

Figure C.26 **Joint Dominance Parameters Locus A =1, Effect Sizes and Broadsense Heritability**

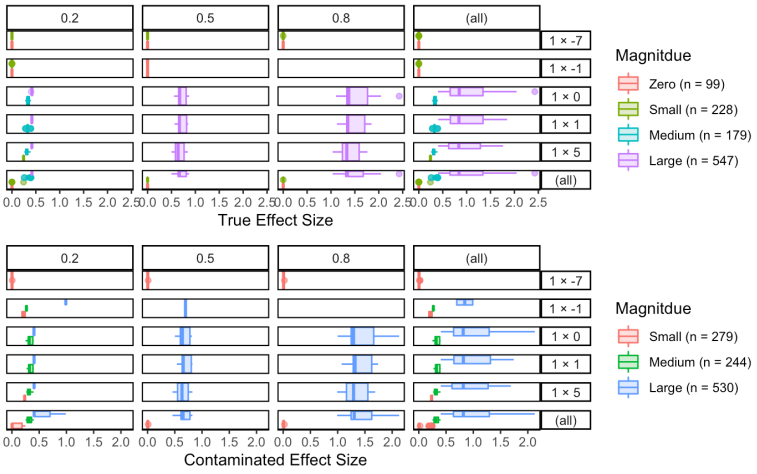

Figure C.27 **Joint Dominance Parameters Locus A =-1, Effect Sizes and Broadsense Heritability**

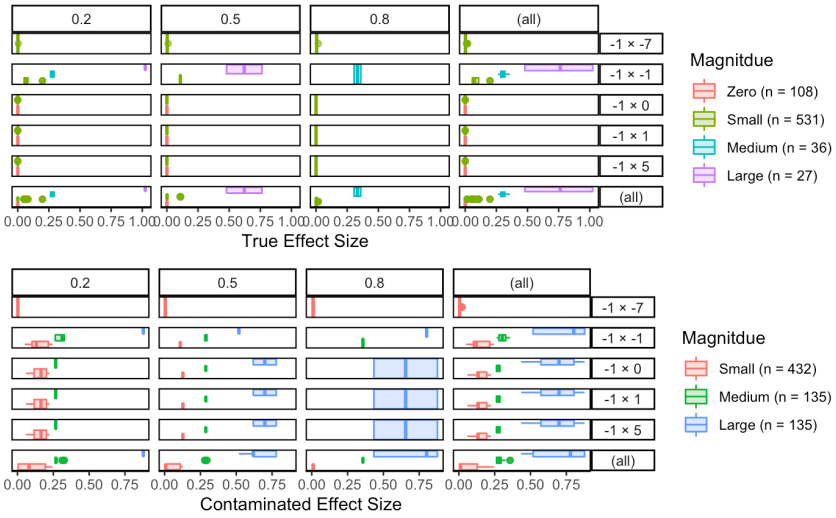

Figure C.28 **Joint Dominance Parameters Locus A =0, Effect Sizes and Broadsense Heritability**

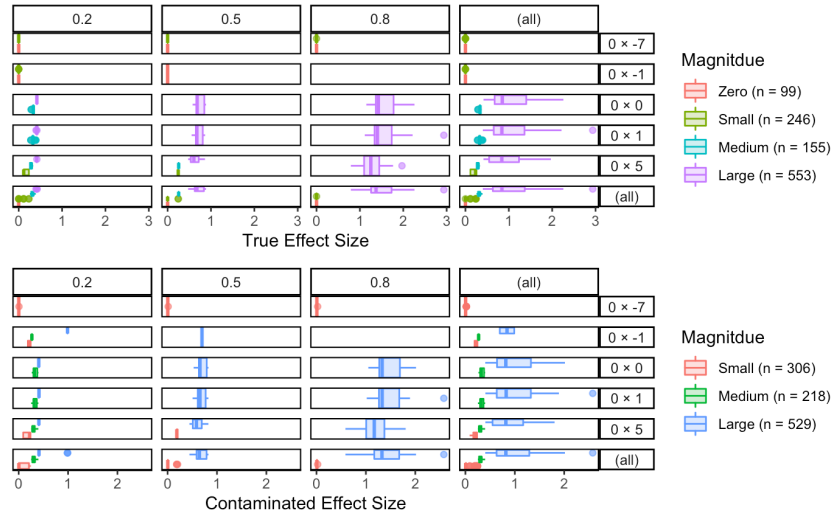

Figure C.29 Joint Dominance Parameters Locus A =2, Effect Sizes and Broadsense Heritability

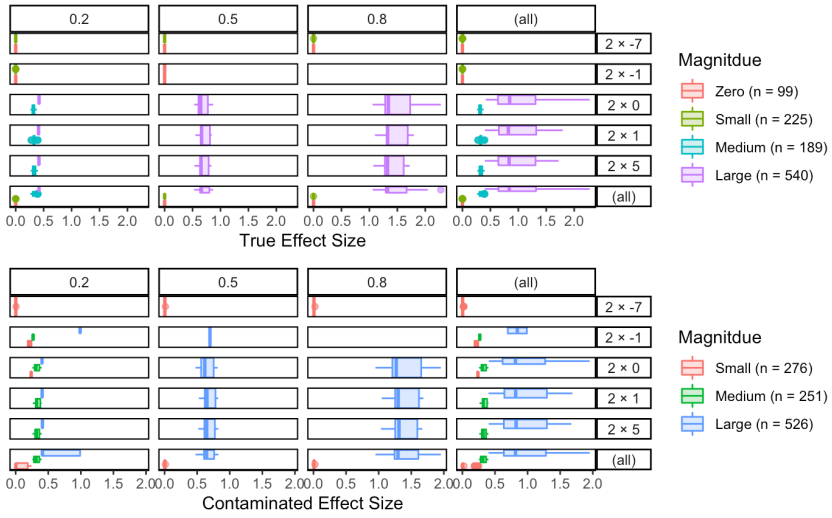

Figure C.30 Joint Dominance Parameters Locus A =-6, Effect Sizes and Broadsense Heritability

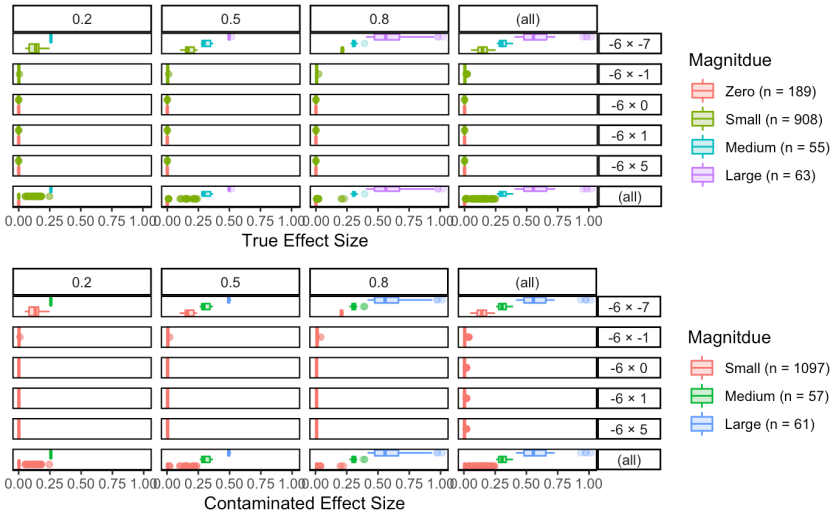

Figure C.31 **Joint Additive Parameters, True Effect Size and Broadsense Heritability**

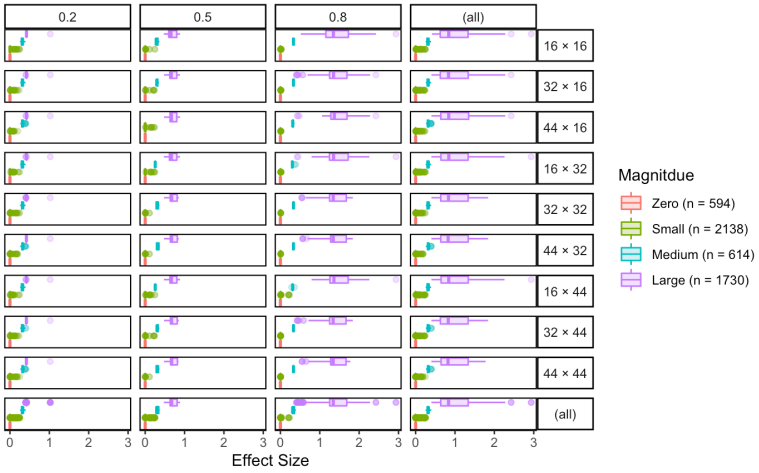

Figure C.32 **Joint Additive Parameters, Contaminated Effect Size and Broadsense Heritability**

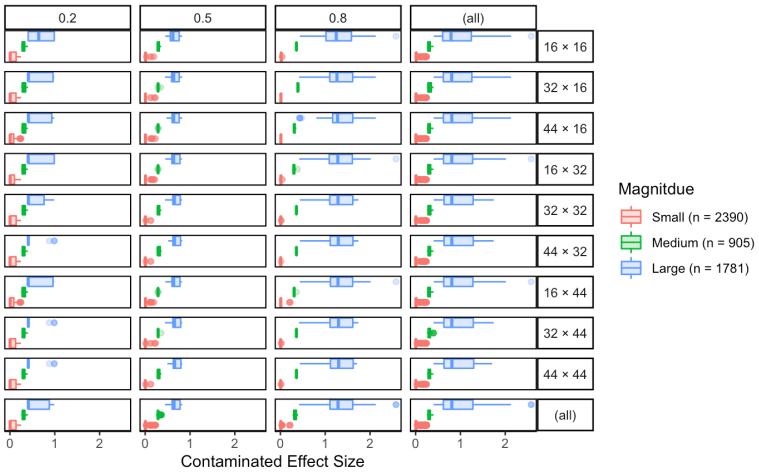

Appendix D R Code $\Psi'(g)_{Max}$ Architectures

Genetic Seed Values:

```
a1<-c(16,32,44)
d1<-c(0.1,0.5,0.9)
k1<-c(0,1,-1,2,-6)
a2<-c(16,32,44)
d2<-c(0.1,0.5,0.9)
k2<-c(0,1,-1,5,-7)
H2<-c(0.2,0.5,0.8)
```

$\Psi'(g)_{Max}$ Architecture:

```
Max.Architecture(a1,d1,k1,a2,d2,k2,H2) {
  t<-0
  STOREADD<-
rep(0,length(a1)*length(a2)*length(k1)*length(k2)*length(d1)*length(d2)*length(H2))
  STOREDOM<-
rep(0,length(a1)*length(a2)*length(k1)*length(k2)*length(d1)*length(d2)*length(H2))
  STOREEP<-
rep(0,length(a1)*length(a2)*length(k1)*length(k2)*length(d1)*length(d2)*length(H2))
  STOREENV<-
rep(0,length(a1)*length(a2)*length(k1)*length(k2)*length(d1)*length(d2)*length(H2))
  STOREPHEN<-
rep(0,length(a1)*length(a2)*length(k1)*length(k2)*length(d1)*length(d2)*length(H2))
  STOREEFF<-
rep(0,length(a1)*length(a2)*length(k1)*length(k2)*length(d1)*length(d2)*length(H2))
  Architecture<-
c(1:(length(a1)*length(a2)*length(k1)*length(k2)*length(d1)*length(d2)*length(H2)))
  MaxSTOREAVL1<-
rep(0,length(a1)*length(a2)*length(k1)*length(k2)*length(d1)*length(d2)*length(H2))
  MaxSTOREKVL1<-
rep(0,length(a1)*length(a2)*length(k1)*length(k2)*length(d1)*length(d2)*length(H2))
  MaxSTOREDVL1<-
rep(0,length(a1)*length(a2)*length(k1)*length(k2)*length(d1)*length(d2)*length(H2))
  MaxSTOREAVL2<-
rep(0,length(a1)*length(a2)*length(k1)*length(k2)*length(d1)*length(d2)*length(H2))
  MaxSTOREKVL2<-
rep(0,length(a1)*length(a2)*length(k1)*length(k2)*length(d1)*length(d2)*length(H2))
  MaxSTOREDVL2<-
rep(0,length(a1)*length(a2)*length(k1)*length(k2)*length(d1)*length(d2)*length(H2))
  MaxSTOREH2<-
rep(0,length(a1)*length(a2)*length(k1)*length(k2)*length(d1)*length(d2)*length(H2))

set.seed(100)
for (i in seq_along(a1)){
  for (j in seq_along(k1)) {
     for (k in seq_along(d1)) {
       for (l in seq_along(a2)) {
         for (m in seq_along(k2)) {
           for (o in seq_along(d2)) {
             for ( p in seq_along(H2)) {

               AVL1<-a1[i]
               KVL1<-k1[j]
```

```
DVL1<-d1[k]
AVL2<-a2[l]
KVL2<-k2[m]
DVL2<-d2[o]
H2a<-H2[p]

GVL1<-c(0,(1+k1[j])*a1[i],2*a1[i])
GVL2<-c(0,(1+k2[m])*a2[l],2*a2[l])
PR1<-c(1-d1[k]^2,2*d1[k]*(1-d1[k]),(d1[k])^2)
PR2<-c(1-d2[o]^2,2*d2[o]*(1-d2[o]),(d2[o])^2)
JDIST<-matrix(0, nrow=length(PR1), ncol=length(PR2))
JDIST<-PR1%*%t(PR2)
GVALS<-matrix(0,nrow=length(GVL1), ncol=length(GVL2))
for (q in seq_along(GVL1)) {
  for (r in seq_along(GVL2)) {
    GVALS[q,r] <-pmax(GVL1[q], GVL2[r])
  }
}
GRANDMEAN<-sum(JDIST*GVALS)
TOTGENVAR<-sum(JDIST*(GVALS-GRANDMEAN)^2)
u<- rep(1,3)
CML1<-(solve(diag(PR1)) %*% (JDIST*GVALS)) %*% u
CML2<-(solve(diag(PR2)) %*% (t(JDIST)*t(GVALS))) %*%u
CV<-c(sum(PR1*CML1^2)-GRANDMEAN^2,sum(PR2*CML2^2)-
          GRANDMEAN^2
CONTMEANS<-c(2*(1-d1[k]), 2*(1-d2[o]))
CONTVARS<-c(2*d1[k]*(1-d1[k]), 2*d2[o]*(1-d2[o]))
GCONT<-c(0,1,2)
COV<-c(sum(PR1*(CML1-GRANDMEAN)*GCONT), sum(PR2*(CML2-
    GRANDMEAN)*GCONT))
AVAR<-(COV[1]^2/CONTVARS[1])+(COV[2]^2/CONTVARS[2])
DOMVAR<-CV[1]+CV[2]-AVAR
GMAIN<-matrix(nrow=length(GVL1), ncol=length(GVL2))
for (q in seq_along(GVL1)) {
  for (r in seq_along(GVL2)) {
    GMAIN[q,r]<-CML1[q]+CML2[r]-GRANDMEAN
  }
}
EPVAR<-sum(JDIST*(GVALS-GMAIN)^2)
ENVAR<-((1/H2[p]-1))*TOTGENVAR
PHENVAR<-TOTGENVAR+ENVAR
EFFECT<-sqrt(EPVAR/ENVAR)

t<-t+1
STOREADD[t]<-AVAR
STOREDOM[t]<-DOMVAR
STOREEP[t]<-EPVAR
STOREENV[t]<-ENVAR
STOREPHEN[t]<-PHENVAR
STOREEFF[t]<-EFFECT
MaxSTOREAVL1[t]<-AVL1
MaxSTOREKVL1[t]<-KVL1
MaxSTOREDVL1[t]<-DVL1
MaxSTOREAVL2[t]<-AVL2
MaxSTOREKVL2[t]<-KVL2
MaxSTOREDVL2[t]<-DVL2
MaxSTOREH2[t]<-H2a
```

```
                Oadd<-STOREADD/STOREPHEN
                Odom<-STOREDOM/STOREPHEN
                Oepi<-STOREEP/STOREPHEN
                Oenv<-STOREENV/STOREPHEN
                Oeff<-STOREEFF
                Ophen<-STOREPHEN

                Max<<-cbind("Add L1"= MaxSTOREAVL1,
                        "Dom L1"= MaxSTOREKVL1,
                        "Allele-F L1" = MaxSTOREDVL1,
                        "Add L2"  = MaxSTOREAVL2,
                        "Dom L2"= MaxSTOREKVL2,
                        "Allele-F L2" = MaxSTOREDVL2,
                        "H2"= MaxSTOREH2,
                        "Add Omega"=Oadd,
                         "Dom Omega"=Odom,
                        "Ep Omega"=Oepi,
                         "Env Omega"=Oenv,
                         "Effect.S"=Oeff,
                        "Phen Omega"=Ophen)

              }
            }
          }
        }
      }
    }
  }
  x<<-Max
  }
```

$\Psi'(\boldsymbol{g})_{\text{Max}}$ Architecture - Numerical Example:

```
Max.Arch.2<-function(a1,k1,d1,a2,k2,d2,H2) {
for (i in seq_along(a1)){
  for (j in seq_along(k1)) {
     for (k in seq_along(d1)) {
       for (l in seq_along(a2)) {
         for (m in seq_along(k2)) {
           for (o in seq_along(d2)) {
             for ( p in seq_along(H2)) {

               AVL1<-a1[i]
               KVL1<-k1[j]
               DVL1<-d1[k]
               AVL2<-a2[l]
               KVL2<-k2[m]
               DVL2<-d2[o]
               H2a<-H2[p]

               GVL1<-c(0,(1+k1[j])*a1[i],2*a1[i])
               GVL2<-c(0,(1+k2[m])*a2[l],2*a2[l])
               PR1<-c(1-d1[k]^2,2*d1[k]*(1-d1[k]),(d1[k])^2)
               PR2<-c(1-d2[o]^2,2*d2[o]*(1-d2[o]),(d2[o])^2)
               JDIST<-matrix(0, nrow=length(PR1), ncol=length(PR2))
               JDIST<-PR1%*%t(PR2)
               GVALS<-matrix(0,nrow=length(GVL1), ncol=length(GVL2))
               for (q in seq_along(GVL1)) {
```

```
            for (r in seq_along(GVL2)) {
              GVALS[q,r] <-pmax(GVL1[q], GVL2[r])
            }
           }
           GRANDMEAN<-sum(JDIST*GVALS)
           TOTGENVAR<-sum(JDIST*(GVALS-GRANDMEAN)^2)
           u<- rep(1,3)
           CML1<-(solve(diag(PR1)) %*% (JDIST*GVALS)) %*% u
           CML2<-(solve(diag(PR2)) %*% (t(JDIST)*t(GVALS))) %*%u
           CV<-c(sum(PR1*CML1^2)-GRANDMEAN^2,sum(PR2*CML2^2)-
          GRANDMEAN^2)
           CONTMEANS<-c(2*(1-d1[k]), 2*(1-d2[o]))
           CONTVARS<-c(2*d1[k]*(1-d1[k]), 2*d2[o]*(1-d2[o]))
           GCONT<-c(0,1,2)
           COV<-c(sum(PR1*(CML1-GRANDMEAN)*GCONT), sum(PR2*(CML2-
          GRANDMEAN)*GCONT))
           AVAR<-(COV[1]^2/CONTVARS[1])+(COV[2]^2/CONTVARS[2])
           DOMVAR<-CV[1]+CV[2]-AVAR
           GMAIN<-matrix(nrow=length(GVL1), ncol=length(GVL2))
            for (q in seq_along(GVL1)) {
              for (r in seq_along(GVL2)) {
                GMAIN[q,r]<-CML1[q]+CML2[r]-GRANDMEAN
              }
            }
           EPEFF<-JDIST*(GVALS-GMAIN)
           EPVAR<-sum(JDIST*(GVALS-GMAIN)^2)
           ENVAR<-((1/H2[p]-1))*TOTGENVAR
           PHENVAR<-TOTGENVAR+ENVAR
           EFFECT<-sqrt(EPVAR/ENVAR)

          }
        }
       }
      }
     }
  }
}

f.3<<-list(Gvl1=GVL1, Pr1=PR1, Pr2=PR2,Gvl2=GVL2, Jdist=JDIST,Gvals=GVALS,
Gmain=GMAIN, Epdeviations=EPEFF,
Avar=AVAR,Domvar=DOMVAR,Epvar=EPVAR, Effect=EFFECT,phenotypicvariance
=PHENVAR, OmegaAdd=AVAR/PHENVAR, OmegaDom=DOMVAR/PHENVAR,
OmegaEp=EPVAR/PHENVAR, TotalGenVar=TOTGENVAR)

return(f.3)
}
```

Appendix E R Code $\Psi'(g)_{\text{Min}}$ Architectures

Genetic Seed Values:

```
a1<-c(16,32,44)
d1<-c(0.1,0.5,0.9)
k1<-c(0,1,-1,2,-6)
a2<-c(16,32,44)
d2<-c(0.1,0.5,0.9)
k2<-c(0,1,-1,5,-7)
H2<-c(0.2,0.5,0.8)
```

$\Psi'(g)_{\text{Min}}$ Architecture:

```
Min.Genetic.Architecture<-function(a1,d1,k1,a2,d2,k2,H2){
t<-0
STOREADDmin<-
rep(0,length(a1)*length(a2)*length(k1)*length(k2)*length(d1)*length(d2)*length(H2))
STOREDOMmin<-
rep(0,length(a1)*length(a2)*length(k1)*length(k2)*length(d1)*length(d2)*length(H2))
STOREEPmin<-
rep(0,length(a1)*length(a2)*length(k1)*length(k2)*length(d1)*length(d2)*length(H2))
STOREENVmin<-
rep(0,length(a1)*length(a2)*length(k1)*length(k2)*length(d1)*length(d2)*length(H2))
STOREPHENmin<-
rep(0,length(a1)*length(a2)*length(k1)*length(k2)*length(d1)*length(d2)*length(H2))
STOREEFFmin<-
rep(0,length(a1)*length(a2)*length(k1)*length(k2)*length(d1)*length(d2)*length(H2))
MinSTOREAVL1<-
rep(0,length(a1)*length(a2)*length(k1)*length(k2)*length(d1)*length(d2)*length(H2))
MinSTOREKVL1<-
rep(0,length(a1)*length(a2)*length(k1)*length(k2)*length(d1)*length(d2)*length(H2))
MinSTOREDVL1<-
rep(0,length(a1)*length(a2)*length(k1)*length(k2)*length(d1)*length(d2)*length(H2))
MinSTOREAVL2<-
rep(0,length(a1)*length(a2)*length(k1)*length(k2)*length(d1)*length(d2)*length(H2))
MinSTOREKVL2<-
rep(0,length(a1)*length(a2)*length(k1)*length(k2)*length(d1)*length(d2)*length(H2))
MinSTOREDVL2<-
rep(0,length(a1)*length(a2)*length(k1)*length(k2)*length(d1)*length(d2)*length(H2))
MinSTOREH2<-
rep(0,length(a1)*length(a2)*length(k1)*length(k2)*length(d1)*length(d2)*length(H2))

set.seed(100)
for (i in seq_along(a1)){
  for (j in seq_along(k1)) {
     for (k in seq_along(d1)) {
       for (l in seq_along(a2)) {
         for (m in seq_along(k2)) {
           for (o in seq_along(d2)) {
             for ( p in seq_along(H2)) {

               minAVL1<-a1[i]
               minKVL1<-k1[j]
               minDVL1<-d1[k]
               minAVL2<-a2[l]
```

```
  minKVL2<-k2[m]
  minDVL2<-d2[o]
  minH2a<-H2[p]
  locus1 specific genotypic value
  GVL2min<-c(0,(1+k2[m])*a2[l],2*a2[l]) value
  PR1min<-c(1-d1[k]^2,2*d1[k]*(1-d1[k]),(d1[k])^2)
  PR2min<-c(1-d2[o]^2,2*d2[o]*(1-d2[o]),(d2[o])^2)
  JDISTmin<-matrix(0, nrow=length(PR1min), ncol=length(PR2min))
  JDISTmin<-PR1min%*%t(PR2min)
  GVALSmin<-matrix(0,nrow=length(GVL1min),
ncol=length(GVL2min))
  for (q in seq_along(GVL1min)) {
    for (r in seq_along(GVL2min)) {
      GVALSmin[q,r] <-pmin(GVL1min[q], GVL2min[r])
    }
  }
 GRANDMEANmin<-sum(JDISTmin*GVALSmin)
 TOTGENVARmin<-sum(JDISTmin*(GVALSmin-          GRANDMEANmin)^2)
 u<- rep(1,3)
 CML1min<-(solve(diag(PR1min)) %*% (JDISTmin*GVALSmin)) %*% u
 CML2min<-(solve(diag(PR2min)) %*% (t(JDISTmin)*t(GVALSmin)))
%*%u
CVmin<-c(sum(PR1min*CML1min^2)-
GRANDMEANmin^2,sum(PR2min*CML2min^2)-GRANDMEANmin^2
 CONTMEANSmin<-c(2*(1-d1[k]), 2*(1-d2[o]))
 CONTVARSmin<-c(2*d1[k]*(1-d1[k]), 2*d2[o]*(1-d2[o]))
 GCONT<-c(0,1,2)
 COVmin<-c(sum(PR1min*(CML1min-GRANDMEANmin)*GCONT),
sum(PR2min*(CML2min-GRANDMEANmin)*GCONT))
 AVARmin<-
(COVmin[1]^2/CONTVARSmin[1])+(COVmin[2]^2/CONTVARSmin[2])
 DOMVARmin<-CVmin[1]+CVmin[2]-AVARmin
 GMAINmin<-matrix(nrow=length(GVL1min), ncol=length(GVL2min))
  for (q in seq_along(GVL1min)) {
    for (r in seq_along(GVL2min)) {
      GMAINmin[q,r]<-CML1min[q]+CML2min[r]-GRANDMEANmin
    }
  }
 EPVARmin<-sum(JDISTmin*(GVALSmin-GMAINmin)^2)
 ENVARmin<-((1/H2[p]-1))*TOTGENVARmin
 PHENVARmin<-TOTGENVARmin+ENVARmin
 EFFECTmin<-sqrt(EPVARmin/ENVARmin)

 t<-t+1
 STOREADDmin[t]<-AVARmin
 STOREDOMmin[t]<-DOMVARmin
 STOREEPmin[t]<-EPVARmin
 STOREENVmin[t]<-ENVARmin
 STOREPHENmin[t]<-PHENVARmin
 STOREEFFmin[t]<-EFFECTmin

 MinSTOREAVL1[t]<-minAVL1
 MinSTOREKVL1[t]<-minKVL1
 MinSTOREDVL1[t]<-minDVL1
 MinSTOREAVL2[t]<-minAVL2
 MinSTOREKVL2[t]<-minKVL2
 MinSTOREDVL2[t]<-minDVL2
 MinSTOREH2[t]<-minH2a
```

```
            Oaddmin<-STOREADDmin/STOREPHENmin
            Odommin<-STOREDOMmin/STOREPHENmin
            Oepimin<-STOREEPmin/STOREPHENmin
            Oenvmin<-STOREENVmin/STOREPHENmin
            Oeffmin<-STOREEFFmin
            Ophenmin<-STOREPHENmin


            Min<<-cbind("Add L1"= MinSTOREAVL1,
                    "Dom L1"= MinSTOREKVL1,
                    "Allele-F L1" = MinSTOREDVL1,
                    "Add L2"  = MinSTOREAVL2,
                    "Dom L2"= MinSTOREKVL2,
                    "Allele-F L2" = MinSTOREDVL2,
                    "H2"= MinSTOREH2,
                    "Add Omega"=Oaddmin,
                     "Dom Omega"=Odommin,
                    "Ep Omega"=Oepimin,
                     "Env Omega"=Oenvmin,
                     "Effect.S"=Oeffmin,
                    "Phen Omega"=Ophenmin)
          }
        }
      }
    }
  }
}
return(Min)
}
```

Appendix F R Code $\Psi'(g)_{\text{MaxGE}}$ Architectures

Genetic Seed Values:

```
a1<-c(16,32,44)
d1<-c(0.1,0.5,0.9)
k1<-c(0,1,-1,2,-6)
a2<-c(16,32,44)
d2<-c(0.1,0.5,0.9)
k2<-c(0,1,-1,5,-7)
H2<-c(0.2,0.5,0.8)
```

$\Psi'(g)_{\text{MaxGe}}$ Architecture:

```
t<-0
StoreENV<-
numeric(length(a1)*length(a2)*length(k1)*length(k2)*length(d1)*length(d2)*length(H2))
StorePHEN<-
numeric(length(a1)*length(a2)*length(k1)*length(k2)*length(d1)*length(d2)*length(H2))
StorePHENA<-
numeric(length(a1)*length(a2)*length(k1)*length(k2)*length(d1)*length(d2)*length(H2))
StoreINT<-
numeric(length(a1)*length(a2)*length(k1)*length(k2)*length(d1)*length(d2)*length(H2))
StoreCOV<-
numeric(length(a1)*length(a2)*length(k1)*length(k2)*length(d1)*length(d2)*length(H2))
StoreCORR<-
numeric(length(a1)*length(a2)*length(k1)*length(k2)*length(d1)*length(d2)*length(H2))
StoreADD<-
numeric(length(a1)*length(a2)*length(k1)*length(k2)*length(d1)*length(d2)*length(H2))
StoreDOM<-
numeric(length(a1)*length(a2)*length(k1)*length(k2)*length(d1)*length(d2)*length(H2))
StoreEP<-
numeric(length(a1)*length(a2)*length(k1)*length(k2)*length(d1)*length(d2)*length(H2))
StoreEFFECT<-
numeric(length(a1)*length(a2)*length(k1)*length(k2)*length(d1)*length(d2)*length(H2))
StoreIADD<-
numeric(length(a1)*length(a2)*length(k1)*length(k2)*length(d1)*length(d2)*length(H2))
StoreIDOM<-
numeric(length(a1)*length(a2)*length(k1)*length(k2)*length(d1)*length(d2)*length(H2))
StoreIEP<-
numeric(length(a1)*length(a2)*length(k1)*length(k2)*length(d1)*length(d2)*length(H2))
StoreIEFFECT<-
numeric(length(a1)*length(a2)*length(k1)*length(k2)*length(d1)*length(d2)*length(H2))
STOREAVL1Bias<-
numeric(length(a1)*length(a2)*length(k1)*length(k2)*length(d1)*length(d2)*length(H2))
STOREKVL1Bias<-
numeric(length(a1)*length(a2)*length(k1)*length(k2)*length(d1)*length(d2)*length(H2))
STOREDVL1Bias<-
numeric(length(a1)*length(a2)*length(k1)*length(k2)*length(d1)*length(d2)*length(H2))
STOREAVL2Bias<-
numeric(length(a1)*length(a2)*length(k1)*length(k2)*length(d1)*length(d2)*length(H2))
STOREKVL2Bias<-
numeric(length(a1)*length(a2)*length(k1)*length(k2)*length(d1)*length(d2)*length(H2))
STOREDVL2Bias<-
numeric(length(a1)*length(a2)*length(k1)*length(k2)*length(d1)*length(d2)*length(H2))
```

```
STOREH2Bias<-
numeric(length(a1)*length(a2)*length(k1)*length(k2)*length(d1)*length(d2)*length(H2))

#Imatep.max.1<<-matrix(c(rnorm(9,sd=1)),nrow=3)
Imatep.max<-matrix(c(-0.360,0.090,0.096, -0.202,  0.740,0.123, -0.029, -0.389,
0.511),nrow=3)

Bias.Arch.Max<-function(a1,k1,d1,a2,k2,d2,H2) {
 for (i in seq_along(a1)){
   for (j in seq_along(k1)) {
     for (k in seq_along(d1)) {
       for(l in seq_along(a2)) {
         for (m in seq_along(k2)) {
           for (o in seq_along(d2)) {
             for (p in seq_along(H2)) {

               AVL1bias<-a1[i]
               KVL1bias<-k1[j]
               DVL1bias<-d1[k]
               AVL2bias<-a2[l]
               KVL2bias<-k2[m]
               DVL2bias<-d2[o]
               H2abias<-H2[p]

               Gvl1<-c(0,(1+k1[j])*a1[i],2*k1[j])
               Gvl2<-c(0,(1+k2[m])*a2[l],2*k2[m])
               Pr1<-c(1-d1[k]^2,2*d1[k]*(1-d1[k]),(d1[k])^2)
               Pr2<-c(1-d2[o]^2,2*d2[o]*(1-d2[o]),(d2[o])^2)
               Jdist<-matrix(0, nrow=length(Pr1), ncol=length(Pr2))
               Jdist<-Pr1%*%t(Pr2)
               Gvals<-matrix(0,nrow = length(Gvl1), ncol= length(Gvl2)) #genotypic values
               for (q in seq_along(Gvl1)) {
                 for (r in seq_along(Gvl2)) {
                   Gvals[q,r]<-pmax(Gvl1[q],Gvl2[r])
                 }
               }

               MuG<-sum(Jdist*Gvals)
               TotalGenVar<-sum(Jdist*(Gvals-MuG)^2)
               u<-rep(1,3)
               CmL1<-(solve(diag(Pr1))%*%(Jdist*Gvals))%*%u
               CmL2<-(solve(diag(Pr2))%*%(t(Jdist)*t(Gvals)))%*%u
               Cvar<-c(sum(Pr1*CmL1^2)-MuG^2,sum(Pr2*CmL2^2)-MuG^2)
               ContMeans<-c(2*(1-d1[k]), 2*(1-d2[o]))
               Contvars<-c(2*d1[k]*(1-d1[k]), 2*d2[o]*(1-d2[o]))
               Gcont<-c(0,1,2)
               Cov<-c(sum(Pr1*(CmL1-MuG)*Gcont),sum(Pr2*(CmL2-MuG)*Gcont))
               #gene content and genotypic value covaraince
               #Matrix of main effect fitted values
               Gmain<-matrix(nrow=length(Gvl1),ncol=length(Gvl2))
               for (q in seq_along(Gvl1)){
                 for (r in seq_along(Gvl2)) {
                   Gmain[q,r]<-CmL1[q]+CmL2[r]-MuG
                 }
               }
               #Variances
               Avar<-(Cov[1]^2/Contvars[1])+(Cov[2]^2/Contvars[2])
               Domvar<-Cvar[1]+Cvar[2]-Avar
```

```
EpVar<-sum(Jdist*(Gvals-Gmain)^2)

Iccm<-Gvals+Imatep.max
MuE<-sum(Jdist*Imatep.max)
MuZ<-MuG+MuE
Icml1<-(solve(diag(Pr1))%*%(Jdist*Iccm))%*%u
Icml2<-(solve(diag(Pr2))%*%(t(Jdist)*t(Iccm)))%*%u
 Icvar<-c(sum(Pr1*Icml1^2)-MuZ^2, sum(Pr2*Icml2^2)-MuZ^2)
Icov<-c(sum(Pr1*(Icml1-MuZ)*Gcont), sum(Pr2*(Icml2-MuZ)*Gcont))
Iavar<-(Icov[1]^2/Contvars[1])+(Icov[2]^2/Contvars[2])
Idomvar<-(Icvar[1]+Icvar[2])-Iavar
Igxevar<-sum(Jdist*(Imatep.max-MuE)^2)
covGE<-sum(Jdist*Imatep.max*Gvals)-MuG*MuE
corrGE<-covGE/sqrt(Igxevar*TotalGenVar)
IGmain<-matrix(nrow=length(Gvl1),ncol=length(Gvl2))
for (q in seq_along(Gvl1)) {
  for (r in seq_along(Gvl2)){
    IGmain[q,r]<-Icml1[q]+Icml2[r]-MuZ
  }
}

Iepvar<-sum(Jdist*(Iccm-IGmain)^2)
VarER<-((1/H2[p])-1)*TotalGenVar-2*covGE-Igxevar
Phenvar<-sum(Jdist*(Iccm-MuZ)^2)+VarER
Phenvarch<-TotalGenVar+2*covGE+Igxevar+VarER
if (VarER > 0) {Effect<-sqrt(EpVar/VarER); Ieffect<-sqrt(Iepvar/VarER)}
else {Effect<--10;Ieffect<- -10}
t<-t+1
StoreENV[t]<-VarER
StorePHEN[t]<-Phenvar
StorePHENA[t]<-Phenvarch
StoreINT[t]<-Igxevar
StoreCOV[t]<-covGE
StoreCORR[t]<-corrGE
StoreADD[t]<-Avar
StoreDOM[t]<-Domvar
StoreEP[t]<-EpVar
StoreEFFECT[t]<-Effect
StoreIADD[t]<-Iavar
StoreIDOM[t]<-Idomvar
StoreIEP[t]<-Iepvar
StoreIEFFECT[t]<-Ieffect

STOREAVL1Bias[t]<-AVL1bias
STOREKVL1Bias[t]<-KVL1bias
STOREDVL1Bias[t]<-DVL1bias
STOREAVL2Bias[t]<-AVL2bias
STOREKVL2Bias[t]<-KVL2bias
STOREDVL2Bias[t]<-DVL2bias
STOREH2Bias[t]<-H2abias
          }
        }
      }
    }
  }
 }
}
```

```
e<<-cbind("ADD L1" = STOREAVL1Bias[StoreEFFECT!=-10],
        "DOM L1" = STOREKVL1Bias[StoreEFFECT!=-10],
        "AF- L1" = STOREDVL1Bias[StoreEFFECT!=-10],
        "ADD L2" = STOREAVL2Bias[StoreEFFECT!=-10],
        "DOM L2" = STOREKVL2Bias[StoreEFFECT!=-10],
        "AF-L2" =  STOREDVL2Bias[StoreEFFECT!=-10],
        "H2" = STOREH2Bias[StoreEFFECT!=-10],
        "Resid.Env.Var"= StoreENV[StoreEFFECT!=-10],
        "Phenotypic.Var"= StorePHEN[StoreEFFECT!=-10],
        "Interaction.Var" = StoreINT[StoreEFFECT!=-10],
        "Covariance" = StoreCOV[StoreEFFECT!=-10],
       "Correlation" = StoreCORR[StoreEFFECT!=-10],
        "Additive Var" = StoreADD[StoreEFFECT!=-10],
        "Dominance Var" = StoreDOM[StoreEFFECT!=-10],
        "Epistatic Var" = StoreEP[StoreEFFECT!=-10],
        "Additive Var.Cont" = StoreIADD[StoreEFFECT!=-10],
        "Dominance Var.Cont" = StoreIDOM[StoreEFFECT!=-10],
        "Epistatic Var.Cont" = StoreIEP[StoreEFFECT!=-10],
        "Effect.Cont" = StoreIEFFECT[StoreEFFECT!=-10],
        "OmegaAdd"=StoreADD[StoreEFFECT!=-10]/StorePHEN[StoreEFFECT!=-10],
        "OmegaDom"=StoreDOM[StoreEFFECT!=-10]/StorePHEN[StoreEFFECT!=-10],
        "OmegaEp"=StoreEP[StoreEFFECT!=-10]/StorePHEN[StoreEFFECT!=-10],
        "OmegaAdd.C"=StoreIADD[StoreEFFECT!=-10]/StorePHEN[StoreEFFECT!=-10],
        "OmegaDom.C"=StoreIDOM[StoreEFFECT!=-10]/StorePHEN[StoreEFFECT!=-10],
         "OmegaEp.C"=StoreIEP[StoreEFFECT!=-10]/StorePHEN[StoreEFFECT!=-10],
          "OmegaEnv"=StoreENV[StoreEFFECT!=-10]/StorePHEN[StoreEFFECT!=-10],
          "OmegaAssociation"=StoreINT[StoreEFFECT!=-10]/StorePHEN[StoreEFFECT!=
            10],
          "OmegaResidual"=StoreENV[StoreEFFECT!=-10]/StorePHEN[StoreEFFECT!=-10],
          "Effect.C" =StoreIEFFECT[StoreEFFECT!=-10],
          "Effect" = StoreEFFECT[StoreEFFECT!=-10],
          "Phen"= StorePHEN[StoreEFFECT!=-10],
          "Bias"=StoreIEFFECT[StoreEFFECT!=-10]-StoreEFFECT[StoreEFFECT!=-10],
          "Bias.Add"=(StoreIDOM[StoreEFFECT!=-10]/StorePHEN[StoreEFFECT!=-10])-
(StoreADD[StoreEFFECT!=-10]/StorePHEN[StoreEFFECT!=-10]),
          "Bias.Dom"=(StoreIDOM[StoreEFFECT!=-10]/StorePHEN[StoreEFFECT!=-10])-
(StoreDOM[StoreEFFECT!=-10]/StorePHEN[StoreEFFECT!=-10]),
       "Bias.Ep"=(StoreIEP[StoreEFFECT!=-10]/StorePHEN[StoreEFFECT!=-10])-
(StoreEP[StoreEFFECT!=-10]/StorePHEN[StoreEFFECT!=-10]))

return(head(e))
}
```

Appendix G R Code $\Psi'(g)_{\text{MinGE}}$ Architectures

Genetic Seed Values:

```
a1<-c(16,32,44)
d1<-c(0.1,0.5,0.9)
k1<-c(0,1,-1,2,-6)
a2<-c(16,32,44)
d2<-c(0.1,0.5,0.9)
k2<-c(0,1,-1,5,-7)
H2<-c(0.2,0.5,0.8)
```

$\Psi'(g)_{\text{MinGe}}$ Architecture:

```
t<-0
 StoreENV.min<-
numeric(length(a1)*length(a2)*length(k1)*length(k2)*length(d1)*length(d2)*length(H2))
 StorePHEN.min<-
numeric(length(a1)*length(a2)*length(k1)*length(k2)*length(d1)*length(d2)*length(H2))
 StorePHENA.min<-
numeric(length(a1)*length(a2)*length(k1)*length(k2)*length(d1)*length(d2)*length(H2))
 StoreINT.min<-
numeric(length(a1)*length(a2)*length(k1)*length(k2)*length(d1)*length(d2)*length(H2))
 StoreCOV.min<-
numeric(length(a1)*length(a2)*length(k1)*length(k2)*length(d1)*length(d2)*length(H2))
 StoreCORR.min<-
numeric(length(a1)*length(a2)*length(k1)*length(k2)*length(d1)*length(d2)*length(H2))
 StoreADD.min<-
numeric(length(a1)*length(a2)*length(k1)*length(k2)*length(d1)*length(d2)*length(H2))
 StoreDOM.min<-
numeric(length(a1)*length(a2)*length(k1)*length(k2)*length(d1)*length(d2)*length(H2))
 StoreEP.min<-
numeric(length(a1)*length(a2)*length(k1)*length(k2)*length(d1)*length(d2)*length(H2))
 StoreEFFECT.min<-
numeric(length(a1)*length(a2)*length(k1)*length(k2)*length(d1)*length(d2)*length(H2))
 StoreIADD.min<-
numeric(length(a1)*length(a2)*length(k1)*length(k2)*length(d1)*length(d2)*length(H2))
 StoreIDOM.min<-
numeric(length(a1)*length(a2)*length(k1)*length(k2)*length(d1)*length(d2)*length(H2))
 StoreIEP.min<-
numeric(length(a1)*length(a2)*length(k1)*length(k2)*length(d1)*length(d2)*length(H2))
 StoreIEFFECT.min<-
numeric(length(a1)*length(a2)*length(k1)*length(k2)*length(d1)*length(d2)*length(H2))
 STOREAVL1Bias.min<-
numeric(length(a1)*length(a2)*length(k1)*length(k2)*length(d1)*length(d2)*length(H2))
 STOREKVL1Bias.min<-
numeric(length(a1)*length(a2)*length(k1)*length(k2)*length(d1)*length(d2)*length(H2))
 STOREDVL1Bias.min<-
numeric(length(a1)*length(a2)*length(k1)*length(k2)*length(d1)*length(d2)*length(H2))
 STOREAVL2Bias.min<-
numeric(length(a1)*length(a2)*length(k1)*length(k2)*length(d1)*length(d2)*length(H2))
 STOREKVL2Bias.min<-
numeric(length(a1)*length(a2)*length(k1)*length(k2)*length(d1)*length(d2)*length(H2))
 STOREDVL2Bias.min<-
numeric(length(a1)*length(a2)*length(k1)*length(k2)*length(d1)*length(d2)*length(H2))
```

```
  STOREH2Bias.min<-
numeric(length(a1)*length(a2)*length(k1)*length(k2)*length(d1)*length(d2)*length(H2))
  #Imatep.min1<<-matrix(c(rnorm(9,sd=1)),nrow=3)
  Imatep.min<<-matrix(c(-0.502,0.131,-0.078, 0.886,0.116,0.318, -0.581, 0.714, -
0.825),nrow=3)

Bias.Arch.Min<-function(a1,k1,d1,a2,k2,d2,H2) {
          for (i in seq_along(a1)){
             for (j in seq_along(k1)) {
               for (k in seq_along(d1)) {
                 for(l in seq_along(a2)) {
                   for (m in seq_along(k2)) {
                     for (o in seq_along(d2)) {
                       for (p in seq_along(H2)){

                         AVL1bias.min<-a1[i]
                         KVL1bias.min<-k1[j]
                         DVL1bias.min<-d1[k]
                         AVL2bias.min<-a2[l]
                         KVL2bias.min<-k2[m]
                         DVL2bias.min<-d2[o]
                         H2abias.min<-H2[p]

                         Gvl1.min<-c(0,(1+k1[j])*a1[i],2*k1[j])
                         Gvl2.min<-c(0,(1+k2[m])*a2[l],2*k2[m])
                         Pr1.min<-c(1-d1[k]^2,2*d1[k]*(1-d1[k]),(d1[k])^2)
                         Pr2.min<-c(1-d2[o]^2,2*d2[o]*(1-d2[o]),(d2[o])^2)
                         Jdist.min<-matrix(0, nrow=length(Pr1.min), ncol=length(Pr2.min))
                         Jdist.min<-Pr1.min%*%t(Pr2.min)
                         Gvals.min<-matrix(0,nrow = length(Gvl1.min), ncol= length(Gvl2.min))
                         #genotypic values
                         for (q in seq_along(Gvl1.min)) {
                           for (r in seq_along(Gvl2.min)) {
                             Gvals.min[q,r]<-pmin(Gvl1.min[q],Gvl2.min[r])
                           }
                         }
                         MuG.min<-sum(Jdist.min*Gvals.min)
                         TotalGenVar.min<-sum(Jdist.min*(Gvals.min-MuG.min)^2)
                         u<-rep(1,3) #conditional means and conditional variances
                         CmL1.min<-(solve(diag(Pr1.min))%*%(Jdist.min*Gvals.min))%*%u
                         #conditional mean for locus 1
                         CmL2.min<-(solve(diag(Pr2.min))%*%(t(Jdist.min)*t(Gvals.min)))%*%u
                          Cvar.min<-c(sum(Pr1.min*CmL1.min^2) -
                        MuG.min^2,sum(Pr2.min*CmL2.min^2)-MuG.min^2
                         ContMeans.min<-c(2*(1-d1[k]), 2*(1-d2[o]))
                         Contvars.min<-c(2*d1[k]*(1-d1[k]), 2*d2[o]*(1-d2[o]))
                         Gcont.min<-c(0,1,2)
                         Cov.min<-c(sum(Pr1.min*(CmL1.min-MuG.min)*Gcont.min),
                                 sum(Pr2.min*(CmL2.min-MuG.min)*Gcont.min))
                         #gene content and genotypic value covaraince
                         #Matrix of main effect fitted values
                         Gmain.min<-matrix(nrow=length(Gvl1.min),ncol=length(Gvl2.min))
                         for (q in seq_along(Gvl1.min)){
                           for (r in seq_along(Gvl2.min)) {
                             Gmain.min[q,r]<-CmL1.min[q]+CmL2.min[r]-MuG.min
                           }
                         }
```

```
Avar.min<-
(Cov.min[1]^2/Contvars.min[1])+(Cov.min[2]^2/Contvars.min[2])
Domvar.min<-Cvar.min[1]+Cvar.min[2]-Avar.min
 EpVar.min<-sum(Jdist.min*(Gvals.min-Gmain.min)^2)

 Iccm.min<-Gvals.min+Imatep.min
 MuE.min<-sum(Jdist.min*Imatep.min)
 MuZ.min<-MuG.min+MuE.min
 Icml1.min<-(solve(diag(Pr1.min))%*%(Jdist.min*Iccm.min))%*%u
 Icml2.min<-(solve(diag(Pr2.min))%*%(t(Jdist.min)*t(Iccm.min)))%*%u
 Icvar.min<-c(sum(Pr1.min*Icml1.min^2)-MuZ.min^2,
          sum(Pr2.min*Icml2.min^2)-MuZ.min^2)
 Icov.min<-c(sum(Pr1.min*(Icml1.min-MuZ.min)*Gcont.min),
         sum(Pr2.min*(Icml2.min-MuZ.min)*Gcont.min))
 Iavar.min<-
(Icov.min[1]^2/Contvars.min[1])+(Icov.min[2]^2/Contvars.min[2])
 Idomvar.min<-(Icvar.min[1]+Icvar.min[2])-Iavar.min
 Igxevar.min<-sum(Jdist.min*(Imatep.min-MuE.min)^2)
 covGE.min<-sum(Jdist.min*Imatep.min*Gvals.min)-
MuG.min*MuE.min
 corrGE.min<-covGE.min/sqrt(Igxevar.min*TotalGenVar.min)
 IGmain.min<-matrix(nrow=length(Gvl1.min),ncol=length(Gvl2.min))
 for (q in seq_along(Gvl1.min)) {
  for (r in seq_along(Gvl2.min)){
   IGmain.min[q,r]<-Icml1.min[q]+Icml2.min[r]-MuZ.min
  }
 }

 Iepvar.min<-sum(Jdist.min*(Iccm.min-IGmain.min)^2)
 VarER.min<-((1/H2[p])-1)*TotalGenVar.min-2*covGE.min-Igxevar.min
 Phenvar.min<-sum(Jdist.min*(Iccm.min-MuZ.min)^2)+VarER.min
 Phenvarch.min<-
TotalGenVar.min+2*covGE.min+Igxevar.min+VarER.min
 if (VarER.min > 0) {Effect.min<-sqrt(EpVar.min/VarER.min);
 Ieffect.min<-sqrt(Iepvar.min/VarER.min)}
 else {Effect.min<--10;Ieffect.min<- -10}

 t<-t+1

 StoreENV.min[t]<-VarER.min
 StorePHEN.min[t]<-Phenvar.min
 StorePHENA.min[t]<-Phenvarch.min
 StoreINT.min[t]<-Igxevar.min
 StoreCOV.min[t]<-covGE.min
 StoreCORR.min[t]<-corrGE.min
 StoreADD.min[t]<-Avar.min
 StoreDOM.min[t]<-Domvar.min
 StoreEP.min[t]<-EpVar.min
 StoreEFFECT.min[t]<-Effect.min
 StoreIADD.min[t]<-Iavar.min
 StoreIDOM.min[t]<-Idomvar.min
 StoreIEP.min[t]<-Iepvar.min
 StoreIEFFECT.min[t]<-Ieffect.min

 STOREAVL1Bias.min[t]<-AVL1bias.min
 STOREKVL1Bias.min[t]<-KVL1bias.min
 STOREDVL1Bias.min[t]<-DVL1bias.min
 STOREAVL2Bias.min[t]<-AVL2bias.min
```

```
            STOREKVL2Bias.min[t]<-KVL2bias.min
            STOREDVL2Bias.min[t]<-DVL2bias.min
            STOREH2Bias.min[t]<-H2abias.min
          }
        }
      }
    }
  }
}

z<<-cbind("ADD L1" = STOREAVL1Bias.min[StoreEFFECT.min!=-10],
      "DOM L1" = STOREKVL1Bias.min[StoreEFFECT.min!=-10],
      "AF- L1" = STOREDVL1Bias.min[StoreEFFECT.min!=-10],
      "ADD L2" = STOREAVL2Bias.min[StoreEFFECT.min!=-10],
      "DOM L2" = STOREKVL2Bias.min[StoreEFFECT.min!=-10],
      "AF-L2" =  STOREDVL2Bias.min[StoreEFFECT.min!=-10],
      "H2" = STOREH2Bias.min[StoreEFFECT.min!=-10],
      "Env Var.Min"= StoreENV.min[StoreEFFECT.min!=-10],
      "Phenotypic Var.Min"= StorePHEN.min[StoreEFFECT.min!=-10],
      "Interaction Var.Min" = StoreINT.min[StoreEFFECT.min!=-10],
      "Covariance.Min" = StoreCOV.min[StoreEFFECT.min!=-10],
     "Correlation.Min" = StoreCORR.min[StoreEFFECT.min!=-10],
      "Additive Var.Min" = StoreADD.min[StoreEFFECT.min!=-10],
      "Dominance Var.Min" = StoreDOM.min[StoreEFFECT.min!=-10],
      "Epistatic Var.Min" = StoreEP.min[StoreEFFECT.min!=-10],
      "Additive Var.Cont.Min" = StoreIADD.min[StoreEFFECT.min!=-10],
      "Dominance Var.Cont.Min" = StoreIDOM.min[StoreEFFECT.min!=-10],
      "Epistatic Var.Cont.Min" = StoreIEP.min[StoreEFFECT.min!=-10],
      "Effect.Cont.Min" = StoreIEFFECT.min[StoreEFFECT.min!=-10],
      "OmegaAdd.Min"=StoreADD.min[StoreEFFECT.min!=-
        10]/StorePHEN.min[StoreEFFECT.min!=-10],
      "OmegaDom.Min"=StoreDOM.min[StoreEFFECT.min!=-
        10]/StorePHEN.min[StoreEFFECT.min!=-10],
      "OmegaEp.Min"=StoreEP.min[StoreEFFECT.min!=-
        10]/StorePHEN.min[StoreEFFECT.min!=-10],
      "OmegaAdd.C.Min"=StoreIADD.min[StoreEFFECT.min!=-
        10]/StorePHEN.min[StoreEFFECT.min!=-10],
      "OmegaDom.C.Min"=StoreIDOM.min[StoreEFFECT.min!=-
        10]/StorePHEN.min[StoreEFFECT.min!=-10],
       "OmegaEp.C.Min"=StoreIEP.min[StoreEFFECT.min!=-
        10]/StorePHEN.min[StoreEFFECT.min!=-10],
       "Effect.Min"=StoreEFFECT.min[StoreEFFECT.min!=-10],
       "Effect.C" =StoreIEFFECT.min[StoreEFFECT.min!=-10],
       "Env.Min"=StoreENV.min[StoreEFFECT.min!=-
        10]/StorePHEN.min[StoreEFFECT.min!=-10],
       "Phen.Min"= StorePHEN.min[StoreEFFECT.min!=-10])


y<<-cbind("ADD L1" = STOREAVL1Bias.min[StoreEFFECT.min!=-10],
      "DOM L1" = STOREKVL1Bias.min[StoreEFFECT.min!=-10],
      "AF- L1" = STOREDVL1Bias.min[StoreEFFECT.min!=-10],
      "ADD L2" = STOREAVL2Bias.min[StoreEFFECT.min!=-10],
     "DOM L2" = STOREKVL2Bias.min[StoreEFFECT.min!=-10],
      "AF-L2" =  STOREDVL2Bias.min[StoreEFFECT.min!=-10],
       "H2" = STOREH2Bias.min[StoreEFFECT.min!=-10],
          "OmegaAdd.Min"=StoreADD.min[StoreEFFECT.min!=-
        10]/StorePHEN.min[StoreEFFECT.min!=-10],
```

```
    "OmegaDom.Min"=StoreDOM.min[StoreEFFECT.min!=-
          10]/StorePHEN.min[StoreEFFECT.min!=-10],
    "OmegaEp.Min"=StoreEP.min[StoreEFFECT.min!=-
          10]/StorePHEN.min[StoreEFFECT.min!=-10],
    "OmegaAdd.C.Min"=StoreIADD.min[StoreEFFECT.min!=-
          10]/StorePHEN.min[StoreEFFECT.min!=-10],
    "OmegaDom.C.Min"=StoreIDOM.min[StoreEFFECT.min!=-
          10]/StorePHEN.min[StoreEFFECT.min!=-10],
     "OmegaEp.C.Min"=StoreIEP.min[StoreEFFECT.min!=-
          10]/StorePHEN.min[StoreEFFECT.min!=-10],
     "Effect.Min"=StoreEFFECT.min[StoreEFFECT.min!=-10],
     "Effect.C" =StoreIEFFECT.min[StoreEFFECT.min!=-10],
    "Env.Min"=StoreENV.min[StoreEFFECT.min!=-
          10]/StorePHEN.min[StoreEFFECT.min!=-10],
     "Phen.Min"= StorePHEN.min[StoreEFFECT.min!=-10])


return(head(z))

}
```

Appendix H R Code Corollary Relationships

Partition Empirical distributions into the 1st, 2nd, 3rd quantiles:

```
Effect.Size.small<-function(x) {
  quantiles <- quantile(x$`Effect.S`)

  q25 <- quantiles[2]
  q50 <- quantiles[3]
  q75 <- quantiles[4]

  a<-which(x$`Effect.S` <= q75)
  b<-which(x$`Effect.S` > q25)

  identical(a,b)
    smalleffect<<-x[which(x$`Effect.S` <= q25),] #25 quantile
    return(smalleffect)
}


Effect.Size.medium<-function(x) {
  quantiles <- quantile(x$`Effect.S`)

  q25 <- quantiles[2]
  q50 <- quantiles[3]
  q75 <- quantiles[4]

  a<-which(x$`Effect.S` <= q75)
  b<-which(x$`Effect.S`> q25)

  identical(a,b)
  mediumeffect<<-x[intersect(a,b),] #inbetween 25 and 75
  return(mediumeffect)
}


Effect.Size.large<-function(x) {
  quantiles <- quantile(x[,12])

  q25 <- quantiles[2]
  q50 <- quantiles[3]
  q75 <- quantiles[4]

  a<-which(x$`Effect.S` <= q75)
  b<-which(x$`Effect.S` > q25)

  identical(a,b)
  largeeffect<<-x[which(x$`Effect.S`> q75),]#75quantile
  return(largeeffect)
}
```

ANOVA Decomposition of 127 estimable effects:

```
Anova<-function(x) {
library(dplyr)
library(sjstats)
```

```
x.fact<-x %>% mutate_at(vars(`Add.L1`, `Dom.L1`, `Allele.F.L1`,`Add.L2`, `Dom.L2`,
`Allele.F.L2`, `H2`), as.factor)
model<<-aov(Effect.S ~`Add.L1`*`Dom.L1`*`Allele.F.L1`*`Add.L2`* `Dom.L2`
*`Allele.F.L2`*
  `H2`, data = x.fact)
partial.omega<<-omega_sq(model, partial=TRUE)
omegasq.max<<-omega_sq(model)
omega.table<<-merge(omegasq.max,partial.omega) %>%
  arrange(desc(omegasq.max)) %>%
  filter(omegasq.max >=0.01) %>%
  mutate_at(vars(omegasq.max,partial.omegasq),round,3) %>%
  return()
return(omega.table)
}
```

Appendix I R Code Power

Seed Values:

```
n<-c(10,20,50,100,500,1000)
alpha<-c(0.01, 0.05, 0.1, 0.2, 0.3, 0.4)
```

Median Power:

```
Power.Median <-function(n,alpha,x){
 Power.Median<-matrix(0,nrow=(length(n)), ncol=(length(alpha)))
 for (a in seq_along(n)) {
  for (b in seq_along(alpha)) {
   for (c in seq_along(x))
    Power.Median[a,b]<-median(pf(qf(1-alpha[b],4, 9*(n[a]-1)), 4, 9*(n[a]-1),
n[a]*(x$Effect.S), lower.tail = FALSE))
  }
 }
 colnames(Power.Median)<-c(".01",".05",".10", ".20",".30",".40")
 rownames(Power.Median)<-c( "10","20","50","100","500","1000")
 return(Power.Median)
}
```

Proportion of Architectures with Satisfactory Power:

```
Proportion.Power <-function(n,alpha,x){
 Power.9<-matrix(0,nrow=(length(n)), ncol=(length(alpha)))
 for (a in seq_along(n)) {
  for (b in seq_along(alpha)) {
   Power.9[a,b]<-mean(pf(qf(1-alpha[b],4,9*(n[a]-1)), 4,9*(n[a]-1), n[a]*(x$Effect.S^2),
lower. Tail=FALSE) > .90)
  }
 }
 return(Power.9)
}
print(Proportion.Power)
```